Optimisation of Marine Boilers using Model-based Multivariable Control

Industrial Ph.D. Thesis

BRIAN SOLBERG

2008

Aalborg Industries A/S
Gasværksvej 24
9100 Aalborg, Denmark

Dept. of Electronic Systems
Aalborg University
Fredrik Bajers Vej 7C
9220 Aalborg Ø, Denmark

Solberg, Brian
Optimisation of Marine Boilers using Model-based Multivariable Control
ISBN 978-87-90664-42-8
First Edition, August, 2008

Aalborg Industries A/S
Gasværksvej 24
9100 Aalborg
Denmark

Department of Electronic Systems
Aalborg University
Fredrik Bajers Vej 7C
9220 Aalborg Ø
Denmark

Preface and Acknowledgements

The work presented in this thesis has been carried out under the Industrial Ph.D. programme supported by the Danish Ministry of Science, Technology and Innovation. The thesis is submitted in partial fulfilment of the requirements for the degree of Doctor of Philosophy in Control Engineering at Automation and Control, Department of Electronic Systems, Aalborg University, Denmark. The work has been carried out at the Engineering Department, Aalborg Industries A/S and at the section of Automation and Control, Aalborg University in the period August 2004 to August 2007 under supervision of Professor Jakob Stoustrup, Associate Professor Palle Andersen and R&D Project Manager Claus M. S. Karstensen.

I would like to thank all my supervisors for great support and guidance throughout the project period. A special thank you to Palle Andersen and Jakob Stoustrup for the many hours they have invested in discussions on project relevant matters and for their eagerness to share their high level of expertise with me.

I would also like to thank my colleagues at Aalborg Industries A/S for contributing to a pleasant working environment.

Thank you to Professor Jan M. Maciejowski for letting me visit his control group at Cambridge University, helping me find accommodation at Pembroke College and otherwise being a kind host. It has been a privilege to visit the Cambridge control group hosting many dominant figures in the field of systems and control. The high scientific level was very motivating, and participating in MPC group meetings and Friday seminars was very inspiring. Also I would like to thank the Ph.D. students at the Cambridge control group for providing a pleasant social atmosphere.

Brian Solberg
Aalborg, August 2008

Abstract

Traditionally, marine boilers have been controlled using classical single loop controllers. To optimise marine boiler performance, reduce new installation time and to minimise the physical dimensions of these large steel constructions a more comprehensive and coherent control strategy is needed. This research deals with the application of advanced control to a specific class of marine boilers combining well known design methods for multivariable systems.

This thesis presents contributions for modelling and control of the one-pass smoke tube marine boilers as well as for hybrid systems control. Much of the focus has been directed towards water level control which is complicated by the nature of the disturbances acting on the system as well as by low frequency sensor noise. This focus was motivated by an estimated large potential to minimise the boiler geometry by reducing water level fluctuations. Strategies for achieving such goal, based on model predictive control, are suggested while pressure control is achieved by using a multivariable control setup.

The thesis further directs attention towards control of the boilers in load situations requiring on/off switching of the burner. A new strategy for handling such situations based on a generalised hysteresis control approach is presented. The solution is optimal according to a specific performance and the new method prove promising results compared to traditional methods and existing optimisation based methods (finite horizon model predictive control). In the thesis the pressure control is based on this new method when on/off burner switching is required while the water level control is handled by a model predictive controller.

The thesis is presented as a collection of eight papers accompanied by a short introduction of the marine boiler plant, motivation, background, summary and conclusions. The first paper (A) discusses modelling and control of a novel turbocharged burner unit. The derived model is compared with measurement data, and a control strategy for the burner is suggested.

In the second paper (B) a model of the marine boiler is presented along with application of linear quadratic Gaussian control to control pressure and water level in a test boiler. In the third paper (C) a thorough analysis of the marine boiler control properties is

presented. In the following paper (D) a model predictive control strategy for controlling pressure and water level in the boiler is presented along with simulation results. This paper introduces an extra complexity to the control problem by considering cooperation with a waste heat recovery boiler. In the fifth paper (E) results gathered from Papers B, C and D and experience gained over the project period are collected into a statement of limits of performance for the marine boiler along with simple control design guidelines. In the sixth paper (F) finite horizon model predictive control is applied to control of marine boilers when the load situations require on/off burner control. In the seventh paper (G) one of the new strategies suggested in Paper (H) based on a generalised hysteresis control approach is applied to the marine boiler and delivers more appropriate performance than the finite receding horizon strategy presented in paper F.
The final paper (H) discusses problems with finite receding horizon control for systems with discrete input and states converging to a limit cycle. Further, new methods handling these problems are introduced derived from infinite horizon aspects.

Synopsis

Marinekedler har traditionelt været styret af klassiske enkelt sløjfe regulatorer. For at optimere ydeevnen af marinekedlerne, reducere installationstiden samt minimere de fysiske dimensioner af disse store stålkonstruktioner er der brug for en mere omfattende og sammenhængende reguleringsstrategi. Dette projekt omhandler avanceret regulering af en specifik klasse af marinekedler ved at kombinere kendte designmetoder for flervariable systemer.
I afhandlingen præsenteres bidrag inden for modellering og regulering af et-træks røgrørs marinekedler såvel som inden for regulering af hybride systemer. Der er specielt fokuseret på vandstandsregulering, hvilket er kompliceret af karakteren af de forstyrrelser, der påvirker systemet samt af lavfrekvent målestøj. Dette fokus var motiveret af et estimeret stort potentiale for at reducere kedlernes dimensioner ved at minimere fluktuationer i vandstanden. Reguleringsstrategier, baseret på model prædiktiv regulering, fremsættes for at nå målet, mens trykreguleringen er håndteret ved at anvende et flervariabel reguleringssetup.
Afhandlingen retter derudover fokus mod regulering af kedler i last situationer, som kræver tænd/sluk skift af brænderen. En ny strategi, baseret på et generaliseret hysterese reguleringsprincip, til at håndtere sådanne situationer er præsenteret. Løsningen er optimal i forhold til et bestemt ydeevne kriterium, og den viser lovende resultater sammenlignet med traditionelle metoder og eksisterende optimeringsbaserede metoder (endelig horisont model prædiktiv regulering). I afhandlingen baseres trykreguleringen på denne nye metode, når tænd/sluk skift af brænderen kræves, mens vandstandsreguleringen er håndteret med en model prædiktiv regulator.
Afhandlingen består af en samling af otte artikler indledt med en kort introduktion til marinekedler, motivation, baggrund, sammendrag samt konklusion. Den første artikel (A) diskuterer modellering og regulering af en ny turboladet brænder enhed. Den udledte model bliver sammelignet med måle data, og der udvikles en reguleringsstrategi til brænderen.
I den anden artikel (B) opstilles en model af marinekedlen samt en regulator baseret på lineær kvadratisk regulering til regulering af tryk og vandstand i en test kedel. I den tredje artikel (C) præsenteres en grundig analyse af reguleringsegenskaberne for

marinekedler. I den efterfølgende artikel (D) præsenteres simulerings resultater for en model prædiktiv reguleringsstrategi til at styre vandstand og tryk i kedlen. Denne artikel introducerer en ekstra kompleksitet ved at betragte situationer med sammenkørsel med en udstødningsgas kedel. I den femte artikel (E) er resultaterne fra artiklerne B, C, og D samt erfaring samlet gennem projektperioden samlet til en redegørelse for ydeevne begrænsningerne for marinekedlen samt simple retningslinjer til design af regulatorer.
I den sjette artikel (F) er endelig horisont model prædiktiv regulering anvendt til styring af en marinekedel i last situationer, der kræver tænd/sluk brænder styring. I den syvende artikel (G) er en af de nye strategier, som er foreslået i artikel H og baseret på en generaliseret hysterese regulator, anvendt på en marinekedel, hvor den yder mere tilfredsstillende end model prædiktiv regulering med endelig horisont, som præsenteret i artikel F.
I den sidste artikel (H) er problemer med anvendelse af endelig horisont model prædiktiv regulering på systemer med diskrete input og tilstande, som konvergerer til en grænsecyklus, behandlet. Nye metoder til at håndtere disse problemer, udledt fra et uendelig horisont perspektiv, er introduceret.

Contents

1. Introduction

This thesis is concerned with modelling, analysis and control of marine boiler systems. The goal is to develop advanced control strategies capable of handling the complex dynamics of these constructions while seeking to minimise water level variations to allow reduction of the physical boiler dimensions. This must be achieved while maintaining an acceptable pressure performance.

1.1 Background and Motivation

This project was proposed by Aalborg Industries A/S (AI).
AI has 15 subsidiaries located in 13 countries. Each subsidiary has its own markets and competencies. In the year 2006 AI had a net turnover of DKK 2,146.9 million, presenting a result of DKK 109.2 million [AI, 2006]. The number of employees in 2006 averaged 1906 worldwide. AI is the global market leader in steam and heat generating solutions primarily for marine applications. The core business is to supply and service marine and offshore concepts characterised by boilers, inert gas systems, thermal fluid systems, burners, control systems and other related accessories. Further activities are within service and supply of industrial boiler plants. The focus of this thesis is on the marine steam boilers, burners and control systems.
To remain competitive on the marine boiler market AI has found it necessary to make their boilers more compact, cheaper and at the same time more efficient. Furthermore, there is a demand for easier operation, less maintenance and faster and more efficient new installation of marine boilers. Achieving these improvements requires optimisation of the dynamic behaviour of the boiler through control as well as construction. Especially regarding construction, new burner technology in combination with improved boiler heat transfer efficiency have recently allowed for more compact boiler designs. Integrating the boiler construction and control system is further believed to help protect the product against copying.
As marine boilers are operating off shore, security demands are high compared with industrial onshore boiler plants placing high demands on the controller regarding e.g. boiler water level and pressure control. Further, the marine boiler is often vital for ship

operation and high availability is expected. This means that there is a demand for a high level of automation and reliable fault detection and accommodation.
Basically, marine boiler control is a matter of keeping water level and pressure near specified setpoints. Today, the background theory used for designing marine boiler controllers is based on single loop processes (ignoring the multivariable nature of the process) resembling the principle applied to steam engines by James Watt in 1788. These controllers are adjusted by the sevice engineer at commissioning, which requires relatively large resources and further by no means ensures optimal performance. This means that since the first marine boiler was built in Aalborg in 1912 there have been only few developments in the basic control algorithm. However, due to the increased market competition AI has found it necessary to look towards the development of a more comprehensive, versatile and coherent control system. A new control system is currently under development, which together with software tools as MATLAB® /Simulink® and Real-Time Workshop® allows for rapid prototyping and faster implementation of new advanced control strategies. Further, over the past few years AI has initiated many student projects at Aalborg University focused on applying model-based control and fault detection algorithms to a specific boiler family; the oil-fired one-pass smoke tube boiler. This thesis focuses on model-based control of the marine boiler and related topics.

1.2 The Marine Boiler

This section will give a basic introduction to marine boilers in order to make the reader familiar with the application. First, a short introduction to the application of these large steel constructions is given and the basic functionality is explained.
The class of marine boilers described in this work is used for offshore steam production. The offshore carriers span from FPSO[1] vessels, tankers, container ships and bulk carriers to passenger liners. The steam is used in a wide range of applications, among others:

- Keeping heavy fuel in tanks at $\approx 45^{\circ}\mathrm{C}$
- Preheating the fuel to $\approx$ 120-140$^{\circ}\mathrm{C}$ before it enters the ship engine and boiler burner
- Keeping oil and other cargo in tanks at a suitable temperature
- Heating cabins, producing hot water and producing fresh water
- Steam driven cargo pumps
- Tank cleaning.

[1] Floating, Production, Storage and Offloading

The reasons for using steam for these purposes are many; steam has a high energy content, it takes up little space, it is easy to transport and the overall boiler system has a high efficiency.
Typically two types of steam boilers are present on the ships; the oil-fired boiler and the waste heat recovery (WHR) boiler, also sometimes referred to as the exhaust gas boiler[2]. A ship can have more than one of each. The oil-fired boiler is mainly active when the ship is in harbour, whereas when at sea the WHR boiler takes over and is supplemented by the oil-fired boiler when the steam consumption exceeds the WHR boiler's capacity. The two boilers are usually combined in a configuration where the WHR uses the steam space of the oil-fired boiler. However, AI also supply WHR boilers (the smoke tube WHR boilers) which can have their own steam space.
The boiler family addressed in this work is the oil-fired one-pass smoke tube boiler interconnected with the water tube WHR boiler. A drawing of such a configuration is shown in Figure 1.1.

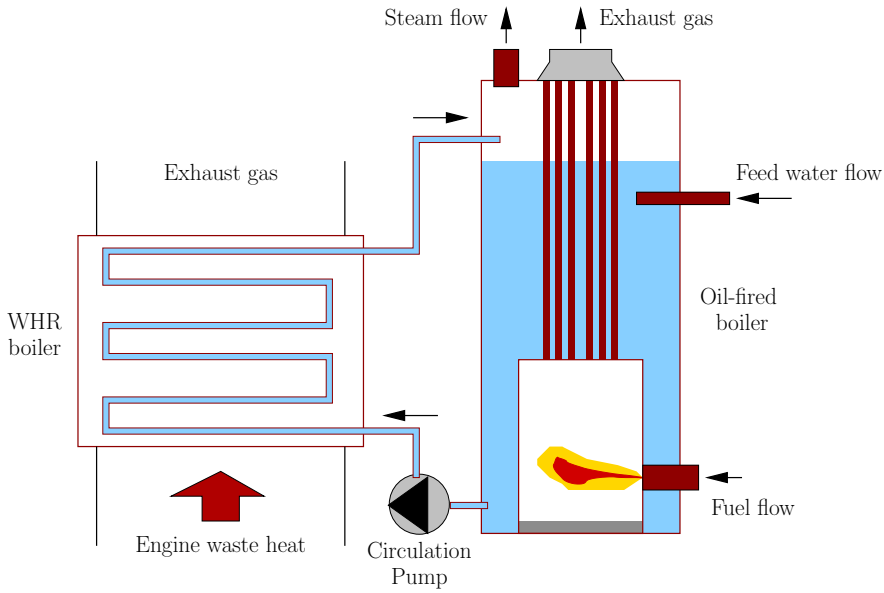

Figure 1.1: Drawing of side-fired marine boiler interconnected with a WHR boiler.

The oil-fired boiler differs from other boiler designs in two ways: it is side-fired and the flue gas passes straight through. These side-fired boilers are simple in design, have larger efficiency compared to other designs and use less steel.
The boiler consists of a furnace and flue gas pipes surrounded by water and steam in

[2]For an extensive overview of boiler designs and functions see [Larsen, 2001; Spirax, 2007].

what will be referred to as the water/steam part or drum of the boiler. In the top left side of the boiler the steam is let out and in the top right side feed water is injected.
A mixture of air and residual fuel is injected into the furnace where it is ignited and burned. A combination of thermal radiation and convection distributes the heat to the furnace jacket and heats the surrounding water. The gas from the combustion (flue gas) leaves the furnace through the flue gas pipes and contributes to heating of the water and steam by thermal convection through the pipe walls.
The WHR boiler is placed in the funnel of the ship. The design sketched in Figure 1.1 is a water tube boiler, especially designed for heat recovery from diesel engine exhaust gas. These boilers use forced circulation. The water inlet is taken from the bottom of the oil-fired boiler. The water is then heated by the engine exhaust gas, and the mixture of steam and water exiting the boiler is injected in the top of the oil-fired boiler.

1.3 State of the Art and Related Work

The steam boiler technology is over 200 years old and constitutes a complicated multivariable nonlinear process. Nevertheless steam boilers are controlled with controllers whose background theory is based on SISO (single input single output) processes. This is general for both industrial and marine steam boilers. The steam pressure is controlled using PID, control in some cases supplemented by a feedforward from the steam flow. The water level is controlled using what is known as single, two or three element control [Pedersen et al., 2003]. Single element control makes use of feedback from the water level only. Two element control adds a feedforward action from the measured steam flow to the feedback law. Finally three element control adds to the feedback a separate loop which has the purpose of continuously adding the same amount of feed water to the boiler as the amount of steam leaving by measuring both flows. The type of water level controller depends on the specific boiler type. However, the water level feedback controller is normally pure proportional action. For small boilers both the water level and pressure can be controlled using a hysteresis controller supplying an on/off control signal to the fuel valve or feed water pump rather than a continuous control signal.
Advanced model-based control has evolved much during the last century and has shown potential in many industries. However, even though model-based control has had success in other industries it has had difficulties being adopted in the marine steam boiler industry. Therefore, there is a potential for improvements which is also backed by economical and competitive incentives:

- A better controller for the water level can allow for more compact boilers with reduced water and steam volumes.
- Using new signals can allow for better combined operation of oil-fired and WHR boilers, which again allows for more compact boilers.

- The performance at low load where on/off burner switching is required can be increased.
- Advanced control strategies can allow for burners which can be combined with more compact boilers.
- Using control system analysis it is possible to find out what limits the achievable performance.

Looking in the literature numerous works can be found on modelling and advanced control of the steam boiler. However, most of these examples are confined to simulation studies. In the field of power plant boilers, advanced control strategies have been studied for some years now. In [Mortensen, 1997; Mortensen et al., 1998], a gain scheduled linear quadratic Gaussian (LQG) regulator designed to improve load following capabilities of once through boilers was presented. In [Hangstrup, 1998], a gain scheduled H_∞ controller was developed for control of steam pressure and temperature in the same process. In [Mølbak, 1990], generalised predictive control was applied for control of super heater temperature. More recently related work was presented in [Rossiter et al., 2002]. In [Lee et al., 2000], a constrained receding horizon algorithm was applied to a nonlinear boiler-turbine model, and in [Kothare et al., 2000] a similar algorithm was applied to level control in the steam generator in a nuclear power plant. Both these later works address extension of the algorithms to linear parameter varying processes.
Even though experience from the power plants can be used there is still a large challenge in introducing advanced control for marine boilers to reach the improvements listed above:

- Introduction of advanced model-based control requires models that reflect the system dynamics with sufficient precision. As new boilers and burners are developed, model-based control requires a considerable effort regarding renewed model work and model fitting for every new boiler type.
- The boiler control must be adjusted to the operating conditions for marine boilers characterised by frequent large variations in the steam load.
- Satisfying demands to the system requires careful consideration of the performance requirements and knowledge of the control properties of the system.
- Optimal on/off burner control requires a new control theory to be developed.

Furthermore, the configuration of the WHR and the oil-fired boiler is a special solution in marine boiler systems.
Dynamic models and hereby also model-based control are relatively new subjects in the field of marine boilers. AI began these studies five years ago and have since initiated student and Ph.D. projects at Aalborg University, see e.g. [Andersen and Jørgensen, 2007; Hvistendahl and Solberg, 2004; Persson and Sørensen, 2006; Sørensen, 2004].

1.3.1 Boiler modelling

As we are interested in controlling the whole boiler system, models of both the boiler, the burner and the feed water system are of interest. We are interested in deriving models based on first principles rather than using system identification techniques to specify a black box model based on e.g. linear parametric models, [Ljung, 1999]. This technique is adopted as these models tend to be valid over a wider operating range. The goal is to derive lumped parameter models that reflect the plant dynamics as well as possible based on knowledge of the system behaviour and measurements. This approach is also taken to achieve insight into the boiler system process. Further, detailed models like these will be of great value as a simulation platform for controller designs.
Early work on lumped first principle dynamic models useful for advanced controller design for the drum boiler can be found in [Chien et al., 1958]. More recent publications are [Pellegrinetti and Bentsman, 1996] and the popular model by Åström and Bell published in [Åström and Bell, 2000]. The main difficulty in modelling the boiler dynamics is caused by the distribution of steam below the water surface. This steam introduces a phenomenon called shrink-and-swell on the water level [Åström and Bell, 2000]. This is seen as a non-minimum phase zero in the response from steam flow, feed water flow and fuel flow to the water level. Many proposals for a description of the distribution of steam bubbles below the water surface have been documented – see e.g. [Åström and Bell, 2000; Andersen and Jørgensen, 2007; Kim and Choi, 2005; Solberg et al., 2005b; Sørensen et al., 2004]. Most of these are based on assumptions and all end up including empirical constants to be estimated to fit the model to process data. In [Kothare et al., 2000], an approach was taken to model the boiler as a collection of linear models in which a non-minimum phase zero is easily inserted. A summary of developments in modelling of boilers can be found in [Sørensen, 2004] where a model of the WHR boiler is also presented.
The feed water system can be modelled using standard expressions for flow through valves and pressure delivered by pumps – see e.g. [Eastop and McConkey, 1993]. Also, the standard pressure atomising burner does not cause any modelling difficulties. However, we must also address a novel burner which instead of a conventional fan is equipped with a gas turbine. The gas turbine is among other parts constructed of a turbocharger. When constructing a model of this burner it is useful to look towards the automotive industry where especially the turbocharger has received much modelling attention – see e.g. [Amstutz and Guzzella, 1998; Jensen et al., 1991; Jung and Glover, 2003; Kolmanovsky and Moraal, 1999; Müller et al., 1998]. Also gas turbine theory is described in [Saravanamuttoo et al., 2001], and a model for stationary gas turbines can be found in [Sekhon et al., 2006]. In most works the flue gas is treated as an ideal gas for which the general physics can be found in e.g. [Serway and Beichner, 2000].

1.3.2 System analysis

It is important to analyse the properties of the system prior to setting up proper performance criteria, selecting control strategy and designing controllers. Many methods exist for evaluating control structure design – see e.g. [Maciejowski, 1989; Skogestad and Postlethwaite, 1996]. We shall use methods for finding a suitable input/output pairing and evaluating performance of decentralised controllers. Measures as the Relative Gain Array (RGA), [Bristol, 1966], and for 2×2 systems, Rijnsdorp's Interaction Measure (RIM), [Rijnsdorp, 1965], are popular analysis tools for linear systems. Both of these are frequency dependent tools which can be used for e.g. input/output pairing, evaluation of potential control difficulties and provision of information on sensitivity to certain types of uncertainty. Further, using these measures stability and performance under decentralised control can be addressed before doing an actual design.
Both the RGA and the RIM are frequency domain measures. However, time domain analysis is equivalently important, especially for nonlinear systems where frequency dependent tools are not suited. The book [Hirsch et al., 2004] on differential equations and dynamical systems along with the book [Lee, 2006] on differential manifold provide time domain tools for analysing linear and nonlinear systems – see also [Khalil, 2002]. These references also provide tools for analysing the existence of limit cycles in nonlinear systems.

1.3.3 Controller design

There are many methods for controlling MIMO (multiple input multiple output) processes such as the marine boiler. These span from classical decentralised control methods based on SISO linear process theory in combination with feedforward control to advanced nonlinear model-based MIMO controllers. As in many other industries the total marine boiler system is a large-scale process, and there is not one but many controllers implemented to take care of various tasks. These controllers are often implemented in a control hierarchy differentiated by the necessary update frequency of the controller and the complexity of the tasks.

Process control hierarchy

In Figure 1.2 a pyramid showing the industrial process control hierarchy is shown. This structure allows for handling of the increasing complexity in industrial processes. From the figure it can be seen that the closer we get to the process, the closer we get to the bottom of the pyramid.
The controllers at the bottom level handle e.g. flow and supply pressure control. The dynamics and actuators in these processes are fast, usually much faster than the dynamics seen at the middle level. Furthermore, the controllers used in these systems are usually SISO controllers with update times, T_s, specified in seconds or less, $T_s \sim \mathrm{s}$. The bottom level controllers are often combined with the middle level controllers in a

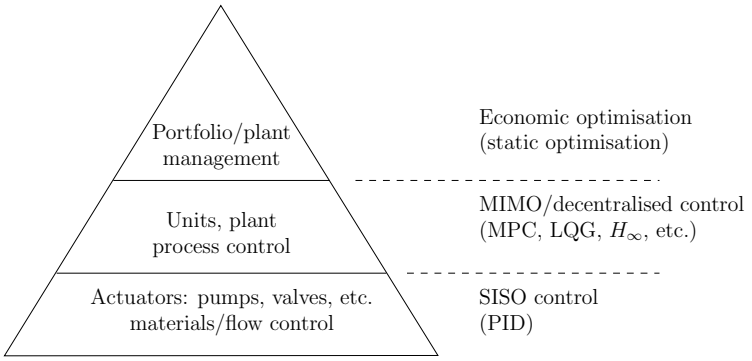

Figure 1.2: Illustration of the process control hierarchy as employed in the industry. The different levels seen from the bottom corresponds to task of increasing complexity and hence longer controller update times. Further, the models used for controller design at the bottom two levels are dynamic whereas the models used at the top level are often static.

cascade configuration. The models used in control designs at this level are dynamic. The controllers at this level often have the purpose of linearising gains, reducing input uncertainty and attenuating input disturbances.
The middle level controllers are the process controllers, e.g. the boiler pressure and water level controllers. These controllers are often more complex than at the lower level and the MIMO nature of the process is efficiently handled at this level. The update time at this level is in the range of minutes or less, $T_s \sim \mathrm{min}$. Also the models used for the controller designs are dynamic.
In relation to the marine boiler system the top level of the hierarchy could be seen as the overall ship-wide control, if such control existed. This could be overall ship efficiency optimisation. The update frequency of controllers at this level will usually be in the range of hours $T_s \sim \mathrm{h}$. Furthermore, the models used at this level are often static. The output of these controllers are future setpoints for the middle level controllers.
At both the top and middle levels it is often necessary to be able to handle constraints on process outputs, e.g. water level, pressure or NO_x concentration in the exhaust gas. In this thesis we will work on the bottom and middle levels of the hierarchy. Especially we will later address the model predictive controller (MPC) which is found at the middle level.

Control methods

See e.g. [Åström and Hägglund, 2006; Franklin et al., 1994, 1998; Haugen, 1994; Skogestad, 2003] for design and tuning rules for the PID controllers and feedforward elements for SISO processes. It is possible to take the cross couplings in MIMO processes into account while still allowing for a controller design based on SISO process

theory. This can be achieved by introducing a decoupling between the loops that interact, – see e.g. [Gagnon et al., 1998; Luyben, 1970; Wade, 1997]. Seen from the input to the decoupling element, the decoupling element plus the process represent a diagonal process. We will use a decoupling scheme to analyse the benefits of MIMO control.
Apart from the classical control strategies there are a number of advanced model-based control strategies relevant for control of the marine boiler. These are e.g. optimal control, robust control, nonlinear control and adaptive/self-tuning control.
There are many variants of optimal control, [Athans and Falb, 1966; Lee and Markus, 1967]. We will use both time-optimal control, [Lim, 1969; Sontag, 1998] and the linear quadratic Gaussian (LQG) control. Loop transfer recovery (LTR) is a method for robust tuning of LQG controllers. The LQG/LTR procedure can be found in [Doyle and Stein, 1981; Maciejowski, 1985, 1989; Saberi et al., 1993], which includes both the continuous time and discrete time case.
The robust controller addresses model uncertainty directly in the controller design and allows for designing controllers that stabilise a chosen family of plants and further provides robust performance, – see e.g. [Doyle et al., 1990; Dullerud and Paganini, 2000; Zhou et al., 1996]. Tools such as linear matrix inequalities (LMI), [Boyd et al., 1994], and semi-definite programming (SDP) allows for very complex robust controller designs and especially offers methods for multiobjective designs.
Nonlinear control is still a topic of much research and is a very broad topic, [Khalil, 2002], and also exists as versions of robust and optimal control. One especially attractive method is gain scheduling, which covers methods such as inverting the plant gain and combining multiple controllers into one controller by scheduling. The feed water system is an obvious plant to apply gain scheduling to as the plant gain can be inverted relatively easily.
Another class of control strategies relevant to the marine boiler plant is the auto-tuning controllers and the adaptive/self-tuning controllers. Strategies for automatic tuning of PID controllers are described in [Åström et al., 1993]. We here refer to the methods which consists of performing an experiment on the open or closed loop process and from these find a set of controller parameters to be implemented in the control system for future operation. Such a scheme would be rather straight forward to apply to the marine boiler system if local loops around the feed water and fuel supply had been closed. There are also methods that continuously adapt parameters to the plant – see e.g. [Åström and Wittenmark, 1989]. These are for instance adaptive and self-tuning control of which an example is presented in [Bitmead et al., 1990] using optimal control. These methods also include the iterative identification and control schemes such as presented in [Hjalmarsson, 2002; Van den Hof and Schrama, 1995; Zang et al., 1995]. Especially closed-loop identification techniques are of interest when using these methods, [Forssell and Ljung, 1999; van Donkelaar and Van den Hof, 1999; Zhu and Butoyi, 2002].
Many other control design methods exist, but especially one receives much attention in this thesis. We have the intention of designing a controller taking into account constraints on both inputs and outputs. Further, we are interested in minimising the variance

of water level and pressure variations which naturally leads to MPC.

Model predictive control

Model predictive control is a widely applied advanced control strategy for industrial applications [Qin and Badgwell, 1997, 2003]. In relation to boiler control, examples are documented in [Kothare et al., 2000; Lee et al., 2000; Rossiter et al., 2002]. MPC refers to the control algorithms that explicitly make use of a process model to predict future responses. The algorithm implementation is also known as receding horizon control. At each controller update the predictions are based on current measurements gathered from the plant. They are used to evaluate a performance function and an optimisation problem is solved to find the input sequence which optimises the predicted performance over a chosen horizon. Now the first input in the sequence is applied to the plant, and the same procedure is repeated at the next controller update.

Motivation The model used in the predictions can be both linear and nonlinear. In this thesis we will look at MPC using linear models and a special kind of nonlinear models called hybrid models, which we will treat later. For an overview of linear MPC see e.g. [Maciejowski, 2001; Rossiter, 2003]. MPC has a number of advantages over other advanced control strategies. First of all, as finding the optimal input consists of solving an optimisation problem, it is possible to incorporate constraints on both inputs, rate of change of inputs, outputs and internal state variables into the controller. This obviously means that even though we refer to it as linear MPC, the controller is not linear. The MPC controller is also pro-active, meaning that future trajectories of setpoints and disturbances can be handled in the control setup. Further, MPC naturally handles MIMO processes and has the advantages over linear controllers that it allows for moving the setpoints closer to the constraints without increasing the number of constraint violations.

The process control hierarchy In relation to the process control hierarchy discussed in the previous section, the MPC controller can be found at the middle level. The reason for this is mostly computational complexity and complexity of implementation, which means that it is difficult to apply MPC at the lower level where the SISO PID controllers are most popular. However, lately results have shown that even in the SISO case MPC should be considered over PID as the computational demands of the SISO MPC controller are similar to those of PID control, and further the MPC controller in general outperforms the PID controller regarding setpoint changes, disturbance rejection and constraint handling – see [Pannocchia et al., 2005].

Computational aspects The optimisation problem arising in linear MPC using a quadratic performance function is a convex quadratic programming problem. Such problems are the topic of [Boyd and Vandenberghe, 2004]. It is possible to exploit the struc-

ture of the MPC problem setup to arrive at very efficient solutions to the optimisation problem – see e.g. [Rao et al., 1998]. However, the complexity and the computational resources needed to implement the control law might be very high. Therefore, different methods to reduce the online computational load have been suggested. These are for instance the explicit MPC controller found by means of multi-parametric programming, [Bemporad et al., 2002c]. Another way to reduce the complexity is to reduce the number of free variables. This is done by introducing input blocking [Cagienard et al., 2007; Qin and Badgwell, 1997] which refers to the approach of constraining the input sequence to only change at certain times throughout the prediction horizon. We will use this approach in the marine boiler example. In [Ling et al., 2006], the authors suggest another method for reducing the online computational load. A multiplexed MPC scheme is presented where the MPC problem for each subsystem is solved sequentially. Work has also been done in the direction of decentralised MPC – see e.g. [Venkat, 2006]. The latter three methods for reducing online computational load are suboptimal solutions to the original problem whereas the explicit MPC controller is equivalent to the original controller.

Stability It is possible to construct an MPC controller with guaranteed stability at least for the nominal case [Mayne et al., 2000; Pannocchia and Rawlings, 2003; Rawlings and Muske, 1993]. In fact stability can be ensured even when using input blocking [Cagienard et al., 2007]. In particular, it is also possible to construct the MPC controller in such a way that it defines the constrained linear quadratic infinite horizon regulator (CLQR) – see e.g. [Chmielewski and Manousiouthakis, 1996; Grieder et al., 2004; Scokaert and Rawlings, 1998].

Output feedback and integral action It is worth noting that MPC assumes that the state vector of the plant can be measured. In order to achieve output feedback the MPC controller must be combined with a state observer as for instance the Kalman filter [Grewal and Andrews, 2001]. This means that the stability results referred to above will not hold in the output feedback situation. Different attempts have been made to fix this – see e.g. [Bernussou et al., 2005; Kothare et al., 1996].
It is also through the state observer that integral action in the MPC controller is normally incorporated, [Muske and Rawlings, 1993]. When the model is not identical to the plant it is not enough to use a model formulation with input changes (integrator at the input), which is why integrating disturbances put in the direction of e.g. the inputs or outputs are estimated to explain the difference between model and plant.

Controller tuning Tuning of the MPC controller then becomes a matter of both tuning the gains and horizon in the performance function of the controller and for instance the covariances of the state and measurement noise in a Kalman filter. Depending on the problem size, this leaves quite a lot of parameters to be chosen. To aid this procedure

there are methods such as the autocovariance least-squares method for estimating noise covariances [Odelson et al., 2006a,b]. Another method which we will use on the marine boiler example is the loop transfer recovery (LTR) method (the LQG/LTR approach). Notes on LTR can be found in e.g. [Doyle and Stein, 1981; Maciejowski, 1985, 2001, 1989; Saberi et al., 1993]. This approach is for linear controllers, however, for an example of application to MPC, see [Rowe and Maciejowski, 1999].

Robustness and nonlinearity Work has also been carried out in the area of robust model predictive control. However, this direction is still in the development phase and not yet suited for industrial applications. Two sources of uncertainty are dealt with in the robust predictive control framework: model uncertainty and uncertainty with respect to disturbances – see e.g. [Chisci et al., 2001; Gaulart and Kerrigan, 2006; Kothare et al., 1996; Smith, 2006].
As mentioned earlier this thesis deals with MPC using linear models. However, such schemes only work well when the nonlinear system to be controlled is working around an operating point. When the operating point is changed from the nominal situation, the controller might not perform well due to model mismatch. One way of tackling this by still using linear models is to switch among a set of these according to the current plant state. Examples of this can be found in e.g. [Kothare et al., 2000; Pedret et al., 2000] where the latter refers to this method as model-varying predictive control. This method has not been used in this thesis but might become relevant in the future.
There exists a number of tools to assist the engineer in performing design, analysis and development of his MPC controller. The ones that have been used in this thesis, apart from the authors own algorithms, are the multi-parametric toolbox (MPT-toolbox), [Kvasnica et al., 2004] and the MPC-toolbox from the The MathWorks , [Bemporad et al., 2006], which are both software packages for MATLAB® .

Hybrid/switching control

In many industrial processes, e.g. the thermodynamical and chemical processes a mixture of on/off valves and heating elements might be present. When describing such systems they fall into the class of hybrid systems. The marine boiler is such a system as both the burner and feed water valve can be operated continuously down to some minimum level whereafter the output from these systems must be switched off to reduce the load further. This means that when operated at low load some switching control must take place. Traditional methods for controlling such systems are hysteresis control and pulse width modulation (PWM). However, both these methods have a number of shortcomings discussed in [Solberg et al., 2008a]. For the feed water system these shortcomings are not crucial and here we shall use PWM. However, for the burner system things are more complicated, and in this thesis we will investigate how to optimally control processes which require switching control.
A special property of the systems with discrete inputs is that in some cases the optimal

state trajectory does not converge to an equilibrium point but to a limit cycle. Such a case arise in the marine boiler example.
Optimal control of hybrid systems is discussed in e.g. [Bemporad et al., 2002a,b; Egerstedt et al., 2006; Giua et al., 2001a,b; Hedlund and Rantzer, 1999; Riedinger et al., 1999; Seatzu et al., 2006; Verriest et al., 2005; Xuping and Antsaklis, 2003]. Many authors have focused on switched linear and affine autonomous systems e.g. [Giua et al., 2001b; Seatzu et al., 2006; Xuping and Antsaklis, 2003]. In particular, it is noticed that when the switching sequence is predetermined, the optimal control reduces to a state feedback. However, the focus is restricted to a finite number of switches. In [Giua et al., 2001a], the stability of these systems when the number of switches goes to infinity, is studied. However, this is for stable dynamics and with no switching cost.
We will also make use of terminology from [Frazzoli, 2001; Frazzoli et al., 1999] presenting robust motion planing for autonomous vehicles.
However, to solve our problem we will move in the direction of MPC and time-optimal control. In the MPC framework there are tools such as the Mixed Logic Dynamical (MLD) modelling framework, which in combination with MPC is an approach which allows standard tools to be applied to obtain an optimising control law – see e.g. [Bemporad and Morari, 1999; Torrisi and Bemporad, 2004]. In [Mignone, 2002; Tsuda et al., 2000], approaches to handle when the states converge to a limit cycle are presented. Furthermore, a simulation with the MLD framework on an industrial process is presented in [Larsen et al., 2005]. A few offline techniques based on multi-parametric programming and dynamic programming have been suggested in the literature for defining the explicit control law – see e.g. [Bemporad et al., 2000; Borrelli et al., 2005]. However, these methods are most suitable for relatively small systems using a relatively short prediction horizon.
In [Sarabia et al., 2005], another approach to MPC of hybrid systems is presented. This approach uses a nonlinear process model, and instead of optimising over both continuous and discrete input variables over the control horizon, the optimisation is performed over continuous variables and switching times of the discrete variables. In this thesis we will show shortcomings of many of the above listed methods and suggest a new approach for controlling systems with discrete decision variables.

1.4 Vision for the Marine Boiler Controller

Today all installed controllers on marine boiler plants are adjusted during commissioning and no model-based approaches are employed. This means that each unit of the plant is adjusted independently, and overall plant performance is rather arbitrary and highly dependent on time schedule and the skill of the assigned service engineer.
This section expresses the author's opinion on what parts the future marine boiler control system should consist of. To a large extent many of these visions are made possible by the control system currently under development at AI. The vision is to have a marine

boiler control concept, which includes automatic parameter identification of a process model to be used for actuator and boiler controller design. This system must be capable of allowing still smaller boiler geometry, meaning that the autonomy of the plant must not be at the expense of water level and pressure performance. A complete control system must also include fault detection and accommodation algorithms.
For control purposes, the boiler plant should be divided into modules representing e.g. feed water system, burner and boiler. Each module has its own controller and the overall controller has a hierarchy of control loops combined in a cascade configuration. (This is of course a somewhat oversimplified picture as each module e.g. the burner and oil system will contain both a loop for stabilising the oil pressure, heating the oil and injecting the correct fuel amount to the furnace.) Such a configuration has many advantages. Regarding control, inner loops on actuator systems are in general known in the process industry to linearise valve gains and attenuate disturbances at the plant input allowing an outer loop to treat it as a linear system. However, a much more transparent advantage of such a strategy is the flexibility it allows in combining modules. Of course such ability requires the aforementioned automatic parameter identification to be implemented in order for outer loops to base their control actions on the correct process model. When changes are made to the boiler plant, only the controller which is assigned to the module that is affected needs to be updated. Simulink® and Real-Time Workshop® supports automatic code generation for subsystems in a plant/controller diagram.
It should then be possible to create a marine boiler control library containing models of each process submodule to allow testing in a simulation environment. Apart from the process models such library must contain controllers for each module. These controllers should be general enough to allow simple configuration to adopt the controller to a specific element within its class. E.g. boilers in the same family can use the same control structure. The software tools for implementing the model and control library could be e.g. MATLAB® /Simulink® in combination with Modelica [Modelica, 2007]. The latter supports object-oriented modelling of thermodynamical plants and can easily interface with Simulink® . See e.g. [Casella and Leva, 2003; Eborn and Åström, 2000] for Modelica examples of boiler modelling and power plant library design.
Regarding the control strategy, the scheme shown in Figure 1.3 supports the discussion above and is the scheme used in this project. The inner loops around the actuators are not shown in details in Figure 1.3. This scheme only applies to non-load sharing boiler operation.
There are two new things to this figure; one is the green box including setpoint control and burner decision control, the other is the external input. The external input covers possible signals about load changes from the ship engine or cargo pumps. Such signals can be used to improve the water level control in a feedforward and can be made available. The setpoint optimisation is meant to use these signals together with possible estimates of other disturbances acting on the boiler in order to calculate setpoints for the water level, which are safe. Here safe means that the water level can be held within

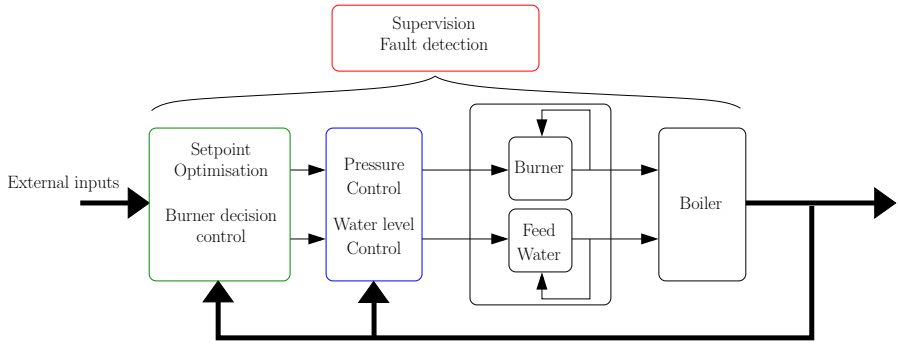

Figure 1.3: Control strategy for marine boiler plant.

the upper and lower constraints for all possible future disturbances. The burner decision control is a matter of deciding whether the burner should be turned off or turned on. This is important when the steam demand is smaller than that corresponding to the minimum burner load. More information on the function of the green box is given in [Solberg et al., 2007a] and [Solberg et al., 2008b].
The vision described above assumes that the boiler control system is separated from the control systems for ship propulsion and steam consuming units as is the case today. However, integrating control of all these units in a ship-wide control system can allow for much more efficient control resembling that of modern power plants. As an example this will allow for the boiler steam demand to be changed in an optimal way corresponding to the boiler dynamics. However, introduction of such systems is still in the early stages and requires many of the unit suppliers to cooperate.

1.4.1 Project objectives

In this project focus has been on the introduction of model-based control to the marine boilers. In particular, the goal has been to find systematic design procedures limiting the current need for time consuming manual controller tuning.
The main objective of the project is to develop control strategies for the oil-fired one-pass smoke tube marine boiler which allows for reduction of the physical boiler dimensions. Model predictive control (MPC) was thought as the solution to the control problem as it naturally incorporates constraints on inputs and outputs and gives large degrees of freedom in choosing the performance function to be optimised. Further, MPC has proved the most successful advanced control strategy in the process industry, [Qin and Badgwell, 2003]. Especially in the chemical and petrol industry, large improvements using MPC in replacement of classical control are reported, resulting in

remarkably increased production rates.

1.5 Outline of the Thesis

This thesis is based on a collection of publications. The thesis is divided into two parts. The first part is an introduction and summary of the contributions, and the second part presents the related publications. The organisation is as follows:
Part 1: Chapter 2 presents a description of the marine boiler plant together with control challenges hereof, and a few specific details of the test boiler are given. Chapter 3 gives a summary of the contributions. In Chapter 4, conclusions and perspectives are presented.
Part 2: In this part the eight publications made during the project are presented in the following order:

A [Solberg et al., 2008c]. Brian Solberg, Palle Andersen and Jakob Stoustrup. Modelling and control of a turbocharged burner unit. ECOS 2008 Conference, Kraków, Poland, 2008.

B [Solberg et al., 2005b]. Brian Solberg, Claus M. S. Karstensen, Palle Andersen, Tom S. Pedersen and Poul U. Hvistendahl. Model-based control of a bottom fired marine boiler. In P. Horacek, editor, 16th IFAC World Congress, Prague, Czech Republic, 2005.

C [Solberg et al., 2007b]. Brian Solberg, Claus M. S. Karstensen and Palle Andersen. Control properties of bottom fired marine boilers. Energy, 2007.
(Journal version of the conference paper [Solberg et al., 2005a])

D [Solberg et al., 2007a]. Brian Solberg, Palle Andersen and Jakob Stoustrup. Advanced water level control in a one-pass smoke tube marine boiler. Technical report, Department of Electronic Systems, Aalborg University, Aalborg, Denmark, 2007.

E [Solberg et al., 2008d]. Brian Solberg, Palle Andersen and Jakob Stoustrup. The one-pass smoke tube marine boiler - limits of performance. ECOS 2008 Conference, Kraków, Poland, 2008.

F [Solberg et al., 2008a]. Brian Solberg, Palle Andersen, Jan M. Maciejowski and Jakob Stoustrup. Hybrid model predictive control applied to switching control of burner load for a compact marine boiler design. In D. D. Cho, editor, 17th IFAC World Congress, Seoul, Korea, 2008.

G [Solberg et al., 2008b]. Brian Solberg, Palle Andersen, Jan M. Maciejowski and Jakob Stoustrup. Optimal switching control of burner setting for a compact marine boiler design. Submitted March 2008 for journal publication, 2008.

H [Solberg et al., 2008e]. Brian Solberg, Palle Andersen and Jakob Stoustrup. Optimal switching strategy for systems with discrete inputs using a discontinuous cost functional. Submitted March 2008 for publication in International Journal of Control, 2008.

2. The Marine Boiler Plant

The purpose of this chapter is to describe in detail the marine boiler plant introduced in Section 1.2. Both the environment in which the boiler operates and the load characteristics are presented in order to be able to formulate requirements for the marine boiler control system. Also different control challenges special to the marine boiler are discussed. In the end of the chapter the plant used during tests in the project will be described shortly.

2.1 Operating Conditions

2.1.1 Environment

In this section we will look at the environment in which the boilers are operating. Apart from the natural rolling of the ship due to high sea there are a few notable characteristics about the environment.

Oil-fired boiler

The oil-fired boiler is placed in the engine room of the ship. The air for the burner is taken from inside the engine room. The temperature of this air varies depending on the outside temperature. In the extremes some plants are designed to operate with air temperatures ranging from 0-35°C.
As the ventilation system in the engine room operates continuously, the pressure in the engine room can vary. This influences the fan and hence the combustion. The ventilation is to ensure air for the burner and engine without creating too much vacuum in the engine room.

WHR boiler

The air for the engine is taken from inside the engine room. However, as mentioned in the previous section the temperature of this air can vary depending on the outside temperature. This causes the engine efficiency to vary as well. For this reason the

heat absorbed in the WHR boiler for the same engine load depends on the outside temperature (e.g. Arctic waters or the tropics). A typical WHR boiler for a $4000\frac{\text{kg}}{\text{h}}$ oil-fired boiler has a steam production in the range of $500 - 4000\frac{\text{kg}}{\text{h}}$ of steam.

2.1.2 Operational situation

There is a collection of different operational situations for the marine boiler plant. This gives a number of different states the system can be in. These states are sketched below:

OF \ WHR	off	on	start-up	shutdown
off	X_{11}	X_{12}	X_{13}	X_{14}
on	X_{21}	X_{22}	X_{23}	X_{24}
start-up	X_{31}	X_{32}	X_{33}	X_{34}
shutdown	X_{41}	X_{42}	X_{43}	X_{44}

where OF means oil-fired boiler. The WHR boiler produces steam as long as the engine is running, and start-up and shutdown of this boiler are completely dependent on the engine operating condition. When to start or stop the oil-fired boiler is currently controlled by monitoring the pressure. On/off control of the oil-fired boiler is necessary in situations where the steam consumption is just above the capacity of the WHR boiler, or if the WHR boiler is off when the steam consumption is lower than the minimum capacity of the burner.

2.2 Water-steam Circuit

Here we look at the water-steam circuit for the marine boiler configuration: one oil-fired boiler and one WHR boiler. The purpose is to introduce the most important terminology used in the thesis and to make the reader more familiar with marine boiler plants. In Figure 2.1 a principle diagram of the water-steam circuit is shown. Only the valves important for the present work are presented, and none of the redundant systems have been displayed.
The numbers in the figure have the following interpretation:

1 Oil-fired boiler.

2 WHR boiler.

3 Steam dump condenser.

4 Hot well. This works as the open feed water tank and further collects the condensate returned from the consumer or dumped by the control system. The water in the hot well is kept at a temperature $> 80°\text{C}$ in order to increase boiler efficiency

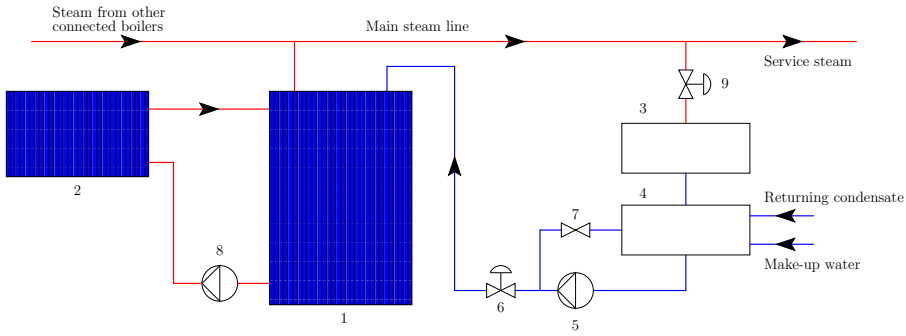

Figure 2.1: Principle diagram of marine boiler plant water-steam circuit.

and reduce oxygen content [Pedersen et al., 2003]. This is handled by blowing steam into the water.

5 Feed water pump. Usually this is designed to be able to supply a flow of 1.25-1.50 times the maximum steam production.

6 Feed water control valve.

7 Feed water return valve. The feed water pump is running at constant speed. The return valve is installed to ensure that the pump will not be pumping against a closed valve which would cause the energy delivered by the pump to heat up the feed water which in the end could damage the pump. Also this valve can change the characteristic of the pressure just after the pump, which has similar behaviour as changing the pump speed.

8 Circulation pump. The pump has a design capacity of 5-7 times the maximum steam production depending on which engine operating load it is designed for. The reason for keeping such high circulation numbers is to prevent a too high steam quality or super heating in the tubes. Especially in the water tube WHR boilers there is a risk of starting a soot fire caused by an engine spark if there is insufficient cooling of the water tubes. This can damage the tubes.

The distribution of water and steam in the water tube boilers is expected to look like shown in Figure 2.2. The z variable describes the distance from the entry to the WHR boiler to an arbitrary point in the WHR boiler. It can be seen that for high steam qualities a water film is expected to form on the pipes. A high circulation number is needed to avoid braking this film.

9 Steam dump valve. On plants equipped with both the oil-fired boiler and the WHR boiler this valve is controllable.

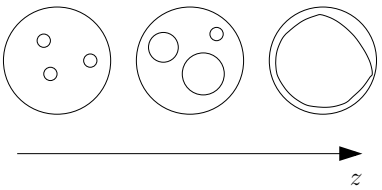

Figure 2.2: Three cross sections of the water tubes in the WHR boiler. z is distance from the entry to the boiler.

2.3 The Water Level

It is important to keep both pressure and water level in the boilers close to their set-points. Especially the water level is difficult to control. In this section we will explain why.
For safety reasons it is necessary to keep the water level above a certain level in order to have sufficient cooling of the metal parts, and to ensure a high steam quality it is also important to keep the water level below a certain level. The lower level is indicated by a low water level (LWL) alarm and the high level is indicated by a high water level (HWL) alarm. In general, a normal water level (NWL) is defined and used as setpoint in the level controller. The difficulties in keeping the level around this setpoint arise from what is known as the shrink-and-swell phenomenon. This phenomenon introduces an initial inverse response on the water level seen from both the steam flow and engine load disturbance but also from the feed water flow and burner load. This inverse response refers to the process control term non-minimum phase and basically means that the process variable considered responds to an input by first moving in the opposite direction before it moves in the long term direction. Details are listed below:

- Engine load changes:
  - Swell: Occurs under start of the engine and under positive load changes. When the power delivered to the WHR boiler increases the mass fraction of steam in the boiler increases. At low pressure, steam occupies much more space than water, which leads to large amounts of water being pushed into the oil-fired boiler, and the water level increases.
  - Shrink: Occurs under engine shutdown and negative load changes. When the power delivered to the WHR boiler decreases the mass fraction of steam decreases. This allows for more water in the WHR boiler, which is pumped from the oil-fired boiler in which the water level decreases.
- Steam load changes:

  - Swell: The phenomenon is caused by the distribution of steam bubbles below the water surface in the boiling process. When the steam flow is increased the pressure drops instantly. This causes the bubbles below the water surface to expand and the boiling point to decrease creating more bubbles. As a consequence the water level will apparently rise.
  - Shrink: Opposite of swell.

- Feed water flow changes:
  - Swell: Opposite of shrink.
  - Shrink: The phenomenon is again caused by the steam bubbles under the water surface. The feed water is cooler than the saturation temperature in the boiler. When the feed water flow is increased the cooler water causes steam bubbles below the water surface to condensate as energy is required to get the system in thermal equilibrium. As water takes up less space than steam this causes the water level to drop.

- Burner load changes:
  - Swell: Increasing the firing rate has much the same consequences as engine load changes. The increase in firing rate causes vaporisation of water beneath the water surface to increase resulting in an increased volume of steam in the water causing a raise in the water level.
  - Shrink: Opposite of swell.

The distances from LWL alarm to NWL and from NWL to HWL alarm are calculated based on the water volume in the WHR transferred from the oil-fired boiler in case of shrink and to the oil-fired boiler in case of swell. In case no WHR boiler is present more heuristic measures are imposed. In some cases it is found that the boiler must be taller than the maximum allowed. Further, some shipyards have problems handling the tall boilers. It is expected that by introducing advanced control, less conservative estimates of LWL alarm and HWL alarm levels can be generated.
Apart from the shrink-and-swell phenomenon, the variance on the water level makes it difficult to measure it and in turn difficult to control. It has been observed that the water level variance is correlated with the steam load. Also the water level measurement used in this project is based on one measurement placed in one side of the boiler, which means that it only gives information about a very small surface area. It is known from studying the water level through a glass in the drum that even though the level measurement does not vary a lot the water level is very chaotic.
For the one-pass smoke tube boiler concerned in this project, observations has also shown that the water level in the boiler rises from the sides towards the middle of the boiler. The level has the shape of a cone. This phenomenon is expected to be caused by the strong heating in the center of the boiler along the flue gas pipes, creating many

steam bubbles in the water which raises the surface. See Figure 2.3. Occasionally this cone seems to collapse creating a wave on the surface. In summary, one must keep in mind that when speaking of controlling the water level it is the number returned from a water level measurement that is controlled and not the actual chaotic water surface.

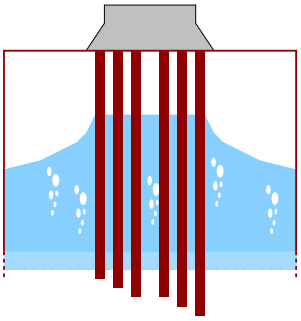

Figure 2.3: Water surface in one-pass smoke tube boiler. Note that the surface is rising towards the flue gas pipes.

2.4 Consumer and Load Characteristics

The steam consumers onboard ships are mostly represented by ruthless on/off operation of valves. Even on tank ships the controllers for the cargo pumps, driven by steam turbines, react very fast compared to the marine boiler dynamics. However, generally there is a mixture of load situations listed below:

- Ramps: turbine units changing load will generate a ramp in the steam flow disturbance.
- Steps: on/off switching of e.g. heating sections for cargo or fuel.

Regarding the step disturbances they are usually in the range from 10-30$\%$, however, there is no onboard boiler equipment which prevents larger steps from occurring. However, at this point, by informing the consumer, AI tries to limit the load changes to about $10\frac{\%}{\text{min}}$ to avoid tripping[1] the boiler.
The steam load is interpreted as a disturbance in the boiler control system. The reason is that the consumer has full authority of the main steam line. This means that in theory, if sufficient firing is sustained, the consumer can empty the boiler for steam/water if the consumption is high enough.
The type of disturbance and the frequency with which the disturbance occurs differ from one ship type to another. However, also within the same ship type the disturbance

[1]Tripping here refers to the forced burner shutdown caused by activating the water level alarms.

characteristics vary. This can for instance be due to changing cargo or the environment in which the ship is sailing; tropical versus arctic waters where different heat consumptions are required. Real life measurement of the load pattern is not available. In fact currently this pattern is not well known.
Some applications require very large amounts of steam while others do not. Oil-fired boilers that can produce more than $30000\frac{\mathrm{kg}}{\mathrm{h}}$ are used to drive cargo pumps. In these applications usually only relatively small WHR boilers, compared to the volume of the oil-fired boiler, are used. For this reason the shrink-and-swell phenomenon caused by engine load changes is less pronounced. However, the boiler family treated in this project consists of relatively small boilers capable of delivering steam flows in the range from 1200-8000$\frac{\mathrm{kg}}{\mathrm{h}}$. In these boilers the disturbance from the WHR boiler plays a large role.

2.5 Control System Requirements

The requirements for the control system can be split into three types; Those requested by the consumers, those imposed by the boiler construction material and those demanded by the classification societies and authorities. The latter two are mainly safety and environmental concerns.
Requirements imposed by construction material mainly concerns limitations in pressure and temperature gradients in the steel of the boiler drum. These requirements limits the speed at which the boiler becomes available for steam production. Maximum pressure gradients are $\approx 1\frac{\mathrm{bar}}{\mathrm{min}}$ depending on the boiler geometry. In large boilers operating at high pressures delivering steam for turbines, large changes in the steam demand can occur causing the pressure to drop several bars making these gradient limitations important during normal operation as well. However, for the small boilers considered in this project this is usually not a problem.
The most important requirement set by the classification societies for the control system is a lower bound on the water level. The flue gas pipes must be under water up to the point at which the flue gas drops below $600^{\circ}\mathrm{C}$ to avoid too high temperatures in the steel structure. Of course this bound must in any case be somewhat conservative as it is at a constant level, whereas the point would in reality change with the load. The boiler is equipped with a LWL alarm to indicate when the water level is within a certain range from this point (typically 45-60mm). This limit the allowable fluctuations on the water level.
Large penalties are often assigned by authorities to ship owners if the smoke coming out of the stacks is too harmful for the environment. This makes requirements on the burner control, which must keep clean combustion at all times. This is a matter of keeping a proper ratio between the fuel and air flow supplied to the combustion. The requirements set by the authorities are different from harbour to harbour. However, keeping the oxygen level in the exhaust gas above 3% is enough to ensure a minimum

of polluting gasses leaving the stacks. Keeping the oxygen level low also has the benefit of improving combustion performance and hence increasing boiler plant efficiency.

2.5.1 Consumer

Of course the requirements for the boiler output (steam flow and pressure) depend on the type of application which the steam is to be used for. The most stringent requirements occur when the steam is to be used to drive a turbine. In this case the turbine efficiency is very dependent on the steam temperature and further wet steam can damage the turbine blades. However, the requirements are less stringent in the applications in which the one-pass smoke tube boiler is used.
The consumer requirements fall into three categories:

- Plant stability: The capability of the plant to supply steam at a predefined temperature/pressure to the consumer when in operation. This is mostly a matter of correct sizing of the actuators. The consumer also plays an important role when it comes to plant stability. The reason is that the steam flow disturbance is completely controlled by the consumer as mentioned in Section 2.4. This means that he can by choice of the disturbance profile cause tripping of the boiler if this profile does not comply with the plant design. To avoid tripping the boiler is again a matter of proper water level control. Basically this means that the control system has to expect the worst from the consumer which is frequent, large steps in the steam flow.

- Output variance: When purchasing a new boiler the consumer normally only specifies a certain steam flow capacity at a certain pressure. For this reason it is difficult to set up requirements for the control system regarding the output variance. However, the following can be observed: the reason why the consumer wants a constant pressure is that this implies a constant temperature (i.e. saturation temperature), and all heat consuming applications and pipe systems are designed for saturated steam pressure. Especially heat exchangers require constant pressure as industrial processes often require a constant temperature.

- Steam quality: Water drops in the steam should be avoided in general. The reason is that water from the drum can carry salts and oil into the steam supply line damaging the pipe system. Further, water drops at high velocity can hit the pipe walls in pipe bends causing wear on the pipeline. Keeping high steam quality is a matter of appropriate water level control. The higher the water level, the higher the risk of carrying water drops into the steam supply line. However, a new mechanical installation above the steam space in the boiler drum has reduced this dependency. In the boilers treated in this project the matter of keeping water drops from entering the steam outlet can be formulated as a hard water level constraint. If this constraint is exceeded water will get into the steam supply

line. This constraint is indicated with the HWL alarm activated before the hard constraint is exceeded.

One natural way to evaluate the performance of the boiler system seen from a consumer's point of view would be to look at the response from a step in the steam valve to produced steam flow. In this way, classical measurements such as rise time, settling time and overshoot can be evaluated. However, no such specifications for this variable are available but could be defined in collaboration with AI customers.

2.5.2 Controlled variables

In summary, the controlled variables are pressure, water level in the drum and oxygen percentage in the exhaust gas. These variables must be kept approximately constant for all potential disturbance profiles.

2.5.3 Boiler types

It is desirable that the developed control algorithms are generic in such a way that they can be applied to other AI boiler types than the one-pass smoke tube boiler. AI has announced that they do not have any problems controlling the water level in the stand-alone oil-fired one-pass smoke tube boiler. Even so, the small boilers serve as good test boilers because large boilers are difficult to access. Further, it is assumed that theory developed for these small boilers can be used for the larger boilers without large modifications.
Therefore, it is assumed that the results presented in this thesis can be extended to a wider use on other boiler families in AI's product range. Of particular interest here is the large drum boilers that produce steam to drive steam turbines. In these boilers there is a much higher demand for good pressure performance.

2.6 Control Challenges

Having introduced some of the basics regarding the marine boiler plant and control system requirements, attention is now directed towards control challenges present for the marine boiler. Below is a list of properties of the marine boiler system which complicate drum pressure and water level regulation.

- *Actuator nonlinearities*. Both the feed water system and the burner are complicated systems consisting of numerous valves, pipes and pumps. They are difficult to describe yet they still have a large effect on the achievable controller performance if no special attention is given to these in the controller design.

- *Actuator saturation* (integrator windup). Obviously both oil flow to the burner and feed water flow are limited. This introduces further nonlinearities at the

plant input. When the designed controller has integral action, special precautions must be taken.

- *Discontinuous input flows*. Both the burner and the feed water system are characterised by having discontinuities in the delivered output. Usually continuous operation of the feed water valve is reliable down to an opening degree of 10%; from here to fully closed the valve position is unreliable. To overcome this problem the valve might be operated in on/off mode for low openings. As the burner turndown ratio[2] cannot be infinite the burner has to be operated in on/off mode for low steam consumptions.

- *High disturbance bandwidth*. The steam flow disturbance instantly affects the steam pressure and as mentioned in Section 2.3 also the water level, creating the shrink-and-swell phenomenon. The marine boiler control system receives no prior information about the steam load changes which makes this disturbance difficult to handle and requires frequent updates in the monitoring of the steam pressure to be able to respond fast to the disturbance for good control performance.

- *Shrink-and-swell*. When present in the response from control input to control variable it limits the achievable performance using single input single output (SISO) strategies as it introduces a non-minimum phase zero. However, this zero from feed water to water level is not pronounced in the one-pass smoke tube boiler. The shrink-and-swell caused by engine load changes was previously described and has a large affect on the water level.

- *Measurement noise*. Here we refer to the water level measurement. As mentioned in Section 2.3 the water surface is rather chaotic causing some measurement techniques to deliver a signal subject to noise. This makes it difficult to obtain a high bandwidth of the closed loop system.

As can be seen, the factors contributing to complication of the boiler control fall into two groups; One group is concerned with the supply systems and the actuators, and the other group is concerned with disturbances and noise. The reason why plant nonlinearities are not mentioned is that in the boiler family addressed in this project these are not pronounced in the frequency band around the desired crossover frequency [Solberg et al., 2007b].
The largest challenge is to improve the current water level control in such a way that the boiler geometry can be minimised (by reducing the necessary distance between LWL alarm and HWL alarm – see Section 2.3) without compromising steam quality and steam output. Improved level control further makes it possible to increase efficiency of existing boilers by moving the level setpoint closer to the HWL alarm level. It is

[2]Turndown ratio is defined as the ratio between the maximum and minimum possible fuel flow which results in an acceptable burner performance during boiler operation.

expected that to improve level control, introduction of advanced control methods is required. The controller must take into account the complications discussed above.
There is also a large challenge in making the control system more autonomous. This concerns auto tuning of the control system and reliable fault detection and accommodation. The focus in this project is on the water level and pressure control.

2.6.1 Time-varying plant dynamics

Due to sooting of the heating surfaces in the boilers the heat transfer coefficients will change during the boiler lifetime. The sooting also changes the equlibrium to withhold a certain steam demand, and there is a risk of soot fires. The soot can be removed again using soot blowers. Also a stone layer can build up on the heating surface on the water side if the feed water is not properly treated and has too many salts in it, which when the water evaporates settle on the heating surface as stones. This highly increases the temperature in the heating surface and should be avoided. If the feed water should contain small amounts of oil this can burn onto the heating surface and create an insulating layer just as with the stone layer. Both the salt and the oil content in the feed water is monitored on line to avoid damaging the heating surface. Special valve systems are installed to remove the oil and other substances from the drum water.
Wear on e.g. valves will also cause the dynamics and gains in the actuator systems to change over time.

2.7 Test Plant

The test plant available during this project was a full-scale MISSION^{TM} OB marine boiler situated in AI's test centre. We will only give a few details about the MISSION^{TM} OB plant. The boiler is connected to AI's new control system, which can be used both for data acquisition and plant control. Besides the standard equipment, the boiler is equipped with additional sensors used for test purposes only.
The boiler is an oil-fired one-pass smoke tube boiler capable of delivering $1800\frac{\mathrm{kg}}{\mathrm{h}}$ of steam at $8\mathrm{bar}$ when equipped with the current burner. A drawing of this boiler principle is shown in Figure 1.1. The water-steam circuit for the test plant is similar to the one illustrated in Figure 2.1 without the WHR boiler. Further, all steam is dumped and only one test boiler is operating on the main steam line at a time.

2.7.1 Sensors and actuators

The actuators on the boiler are the feed water valve and the return valve in the oil system controlling how much oil is fed to the atomiser. The principle of the feed water system was shown in Figure 2.1. It is capable of delivering a water flow of 0-$2100\frac{\mathrm{kg}}{\mathrm{h}}$.

The oil system is a bit more complicated, and we will not show any diagram hereof. The burner is a pressure atomising burner. The specific burner on the test boiler has a relatively large turndown ratio of 1:5.7. At fuel flows below the minimum allowable fuel flow there is not enough pressure to allow for proper atomising. In such case the combustion is incomplete which leads to more pollution, poor utilisation of the fuel energy, risk of carbon deposits in the furnace and flue gas pipes. In such case, the combustion air flow could be increased giving a higher excess air number, but at the risk of cooling the flame which also gives poor combustion, more CO_2 and NO_x emissions and less efficiency.
The air flow supplied to the combustion in the test boiler is adjusted by a damper after the fresh air fan. The amount of air is controlled electronically and determined as a function of the current wanted fuel flow. This function is not treated in the present work. The maximum fuel flow is $154\frac{\mathrm{kg}}{\mathrm{h}}$ and the minimum fuel flow is $27\frac{\mathrm{kg}}{\mathrm{h}}$.
The sensors on the boiler for measuring pressure and temperature are all standard equipment and so is the water level sensor. However, the water level sensor is interesting as we will see that it limits the speed of the water level feedback loop. It is based on the capacitive measurement principle where an electrode rod is submerged in the water acting as one plate of a capacitor, and the boiler drum walls act as the other plate. The water acts as the dielectric. When the water level changes, the capacitor changes as the dielectric between the plates changes. This change is detected and converted into an output signal. The change in capacitance is proportional to the change in level. Although accurate and placed in a protection tube such, measurement is very sensitive. This also means that the chaotic behaviour of the boiling water level is detected by this device. As the noise on the water level has no specific frequency this makes it difficult to detect whether changes of the water level are due to changes caused by the shrink-and-swell phenomenon or simple bubbles breaking loose from the water surface, or the raised surface towards the flue gas pipes collapsing creating wave motions on the surface. Other devices for measuring liquid surfaces are available also for pressurised vessels containing boiling substances. However, these have not been available throughout the project.

3. Summary of Contributions

This chapter summarises the contributions made in this project. Along with this summary, the challenges in marine boiler control from Section 2.6 are addressed. The purpose is to describe which of these challenges have been solved and how. The chapter is organised in sections describing supply system modelling and control, marine boiler modelling and control and hybrid systems control together with its application to marine boiler burner setting control.

3.1 Supply System Modelling and Control

This section is concerned with modelling and control of the supply systems for the marine boiler. These are the feed water system and the burner. We will see that the results presented here solve the first challenge from Section 2.6 regarding *Actuator nonlinearities*. This is done by designing local compensations for these systems linearising the system gains and allowing the reference to the feed water flow and fuel flow to be used as manipulated variables in the outer controller. Further, these inner loops can easily be designed faster than the outer loop.

3.1.1 Feed water system

The modelling and control of the feed water system was presented in [Solberg et al., 2008d]. The controller adjusts the feed water valve stroke to make the feed water flow equal to the reference. A diagram of the feed water system is shown in Figure 3.1.
The total water-steam circuit was shown in Figure 2.1. p_a is the pressure in the open feed water tank which is equal to the ambient pressure, p_p is the pressure delivered by the pump, p_s is the back pressure seen from the feed water system which is equal to the pressure in the boiler. $\dot{m}_{fw}$ is the feed water flow to the boiler through the controllable feed water valve, and $\dot{m}_r$ is the return flow to the feed water tank through the manually adjustable valve.
An explicit expression for the feed water flow as function of the valve stroke, z_{fw}, and

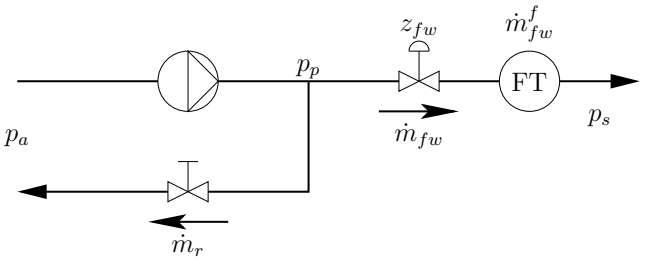

Figure 3.1: Diagram of feed water system. Water pumped from the feed water tank is injected into the boiler in the forward path, and in the return path the water is led back to the feed water tank.

boiler pressure was found as

$$\dot{m}_{fw} = g(z_{fw}, k_r, p_s) = k_f f(z_{fw}) \sqrt{\Delta p_p(z_{fw}, k_r, p_s) + p_a - p_s} \tag{3.1}$$

where Δp_p is given as the solution to a quadratic equation:

$$\Delta p_p = \frac{-a_1(z_{fw}, k_r, p_s) - \sqrt{a_1(z_{fw}, k_r, p_s)^2 - 4a_2(z_{fw}, k_r)a_0(z_{fw}, p_s)}}{2a_2(z_{fw}, k_r)} \tag{3.2}$$

k_f and k_r are the valve gains of the forward control valve and the return valve respectively. a_2, a_1 and a_0 can be found in [Solberg et al., 2008d].
The function $f(\cdot)$ relates the valve stroke, z_{fw}, to the flow:

$$f(z_{fw}) = \frac{1}{R}(R^{z_{fw}} - e^{-R_0 z_{fw}}) \tag{3.3}$$

The function indicates that this is an exponential valve. Further, the last term in the parenthesis involving R_0 is not standard, but is included to describe the valve through the whole operating range. The feed water flow dynamics and the dynamics of the pneumatic valve positioning are fast compared to the flow sensor dynamics which is why this model was constructed purely static. The sensor dynamics were described as:

$$\dot{m}^f_{fw}(s) = G_{fw}(s)\dot{m}_{fw}(s) = \frac{1}{\tau_{fw}s + 1}\dot{m}_{fw}(s) \tag{3.4}$$

This model provides a good fit to measuring data, and the sensor time constant is about $\tau_{fw} = 4\text{s}$. The only parameters in this model that cannot be found from datasheets are the positioning of the return valve, k_r, and the sensor time constant. It is obvious that the system is very nonlinear, which is illustrated in Figure 3.2.
Note that the feed water flow is dependent on the boiler steam pressure, such that $\dot{m}_{fw} \in [0, \overline{\dot{m}}_{fw}(p_s)]$. Further, note that at nominal boiler pressure, $p_s = 8\text{bar}$, the small gain varies up to a factor of 22.

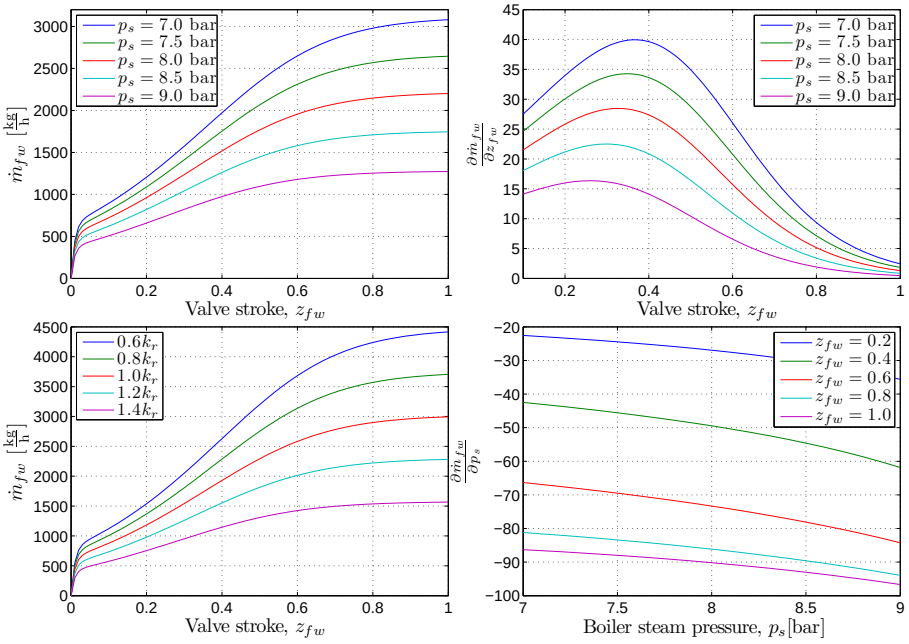

Figure 3.2: Feed water system characteristics. In the top left corner the feed water flow is shown as a function of the valve stroke for different boiler pressures. In the top right corner the partial derivative of the feed water flow with respect to the valve stroke is shown for different boiler pressures. Notice that only valve strokes $z_{fw} \geq 0.1$ are included as the valve positioning is unreliable below this level. In the bottom left corner the feed water flow is shown as a function of the valve stroke for different return valve strokes, and in the bottom right corner the partial derivative of the feed water flow with respect to the boiler pressure is shown for different valve strokes.

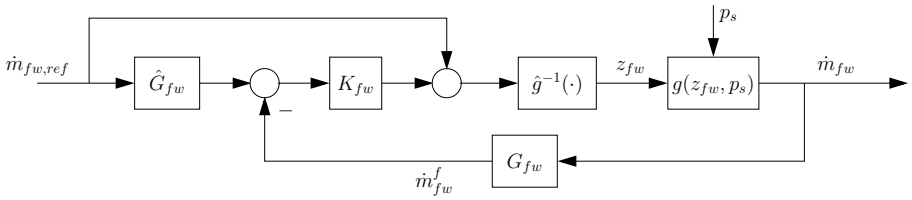

Figure 3.3: Feed water control scheme including both feedforward and feedback. K_{fw} is the feedback controller (a PI controller), $\hat{g}^{-1}$ is a model of the feed water system gain and $\hat{G}_{fw}$ is a model of the feed water sensor dynamics. Notice for $\hat{G}_{fw} = G_{fw}$ and $\hat{g} = g$ we have $\dot{m}^f_{fw} = G_{fw}\dot{m}_{fw,ref}$.

To handle the nonlinearity in the feed water system we suggested the control structure in Figure 3.3.

Note that the boiler pressure is assumed to be an unmeasured disturbance handled by the feedback. The inverse mapping of $g(z_{fw}, p_s)$ is a function mapping a reference flow and a nominal boiler pressure to a valve stroke, $g^{-1} : \mathbb{R}^2 \mapsto \mathbb{R}$.

$$z_{fw,ref} = \frac{1}{\log(R)} \log\left(\frac{\dot{m}_{fw,ref}}{k_f \sqrt{\Delta p_{p,ref}(\dot{m}_{fw,ref}, k_r) + p_a - p_s}} \right) + 1 \tag{3.5}$$

Note that here $f(z_{fw}) = \frac{1}{R} R^{z_{fw}}$, where the term involving R_0 has been omitted, $e^{-R_0 z_{fw}} = 0$. The reason for this is that the gain of the system is very high at low valve strokes and further the positioning of the valve stroke is not accurate enough to actively operate at these small strokes. Instead, pulse width modulation is used for small valve strokes, handling the control challenge *Discontinuous input flows*.
$\Delta p_{p,ref}$ is a function of $\dot{m}_{fw,ref}$ and was found as the solution to a quadratic equation:

$$\Delta p_{p,ref} = \frac{-b_1(\dot{m}_{fw,ref}, k_r) - \sqrt{b_1(\dot{m}_{fw,ref}, k_r)^2 - 4b_2(k_r)b_0(\dot{m}_{fw,ref})}}{2b_2(k_r)} \tag{3.6}$$

where b_2, b_1 and b_0 can be found in [Solberg et al., 2008d]. In [Andersen and Jørgensen, 2007] the inverse (3.5) was approximated by the solution to a quadratic equation in $\dot{m}_{fw,ref}$, which proved to give satisfactory results in practice. Further, integrator windup is handled in a tracking anti-windup scheme – see [Åström and Hägglund, 2006].
To sum up, a model of the feed water system has been derived, and a controller based on gain scheduling and local feedback has been developed.

3.1.2 Burner

The contributions regarding burner control have mainly been concentrated on modelling and control of a novel turbocharged burner unit. However, for completeness we will shortly address the standard pressure atomising burner which we find on boilers that we will discuss control strategies for later.

Pressure atomising burner

The conventional pressure atomising burner has been treated by pure feedforward. For details – see [Andersen and Jørgensen, 2007; Solberg et al., 2008d]. The reason is that the fuel flow is seldom measured on installed boilers of the capacity treated in this project. The position of the damper controlling the air flow required to keep a clean combustion is found through a pre-calculated function of the fuel valve stroke. This function was found in [Andersen and Jørgensen, 2007]. This also means that there is no feedback from the oxygen level in the exhaust gas. No details of the nozzle-lance/atomiser system have been found for which reason a first principle model for the fuel system could not be derived. However, the gain from fuel valve stroke to fuel flow

to the burner has a relatively small variation over a large part of the operating range. For this reason the feedforward is a linear function from fuel flow reference to fuel valve stroke.

Turbocharged burner unit

In [Solberg et al., 2008c] a model and control strategy for a novel turbocharged burner unit developed partly by AI was derived. The overall goal of this work was to develop a control strategy capable of tracking a fuel flow reference while optimising efficiency and ensuring clean combustion measured by the oxygen content in the exhaust gas.
The burner consists of a gas turbine mounted on a furnace. A sketch of the burner unit is shown in Figure 3.4 and the functionality is explained below.

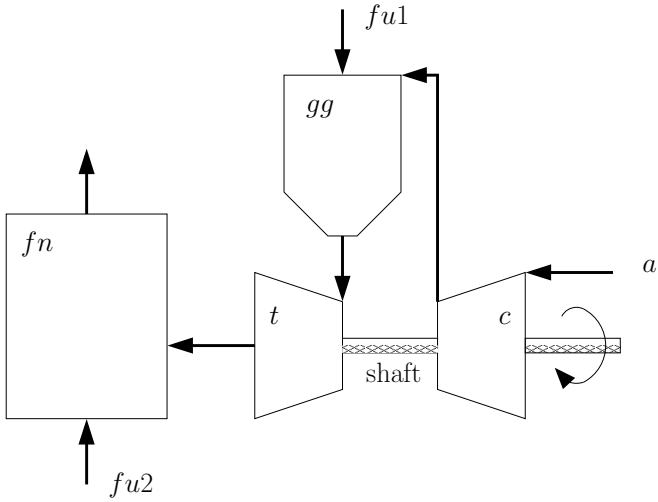

Figure 3.4: Drawing of the turbocharged burner system. c is the compressor, t is the turbine, gg is the gas generator (the first combustion chamber) and fn is the furnace (the second combustion chamber). a is the fresh air inlet, and $fu1$ and $fu2$ are the fuel inputs.

The units c, t and gg comprise the gas turbine. Fuel, $fu1$, is injected and burned in the gas generator, gg, and the hot gas leaving the combustion drives the turbine, t, which rotates the shaft of the turbocharger delivering power to drive the compression process in the compressor, c. Air is sucked in at the compressor inlet, and the hot combustion flue gas leaves the turbine to enter the second combustion chamber, the furnace, fn. Here fuel is added again, $fu2$, and another combustion takes place. More than 70% of the total fuel flow is injected into the furnace. The hot flue gas leaves the furnace and enters the boiler convection part before leaving through the funnel.

The model was based on first principles using mass and energy balances for describing the temperature and pressure dynamics. As flow through and efficiency of the turbocharger was required in these balance equations, approximations of the turbocharger turbine and compressor maps partly based on physical insight were made. The oxygen was modelled by describing mole balances for the oxygen in the gas generator and furnace volumes. The resulting model was of sixth order and presented in descriptor form as:

$$F(x)\frac{dx}{dt} = h(x,u,d) \tag{3.7a}$$

$$y = g(x,u,d) \tag{3.7b}$$

where $u = [\dot{m}_{fu1}, \dot{m}_{fu2}]^T$ is the vector of inputs being the fuel mass flow to the gas generator and the furnace. $d = [T_a, T_{fu}, T_m]^T$ is the vector of disturbances being temperatures of the inlet air, of the fuel and of the metal separating the hot flue gas and the water/steam in the boiler. $x = [p_{gg}, T_{gg}, \omega, T_{fn}, x_{gg,O_2}, x_{fn,O_2}]^T$ is the state vector being pressure in the gas generator, temperature in the gas generator, shaft speed, temperature in the furnace, and oxygen fraction in the gas generator and the furnace. Finally, $y = [\dot{m}_{fu}, \dot{Q}, x_{fn,O_2}]^T$ is the output vector with $\dot{m}_{fu} = \dot{m}_{fu1} + \dot{m}_{fu2}$ and $\dot{Q}$ is the energy transferred to the metal walls. Expanding, (3.7a) reveals the model structure as:

$$\begin{bmatrix} f_{11} & f_{12} & 0 & 0 & 0 & 0 \\ f_{21} & f_{22} & 0 & 0 & 0 & 0 \\ 0 & 0 & f_{33} & 0 & 0 & 0 \\ 0 & 0 & 0 & f_{44} & 0 & 0 \\ 0 & 0 & 0 & 0 & f_{55} & 0 \\ 0 & 0 & 0 & 0 & 0 & f_{66} \end{bmatrix} \begin{bmatrix} \frac{dp_{gg}}{dt} \\ \frac{dT_{gg}}{dt} \\ \frac{d\omega}{dt} \\ \frac{dT_{fn}}{dt} \\ \frac{dx_{gg,O_2}}{dt} \\ \frac{dx_{fn,O_2}}{dt} \end{bmatrix} = \begin{bmatrix} h_1 \\ h_2 \\ h_3 \\ h_4 \\ h_5 \\ h_6 \end{bmatrix} \tag{3.8}$$

where the elements f_{ij} and h_i were found in the model derivation – see [Solberg et al., 2008c]. F is never singular, hence has a well defined inverse, so (3.7a) can be written as an ordinary differential equation: $\dot{x} = f(x,u,d) = F^{-1}(x)h(x,u,d)$.

Validation against measurements collected from the test setup shows good agreement between model and measuring data in terms of capturing the dynamical behaviour. However, in terms of stationary values these are not represented well by the model for other outputs than the oxygen level, see Figure 3.5. This was accepted for now as the main focus was on oxygen control, and constraints on internal states were not considered.

The performance requirements for the controller of the burner were to deliver the requested fuel flow while keeping the oxygen percentage above 3% and maximise efficiency. No requirement regarding off-set free tracking of the fuel flow reference was introduced meaning that differences between requested and actual fuel flow should be handled by e.g. including integral action in the outer controller.

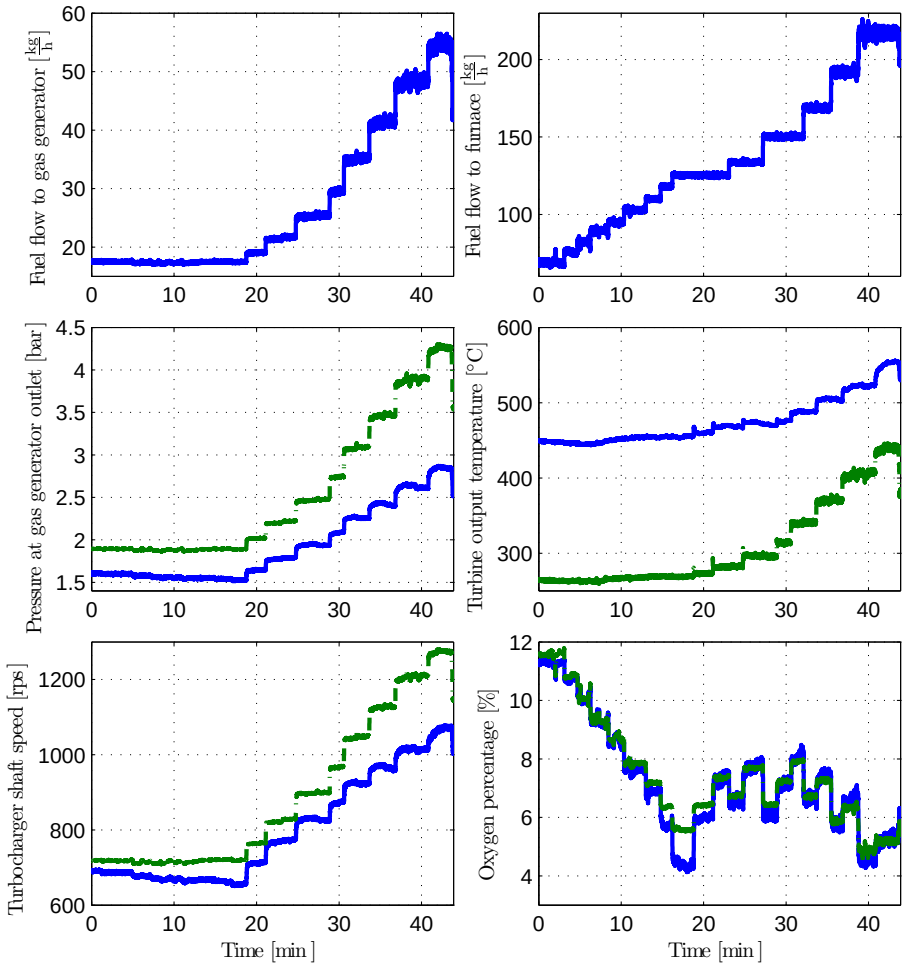

Figure 3.5: Comparison between measurements (blue solid curves) and simulation output (green dashed curves).

It was shown that the feasible region of stationary input fuel flows is convex and further the optimal stationary input distribution was the one keeping a minimum fuel flow to the gas generator burner. Also, both the gains and dynamics from the fuel inputs to oxygen percentage and power delivered to the metal walls proved to be very nonlinear. Further, the response from $\dot{m}_{fu1}$ to x_{fn,O_2} has a non-minimum phase zero. To handle the nonlinearities and non-minimum phase behaviour, the control structure shown in Figure 3.6 was suggested.

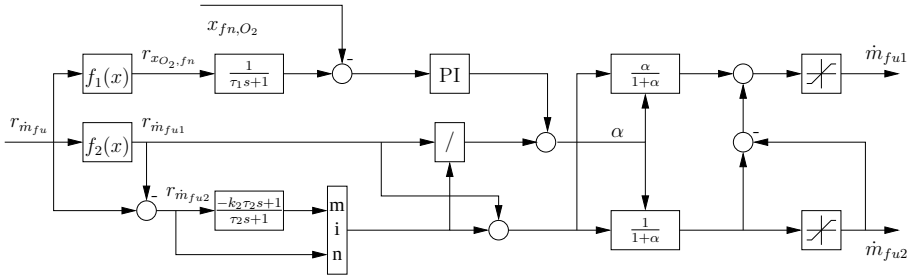

Figure 3.6: Control structure for the burner unit. A nonlinear feedforward is combined with some dynamic compensation to take into account the dynamics of the process. A feedback around the oxygen is closed to handle disturbances and model uncertainty.

Note that this controller consists of a feedback and a feedforward path. The feedforward from the total fuel flow reference, $r_{\dot{m}_{fu}}$, is functions calculating optimal steady state values for the fuel distribution, $r_{\dot{m}_{fu1}} = f_2(r_{\dot{m}_{fu}})$, $r_{\dot{m}_{fu2}} = r_{\dot{m}_{fu}} - r_{\dot{m}_{fu1}}$, and the corresponding oxygen level, $r_{x_{fn,O_2}} = f_1(r_{\dot{m}_{fu}})$. Note that no feedforward compensation is made for disturbances. The feedforward functions are calculated by inverting the steady state version of the model. The functions can be approximated by piecewise quadratic functions consisting of three pieces. The dynamic lag filter, $\frac{k_2\tau_2 s+1}{\tau_2 s+1}$, introduced after the nonlinear feedforward function for $r_{\dot{m}_{fu2}}$ is introduced to accommodate the non-minimum phase behaviour to x_{fn,O_2} when changing $\dot{m}_{fu1}$. The "min" block ensures that air lack never occurs. The other filter $\frac{1}{\tau_1 s+1}$ has a time constant close to that of the closed loop oxygen response. The feedback, a PI controller, adjusts the ratio, $\alpha = \frac{\dot{m}_{fu1}}{\dot{m}_{fu2}}$, between the two fuel flows to correct the oxygen level if the feedforward compensation is not accurate due to disturbances or model uncertainty. Anti-windup compensation, not shown, is made for the PI controller. The input saturation configuration to the right in the diagram ensures that the reference can be achieved even though $\dot{m}_{fu2}$ has saturated.
Simulation results gathered from the nonlinear model are presented in Figure 3.7 and Figure 3.8.
From the simulation results it can be seen that the designed controller is robust against disturbances and capable of tracking the fuel flow reference. Further, the number of constraint violations ($x_{fn,O_2} < 3\%$) is small. Note that the functions used in the nonlinear feedforward are easy to identify during burner commissioning.
Thus regarding burner control, focus was on a new turbocharged burner for which a first principle model was derived and a control strategy based on a nonlinear feedforward and a feedback oxygen controller was suggested.

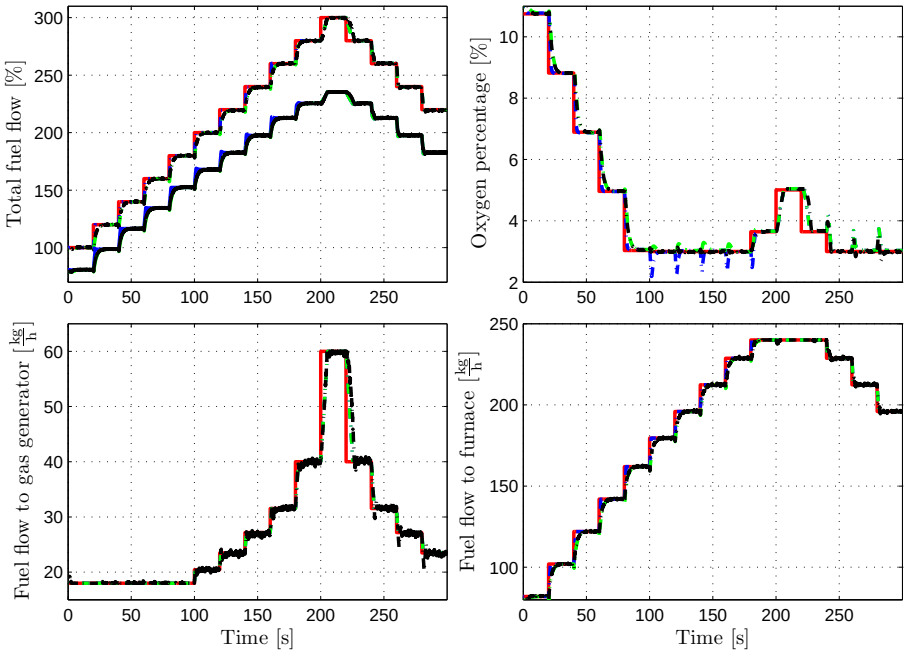

Figure 3.7: Simulation results with a staircase reference change to the total fuel flow. The total fuel flow is shown in the top left plot, upper curves, along with the power delivered to the metal divided by the fuel enthalpy, lower curves. The oxygen percentage is shown in the top right plot. The fuel flow to the gas generator is shown in the bottom left plot and the fuel flow to the furnace in the bottom right plot. The red lines in the top plots are reference curves. The red lines in the bottom plots are feedforward signals. The blue curves are the uncontrolled system with pure feedforward. The green curves have feedforward and the lag filter in the feedforward path. The black curves have both feedforward and feedback.

3.2 Marine Boiler Modelling and Control

In this section we focus on marine boiler modelling and control, and we discuss the contributions made in this area. Different first principle models for the marine boiler of varying complexity (second to eighth order) have been presented in the thesis. The most cited model is the third order model presented in [Solberg et al., 2007a] and [Solberg et al., 2008a] differing only by choice of functions describing the amount of steam escaping the water surface and the heat transfer efficiency. The model has the descriptor form:

$$F(x)\frac{dx}{dt} = h(x,u,d) \tag{3.9a}$$

$$y = g(x) \tag{3.9b}$$

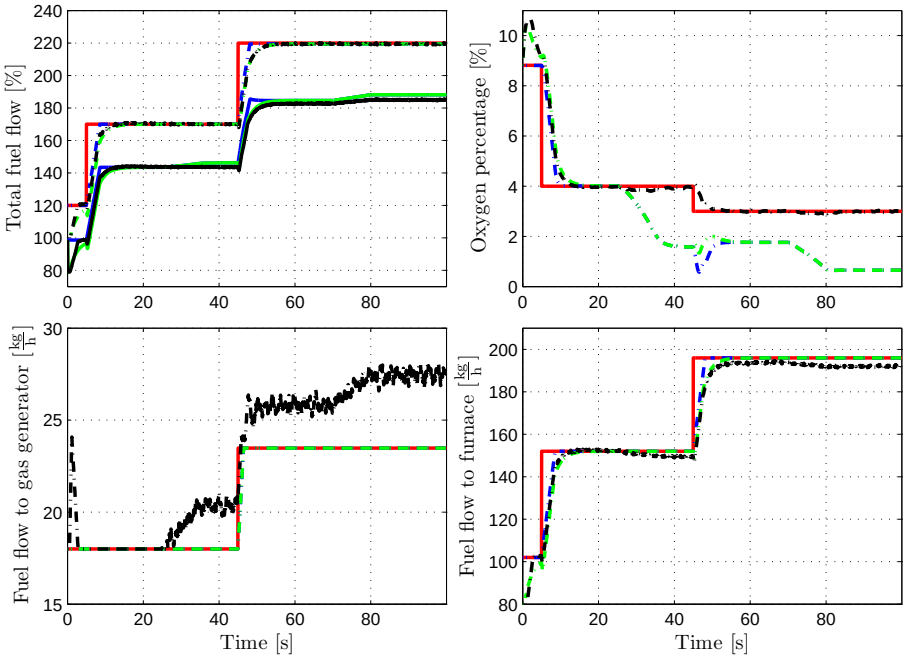

Figure 3.8: Simulation results with a ramp disturbance in engine room pressure of $-500\frac{\text{Pa}}{\text{s}}$ over 10s, from 25s to 35s. Further, a ramp disturbance occurs in the engine room temperature of $3\frac{^\circ\text{C}}{\text{s}}$ over 10s from 70s to 80s. The total fuel flow is shown in the top left plot; upper curves, along with the power delivered to the metal divided by the fuel enthalpy; lower curves. The oxygen percentage is shown in the top right plot. The fuel flow to the gas generator is shown in the bottom left plot and the fuel flow to the furnace in the bottom right plot. The red lines in the top plots are reference curves. The red lines in the bottom plots are feedforward signals. The blue curves are the uncontrolled system with pure feedforward. The green curves have feedforward and lag filter in the feedforward path. The black curves have both feedforward and feedback.

where the state vector is $x = [p_s, V_w, V_b]^T$ with p_s being the steam pressure, V_w the volume of water in the boiler and V_b the volume of steam bubbles below the water surface. The input vector is $u = [\dot{m}_{fu}, \dot{m}_{fw}]^T$ with $\dot{m}_{fu}$ being the oil mass flow to the burner and $\dot{m}_{fw}$ the feed water flow. $d = k$ is the disturbance where k is a variable expressing steam pipe conductance and steam valve stroke and relates the steam pressure to the steam flow, $\dot{m}_s$, as:

$$\dot{m}_s(t) = k(t)\sqrt{p_s(t) - p_a} \tag{3.10}$$

with p_a being the pressure in the feed water tank. The temperature of the feed water is assumed to be constant and therefore not included in d. The output vector is $y = g(x) = [p_s, L_w]^T$ where $L_w(V_w, V_b)$ is the water level. Expanding, (3.9a) reveals the

model structure as:

$$\begin{bmatrix} f_{11} & f_{12} & 0 \\ f_{21} & f_{22} & 0 \\ f_{31} & f_{32} & f_{33} \end{bmatrix} \begin{bmatrix} \frac{dp_s}{dt} \\ \frac{dV_w}{dt} \\ \frac{dV_b}{dt} \end{bmatrix} = \begin{bmatrix} h_1 \\ h_2 \\ h_3 \end{bmatrix} \tag{3.11}$$

where the elements f_{ij} and h_i were found in the model derivation – see [Solberg et al., 2007a]. The total nonlinear simulation model used in the project has the structure shown in Figure 3.9.

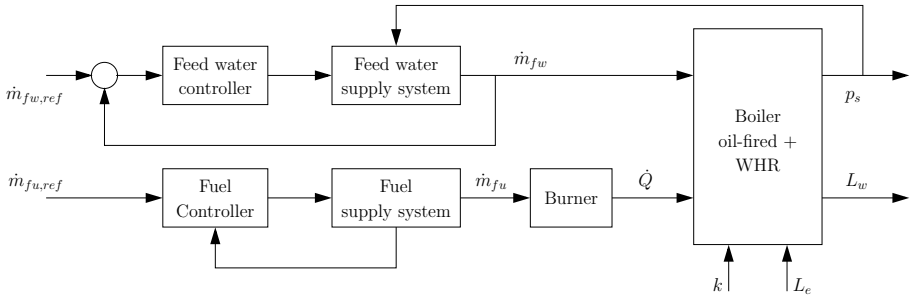

Figure 3.9: Structure of total nonlinear model used for simulation purposes. This structure includes flow controllers for the feed water and oil input.

The WHR boiler, not included in the model (3.9), is also indicated in the figure, and the disturbance L_e corresponds to the engine load.

3.2.1 Limits of performance

Together [Solberg et al., 2007b] and [Solberg et al., 2008d] provide a thorough treatment of control properties and limits of performance for the oil-fired one-pass smoke tube boiler. It was shown that the performance limitations for these plants with the current sensor equipment are determined by the water level measurement noise and to some extent actuator constraints. The consequence of this is that it is natural to have a large separation in the water level and pressure loop bandwidths. This also means that it is difficult to obtain a high bandwidth of the sensitivity function from the steam flow disturbance to the water level using decentralised control.

Besides these limiting factors it was shown that the boiler behaves linearly in a large frequency range for all possible steam loads, and that one linear controller provides acceptable performance. Further, an analysis in [Solberg et al., 2007b] showed that interactions in the process does not pose any stability issues when designing decentralised controllers. Also, a product of [Solberg et al., 2008d] was a reduction of the eighth order nonlinear model in [Solberg et al., 2005b] to a second order nonlinear model capturing the important dynamics for control.

The two differential equations from this model were one originating from the mass balance for the water/steam part:

$$V_w \frac{d\varrho_w}{dp_s}\frac{dp_s}{dt} + (\varrho_w - \varrho_s)\frac{dV_w}{dt} \approx \dot{m}_{fw} - \dot{m}_s \tag{3.12}$$

and one from the energy balance:

$$\frac{dp_s}{dt} \approx \frac{1}{\varrho_w V_w \frac{dh_w}{dp_s}} \left(\dot{Q} - (h_w - h_{fw})\dot{m}_{fw} - h_c \dot{m}_s\right) \tag{3.13}$$

where ϱ_w, ϱ_s and h_w, h_s are the densities and enthalpies of the water and steam respectively. $\dot{Q} = \eta \dot{m}_{fu}$ for some efficiency factor η and $h_c = h_s - h_w$.
These equations describe the evolution of the water volume and steam pressure. The steam bubble volume below the water surface was described as:

$$V_b = \frac{T_d}{\varrho_s}\dot{m}_s \tag{3.14}$$

where $\dot{m}_s$ was a function of k as in (3.10), and T_d expresses the average rise time of steam bubbles in the water. The water level was then found to be:

$$L_w = \frac{V_w + V_b - V_o}{A_{ws}} \tag{3.15}$$

where A_{ws} is the water surface area and V_o is the volume surrounding the furnace. The water level is measured from the furnace top and up. The second order model can then be written as:

$$\dot{x} = f(x, u, d) \tag{3.16a}$$

$$y = c(x, u, d) \tag{3.16b}$$

where $y = [p_s, L_w]^T$, $x = [p_s, V_w]^T$, $u = [\dot{m}_{fu}, \dot{m}_{fw}]$ and $d = k$. This model has a simple linear representation which can be found in [Solberg et al., 2008d].
The work on control properties and limits of performance showed that low order linear models could be used for controller design and further, the achievable performance is limited by the water level sensor noise and actuator constraints.

3.2.2 Model predictive control of marine boilers

In [Solberg et al., 2005b] an LQG control strategy was presented for the oil-fired one-pass smoke tube boiler. Tests conducted during this work proved two important things: multivariable model-based control was applicable to the boiler class treated and further, relying on an estimate of the current steam flow disturbance rather than a measurement does not decrease performance remarkably. In [Solberg et al., 2007a] the natural extension of this work towards constrained LQG using MPC was described.

MPC naturally deals with the control challenge *Actuator saturation* from Section 2.6. The setup included a second order empirical model of the WHR boiler and the third order model of the oil-fired boiler (3.9). The sampled linear approximation of the model was given as:

$$x(k+1) = Ax(k) + Bu(k) + B_d d(k) \tag{3.17a}$$
$$y(k) = Cx(k) \tag{3.17b}$$
$$x \in \mathcal{X},\ u \in \mathcal{U} \tag{3.17c}$$

where $u = [\dot{m}_{fu}, \dot{m}_{fw}]^T$, $x = [p_s, V_w, V_b, x_{ex,1}, x_{ex,2}]^T$, $y = [p_s, L_w]^T$, $d = [k, L_e]^T$, $\mathcal{X} \subset \mathbb{R}^n$ and $\mathcal{U} \subset \mathbb{R}^m$ are compact sets describing constraints on states and inputs respectively. L_e represents engine load changes and $x_{ex,i}$ is a state of the WHR boiler model. A sample time of 2s was used. This update frequency is necessary to handle the control challenge *High disturbance bandwidth*.
To define the controller, a standard quadratic cost function was used:

$$J^N(x_0, \mathbf{u}) = [r(N) - y(N)]^T P [r(N) - y(N)] + \tag{3.18}$$
$$+ \sum_{i=0}^{N-1} [r(i) - y(i)]^T Q [r(i) - y(i)] + \Delta u^T(i) R \Delta u(i)$$

where Q includes weights on the water level and pressure deviations from the references r. R includes weights on the rate of input changes and P is a terminal error penalty. x_0 is the current state, $\mathbf{u}$ is the future input sequence to be found in the MPC update step and N is the prediction horizon. The tuning of the MPC controller was done by using the LQG/LTR procedure for shaping the return ratio of the estimator in such a way that the MPC performance could be compared to that of a classical decentralised PI control strategy. The estimator was designed also to achieve off-set free tracking of the water level and pressure. This was achieved by augmenting the model (3.17) by integrating disturbances in the direction of Γ. Two different choices of Γ were suggested leading to two MPC designs. Design 1 had $\Gamma = B$ and Design 2 had $\Gamma_2 = \left[\frac{1}{2}B\left[\begin{smallmatrix}1\\1\end{smallmatrix}\right]\ B_d\left[\begin{smallmatrix}1\\0\end{smallmatrix}\right]\right]$. Regarding the control challenges *High disturbance bandwidth* and *Measurement noise*, Design 2 showed to increase the bandwidth of the sensitivity function from the steam flow disturbance to the water level without increasing sensitivity to water level measurement noise.
The designed controllers proved in simulations on the nonlinear model of the full-scale boiler to outperform the PI controller, see the simulation results in Figure 3.10.
The reason for this was concluded to be due to the model-based and MIMO nature of the controller rather than superior constraint handling. This was also backed up by the fact that a clipped-LQG scheme achieved similar performance as MPC. Also, the direction of the unmeasured disturbances in the estimator proved very important. Especially, estimating $k \sim \dot{m}_s$ proved very efficient regarding water level control. To demonstrate

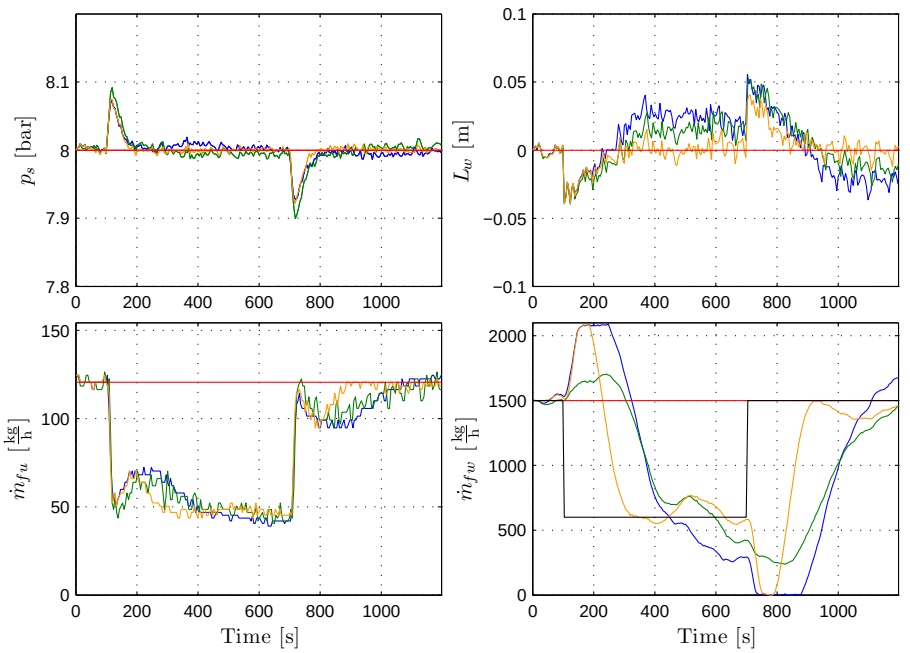

Figure 3.10: Plot of simulation results with a pulse in steam flow of $-900\frac{\text{kg}}{\text{h}}$ shown as the black line in the bottom right plot. The pressure is shown in the top left plot, the water level in the top right plot, the fuel flow in the bottom left plot, and the feed water flow in the bottom right plot. The red lines in the top plots are the references, and the red lines in the bottom plots are the initial steady state value of the inputs. The blue curves represent the PI controller, the green curves represent the MPC controller of Design 1, and the orange curves represent the MPC controller of Design 2.

why this is so, we take a closer look at the unconstrained controller:

$$\begin{bmatrix} \dot{m}_{fu} \\ \dot{m}_{fw} \end{bmatrix} = \begin{bmatrix} u_{11} + u_{12} \\ u_{21} + u_{22} \end{bmatrix} = \begin{bmatrix} K_{11}(z) & K_{12}(z) \\ K_{21}(z) & K_{22}(z) \end{bmatrix} \begin{bmatrix} p_s \\ L_w \end{bmatrix} \tag{3.19}$$

where $K_{ij}(z)$ differs in the three controller designs. In Figure 3.11 each term in the unconstrained MPC controller subject to the same measurements as in Figure 3.10 are shown.

This figure reveals that the controller of Design 2 has a very small coupling from the water level to the fuel flow, whereas the coupling from pressure to feed water holds the estimate of the steam flow. Design 1 has large couplings in both directions. This shows the importance of the MIMO structure and at the same time indicates that adequate performance should be expected using a decentralised control scheme with feedforward from a steam flow estimate to the water level controller.

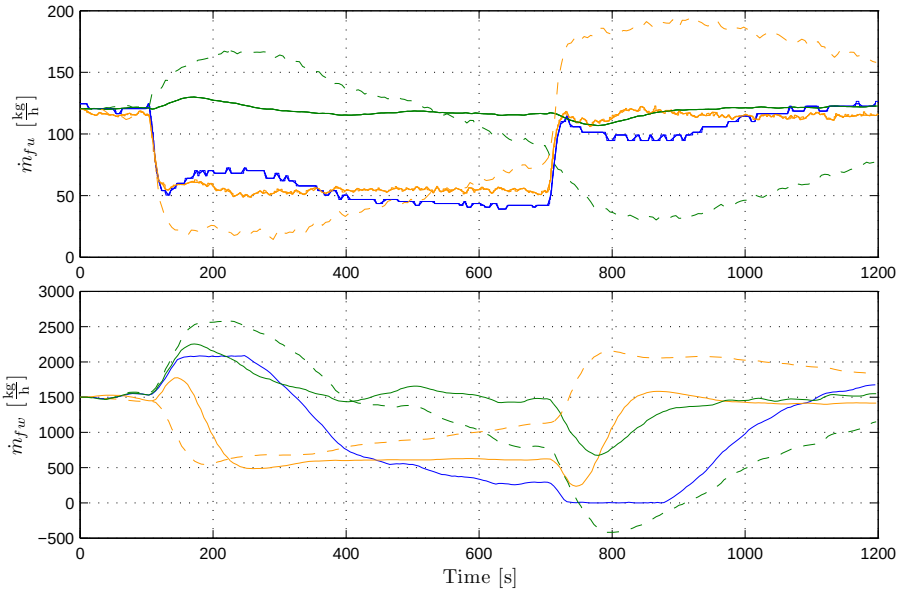

Figure 3.11: Plot of individual terms of the unconstrained controllers. The top plot is the fuel flow and the bottom plot is the feed water flow. The blue curves are the PI controller, u_{11} and u_{22}. The dashed, green and orange curves represent the MPC controller of Design 1, and the solid, green and orange curves represent Design 2. In the top plot the orange curves represent u_{11} and the green curves represent u_{12}. In the bottom plot the orange curves represent u_{21} and the green curves represent u_{22}.

Thus, what really sets the limits of performance for the standalone oil-fired boiler is the ability to generate this steam flow estimate which is influenced by measurement noise and model uncertainty. The reason is, as mentioned in [Solberg et al., 2008d], that we have to accept the shrink or swell occurring from the steam flow changes but can change the speed at which recovery from the disturbance is made. In fact, the feedback itself need not be very fast as other disturbances than the steam flow have much smaller bandwidths. This again points towards MIMO control, in the sense that the steam flow estimate must be generated from both process inputs and outputs.

In the paper [Solberg et al., 2007a] we also investigated the benefits of applying MPC to processes for which future knowledge of disturbance changes is available. This was done by assuming that the engine load changes were known three minutes in advance. The purpose was to address the challenge *Shrink-and-swell*. The efficiency of this scheme is illustrated in the simulation results of Figure 3.12.

Finally, a setpoint control scheme was discussed with the purpose of limiting the necessary distance between the lower and upper water level alarms in such a way that the boiler dimension could be reduced. However, no concrete algorithm was developed.

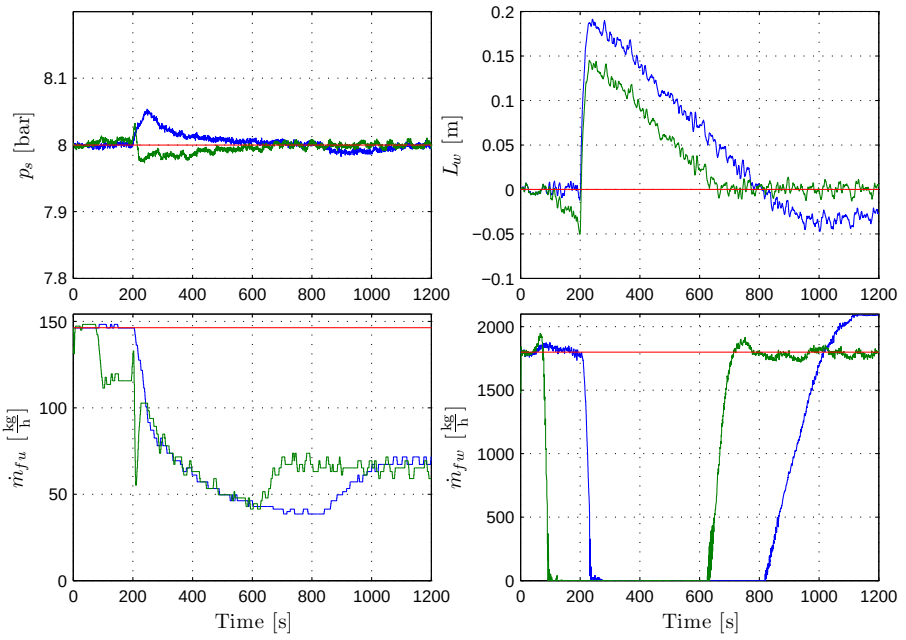

Figure 3.12: Plot of simulation results with a step change in the engine load from $L_e = 0$ to $L_e = 0.35$. The pressure is shown in the top left plot, the water level in the top right plot, the fuel flow in the bottom left plot, and the feed water flow in the bottom right plot. The red lines in the top plots are the references, and the red lines in the bottom plots are the initial steady state value of the inputs. The blue curves represent the PI controller and the green curves represent the MPC controller of Design 1. Notice that the MPC controller acts before the disturbance occurs.

3.2.3 Switching control of burner setting

As mentioned earlier in Section 2.6 a burner can only be operated down to a certain minimum load whereafter on/off operation is required to meet the desired energy request on average. This issue was part of the control challenge *Discontinuous input flows*.
In [Solberg et al., 2008a,b] two different strategies for handling the burner setting switching was presented for boilers equipped with a two-stage burner. The burner can operate in three modes, Burner 1 off and Burner 2 off, Burner 1 on and Burner 2 off, and Burner 1 on and Burner 2 on. Burner 1 is smaller than Burner 2. The burner was modelled as a finite state machine with fixed fuel flow manoeuvres executed during burner switching. This model was combined with a linear model as the one in (3.17) (without the WHR boiler) to have a full model of the boiler system.
Both, strategies set out to solve the following control problem:

Problem 3.1. *At every sample instant k, given the current state $x(k)$, minimise the*

following performance index over $\mathbf{u} = [u(k), u(k+1|k), \dots]$*:*

$$J(x(k), \mathbf{u}) = \lim_{T\to\infty} \frac{1}{T}\Big\{ \sum_{j=1}^{M(T)} h_{i_{j-1},i_j} + \\ + T_s \sum_{j=0}^{T} \left[z^T(j+k|k) Q(j) z(j+k|k) + + \Delta u^T(j+k|k) R(j) \Delta u(j+k|k) \right] \Big\} \tag{3.20}$$

where $\Delta u(j) = u(j) - u(j-1)$*,* $z(j) = r(j) - y(j)$ *with the reference vector* $r(j)$*,* $i \in \{0, 1, 2\}$*,* $M(T)$ *is the total number of burner switches, and* h_{i_{j-1},i_j} *is the cost associated with a switch from burner mode* i_{j-1} *to mode* i_j*.* Q *and* R *are quadratic penalties on error and input changes.*

Hence the control problem poses a trade-off between output (water level and pressure) setpoint deviations and control input action including costs of burner switches.
A special property of the two-stage burner is that the minimum possible power delivered by concurrent operation of the burners is higher than the maximum power delivered by Burner 1 alone. This means that there are two power gap-regions, meaning that the burner cannot deliver power continuously below the minimum load of Burner 1 and neither between the maximum load of Burner 1 and the minimum load of the concurrent burner operation.
It was noted that given the special property of the gap-regions and the cost function in the control problem setup there will be certain disturbance levels for which the optimal continuous solution to the control problem 3.1 forces the state trajectory of the system to converge to a limit cycle.
In [Solberg et al., 2008a] the application of MPC using the mixed logic dynamical framework (MLD) to control burner on/off switches for boilers equipped with a two-stage burner was discussed. We refer to this method as Method A. In the same paper, problems regarding the finite receding horizon framework for controlling these burner on/off switches were discussed. The problems arise exactly when the system to be controlled converges to a limit cycle. In this case the receding horizon control using the MPC/MLD framework suffers from prediction mismatches.
In [Solberg et al., 2008b] a method suggested in [Solberg et al., 2008e] based on a generalised hysteresis framework was applied to the same process in order to handle the shortcomings of MPC/MLD. We refer to this method as Method B. The structure of this new control strategy is shown in Figure 3.13.
The idea behind this new strategy is that the MPC controller is basically the same as designed in [Solberg et al., 2007a] but with variable constraints depending on the burner state. The state estimator estimates when the requested power corresponds to a gap-region. If this is so, the burners are allowed to switch when the states hit a switching surface described by $f(x)$. These switching surfaces are found by seeking the optimal

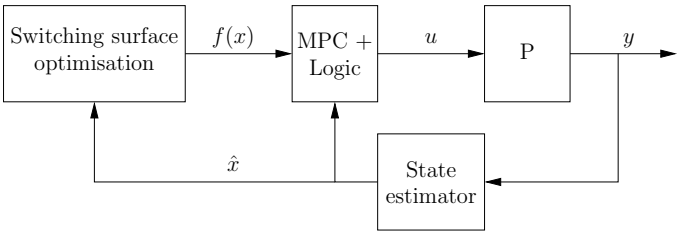

Figure 3.13: Control structure for Method B.

limit cycle (if one exists) given the current requested power demand. The surfaces are described using theory from time-optimal control. The method is only developed for SISO systems with discrete input. For this reason the model used in the optimisation assumed that the MPC water level controller was active. Instead of performing the optimisations on line, a table of switching surfaces was found off line and implemented as a lookup table.
A simulation study showed that this new controller behaved more appropriately than the MPC/MLD controller, see Figure 3.14. The approach is general and can be applied to similar systems governed by actuator systems which are continuous in one region and discrete in another. Further, the method allows for certain sequences to be executed in between input switches.

3.3 Hybrid Systems Control

The contributions in this field are concerned with control of systems having discrete inputs using a discontinuous cost functional. The latter method mentioned (Method B) for control of the burner on/off switches above was originally described in [Solberg et al., 2008e]. In that work it was pointed out that finite receding horizon control of systems whose state converge to a limit cycle is never optimal through the proposition:

Proposition 3.2. *Given a control problem described by a cost functional which has discontinuous jumps. If the optimal state trajectory converges to a limit cycle, finite receding horizon control is never optimal.*

The systems under consideration were:

$$\dot{x}(t) = Ax(t) + Bu(t) \tag{3.21a}$$
$$y(t) = Cx(t) \tag{3.21b}$$

where $x \in \mathbb{R}^n$, $y \in \mathbb{R}$ and $u(t) : [0, \infty) \rightarrow \{\underline{u}, \overline{u}\}$. The input was symmetric, $u(t) \in$

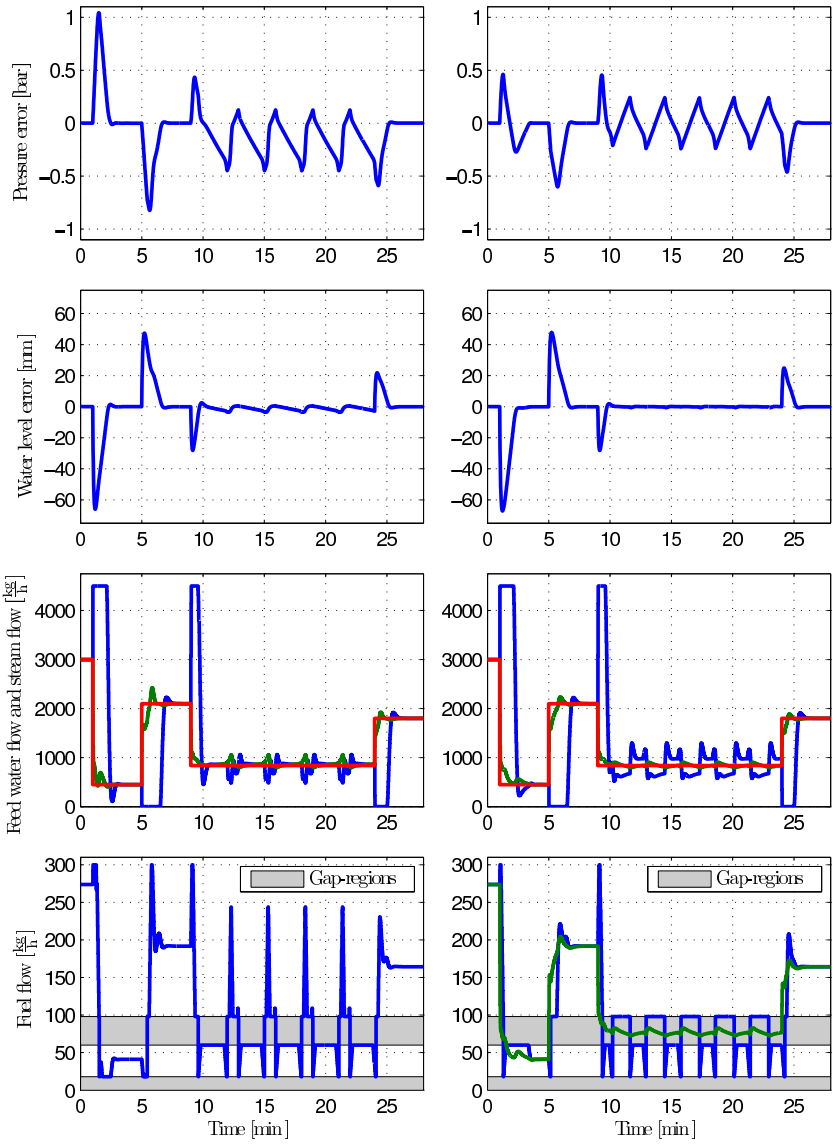

Figure 3.14: Simulation results using Method A left and Method B right. From the top the first row shows pressure error, the second water level error, the third row shows the feed water flow (blue), estimated (green) and measured (red) disturbance both converted to represent requested steam flow, and the bottom row shows fuel flow. The plot on the right includes the estimated steady state fuel input (green), the grey fields correspond to the gap-regions. Notice the spikes in the fuel flow from 12 to 25 min. bottom left and the asymmetry in the pressure error oscillations in the same period top left for Method A.

$\{-1, 1\}$, and we defined $\Delta = u(0)$, such that:

$$u(t) = \begin{cases} \Delta \text{ for } 0 \leq t \leq T_1 \\ -\Delta \text{ for } T_1 < t \leq T_2 \\ \Delta \text{ for } T_2 < t \leq T_3 \text{ etc.} \end{cases} \tag{3.22}$$

The general cost functional treated was:

$$J(x(0), u(\cdot)) = \lim_{T \to \infty} \frac{1}{T} \int_0^T l(e(\tau), u(\tau)) d\tau \tag{3.23}$$

where $e(\tau) = r(\tau) - y(\tau)$ and the piecewise continuous $l(e(\tau), u(\tau)) : \mathbb{R} \times \{\underline{u}, \overline{u}\} \to \mathbb{R}$ included a quadratic penalty on the tracking error and a cost of switching the input. Hence:

$$l(e(\tau), u(\tau)) = qe^2(\tau) + \rho \left(\delta \left(\tau - T_1 \right) + \delta \left(\tau - T_2 \right) + \dots \right), \tag{3.24}$$

where $q > 0$ is the cost associated with output deviations from the reference, and $\rho > 0$ is the cost assigned to the changes in the input signal. $\delta(\cdot)$ is the Dirac delta function, and T_i is the time of the i'th input change.
A new sampled optimisation problem for solving the infinite horizon control problem minimising (3.23) was introduced. However, as a considerable amount of computational resources would still be required for this approach, two approximations to the infinite horizon strategy were proposed. The strategy behind both these methods was first, offline, to find the optimal limit cycle the state would converge to given some performance function and subsequently in an online control scheme track this cycle. One approach referred to as Method A* penalises the deviations from the predetermined optimal limit cycle in a cost functional of a finite receding horizon controller. The other, Method B*, uses a generalisation of hysteresis control taking a geometrical approach looking at a hypersurface in the state space to determine switches in the input. The steps in designing the latter controller are:

1 Find the optimal limit cycle by solving an optimisation problem.

2 Calculate switching surfaces and their domains, starting from the points x^+ and x^- respectively, using techniques from time-optimal control.

3 The control law aims to evaluate the functions representing the switching surfaces and to check their sign. Based on this information the control input can be set to either $u(t) = -1$, $u(t) = 1$.

x^+ and x^- are points on the limit cycle where a switch in the input from negative to positive and positive to negative respectively occurs.
Examples of both methods were presented in [Solberg et al., 2008e]. One example was the triple integrator which we repeat here:

Example 3.3. *Triple integrator: the differential equation is simply* $\dddot{x}_1(t) = u(t)$*, which for constant* $u(t) = \Delta$ *has the solution:*

$$\begin{bmatrix} x_1 \\ x_2 \\ x_3 \end{bmatrix} = \begin{bmatrix} \frac{1}{6}\Delta & \frac{1}{2}x_3(0) & x_2(0) & x_1(0) \\ 0 & \frac{1}{2}\Delta & x_3(0) & x_2(0) \\ 0 & 0 & \Delta & x_3(0) \end{bmatrix} \begin{bmatrix} t^3 \\ t^2 \\ t \end{bmatrix} \tag{3.25}$$

The input is limited to $u(t) \in \{-1, 1\}$ *and* $y(t) = x_1(t)$ *and* $r(t) = 0$*. The design parameters are:* $q = 1$ *and* $\rho = 50\pi$*. Now find the optimal limit cycle to get switching points* x^+*,* x^- *and the optimal period* T_p^**. The limit cycle is symmetric and hence the duty cycle is* $D_c = 1/2$*. Next we seek the switching surfaces. First, find* Γ^-*, the curve along which the state approaches* x^- *with negative input* $u(t) = -1$ *by setting* $t = -\tau$ *(*$\tau > 0$*) in* (3.25) *and eliminating* τ*. This curve is given by the intersection of the two hypersurfaces:*

$$f_1^-(x) = \frac{1}{6}(x_{32} - x_3^0)^3 + \frac{1}{2}x_3^0(x_{32} - x_3^0)^2 - x_2^0(x_{32} - x_3^0) + x_1^0 - x_{12} = 0 \tag{3.26}$$

$$f_2^-(x) = -\frac{1}{2}(x_{32} - x_3^0)^2 - x_3^0(x_{32} - x_3^0) + x_2^0 - x_{22} = 0 \tag{3.27}$$

over the domain $\{x | x_3^0 < x_3\}$*. The next step is to find the surface,* W^+*, on which a positive input can bring the state to the curve* Γ^-*. To do this, set* $t = -s$ *(*$s \geq 0$*) in* (3.25) *and set the initial condition to the points on* Γ^- *defined by* $f_1^- = 0, f_2^- = 0$*. By eliminating* s *and points on* Γ^- *from the equation, the following expression for the surface can be derived:*

$$g^+(x) = \frac{1}{6}(x_{32} - x_3)^3 + \frac{1}{2}x_{32}(x_{32} - x_3)^2 + x_{22}(x_{32} - x_3) + x_{12} - x_1 = 0 \tag{3.28}$$

with x_{12}, x_{22}, x_{32} *being points on* Γ^- *found from* (3.26), (3.27) *and:*

$$x_{32} = \left(\frac{1}{2}(x_3^2 + {x_3^0}^2) + x_2^0 - x_2\right)^{1/2} \tag{3.29}$$

The domain $X_{W^+} \subset \mathbb{R}^3$ *on which* W^+ *is defined is:*

$$X_{W^+} = \left\{ x \middle| x_2 < \begin{cases} \frac{1}{2}(x_3^2 - {x_3^0}^2) + x_2^0 \text{ for } x_3 \leq 0 \\ -\frac{1}{2}|x_3^2 - {x_3^0}^2| + x_2^0 \text{ for } x_3 > 0 \end{cases} \right\} \tag{3.30}$$

The curve and surface Γ^+ *and* W^- *can be found in a similar manner starting from the point* x^+*. Now define a new function describing the surface dividing the state space* $M = W^+ \cup W^-$*. This function is given as:*

$$g(x) = \begin{cases} g^+(x) \text{ for } x(t) \in X_{W^+} \\ g^-(x) \text{ for } x(t) \in X_{W^-} \end{cases} \tag{3.31}$$

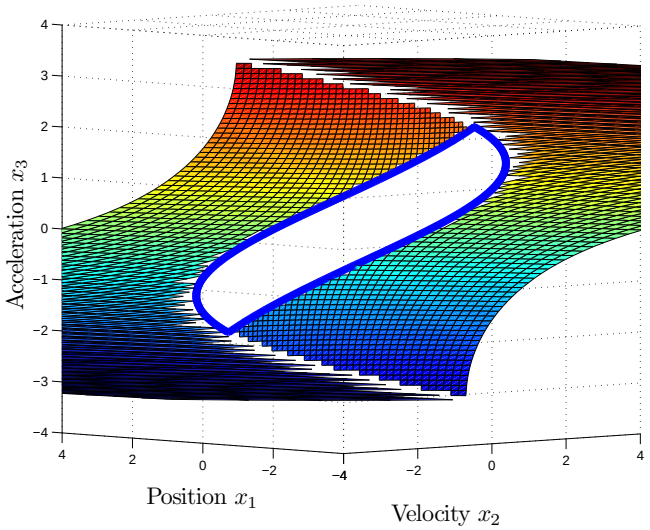

Figure 3.15: Switching surfaces and optimal limit cycle for the triple integrator example.

Finally, define the space above the surface M as M^- and the space below as M^+ being regions of the state space where a negative input or a positive input can take the state to one of the switching surfaces.
Now a feedback law can be designed to steer the state to the limit cycle as:

$$u(t) = \begin{cases} 1 \text{ for } x(t) \in M^+ \\ -1 \text{ for } x(t) \in M^- \\ 1 \text{ for } x(t) \in W^+ \setminus \Gamma^- \\ -1 \text{ for } x(t) \in W^- \setminus \Gamma^+ \\ 1 \text{ for } x(t) \in \Gamma^+ \\ -1 \text{ for } x(t) \in \Gamma^- \\ u(t) \text{ for } x(t) \in \mathbb{R}^3 \setminus (X_{W^+} \cup X_{W^-}) \end{cases} \tag{3.32}$$

The switching surfaces for this control law are shown in Figure 3.15. The optimal limit cycle is also plotted as a blue curve.
The control law (3.32) *and the one using Method A* have been simulated, and the results are shown in Figure 3.16.*
The top plot shows the value of the cost functional. The blue line corresponds to the cost associated with the optimal limit cycle. The red line is the cost achieved by applying Method A, and the green line is the cost achieved by applying Method B*. The performance is evaluated using the performance function in* (3.33)*. The bottom plots*

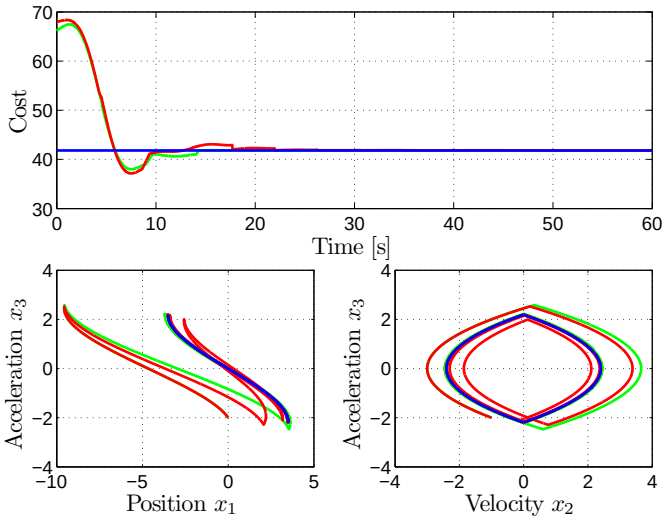

Figure 3.16: Simulation results for triple integrator example. Top: performance plots. Bottom: state trajectory in the phase plane.

show the trajectory of the closed loop in the phase plane projected onto the x_1, x_3 plane left and onto the x_2, x_3 plane right. The red curve is the state evolution using Method A*, the green curve is the state evolution using Method B*, and the blue curve is the state trajectory corresponding to the optimal limit cycle.
As can be seen, both methods result in the state converging to the limit cycle.

The actual performance curve over a period in the above example is evaluated from the following integral:

$$J^a(x,t) = \frac{1}{T_p^a}\Big(\int_t^{T_p^a+t} qx_1^2(\tau)d\tau + 2\rho\Big), \tag{3.33}$$

where T_p^a, the actual period, is defined as:

$$T_p^a = \min(T_2 + T_0, T_3), \tag{3.34}$$

with T_0 being the time since the last input change and T_2 and T_3 being the future times at which the second and third input change take place respectively.
Method B* proved to allow considerably faster online computations than Method A* for the treated examples. Both methods have only been solved for relatively small systems and problems might be encountered when increasing the model order. Further, MIMO systems and mixed continuous/discrete decision variables are not systematically

handled. However, an approach to do so was discussed above for control of the two-stage burner.
We might conclude by raising two questions:

- Why do we need an infinite horizon?
- What is the consequence of running with a finite horizon?

To answer the latter question first, we saw in [Solberg et al., 2008e] that for hybrid systems the choice of horizon changes the solution dramatically. This is different from linear systems and standard MPC where convergence is much faster in the horizon length. An infinite horizon is often used in linear MPC to achieve stability guarantees or approximate the constrained LQR controller. However, when predicting over this infinite horizon, disturbances, references, system dynamics, etc. are often assumed not to change. This is of cause never true in practice. However, hoping that by choice of an infinite horizon, the stability properties of linear MPC can be carried over to the hybrid case, this is motivation enough. Also, if no information about any future changes altering the solution is available, the infinite horizon solution provide consistent predictions as long as no alterations occur, whereas the finite horizon method will be subject to prediction mismatches.

3.4 Solved Control Challenges

Here we shortly summarise the solved challenges.

- *Actuator nonlinearities*. This challenge was solved for both the feed water system and the turbocharged burner unit. For the feed water system this was handled by inverting the plant gain in a gain scheduling strategy combined with a local feedback. For the burner, nonlinear feedforward functions from the reference were used to find the correct distribution of fuel flows.
- *Actuator saturation* (integrator windup). On the actuator control level this was handled by tracking anti-windup schemes. But seen from the boiler controller the saturation (constraints) were handled using MPC.
- *Discontinuous input flows*. This challenge was handled by developing and implementing hybrid system control schemes based on MLD/MPC and generalised hysteresis control.
- *High disturbance bandwidth*. A high sample rate ensured that step disturbance changes were spotted fast. Further, the bandwidth of the sensitivity function from the unmeasured steam flow to water level was increased by generating a steam flow estimate.

- *Shrink-and-swell*. The shrink-and-swell caused by steam flow changes had to be accepted though the recovery speed was increased. The more pronounced phenomenon caused by engine load changes was handled by exploiting the proactive nature of the MPC controller and further, a setpoint control scheme was suggested.

- *Measurement noise*. The measurement noise on the water level limited the achievable bandwidth of the water level loop. However, the most pronounced disturbance is the steam flow, and the bandwidth of the sensitivity function from this to the water level was increased through a steam flow estimate generated mainly from the pressure measurement.

It has been shown that a better water level control could be achieved without compromising pressure performance by using MPC. Further, a setpoint control scheme was discussed allowing to increase the water level setpoint closer to the upper constraint. The influence of the time-varying plant dynamics is reduced to a minimum by the choice of control structure.

4. Conclusion

In this thesis various topics within marine boiler modelling and control have been discussed. The work is presented in a collection of papers enclosed in the final part of this report. These papers describe application of advanced control to a specific class of marine boilers, and new results within hybrid systems control are discussed. Further, a thorough analysis of the boiler control properties is reported.
The contributions of the project are in the area of marine boiler modelling and control and hybrid systems control.
In the area of marine boilers the work can be divided into two branches; one concerning burner control and one concerning overall boiler control. Regarding burner control, the main contributions are:

- Construction of a first principle model describing a turbocharged burner unit. Published in [Solberg et al., 2008c].
- Design of a power controller with oxygen constraints for the turbocharged burner unit. Published in [Solberg et al., 2008c].

Regarding boiler modelling and control, the main contributions are:

- A thorough analysis of control properties of the one-pass smoke tube boiler. Published in [Solberg et al., 2007b].
- A description of limits of performance in marine boiler control. Published in [Solberg et al., 2008d].
- An LQG controller capable of controlling water level and pressure utilising an estimate of the steam flow disturbance. Published in [Solberg et al., 2005b].
- A novel approach to control marine boilers allowing a power consumption which requires on/off burner control. Published in [Solberg et al., 2008a] and [Solberg et al., 2008b].
- Steps towards a model predictive control structure for marine boilers using an outer water level setpoint optimiser to improve efficiency and allow smaller boiler geometry. Published in [Solberg et al., 2007a].

In the area of hybrid systems control, the following contributions have been made:

- Illustration of problems using a receding finite horizon control law for systems whose solution converge to a limit cycle. In this context the need for infinite horizon strategies is pointed out. Published in [Solberg et al., 2008e].
- Two methods for handling the above problem have been developed. Published in [Solberg et al., 2008e].

The overall marine boiler plant is a complicated large-scale nonlinear process. However, in this thesis we have shown that when focusing on different modules of the process, i.e. the actuator systems and boiler process in isolation, rather simple control algorithms can be derived for the entire process.
Both the burner, the feed water system and the boiler process have been treated in the thesis. First principle models of these submodules have been derived and controllers developed.
It turned out that the boiler process itself did not pose large theoretical challenges regarding modelling or control in normal situations. This was emphasised by developing a second order model of the boiler describing the relationship between fuel, feed water, steam flow and water level and pressure. Further, the plant behaved linearly over a large frequency range including the crossover frequency. Regarding the control, the noise on the water level measurement made it impossible to achieve as high a bandwidth for the water level loop as possible with the pressure loop when relying on single loop strategies. As a consequence, benefit could be gained from a multivariable control structure as this allowed for speeding up the response from the steam flow disturbance to the water level through a disturbance estimate. This estimate was generated by a Kalman filter including an internal model of the steam flow disturbance.
Instead it was the actuator systems that introduced the nonlinear behaviour in the plant. For the feed water system, the nonlinear gain could be linearised in a gain scheduling strategy inverting the plant gain combined with a local feedback allowing to set a reference for the feed water flow in an outer loop. Regarding the burner system the nonlinearities were introduced by the complexity of a turbocharged burner unit and as a consequence of the necessary on/off operation for low burner loads. This latter behaviour characterises the system as having a hybrid nature. Techniques to deal with this hybrid nature were developed. Further, a first principle model of the turbocharged burner unit was derived, and a control strategy based on a nonlinear feedforward and a local feedback for oxygen control was presented.
Much of the project has been concerned with the application of MPC and its variants. The reason for this was the original purpose of the project to minimise the boiler water/steam space. It was then thought that the process was highly nonlinear with extensive cross couplings and pronounced shrink-and-swell behaviour. Given both the hard water level, pressure and actuator constraints it seemed natural to use MPC. In [Solberg et al., 2007a] simulation results gathered from a model of a full-scale plant indicated

that MPC is applicable for marine boiler control. This paper concluded that it was especially the model-based nature of the MPC controller that allowed this strategy to outperform the classical PI controller. The superior constraint handling and pro-active nature offered by MPC proved less important when no information of future disturbance or setpoint changes were available. Further, the disturbance model used proved to be very important for improving performance. This model should be designed to estimate the unmeasured steam flow disturbance.
Simulation results also indicated that when the pro-active nature of MPC was not used, MPC delivered similar performance to a clipped-LQG controller. This is important as implementing the clipped-LQG controller eliminates the need for a quadratic programming solver in the marine boiler control system.
It was argued in [Solberg et al., 2008d] that one has to accept the shrink or swell originating from steam flow changes. However, using MPC the water level was brought back to its setpoint faster than with the classical decentralised PI controller. In order still to allow reduction of the steam space, a setpoint control scheme was discussed. Such a scheme can work for both the stand-alone oil-fired boiler and when this is equipped with a WHR boiler. Especially under the concurrent operation of the oil-fired boiler and the WHR boiler such a setpoint scheme can allow for reducing the height of the oil-fired boiler. Combining the setpoint controller with an MPC controller which receives prior knowledge about engine load changes showed potentials in [Solberg et al., 2007a]. However, even for the stand-alone oil-fired boiler, improvements could be expected through setpoint control.
It was found necessary to deal with the burner on/off switching at the same level as the water level and pressure control. This characterised the boiler as a hybrid system. Two strategies for controlling the boiler in situations requiring this on/off switching were suggested. One was based on MPC and the mixed logic dynamical (MLD) framework requiring a mixed integer optimisation problem to be solved on line. The other strategy used a generalised hysteresis (GH) framework developed in [Solberg et al., 2008e] in combination with MPC. The GH/MPC method required either an online optimisation of switching surfaces for the hysteresis or the implementation of a lookup table. In this work a lookup table was constructed. It was shown through simulations that the GH/MPC method in general produces better responses than the MLD/MPC framework. The main reason for this is argued to be due to the infinite horizon used in the GH/MPC method reducing prediction mismatches. The GH/MPC method is further found computationally more attractive than MLD/MPC framework for online implementation.

4.1 Perspectives

In this last section the author's suggestions for future research in the area of marine boiler control will be presented.

- Regarding the one-pass smoke tube boiler, focus should be moved from the con-

trol algorithms towards fault detection and accommodation algorithms. There is a huge potential in being able to automatically detect and isolate faults. Both to avoid damaging the plant but also to assist service engineers in fault accommodation. Such schemes might be based on very simple models of the plant submodules together with the extensive knowledge and experience gathered by service engineers over the years.

- The developed MPC controller should be decoupled and a decentralised scheme applied. This is achieved by closing a fast pressure loop by PI/MPC control. The water level loop can then run at a much lower sample frequency allowing longer computation times. However, it is still important to generate the steam flow estimate as this is what improves the water level control over traditional PI control. Whether this estimate should be generated from the current fuel flow alone or in a Kalman filter as in this thesis can be investigated. The benefit in such a setup is that it is less sensitive to uncertainty in the cross couplings. Such a decentralised strategy is also in line whith our proposed generalised hysteresis control structure.

- Regarding control there are supposedly a large challenge in controlling the large drum type marine boilers. This is backed by observations made by AI. The problem in these boilers is the relatively small water volume compared to the steam load. This makes the phenomena present in the one-pass smoke tube boiler more pronounced in this boiler type. However, the drum boiler is a popular example in the literature both regarding modelling and control and it should not be difficult to adjust these results to the environment in which the marine drum boiler operates.

- Modelling and control of the combustion process to improve burner efficiency and reduce the risk of furnace pressure pulsations which can cause plants to require shutdown.

- Water level measurement. Introducing a measurement of the water volume in the one-pass smoke tube boiler would be beneficial as the need for fast feedback from a noisy water level measurement would be eliminated. It was illustrated in [Solberg et al., 2008d] how such a measurement could be used in a control scheme.

- Further, development is required regarding introduction of the WHR boiler to the one-pass smoke tube boiler. Especially a first principle model of the boiler verified against measuring data is needed. Regarding control, the setpoint optimisation scheme suggested in [Solberg et al., 2007a] should be further developed.

- Regarding control of hybrid systems whose state trajectory converge to a limit cycle, much more work is required in the direction towards infinite horizon strate-

gies. This is important as systems having such properties often arise in the industry.

References

K. J. Åström and R. D. Bell. Drum boiler dynamics. *Automatica*, 36:363–378, 2000.

K. J. Åström and T. Hägglund. *Advanced PID Control*. ISA - Instrumentation, Systems, and Automation Society, 2006.

K. J. Åström and B. Wittenmark. *Adaptive Control*. Addison-Wesley, 1989.

K. J. Åström, T. Hägglund, C. C. Hang, and W. K. Ho. Automatic tuning and adaption for pid controllers - a survey. *Control Eng. Practice*, 1:699–714, 1993.

AI. Aalborg Industries A/S, Annual Report, 2006.

A. Amstutz and L. Guzzella. Control of diesel engines. *IEEE Control Systems Magazine*, 18(5):53–71, 1998.

S. Andersen and L. Jørgensen. Scheme for auto tuning control of marine boilers. Master's thesis, Aalborg University, June 2007.

M. Athans and P. L. Falb. *Optimal control : an introduction to the theory and its applications*. New York McGraw-Hill, 1966.

A. Bemporad and M. Morari. Control of systems integrating logic, dynamics, and constraints. *Automatica*, 35:407–427, 1999.

A. Bemporad, F. Borelli, and M. Morari. Piecewise linear optimal controlles for hybrid systems. In *American Control Conference*, pages 1190–1194, June 2000.

A. Bemporad, F. Borrelli, and M. Morari. On the optimal control law for linear discrete time hybrid systems. In *HSCC '02: Proceedings of the 5th International Workshop on Hybrid Systems: Computation and Control*, pages 105–119, London, UK, 2002a. Springer-Verlag.

A. Bemporad, A. Giua, and C. Seatzu. A master-slave algorithm for the optimal control of continuous-time switched affine systems. In *Proceedings of the IEEE Conference on Decision and Control*, volume 2, pages 1976–1981, 2002b.

A. Bemporad, M. Morari, V. Dua, and E. N. Pistikopoulos. The explicit linear quadratic regulator for constrained systems. *Automatica*, 38:3–20, 2002c.

A. Bemporad, M. Morari, and N. L. Ricker. MATLAB®: Model predictive control toolbox™ v. 2.2.3, 2006.

J. Bernussou, E. Granado, W. Colmenares, and G. Garcia. Dynamic output controller MPC via LMI. In *16th IFAC World Congress*, 2005.

R. Bitmead, M. Gevers, and V. Wertz. *Adaptive Optimal Control: The Thinking Man's GPC*. Prentice Hall International, 1990.

F. Borrelli, M. Baotic, A. Bemporad, and M. Morari. Dynamic programming for constrained optimal control discrete-time linear hybrid systems. *Automatica*, 41:1709–1721, 2005.

S. Boyd and L. Vandenberghe. *Convex Optimization*. Cambridge: Cambridge University Press, 2004.

S. Boyd, L. E. Ghaoui, E. Feron, and V. Balakrishnan. *Linear Matrix Inequalities in System and Control Theory*. Society for Industrial and Applied Mathematics (SIAM), 1994.

E. H. Bristol. On a new measure of interactions for multivariable process control. *IEEE Transactions on Automatic Control*, AC-II:133–134, 1966.

R. Cagienard, P. Grieder, E. C. Kerrigan, and M. Morari. Move blocking strategies in receding horizon control. *Journal of Process Control*, 17:563–570, 2007.

F. Casella and A. Leva. Modelica open library for power plant simulation: design and experimental validation. In *The 3rd International Modelica Conference*, pages 41–50, 2003.

K. L. Chien, E. I. Ergin, C. Ling, and A. Lee. Dynamics analysis of a boiler. *ASME Transactions*, 80:1809–1819, 1958.

L. Chisci, J. A. Rossiter, and G. Zappa. Systems with persistent disturbances: predictive control with restricted constraints. *Automatica*, 37:1019–1028, 2001.

D. Chmielewski and V. Manousiouthakis. On constrained infinite-time linear quadratic optimal control. *Systems & Control Letters*, 29:121–129, 1996.

J. Doyle and G. Stein. Multivariable feedback design: Concepts for a classical/modern synthesis. *IEEE Transactions on Automatic Control*, 26:4–16, 1981.

J. Doyle, B. Francis, and A. Tannenbaum. *Feedback Control Theory*. Macmillan Publishing Co., 1990.

G. E. Dullerud and F. Paganini. *A Course in Robust Control Theory: A Convex Approach*. Springer, 2000.

T. D. Eastop and A. McConkey. *Applied Thermodynamics for Engineering Technologists*. Addison Wesley Longman, 1993.

J. Eborn and K. J. Åström. Modeling of a boiler pipe with two-phase flow instabilities. In *Modelica Workshop*, pages 79–88, 2000.

M. Egerstedt, Y. Wardi, and H. Axelsson. Transition-time optimization for switched-mode dynamical systems. *IEEE Transactions on Automatic Control*, 51(1):110–115, 2006.

U. Forssell and L. Ljung. Closed-loop identification revisited. *Automatica*, 35:1215–1241, 1999.

G. F. Franklin, A. Emami-Naeini, and J. D. Powell. *Feedback Control of Dynamic Systems*. Addison-Wesley, 1994.

G. F. Franklin, J. D. Powell, and M. L. Workman. *Digital Control of Dynamic Systems*. Addison Wesley Longman, 1998.

E. Frazzoli. *Robust Hybrid Control for Autonomous Vehicle Motion Planning*. PhD thesis, MIT, June 2001.

E. Frazzoli, M. Dahleh, and E. Feron. A hybrid control architecture for aggressive maneuvering of autonomous helicopters. In *Proceedings of the 38th IEEE Conference on Decision and Control*, volume 3, pages 2471–2476, December 1999.

E. Gagnon, A. Pomerleau, and A. Desbiens. Simplified, ideal or inverted decoupling? *ISA Transactions*, 37:265–276, 1998.

P. J. Gaulart and E. C. Kerrigan. A convex formulation for receding horizon control of constrained discrete-time systems with guaranteed ℓ_2 gain. In *Proceedings of the 45th IEEE Conference on Decision & Control*, 2006.

A. Giua, C. Seatzu, and C. Van der Mee. Optimal control of switched autonomous linear systems. In *Proceedings of the IEEE Conference on Decision and Control*, volume 3, pages 2472–2477, 2001a.

A. Giua, C. Seatzu, and C. Van der Mee. Optimal control of autonomous linear systems switched with a pre-assigned finite sequence. In *IEEE International Symposium on Intelligent Control - Proceedings*, pages 144–149, 2001b.

M. S. Grewal and A. P. Andrews. *Kalman Filtering: Theory and Practice using* MATLAB® . John Wiley & Sons, 2001.

P. Grieder, F. Borrelli, F. Torrisi, and M. Morari. Computation of the constrained infinite time linear quadratic regulator. *Automatica*, 40:701–708, 2004.

M. E. Hangstrup. *Strategies for Industrial Multivariable Control - with Application to Power Plant Control*. PhD thesis, Aalborg University, Department of Control Engineering, Aalborg, Denmark, 1998.

F. Haugen. *Regulering av Dynamiske Systemer*. Tapir Forlag, 1994.

S. Hedlund and A. Rantzer. Optimal control of hybrid systems. In *Proceedings of the 38th IEEE Conference on Decision and Control*, volume 4, pages 3972–3977, 1999.

M. W. Hirsch, S. Small, and R. L. Devaney. *Differential Equations, Dynamical Systems & An Introduction to Chaos*, volume 60 of *Pure and Applied Mathematics*. Elsevier Academic Press, 2 edition, 2004.

H. Hjalmarsson. Iterative feedback tuning - an overview. *Int. J. Adapt. Control Signal Process*, 16:373–395, 2002.

P. U. Hvistendahl and B. Solberg. Modelling and multi variable control of a marine boiler. Master's thesis, Aalborg Universitet, Institute of Electronic Systems, Aalborg, Denmark, 2004.

J. P. Jensen, A. F. Kristensen, S. C. Sorenson, N. Houbak, and E. Hendricks. Mean value modelling of a small turbocharged diesel engine. *SAE Technical Paper Series*, No. 910070, 1991.

M. Jung and K. Glover. Control-oriented linear parameter-varying modelling of a turbocharged diesel engine. In *Proceedings of the IEEE Conference on Control Applications*, June 2003.

H. K. Khalil. *Nonlinear Systems*. Printice Hall, 3 edition, 2002.

H. Kim and S. Choi. A model on water level dynamics in natural circulation drum-type boilers. *International Communications in Heat Transfer*, 32:786–796, 2005.

I. Kolmanovsky and P. Moraal. Turbocharger modeling for automotive control applications. *SAE Technical Paper Series*, 1999-01-0908, March 1999.

M. V. Kothare, V. Balakrishnan, and M. Morari. Robust constrained model predictive control using linear matrix inequalities. *Automatica*, 32:1361–1379, 1996.

M. V. Kothare, B. Mettler, M. Morari, P. Bendotti, and C.-M. Falinower. Level control in the steam generator of a nuclear power plant. *IEEE Transactions on control system technology*, 8, No. 1:55–69, 2000.

M. Kvasnica, P. Grieder, and M. Baotić. Multi-parametric toolbox (MPT), 2004. URL `http://control.ee.ethz.ch/~mpt/`.

K. F. Larsen. *Dampkedler*. K.F. Bogteknik, 2001.

L. F. S. Larsen, T. Geyer, and M. Morari. Hybrid MPC in supermarket refrigeration systems. In *16th IFAC World Congress*, Prague, Czech Republic, 2005.

E. B. Lee and L. Markus. *Foundations of optimal control theory*. New York John Wiley & Sons, 1967.

J. M. Lee. *Introduction to Smooth Manifolds*, volume 218 of *Graduate Texts in Mathematics*. Springer-Verlag, 2006.

Y. S. Lee, W. H. Kwon, and O. K. Kwon. A constrained receding horizon control for industrial boiler systems. In G. Hencsey, editor, *IFAC Symposium on Manufacturing, Modeling, Management and Control (MIM 2000)*, pages 411–416, Patras, Greece, 2000.

H. C. Lim. Classical approach to bang-bang control of linear processes. *Industrial and Engineering Chemistry, Process Design and Development*, 8(3):9, 1969.

K.-V. Ling, J. Maciejowski, and B.-F. Wu. Multiplexed model predictive control. Technical report, Department of Engineering, University of Cambridge, UK, 2006.

L. Ljung. *System Identification, Theory for the user*. Pretice Hall, 1999.

W. L. Luyben. Distillation decoupling. *AIChE Journal*, 16:198–203, 1970.

J. M. Maciejowski. Asymptotic recovery for discrete-time systems. *IEEE Transactions on Automatic Control*, 30:602–605, 1985.

J. M. Maciejowski. *Predictive Control With Constraints*. Harlow: Pearson Education Limited, 2001.

J. M. Maciejowski. *Multivariable Feedback Design*. Addison-Wesley, 1989.

D. Q. Mayne, J. B. Rawlings, C. V. Rao, and P. O. M. Scokaert. Constrained model predictive control: Stability and optimality. *Automatica*, 36(6):789–814, June 2000.

D. Mignone. *Control and Estimation of Hybrid Systems with Mathematical Optimization*. PhD thesis, Swiss Federal Institute of Technology (ETH), January 2002.

Modelica. Web page of modelica, 2007. URL `http://www.modelica.org`.

T. Mølbak. *Optimering af Kedelregulering - Udvikling af adaptive og prædiktive strategier*. PhD thesis, Aalborg Universitetscenter, Institut for Elektroniske Systemer, Aalborg, Denmark, 1990.

J. H. Mortensen. *Kontrolstrategi til frigørelse af kraftværkers reguleringsevne*. PhD thesis, Aalborg Universitet, Institute of Energy Technology, Aalborg, Denmark, 1997.

J. H. Mortensen, T. Mølbak, P. Andersen, and T. S. Pedersen. Optimization of boiler control to improve the load-following capability of power-plant units. *Control Engineering Practice*, 6:1531–1539, 1998.

M. Müller, E. Hendricks, and S. C. Sorenson. Mean valve modelling of turbocharged spark ignition engines. *SAE Technical Paper Series*, 980784:125–145, February 1998.

K. R. Muske and J. B. Rawlings. Model predictive control with linear models. *AIChE Journal*, 39:262–287, 1993.

B. J. Odelson, A. Lutz, and J. B. Rawlings. The autocovariance least-squares method for estimating covariances: Application to model-based control of chemical reactors. *IEEE Transactions on Control Systems Technology*, 14:532–540, 2006a.

B. J. Odelson, M. R. Rajamani, and J. B. Rawlings. A new autocovariance least-squares method for estimating noise covariances. *Automatica*, 42:303–308, 2006b.

G. Pannocchia and J. B. Rawlings. Disturbance models for offset-free model-predictive control. *American Institute of Chemical Engineers, AIChE*, 49:426–437, 2003.

G. Pannocchia, N. Laachi, and J. B. Rawlings. A candidate to replace PID control: SISO-constrained LQ control. *American Institute of Chemical Engineers, AIChE*, 51:1178–1189, 2005.

F. H. Pedersen, C. M. S. Karstensen, and K. Christensen. AI control system - general description. Technical report, Aalborg Industries A/S, Aalborg, Denmark, 2003.

C. Pedret, A. Poncet, K. Stadler, A. Toller, A. H. Glattfelder, A. Bemporad, and M. Morari. Model-varying predictive control of a nonlinear system. Technical report, Automatic Control Laboratory, ETH - Swiss Federal Institute of Technology, Zürich, Switzerland, 2000.

G. Pellegrinetti and J. Bentsman. Nonlinear control oriented boiler modeling - a benchmark problem for controller design. *IEEE Transactions on Control Systems Technology*, 4:57–64, 1996.

R. B. Persson and B. V. Sørensen. Hybrid control of a compact marine boiler system. Master's thesis, Aalborg University, Institute of Electronic Systems, 2006.

S. J. Qin and T. A. Badgwell. An overview of industrial model predictive control technology. *AIChE Symposium Series*, 93:232–256, 1997.

S. J. Qin and T. A. Badgwell. A survey of industrial model predictive control technology. *Control Engineering Practice*, 11:733–764, 2003.

C. V. Rao, S. J. Wright, and J. B. Rawlings. Application of interior-point methods to model predictive control. *Journal of Optimization Theory and Applications*, 99: 723–757, 1998.

J. B. Rawlings and K. R. Muske. The stability of constrained receding horizon control. *IEEE Transactions on Automatic Control*, 38:1512–1516, 1993.

P. Riedinger, C. Zanne, and F. Kratz. Time optimal control of hybrid systems. In *Proceedings of the American Control Conference*, volume 4, pages 2466–2470, 1999.

J. E. Rijnsdorp. Interaction in two-variable control systems for distillation columns - I. *Automatica*, 1:15–28, 1965.

J. Rossiter, P. Neal, and L. Yao. Applying predictive control to a fossil-fired power station. *Transactions of the Institute of Measurement and Control*, 24:177.194, 2002.

J. A. Rossiter. *Model-based Predictive Control: A Practical Approach*. CRC Press LLC, 2003.

C. Rowe and J. M. Maciejowski. Tuning robust model predictive controllers using LQG/LTR. In *14th IFAC World Congress*, Beijing, P.R. China, 1999.

A. Saberi, B. M. Chen, and P. Sannuti. *Loop Transfer Recovery: Analysis and Design*. Springer-Verlag, London, 1993.

D. Sarabia, C. de Prada, S. Cristea, and R. Mazaeda. Hybrid model predictive control of a sugar end section. In *European Symposium on Computer Aided Process Engineering, ESCAPE 16*, 2005.

H. I. H. Saravanamuttoo, G. F. C. Rogers, and H. Cohen. *Gas Turbine Theory*. Prentice Hall, 5 edition, January 2001.

P. O. M. Scokaert and J. B. Rawlings. Constrained linear quadratic regulation. *IEEE Transactions on Automatic Control*, 43(8):7, August 1998.

C. Seatzu, D. Corona, A. Giua, and A. Bemporad. Optimal control of continuous-time switched affine systems. *IEEE Transactions on Automatic Control*, 51(5):726–741, May 2006.

R. Sekhon, H. Bassily, J. Wagner, and J. Gaddis. Stationary gas turbines – a real time dynamic model with experimental validation. In *American Control Conference*, Minneapolis, Minnesota, USA, 2006.

R. A. Serway and R. J. Beichner. *Physics for Scientists and Engineers with Modern Physics*. Saunders College Publishing, 2000.

S. Skogestad. Simple analytic rules for model reduction and PID controller tuning. *Journal of Process Control*, 13:291–309, 2003.

S. Skogestad and I. Postlethwaite. *Multivariable Feedback Control: Analysis and Design*. Chichester: John Wiley & Sons Ltd, 1996.

R. S. Smith. Model predictive control of uncertain constrained linear systems; LMI-based methods. Technical report, Department of Engineering, University of Cambridge, UK, 2006.

B. Solberg, C. M. S. Karstensen, and P. Andersen. Control properties of bottom fired marine boilers. In T. Gundersen, editor, *ECOS 2005 Conference*, volume 2, pages 669–678, Trondhjem, Norway, 2005a.

B. Solberg, C. M. S. Karstensen, P. Andersen, T. S. Pedersen, and P. U. Hvistendahl. Model-based control of a bottom fired marine boiler. In P. Horacek, editor, *16th IFAC World Congress*, Prague, Czech Republic, 2005b.

B. Solberg, P. Andersen, and J. Stoustrup. Advanced water level control in a one-pass smoke tube marine boiler. Technical report, Department of Electronic Systems, Aalborg University, Aalborg, Denmark, 2007a.

B. Solberg, C. M. S. Karstensen, and P. Andersen. Control properties of bottom fired marine boilers. *Energy*, 32:508–520, 2007b.

B. Solberg, P. Andersen, J. M. Maciejowski, and J. Stoustrup. Hybrid model predictive control applied to switching control of burner load for a compact marine boiler design. In D. D. Cho, editor, *17th IFAC World Congress*, Seoul, Korea, 2008a.

B. Solberg, P. Andersen, J. M. Maciejowski, and J. Stoustrup. Optimal switching control of burner setting for a compact marine boiler design. Submitted March 2008 for journal publication, 2008b.

B. Solberg, P. Andersen, and J. Stoustrup. Modelling and control of a turbocharged burner unit. In *ECOS 2008 Conference*, volume 2, pages 887–903, Kraków, Poland, 2008c.

B. Solberg, P. Andersen, and J. Stoustrup. The one-pass smoke tube marine boiler - limits of performance. In *ECOS 2008 Conference*, volume 2, pages 867–885, Kraków, Poland, 2008d.

B. Solberg, P. Andersen, and J. Stoustrup. Optimal switching strategy for systems with discrete inputs using a discontinuous cost functional. Submitted March 2008 for publication in International Journal of Control, 2008e.

E. D. Sontag. *Mathematical control theory : deterministic finite dimensional systems*. New York Springer, 1998.

K. Sørensen. *Dynamic Boiler Performance - modelling, simulating and optimizing boilers for dynamic operation*. PhD thesis, Aalborg Universitet, Institute of Energy Technology, Aalborg, Denmark, 2004.

K. Sørensen, C. M. S. Karstensen, T. Condra, and N. Houbak. Optimizing the integrated design of boilers - simulation. In R. Rivero, editor, *Efficiency, Costs, Optimization, Simulation and Environmental Impact of Energy Systems (ECOS 2004)*, volume 3, pages 1399–1410, Guanajuato, Mexico, 2004.

Spirax. Spirax sarco, steam engineering tutorials, 2007. URL `http://www.spiraxsarco.com/resources/steam-engineering-tutorials.asp`.

F. D. Torrisi and A. Bemporad. Hysdel - a tool for generating computational hybrid models for analysis and synthesis problems. *IEEE Transactions on Control Systems Technology*, 12:235–249, 2004.

K. Tsuda, D. Mignone, G. Ferrari-Trecate, and M. Morari. Reconfiguration strategies for hybrid systems. Technical Report AUT00-24, Automatic Control Laboratory, ETH Zurich, 2000.

P. M. J. Van den Hof and R. J. P. Schrama. Identification and control - closed-loop issues. *Automatica*, 31:1751–1770, 1995.

E. T. van Donkelaar and P. M. J. Van den Hof. Analysis of closed-loop identification with a tailor-made parametrization. *European Journal of Control*, 1999.

A. N. Venkat. *Distributed Model Predictive Control: Theory and Applications*. PhD thesis, University of Wisconsin–Madison, 2006.

E. Verriest, M. Egerstedt, Y. Wardi, and M. Boccadoro. Optimal control of switching surfaces in hybrid dynamical systems. *Discrete Event Dynamic Systems*, 14(4):433–448, 2005.

H. L. Wade. Inverted decoupling: a neglected technique. *ISA Transactions*, 36:3–10, 1997.

X. Xuping and P. Antsaklis. Quadratic optimal control problems for hybrid linear autonomous systems with state jumps. In *Proceedings of the American Control Conference*, volume 4, pages 3393–3398, 2003.

Z. Zang, R. R. Bitmead, and M. Gervers. Iterative weighted least-squares identification and weighted LQG control design. *Automatica*, 31:1577–1594, 1995.

K. Zhou, J. Doyle, and K. Glover. *Robust and Optimal Control*. New Jersey: Prentice-Hall, Inc, 1996.

Y. Zhu and F. Butoyi. Case studies on closed-loop identification for MPC. *Control Engineering Practice*, 10:403–417, 2002.

Papers

Paper A

Modelling and Control of a Turbocharged Burner Unit

Brian Solberg & Palle Andersen & Jakob Stoustrup

The paper has been published in:
Proceedings of the 21st International Conference on Efficiency, Cost, Optimization, Simulation and Environmental Impact of Energy Systems (ECOS 2008),
June 24–27, 2008, Kraków, Poland

Abstract

This paper concerns modelling and control of a novel turbocharged burner unit developed for small-scale industrial and marine boilers. The burner consists of a gas turbine mounted on a furnace. The burner has two inputs; oil flow to the gas generator (gas turbine combustion chamber) and oil flow to the furnace, and two outputs; power and oxygen percentage in the exhaust gas. The control objective of the burner unit is to deliver the requested power set by e.g. an outer pressure loop while keeping a clean combustion and optimising efficiency. A first principle model is derived and validated against preliminary test data. The preliminary test shows that the model is capable of capturing the important dynamics of the burner unit while more testing is required to determine the reason for discrepancies in gains. An analysis of the model shows that both dynamics and gains change remarkably over the entire load range. However, local linearised models of low order can be derived and used in a subsequent controller design. Also, the model includes an inverse response (non-minimum phase zero) from the gas generator oil flow to the controlled oxygen level. This means that when changing the oil flow to the gas generator, the oxygen level initially moves in the opposite direction before it moves in the long term direction. A control strategy based on a nonlinear feedforward and a linear feedback controller, adjusting the ratio between the oil flow to the gas generator and to the furnace, is proposed. The feedforward is calculated from an inverse mapping of the requested power output to find the two stationary oil flows while respecting oxygen constraints. Simulation results gathered from the developed nonlinear model with added noise and external disturbances illustrate the efficiency of the proposed control strategy.

1 Introduction

Most burners, shipped with industrial and marine boilers today, are equipped with a fan to supply the combustion with air. Such fans consume considerable amounts of electric power and produce noise. Further, to achieve a high turndown ratio using a conventional burner, more than one atomiser is needed. The burner considered in this paper is a two stage burner in which the first stage drives a gas turbine and the second stage is a conventional furnace burner. This concept has multiple advantages over the aforementioned fan concept. First of all burner efficiency is high as there is no longer a need for electrical fan actuation. Further, the turndown ratio is increased in the way that the gas turbine can operate alone (however, this operation mode is not very thermodynamically efficient). Finally, the gas turbine concept increases the gas velocity through the boiler convection part which leads to a higher heat transfer to the metal.
However, this new burner concept requires a more comprehensive control strategy than the conventional burners to maximise efficiency and keep a clean combustion to e.g. minimise the amount of pollutant expelled from the funnel. This factor is especially

important when the burner is installed on ship boilers as large penalties are assigned to shipowners if the smoke coming out of the stacks is too harmful to the environment.
The control problem is complicated by the high degree of nonlinearities in the system and further, the process exhibits an inverse response from the gas generator (gas turbine combustion chamber) fuel injection to the flue gas oxygen level which is used as a parameter for clean combustion.
In relation to the automotive industry many people have addressed modelling and control of turbocharged diesel engines – see e.g. [Jensen et al., 1991; Jung and Glover, 2003; Kolmanovsky and Moraal, 1999; Müller et al., 1998]. From these works, results on the turbocharger modelling can be used. There is obviously a resemblance between the setup presented in this paper and the gas turbine found on power plants and combined cycle power plants. A model of a stationary gas turbine can be found in [Sekhon et al., 2006].
We derive a model based on first principles rather than using system identification techniques to specify a black box model based on e.g. linear parametric models. This technique is adopted as these models tend to be valid over a wider operating range. The goal is to derive a lumped parameter model that reflects the burner dynamics as well as possible from knowledge of the system behaviour and measurement. This approach is also taken to achieve insight to the burner process. Further, a detailed model like this will be of great value as a simulation platform for controller designs. Model verification experiments have been performed at Aalborg Industries' (AI) test centre.
Regarding controller design, principles such as traditional selector and ratio control of burners can be used – see e.g. [Åström and Hägglund, 2006]. However, many other methods exist and especially model predictive control (MPC) [Maciejowski, 2001; Qin and Badgwell, 2003; Rossiter, 2003] is an interesting candidate as it can naturally handle constraints on inputs and state variables. However, in this paper we focus on the control properties of the burner unit and therefore stick with traditional selector and ratio control with a nonlinear feedforward from setpoint changes.
We show that even though the process is nonlinear and includes inverse responses, a simple ratio controller can control the process. However, if more advanced control methods are to be used it is expected to be necessary to handle the nonlinearities in the control setup.
The paper is organised as follows: First a short system description is given and assumptions made for modelling purposes are presented. Leading is the model derivation followed by a discussion of the control properties. Subsequently the control strategy is described, simulation results presented and conclusions and future work are discussed.

2 System Description

A sketch of the burner unit is shown in Figure 1, and the functionality is explained below.

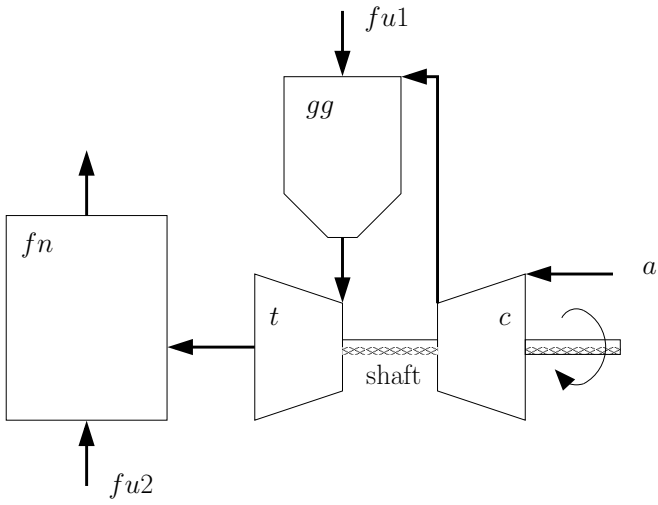

Figure 1: Drawing of the turbocharged burner system. c is the compressor, t is the turbine, gg is the gas generator (the first combustion chamber) and fn is the furnace (the second combustion chamber). a is the fresh air inlet, and $fu1$ and $fu2$ are the fuel inputs.

The units c, t and gg comprise the gas turbine. Fuel, $fu1$, is injected and burned in the gas generator, gg, and the hot gas leaving the combustion drives the turbine, t, which rotates the shaft of the turbocharger delivering power to drive the compression process in the compressor, c. Air is sucked in at the compressor inlet, and the hot combustion flue gas leaves the turbine to enter the second combustion chamber, the furnace, fn. Here fuel is added again, $fu2$, and another combustion takes place. More than 70% of the total fuel flow is injected into the furnace. The hot flue gas leaves the furnace and enters the boiler convection part before leaving through the funnel.
Before proceeding to the model derivation we set up some general assumptions to simplify the modelling process. These assumptions are listed and explained below.

Assumption 2.1. *The ambient pressure is constant.*

The pressure in the engine room on a ship may vary. This will influence the pressure ratio across the compressor as inlet air is taken from the engine room. However, the setup concerned in this project is situated on shore in a test centre where ventilation is expected to cause negligible pressure variations.

Assumption 2.2. *The metal part separating the flue gas and the water-steam part consists of one piece of metal with the same temperature.*

This assumption is justified by the fact that most boilers include a pressure control

loop keeping the pressure around a constant reference value, e.g. $8\mathrm{bar}$, meaning that temperature variations are small.

Assumption 2.3. *All energy losses in the system leave through the funnel.*

This assumption is made because losses in terms of heat are negligible compared to the total amount of energy supplied to the system. A rough estimate of the relative heat losses was shown in [Persson and Sørensen, 2006] to be < 0.0002 per thousand. Furthermore, no friction losses from the shaft of the turbocharger are considered.

Assumption 2.4. *The pressure in the furnace is equal to the ambient pressure.*

Measurement performed over the convection part of the test boiler showed a pressure loss of about $9000\mathrm{Pa}$ which is small compared to the range of operation. The ambient pressure assumption is included to have consistency in the model; no fuel and air flow $\Rightarrow$ no flue gas flow.

Assumption 2.5. *The conditions in the control volumes are homogeneous.*

This assumption reflects the earlier statement that we are constructing a lumped parameter model. Furthermore, we will use a backwards place discretisation. The reason for this is that using for instance a bilinear place discretisation method introduces unwanted right half plane zeros in a linear model [Hvistendahl and Solberg, 2004].

Assumption 2.6. *The specific heat capacity, $c_{p,f}$, and molar mass, M_f, of the flue gas throughout the process are assumed to be constant.*

An analysis of the flue gas carried out in [Hvistendahl and Solberg, 2004] justifies this assumption. In general we do not know M_f. To find this we would have to make use of both a mass balance and a mole balance to find $M_f = \frac{m}{n}$. However, as the analysis of the flue gas in [Hvistendahl and Solberg, 2004] shows; the molar mass of the flue gas even after as stoichiometric combustion is approximately equal to that of atmospheric air. Therefore, we assume a constant molar mass of the flue gas.

Assumption 2.7. *The flue gas can be viewed as an ideal gas.*

The reference level for the enthalpy is set to $T_0 = 273.15\mathrm{K}$ or $0^\circ\mathrm{C}$, however, all temperatures are kept in kelvin ($T[\mathrm{K}]$). The reason for this choice is that many of the specific heat capacity data are only available from $0^\circ\mathrm{C}$ and up.

2.1 Modelling

The modelling is divided into two main sections: one dealing with the thermodynamic properties of the gas turbine and furnace system and another dealing with the oxygen balance. In Figure 2 the gas turbine is presented in a schematic diagram useful for modelling purposes. Attempts have been made to include the four ducts indicated on the figure in the model. This was done by using Euler equations including friction losses. However, the result of modelling these ducts did not contribute to the validity of the resulting model and will be omitted here.

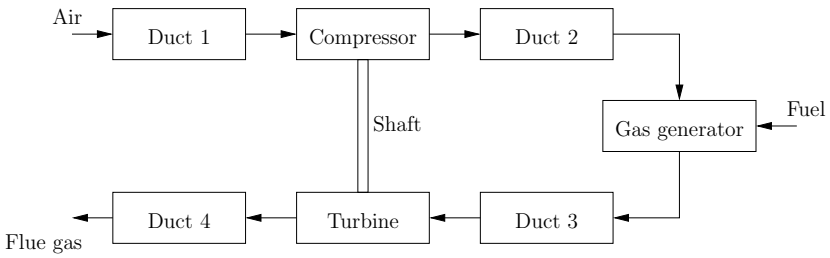

Figure 2: Schematic diagram showing the interconnection of the components that make up the gas turbine.

2.2 Turbocharger Model

There exists a lot of literature concerning mean values modelling of turbocharged engines. The results from this can be applied to this burner unit. Furthermore, the book [Saravanamuttoo et al., 2001] provides a good reference on turbo machinery.
Most of the modelling in this section is based on results from [Amstutz and Guzzella, 1998; Jung and Glover, 2003; Kolmanovsky and Moraal, 1999; Müller et al., 1998]. As mentioned above, heat losses are neglected, and it is assumed that the processes in the compressor and turbine can be viewed as adiabatic reversible compression and expansion respectively. Such processes are called isentropic and have the following properties useful for the model derivation:

Properties of isentropic processes For an ideal gas undergoing an isentropic process, the following relationship is valid [Eastop and McConkey, 1993]:

$$\left(\frac{T_{o_{is}}}{T_i}\right) = \left(\frac{p_o}{p_i}\right)^{\frac{\gamma-1}{\gamma}} \tag{1}$$

where T_i is the inlet temperature of the working fluid, $T_{o_{is}}$ is the outlet temperature under isentropic conditions. p_i and p_o are the inlet and outlet pressure respectively and the adiabatic index $\gamma = \frac{c_p}{c_v} = \frac{c_p}{c_p - \frac{R}{M_f}}$ where $R = M_f(c_p - c_v)$ also known as the ideal gas constant.

Compressor model

To account for the compressor not being ideal in reality, we introduce the compressor isentropic efficiency $0 \leq \eta_c \leq 1$ as the ratio between theoretical isentropic temperature rise and actual temperature rise, [Eastop and McConkey, 1993]:

$$\eta_c = \frac{T_{o_{is},c} - T_{i,c}}{T_{o,c} - T_{i,c}} \tag{2}$$

Equations (1) and (2) can be combined to find an expression for the temperature at the compressor outlet:

$$T_{o,c} = T_{i,c}\left(1 + \frac{1}{\eta_c}\left[\left(\frac{p_{o,c}}{p_{i,c}}\right)^{\frac{\gamma-1}{\gamma}} - 1\right]\right) \tag{3}$$

A common assumption when working with compressor and turbine units is to regard them as steady state steady flow processes (SSSF). The mass in the compressor and turbine is relative low compared to the mass flow rate due to the small compressor and turbine volume. Hence mass, temperature and pressure are all assumed to change instantly with changing inlet conditions rendering the dynamics negligible.
This means that the mass balance for the compressor is given as:

$$0 = \frac{dm_c}{dt} = \dot{m}_{i,c} - \dot{m}_{o,c} \tag{4}$$

Furthermore, the energy balance can be written as:

$$\begin{aligned} 0 &= \frac{d(m_c c_{p,f}(T_{o,c} - T_0) - p_c V_c)}{dt} \\ &= \dot{m}_{i,c} c_{p,f}(T_{i,c} - T_0) - \dot{m}_{o,c} c_{p,f}(T_{o,c} - T_0) + P_c \end{aligned} \tag{5}$$

where P_c is the power delivered from the shaft to the compressor, which, using Equations (4) and (5) can be expressed as:

$$P_c = \dot{m}_c c_{p,f}(T_{o,c} - T_{i,c}) \tag{6}$$

where $\dot{m}_c = \dot{m}_{i,c} = \dot{m}_{o,c}$. Now inserting (3) into this expression gives:

$$P_c = \dot{m}_c c_{p,f} T_{i,c} \frac{1}{\eta_c}\left[\left(\frac{p_{o,c}}{p_{i,c}}\right)^{\frac{\gamma-1}{\gamma}} - 1\right] \tag{7}$$

Turbine model

The turbine in the turbocharger is a fixed geometry turbine (FGT). As in case of the compressor we start by introducing the turbine isentropic efficiency $0 \leq \eta_t \leq 1$ as the ratio between actual temperature drop and theoretical isentropic temperature drop, [Eastop and McConkey, 1993]:

$$\eta_t = \frac{T_{i,t} - T_{o,t}}{T_{i,t} - T_{o_{is},t}} \tag{8}$$

Using Equations (1) and (8) an expression for the temperature at the turbine outlet can be found:

$$T_{o,t} = T_{i,t}\left(1 - \eta_t\left[1 - \left(\frac{p_{o,t}}{p_{i,t}}\right)^{\frac{\gamma-1}{\gamma}}\right]\right) \tag{9}$$

The mass and energy balances for the turbine are equivalent to those of the compressor, except that the work done by the turbine is positive so that energy is transferred from the turbine by means of work. This means that we can find an expression for the power absorbed in the shaft from the turbine:

$$P_t = \dot{m}_t c_{p,f}(T_{i,t} - T_{o,t}) \tag{10}$$

where $\dot{m}_t = \dot{m}_{i,t} = \dot{m}_{o,t}$. Inserting (9) we get:

$$P_t = \dot{m}_t c_{p,f} T_{i,t} \eta_t \left[1 - \left(\frac{p_{o,t}}{p_{i,t}}\right)^{\frac{\gamma-1}{\gamma}}\right] \tag{11}$$

Shaft model

The model of the shaft connecting the compressor and turbine has the purpose of describing the turbocharger speed, ω. This can be done by considering the energy balance for the shaft. The kinetic energy for the shaft is:

$$U_{kin} = \frac{1}{2} I \omega^2 \tag{12}$$

where I is the inertia of the rotating parts. Hence the energy balance is given as:

$$I\omega \frac{d\omega}{dt} = \eta_m P_t - P_c - P_f \tag{13}$$

where P_f is a friction term, which is assumed to be negligible compared to the power delivered by the turbine and the power it takes to drive the compressor. Furthermore, the mechanical efficiency, η_m, is set to 1 below. So inserting the compressor and turbine power terms from (7) and (11), the model for the shaft becomes:

$$\underbrace{\frac{1}{I\omega}}_{f_{33}} \frac{d\omega}{dt} = \underbrace{\frac{\dot{m}_t c_{p,f} T_{i,t} \eta_t \left[1 - \left(\frac{p_{o,t}}{p_{i,t}}\right)^{\frac{\gamma-1}{\gamma}}\right] - \dot{m}_c c_{p,f} T_{i,c} \frac{1}{\eta_c} \left[\left(\frac{p_{o,c}}{p_{i,c}}\right)^{\frac{\gamma-1}{\gamma}} - 1\right]}{I\omega}}_{h_3} \tag{14}$$

This is the equation governing the turbocharger dynamics.

Turbocharger data sheets

We still need to find expressions for the flow through the compressor and turbine as well as expressions for the efficiency of these components. An overview of different methods for deriving such can be found in [Kolmanovsky and Moraal, 1999]. Some are partly based on first principle and others are functions derived from curve fitting techniques. The parameters in both approaches are estimated from turbine and compressor maps. These can be acquired from the turbocharger manufacturer.

Usually the flow and speed data are scaled to make the maps independent of the inlet conditions (p_i, T_i). The scaling is done according to:

$$\dot{\tilde{m}} = \frac{\dot{m}\sqrt{T_i}}{p_i} \left[\frac{\frac{\mathrm{kg}}{\mathrm{s}}\sqrt{\mathrm{K}}}{\mathrm{MPa}} \right], \quad \tilde{N} = \frac{\omega}{2\pi\sqrt{T_i}} \left[\frac{1}{\mathrm{s}\sqrt{\mathrm{K}}} \right] \tag{15}$$

where $\tilde{N}$ is scaled rotations per second. The dependency of the speed and pressure ratios on the flow and efficiency of the compressor and turbine are:

$$\begin{bmatrix} \dot{m}_c \\ \eta_c \end{bmatrix} = g_c \left(\omega, \frac{p_{o,c}}{p_{i,c}} \right), \quad \begin{bmatrix} \dot{m}_t \\ \eta_t \end{bmatrix} = g_t \left(\omega, \frac{p_{o,t}}{p_{i,t}} \right) \tag{16}$$

As discussed in [Kolmanovsky and Moraal, 1999], it is not always easy to find a function g_c, for the compressor map, having flow as output. An alternative mapping for the compressor is possible [Kolmanovsky and Moraal, 1999]:

$$\begin{bmatrix} \frac{p_{o,c}}{p_{i,c}} \\ \eta_c \end{bmatrix} = g_c' \left(\omega, \dot{m}_c \right) \tag{17}$$

Knowledge of the flow can be gained by introducing a control volume corresponding to the manifold connecting the compressor and the gas generator. Using the one-dimensional momentum balance for this control volume gives:

$$\frac{p_{gg} - p_{o,c}}{\rho_c} + gz\cos(\theta) + \frac{dv_c}{dt} z = -h_t(v_c) \tag{18}$$

The compressor mass flow can be found as $\dot{m}_c = \rho_c A v_c$, where A is the diameter of the pipe. This corresponds to using "Model II" in [Kolmanovsky and Moraal, 1999] . This approach has the advantages of allowing for modelling of the pressure drop over the gas generator inlet duct. However, as described in [Kolmanovsky and Moraal, 1999] the new differential equation increases model stiffness.
In this work we will use the mappings shown in (16). The data available for the turbocharger used are limited. For this reason we use a method for approximating the mappings g_c and g_t which is partly based on physical insight instead of e.g. parameterising the data by using regression to fit some polynomial model or train a neural network model. The advantage of this is that the extrapolation of data tends to give better predictions.

Compressor

The method used to describe the compressor flow and efficiency is described in [Jensen et al., 1991]. This is the method investigated in [Kolmanovsky and Moraal, 1999] performing the best when the output is flow and efficiency. Whereas the neural network approach seems to be superior for the alternative model, in [Persson and Sørensen, 2006]

the problems using a neural network model for the compressor unit under consideration was illustrated.
Expressing the enthalpy for the gas undergoing the compression as $h_{i,c} = c_{p,f}T_{i,c}$ and $h_{o,c} = c_{p,f}T_{o,c}$ for the inlet and outlet respectively, we can write Equation (6) as:

$$P_c = \dot{m}_c(h_{o,c} - h_{i,c}) = \dot{m}_c \Delta h_c \tag{19}$$

Using Equation (7) we find the following relation between the enthalpy change and the pressure ratio over the compressor:

$$\Delta h_c = c_{p,f}T_{i,c}\frac{1}{\eta_c}\left[\left(\frac{p_{o,c}}{p_{i,c}}\right)^{\frac{\gamma-1}{\gamma}} - 1\right] \tag{20}$$

Looking at the ideal case $\eta_c = 1$, $\Delta h_{c,ideal}$ can be estimated from Euler's equation for turbomachinery. For this purpose we consider a compressor with radially inclined impeller blades, no pre-whirl and no backsweep [Eastop and McConkey, 1993, p. 372-375]:

$$\Delta h_{c,ideal} = U_o C_{wo} - U_i C_{wi} \tag{21}$$

where U_o is the blade speed at the impeller tip, C_{wo}, is the tangential component of the gas velocity (whirl) leaving the impeller, U_i is the velocity of the impeller at the impeller entry and C_{wi} is the tangential component of the gas velocity entering the impeller. However, as we have assumed no pre-whirl $C_{wi} = 0$ and hence

$$\Delta h_{c,ideal} = U_o C_{wo} = U_c C_c \tag{22}$$

In practice, the whirl velocity C_c is different from the ideal $C_{c,ideal} = U_c$ due to inertia of air trapped between blades. This is known as slip, and

$$\sigma = \frac{C_c}{U_c} \tag{23}$$

is known as the slip factor. Hence:

$$\Delta h_{c,ideal} = \sigma U_c^2 \tag{24}$$

The slip factor is dependent on the mass flow rate through the compressor, meaning that the compressor pressure ratio is a function of both turbocharger speed and mass flow. The ratio between the ideal and actual enthalpy changes across the compressor is the compressor efficiency.

$$\eta_c = \frac{\Delta h_{c,ideal}}{\Delta h_c} \tag{25}$$

Using Equation (20) we have:

$$\Delta h_{c,ideal} = c_{p,f}T_{i,c}\left[\left(\frac{p_{o,c}}{p_{i,c}}\right)^{\frac{\gamma-1}{\gamma}} - 1\right] \tag{26}$$

[Jensen et al., 1991] uses these physical considerations with some empirical assumptions to derive a model for the efficiency and mass flow. They first define the dimensionless parameter Ψ, also known as the temperature coefficient or the blade loading coefficient, which is closely related to the slip factor (and the inverse square of the blade speed ratio as defined later for the turbine), as:

$$\Psi = \frac{c_{p,f} T_{i,c} \left[\left(\frac{p_{o,c}}{p_{i,c}}^{\frac{\gamma-1}{\gamma}} - 1 \right) \right]}{\frac{1}{2} U_c^2} \tag{27}$$

where $U_c = \frac{1}{2} D_c \omega$. The normalised compressor flow rate, Φ, or flow coefficient is defined as:

$$\Phi = \frac{\dot{m}_c}{\rho_a \frac{\pi}{4} D_c^2 U_c} \tag{28}$$

and the inlet Mach number M is:

$$M = \frac{U_c}{\sqrt{\gamma \frac{R}{M_f} T_{i,c}}} \tag{29}$$

The normalised flow and the compressor efficiency are assumed to be functions of Ψ and M:

$$\Phi = \frac{k_3 \Psi - k_1}{k_2 + \Psi}, \quad k_i = k_{i1} + k_{12} M, \quad i = 1, 2, 3 \tag{30}$$

$$\eta_c = a_1 \Phi^2 + a_2 \Phi + a_3, \quad a_i = \frac{a_{i1} + a_{i2} M}{a_{i3} - M}, \quad i = 1, 2, 3 \tag{31}$$

And now

$$\dot{m}_c = \Phi \rho_a \frac{\pi}{4} D_c^2 U_c \tag{32}$$

The method described in [Müller et al., 1998], based on physical insight as well, was also investigated. This method proposes a parametrisation of the enthalpy in (26) using the blade speed and the mass flow. However, the method seems not to be applicable for the compressor at hand and gives a poorer fit than the method described above.

Turbine

Euler's equations can also be used for the turbine, noting that by assuming no swirl at the turbine outlet the tangential component of the gas velocity at the outlet becomes zero, $C_{wt} = 0$. The rest of the equations follow the same lines as for the compressor. However, for the turbine we use a different method for modelling flow and efficiency. Following [Kolmanovsky and Moraal, 1999] we model the flow through the turbine as the flow through nozzles (or diffusers). The well known flow equations are [Saravanamuttoo et al., 2001, p. 449-451]

$$\dot{m}_t = A_t \frac{p_{i,t}}{\sqrt{T_{i,t} R}} \sqrt{\frac{2\gamma}{\gamma - 1} \left[\Pi^{\frac{2}{\gamma}} - \Pi^{\frac{\gamma+1}{\gamma}} \right]} \tag{33}$$

where

$$\Pi = \max(\Pi_t, \Pi_{crit}) = \max(\frac{p_{o,t}}{p_{i,t}}, \Pi_{crit}) \tag{34}$$

Here the critical pressure ratio is: $\Pi_{crit} = \frac{2}{\gamma+1}^{\frac{\gamma}{\gamma-1}}$. A_t is the effective flow area. This is assumed to be a function of the turbocharger speed and the pressure ratio over the turbine given as:

$$A_t(\tilde{N}, \frac{p_{o,t}}{p_{i,t}}) = a_2(\tilde{N}) \left(\frac{p_{o,t}}{p_{i,t}}\right)^2 + a_1(\tilde{N})\frac{p_{o,t}}{p_{i,t}} + a_0(\tilde{N}) \tag{35}$$

where

$$a_i(\tilde{N}) = a_{2i}\tilde{N}^2 + a_{1i}\tilde{N} + a_{0i} \tag{36}$$

this form is not standard but found to be a better fit than the suggestion in [Kolmanovsky and Moraal, 1999].
According to [Kolmanovsky and Moraal, 1999] the efficiency can be modelled as a function of the blade speed ratio:

$$\frac{U_t}{C_t} = \frac{\frac{1}{2}D_t\omega}{\sqrt{2c_pT_{i,t}\left(1 - \left(\frac{p_{o,t}}{p_{i,t}}\right)^{\frac{\gamma-1}{\gamma}}\right)}} \tag{37}$$

where U_t is the velocity of the blade speed at the point where the flow enters, and C_t is the tangential component of the air velocity at the entry to the turbine rotor. The efficiency is then parameterised as:

$$\eta_t = b_2(\tilde{N}) \left(\frac{U_t}{C_t}\right)^2 + b_1(\tilde{N})\frac{U_t}{C_t} + b_0(\tilde{N}) \tag{38}$$

where

$$b_i(\tilde{N}) = b_{1i}\tilde{N} + b_{0i} \tag{39}$$

2.3 Gas Generator Combustion Model

In this paragraph a model used for the combustion taking place in the gas generator is described. The idea is to calculate the adiabatic flame temperature. The approach taken is to construct an artificial infinitesimal combustion control volume. The mass balance for such a control volume is given as:

$$\dot{m}_{cb,gg} = \dot{m}_c + \dot{m}_{fu1} \tag{40}$$

here $\dot{m}_c$ and $\dot{m}_{fu1}$ is the air flow and fuel supplied to the combustion, and $\dot{m}_{cb,gg}$ is the mass flow of the flue gas leaving the combustion. Likewise the energy balance is given as:

$$\dot{m}_{cb,gg}h_{cb,gg} = \dot{m}_c h_c + \dot{m}_{fu1}(h_{fu} + H_{fu}) \tag{41}$$

where h_c, h_{fu1} and $h_{cb,gg}$ are the specific enthalpies of the inflowing and outflowing fluids, and H_{fu} is the calorific value for the fuel. Rearranging to isolate $h_{cb,gg}$ gives:

$$h_{cb,gg} = \frac{\dot{m}_c h_c + \dot{m}_{fu1}(h_{fu} + H_{fu})}{\dot{m}_{cb,gg}} \tag{42}$$

Inserting $h = c_{p,f}(T - T_0)$ gives:

$$T_{cb,gg} = \frac{\dot{m}_c c_{p,f}(T_c - T_0) + \dot{m}_{fu1}(c_{p,fu}(T_{fu} - T_0) + H_{fu})}{\dot{m}_{cb,gg} c_{p,f}} + T_0 \tag{43}$$

2.4 Gas Generator Model

The gas generator is treated as one control volume. The mass balance for the gas generator is given as:

$$\frac{dm_{gg}}{dt} = V_{gg}\frac{d\rho_{gg}}{dt} = \dot{m}_{i,gg} - \dot{m}_{o,gg} = \dot{m}_{cb,gg} - \dot{m}_t \tag{44}$$

where V_{gg} is the volume of the gas generator and ρ_{gg} is the density of the flue gas in the gas generator. m_{gg} is the mass of flue gas in the volume which can be expressed in terms of temperature and pressure through the ideal gas equation:

$$m_{gg} = V_{gg}\rho_{gg}, \;\; \rho_{gg} = \frac{p_{gg}M_f}{RT_{gg}} \tag{45}$$

where T_{gg} is the temperature in the gas generator and p_{gg} is the pressure. The derivative of ρ_{gg} is:

$$\frac{d\rho_{gg}}{dt} = \left(\frac{M_f}{RT_{gg}}\right)\frac{dp_{gg}}{dt} - \left(\frac{p_{gg}M_f}{RT_{gg}^2}\right)\frac{dT_{gg}}{dt} \tag{46a}$$

$$= \frac{\rho_{gg}}{p_{gg}}\frac{dp_{gg}}{dt} - \frac{\rho_{gg}}{T_{gg}}\frac{dT_{gg}}{dt} \tag{46b}$$

Substituting into (44) gives:

$$\underbrace{\frac{1}{p_{gg}}}_{f_{11}}\frac{dp_{gg}}{dt} \underbrace{- \frac{1}{T_{gg}}}_{f_{12}}\frac{dT_{gg}}{dt} = \underbrace{\frac{\dot{m}_{cb,gg} - \dot{m}_t}{m_{gg}}}_{h_1} \tag{47}$$

The energy balance for the gas generator is given as:

$$\frac{d[m_{gg}c_{p,f}(T_{gg} - T_0) - p_{gg}V_{gg}]}{dt} = \dot{m}_{cb,gg}c_{p,f}(T_{cb,gg} - T_0) - \dot{m}_t c_{p,f}(T_{gg} - T_0) \tag{48}$$

Note that we have not included any energy transfer to or storage in the metal construction as these contributions are assumed to be small. Expanding the derivative gives:

$$c_{p,f}(T_{gg} - T_0)\frac{dm_{gg}}{dt} + m_{gg}c_{p,f}\frac{dT_{gg}}{dt} - V_{gg}\frac{dp_{gg}}{dt} = \dot{m}_{cb,gg}c_{p,f}(T_{cb,gg} - T_0) - \dot{m}_t c_{p,f}(T_{gg} - T_0) \tag{49}$$

Now $\frac{dm_{gg}}{dt}$ from (44) can be substituted into (49) and by rearranging we arrive at:

$$\underbrace{-V_{gg}}_{f_{21}}\frac{dp_{gg}}{dt} + \underbrace{m_{gg}c_{p,f}}_{f_{22}}\frac{dT_{gg}}{dt} = \underbrace{\dot{m}_{cb,gg}c_{p,f}(T_{cb,gg} - T_{gg})}_{h_2} \tag{50}$$

The differential equations (14), (47) and (50) constitute the model of the gas turbine. Note that there will be a pressure drop across the gas generator which has not been included in the model.

2.5 Furnace Combustion Model

The furnace combustion model is identical to the combustion model for the gas generator described previously with a change of variables. Hence the flue gas flow and temperature from the combustion and for the furnace can be written as:

$$\dot{m}_{cb,fn} = \dot{m}_t + \dot{m}_{fu2} \tag{51}$$

and

$$T_{cb,fn} = \frac{\dot{m}_t c_{p,f}(T_t - T_0) + \dot{m}_{fu2}(c_{p,fu}(T_{fu} - T_0) + H_{fu})}{\dot{m}_{cb,fn}c_{p,f}} + T_0 \tag{52}$$

respectively.

2.6 Furnace Model

The furnace model is supposed to capture the temperature dynamics in the furnace. Such a model might be divided into multiple control volumes including the convection tubes to achieve a more accurate model. However, here we focus one a single control volume. The mass balance is:

$$\frac{dm_{fn}}{dt} = \dot{m}_{cb,fn} - \dot{m}_{fn} \tag{53}$$

Where $\dot{m}_{fn}$ is the flue gas flow leaving through the funnel. As the pressure in the furnace is regarded as constant, $p_{fn} = p_a$, the energy balance becomes:

$$\frac{[dm_{fn}c_{p,f}(T_{fn} - T_0)]}{dt} = \dot{m}_{cb,fn}c_{p,f}(T_{cb,fn} - T_0) - \dot{m}_{fn}c_{p,f}(T_{fn} - T_0) - \dot{Q} \tag{54}$$

where T_{fn} is the furnace temperature and $\dot{Q} = \alpha_{c,fn}(T_{fn} - T_m)$ is the energy transferred to the metal wall of the furnace and convection part with T_m being the temperature of the wall and $\alpha_{c,fn}$ being the heat transfer coefficient. Expanding the derivatives using (53) and rearranging gives:

$$\underbrace{\frac{1}{f_{44}}}\frac{dT_{fn}}{dt} = \underbrace{\frac{\dot{m}_{cb,fn}c_{p,f}(T_{cb,fn} - T_{fn}) - \dot{Q}}{m_{fn}c_{p,f}}}_{h_4} \tag{55}$$

where m_{fn} is found from:

$$m_{fn} = \rho_{fn}V_{fn} = \frac{p_{fn}M_f}{RT_{fn}}V_{fn} \tag{56}$$

where V_{fn} is the volume of the furnace.
Before finding the output mass flow, $\dot{m}_{fn}$, the change in density, ρ_{fn}, of the flue gas must be found. Such derivations are equivalent to those in (46) and as the pressure is constant, the first term in (46b) is zero leaving the following equation for the change in density:

$$\frac{d\rho_{fn}}{dt} = -\frac{\rho_{fn}}{T_{fn}}\frac{dT_{fn}}{dt} \tag{57}$$

which together with (53) and (55) gives the mass flow:

$$\dot{m}_{fn} = \frac{1}{(T_{fn} + T_0)c_{p,f}}\left(\dot{m}_{cb,fn}c_{p,f}(T_{cb,fn} + T_0) - \dot{Q}\right) \tag{58}$$

2.7 Oxygen Model

The oxygen model is divided into two; one describing the oxygen fraction, x_{gg,O_2}, in the gas generator and another describing the oxygen fraction, x_{fn,O_2}, in the furnace. These models do not treat the combustion meaning that the inputs to these models are the outputs from the combustion. However, the two models are very similar and will be treated in general. First we put up the mole balance for the control volume:

$$\frac{dn}{dt} = \dot{n}_i - \dot{n}_o \tag{59}$$

where $\dot{n}_i$ and $\dot{n}_o$ are the mole flows entering and leaving the container respectively and n is the number of moles accumulated. Now the mole balance for the oxygen can be expressed as:

$$\frac{d(nx_{o,O_2})}{dt} = \dot{n}_i x_{i,O_2} - \dot{n}_o x_{o,O_2} \tag{60}$$

using a backward difference place discretisation, differentiating gives:

$$n\frac{dx_{o,O_2}}{dt} + x_{o,O_2}\frac{dn}{dt} = \dot{n}_i x_{i,O_2} - \dot{n}_o x_{o,O_2} \tag{61}$$

Substituting (59) into this expression and rearranging gives:

$$\frac{dx_{o,O_2}}{dt} = \frac{1}{\tau}(x_{i,O_2} - x_{o,O_2}) \tag{62}$$

where, the time constant is $\tau = \frac{n}{\dot{n}_i}$. Remember also that we can find n as $n = \frac{pV}{RT} = \frac{m}{M_f}$. Using the fact that M_f for the flue gas is assumed constant gives the time constant as $\tau = \frac{m}{\dot{m}_i}$. For the gas generator and furnace the equations are:

$$\underbrace{1}_{f_{55}} \frac{dx_{gg,O_2}}{dt} = \underbrace{\frac{1}{\tau_{gg}}(x_{cb1,O_2} - x_{gg,O_2})}_{h_5} \tag{63}$$

and

$$\underbrace{1}_{f_{66}} \frac{dx_{fn,O_2}}{dt} = \underbrace{\frac{1}{\tau_{fn}}(x_{cb2,O_2} - x_{fn,O_2})}_{h_6} \tag{64}$$

respectively.
As is apparent from these equations we need to know both, n_i and x_{i,O_2} to make use of the differential equation. These are determined by studying the combustion taking place.

Combustion in gas generator

The combustion is assumed to be complete. A complete combustion is a process which burns all the carbon C to CO_2, all the hydrogen H to H_2O and all sulfur S to SO_2. If there are any unburned components in the exhaust gas such as C, H_2 and CO the combustion process is incomplete. The mole flows of carbon and hydrogen coming in with the fuel are:

$$\dot{n}_{C1} = \frac{\dot{m}_{fu1} y_C}{M_C}, \quad \dot{n}_{H1} = \frac{\dot{m}_{fu1} y_H}{M_H} \tag{65}$$

where y_C and y_H are the mass fractions of carbon and hydrogen in the fuel. We assume here that $y_H = 1 - y_C$ hence ignoring sulphur and other purely represented components in diesel and heavy fuel used for marine boilers.
We assume that the atmospheric air for the combustion consists of 21% O_2 and 79% N_2, here the percentages represent mole percentage and we denote the oxygen fraction as $x_{O_2,atm}$. Next the reaction schemes for the process are laid down to be able to determine how much oxygen is left in the flue gas after combustion and what the different compounds in the flue gas are. Reaction schemes:

$$\dot{n}_C \mathrm{C} + \dot{n}_C \mathrm{O_2} \longrightarrow \dot{n}_C \mathrm{CO_2} \tag{66}$$

$$\dot{n}_H \mathrm{H} + \frac{1}{4}\dot{n}_H \mathrm{O_2} \longrightarrow \frac{1}{2}\dot{n}_H \mathrm{H_2O} \tag{67}$$

Hence the mole flow of oxygen leaving the combustion is:

$$\dot{n}_{cb1,O_2} = \dot{n}_{c,O_2} - (\dot{n}_{C1} + \frac{1}{4}\dot{n}_{H1}) \tag{68}$$

where $\dot{n}_{c,O_2} = \dot{n}_c x_{O_2,atm}$ with $\dot{n}_c = \frac{\dot{m}_c}{M_{air}} = \frac{\dot{m}_c}{M_f}$. We also have $\dot{n}_{N_2,c} = \dot{n}_c(1 - x_{O_2,atm})$. Finally, the total amount of moles leaving the combustion is given as:

$$\dot{n}_{cb1} = \dot{n}_{cb,O_2} + \dot{n}_{N_2} + \dot{n}_C + \frac{1}{2}\dot{n}_H \tag{69}$$

This equation works only for combustion with atmospheric air as is the case in the gas generator. The reason is that we do not keep track of the components in the flue gas during the rest of the process. However, we notice that, as we have assumed that M_f is constant, we can find the total amount of mole leaving the combustion as $\dot{n}_{cb1} = \frac{\dot{m}_c + \dot{m}_{fu1}}{M_f}$. The expression for the oxygen fraction entering the gas generator then becomes:

$$x_{cb1,O_2} = \frac{\dot{n}_{cb1,O_2}}{\dot{n}_{cb1}} = \frac{\dot{m}_{cb1,O_2}}{\dot{m}_{cb1}} \left(\frac{M_f}{M_{O_2}} \right) \tag{70}$$

Now in the mean time the last bracket on the right hand side of Equation (70) is close to unity ($M_f/M_{O_2} \approx 0.9$). Hence an approximate solution could be obtained by treating the mole and mass fraction as equal.

Combustion in furnace

The derivation of the expression for the oxygen fraction of the flue gas leaving the furnace combustion is identical to that of the gas generator combustion due to the assumption of constant molar mass of the flue gas. The combustion air is the flue gas leaving the turbine having the oxygen fraction x_{gg,O_2}. The oxygen fraction is given as:

$$x_{cb2,O_2} = \frac{\dot{n}_{cb2,O_2}}{\dot{n}_{cb2}} \tag{71}$$

Fuel

In relation to combustion we need to know what fuel we are using to find out the ratio between carbon and hydrogen. In case of heavy fuel, one can order an analysis of the fuel to obtain such data. In case of diesel we assume that we know the structure of the main molecule. Assuming that it consists only of carbon and hydrogen atoms the general molecule looks like:

$$\text{Diesel}: \quad \mathrm{C}_X\mathrm{H}_Y \tag{72}$$

The mole fraction of carbon and hydrogen in the diesel can be found as:

$$x_C = \frac{X}{X+Y}, \quad x_H = 1 - x_C = \frac{Y}{X+Y} \tag{73}$$

From this we can find the average molar mass of diesel as:

$$\bar{M}_{fu} = x_C M_C + x_H M_H \tag{74}$$

and so the mass fractions of carbon and hydrogen are:

$$y_C = x_C \frac{M_C}{\bar{M}_{fu}}, \quad y_H = x_H \frac{M_H}{\bar{M}_{fu}} \tag{75}$$

In this work we assume $X = 15$ and $H = 32$.

2.8 Model Summary

The total model is best presented in descriptor form as:

$$F(x)\frac{dx}{dt} = h(x, u, d) \tag{76a}$$

$$y = g(x, u, d) \tag{76b}$$

where $u = [\dot{m}_{fu1}, \dot{m}_{fu2}]^T$, $d = [T_a, T_{fu}, T_m]^T$, $x = [p_{gg}, T_{gg}, \omega, T_{fn}, x_{gg,O_2}, x_{fn,O_2}]^T$ and $y = [\dot{m}_{fu}, \dot{Q}, x_{fn,O_2}]^T$, $\dot{m}_{fu} = \dot{m}_{fu1} + \dot{m}_{fu2}$. Expanding, (76a) has the form:

$$\begin{bmatrix} f_{11} & f_{12} & 0 & 0 & 0 & 0 \\ f_{21} & f_{22} & 0 & 0 & 0 & 0 \\ 0 & 0 & f_{33} & 0 & 0 & 0 \\ 0 & 0 & 0 & f_{44} & 0 & 0 \\ 0 & 0 & 0 & 0 & f_{55} & 0 \\ 0 & 0 & 0 & 0 & 0 & f_{66} \end{bmatrix} \begin{bmatrix} \frac{dp_{gg}}{dt} \\ \frac{dT_{gg}}{dt} \\ \frac{d\omega}{dt} \\ \frac{dT_{fn}}{dt} \\ \frac{dx_{gg,O_2}}{dt} \\ \frac{dx_{fn,O_2}}{dt} \end{bmatrix} = \begin{bmatrix} h_1 \\ h_2 \\ h_3 \\ h_4 \\ h_5 \\ h_6 \end{bmatrix} \tag{77}$$

where the elements f_{ij} and h_i were indicated in the model derivation in Equations (14), (47), (50), (55), (63) and (64).
F is never singular, hence it has a well defined inverse, so (76a) can be written as an ordinary differential equation: $\dot{x} = f(x, u, d) = F^{-1}(x)h(x, u, d)$.

2.9 Model Verification

Preliminary test data have been collected from AI's test centre. These are used to verify the constructed model. In Figure 3 both the measurement data and the simulation outputs are shown.
It should be mentioned that the measurement of the temperature at the turbine inlet is unreliable as the sensor was placed close to the gas generator outlet where sufficient gas mixing had not yet occurred, meaning that the temperature was very dependent on the placement in the cross section. Instead the turbine outlet temperature is shown in

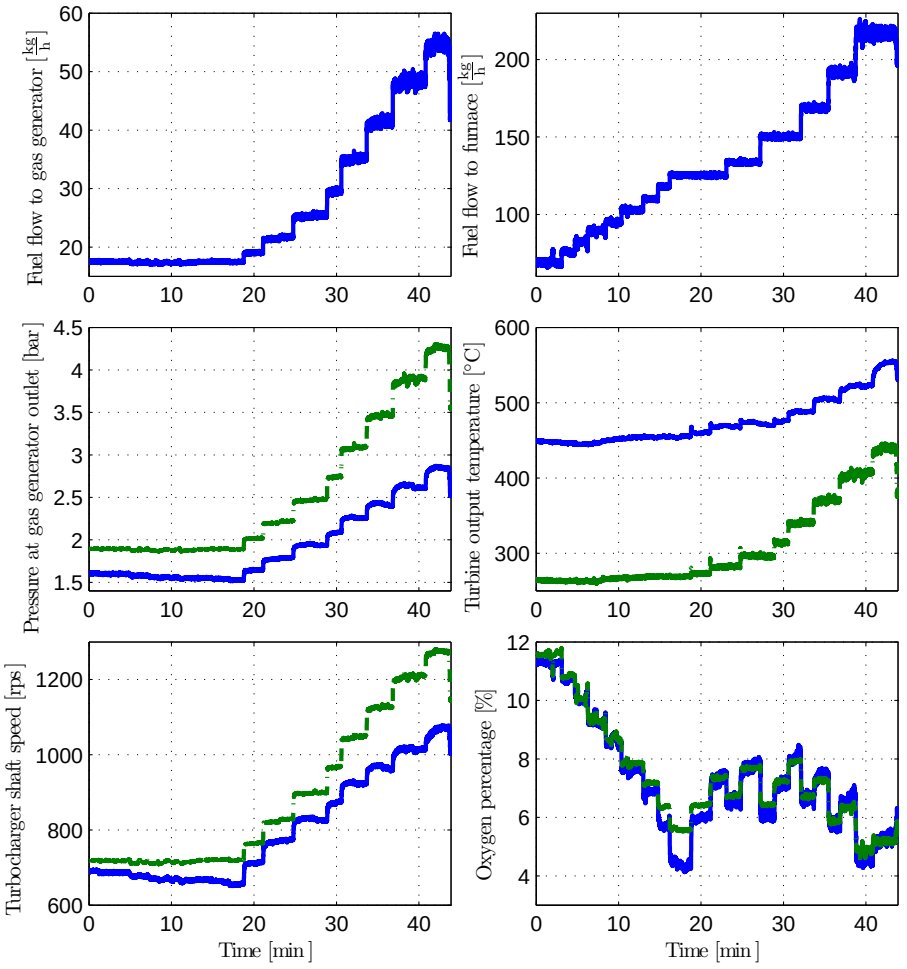

Figure 3: Comparison between measurements (blue solid curves) and simulation output (green dashed curves).

the plot. However, this measurement has a large time constant not modelled. Also the actual gas generator pressure is not measured, and the data shown are constructed from another measurement of differential pressure across the turbine, assuming close to ambient pressure at the turbine outlet. Finally, the measurement of the fuel input is based on the return pressure in the fuel line to each burner rather than the mass flow measurement.

For these reasons the parameters in the model are estimated on the basis of the shaft

velocity and oxygen level alone and a low weighted funnel temperature. The parameters that were estimated using quadratic prediction error performance criteria were: fuel calorific value H_{fu}, heat transfer coefficient $\alpha_{c,fn}$, inertia of turbocharger shaft I.
The figure shows good agreement between model and measurement data in terms of capturing the dynamical behaviour, however, in terms of stationary values these are not represented well by the model for other outputs than the oxygen level. The pressure, temperature and shaft speed differences can be due to poor turbocharger maps, however, it can also originate from the non-modelled pressure losses over the gas generator or the pipes leading from and to the compressor and turbine, which can be introduced by allowing at least one more control volume, and by using Bernoulli's equations. Attempts to model pipe losses have, however, not improved the model. For now we accept these discrepancies as our purpose is to develop an oxygen controller.

2.10 Control Properties

In this section some control properties of the system are discussed. It is obvious that the burner can be operated in two modes; one where only the gas turbine is running and one where both the gas turbine and furnace burner are on. The first mode is less interesting and below we will only address the second. The focus is on the feasible steady state fuel input distribution, optimal steady state fuel distribution and nonlinearities in the dynamics and gain.
The control objectives are to follow the fuel flow setpoint or in fact a power setpoint while optimising efficiency and keeping a clean combustion, measured as an oxygen level above 3%.
In Figure 4 the steady state oxygen level in the flue gas leaving the funnel is shown as a function of the two fuel flows. The plot indicates the feasible steady state fuel flows as the input region where the oxygen level is above 3%. Note that this region is convex.
Further, in Figure 5 a plot of the power delivered to the furnace walls as a function of the total fuel input is shown. From this plot it can be seen that at all times the fuel flow to the gas generator should be kept at a minimum, respecting the oxygen constraint, to achieve the highest efficiency of the burner.
If needed for control design or model estimation, the curve of optimal fuel distribution can be determined on line using simple experiments.
To illustrate the nonlinear behaviour of the system, normalised step responses of linear models linearised along the optimal fuel input distribution from minimum to maximum load are shown in Figure 6. The normalisation is done with respect to the absolute value of the local model steady state gain. From these plots it is obvious that the dynamics change remarkably over the burner operating range. Further, it is noticed that the response from $\dot{m}_{fu1}$ to the oxygen level included a non-minimum phase behaviour. This can limit the performance if a loop is closed around this subsystem. However, it turns out that the inverse response is not pronounced, meaning that the undershoot is relatively small and even difficult to spot in measurements, though it does introduce a

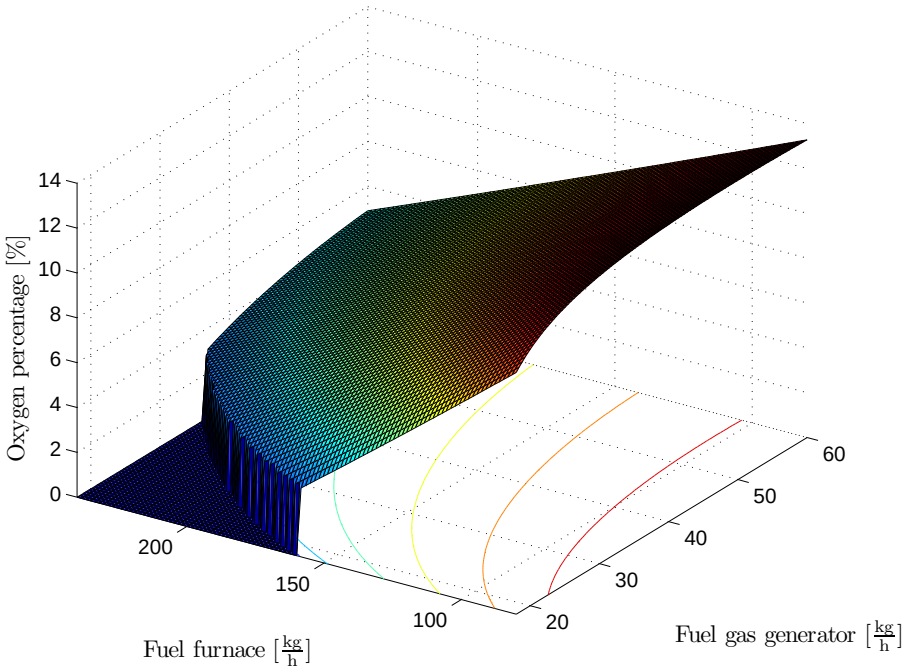

Figure 4: Flue gas oxygen percentage as a function of the two fuel flows. The region where the oxygen percentage is $\geq 3\%$ is indicated in the figure. Note that this region is convex.

delay of < 1s. It is worth noting that these local linear models of 6th order are well approximated by 3rd order models using Hankel norm model reduction – see e.g. [Zhou et al., 1996].

In Table 1 the static gains used in the normalisation before are shown as a function of the static fuel flow. This table shows that not only the dynamics but also the gain in the system change remarkably over the operating range.

These properties might be necessary to incorporate in a controller design which will be discussed in the following section. In control of turbocharged diesel engines one of the concerns is the temperature of the inlet air to the turbine and outlet of the compressor as too high temperatures can accelerate wear and cause breakdowns. However, in the present setup there are no control authority to adjust this temperature independently of the gas generator inlet fuel. Further, there does not seem to be problems with too high temperatures during load changes, caused by the dynamics of the gas generator, which could have limited the gradient at which the load could be increased or decreased. For these reasons constraints on these temperatures are not included in the controller design but could be converted into constraints on the input. This means that the mechanical

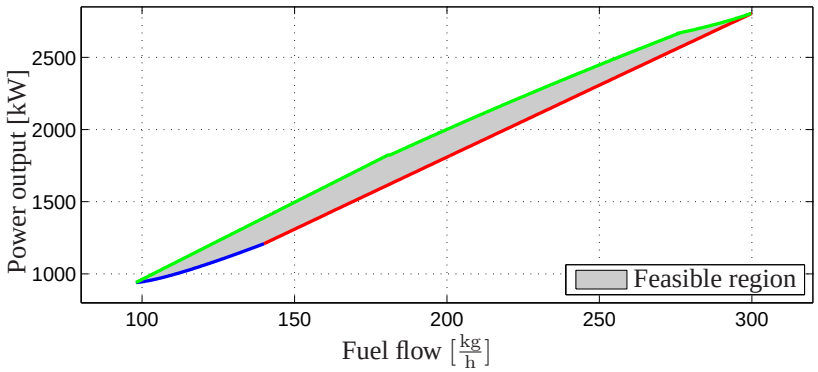

Figure 5: Plot of the burner power output as a function of the total fuel flow supply. For any fuel flow between minimum and maximum there are infinitely many ways to distribute the two fuel flows. As can be seen only one choice is optimal. The blue curve corresponds to increasing the gas generator fuel alone. The red curve corresponds to increasing only the furnace fuel flow. The green curve is the optimal amount of fuel for a given load. Finally, the grey area is the feasible region.

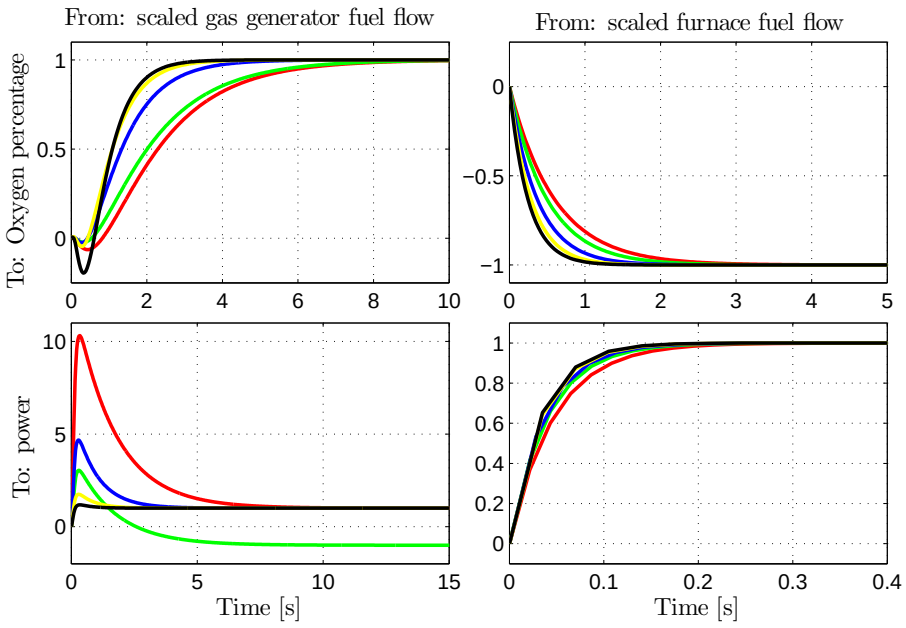

Figure 6: Normalised step responses from fuel flows to the oxygen level in the funnel and power delivered to the metal. The responses are made from linear models gathered from linearising the model over the load range with optimal fuel distribution. The colour ordering is as follows with the first colour being the lowest load: red, green, blue, yellow and black.

design of the gas turbine should be such that too high temperatures are never achieved at the turbine inlet and compressor outlet. If such temperatures are detected during operation, it could be due to a mechanical fault, and the unit should be stopped for service or a different control strategy should be inserted to limit the gas turbine load till service has been carried out. It could also be due to disturbances or changing environment/operating conditions and in these cases a control strategy taking these external factors into account could be used or the input constraints could be adjusted. However, in this preliminary work we do not focus on this special situation.

3 Controller Design

There exist many approaches to fuel/air control of which a few were mentioned in the book on PID controllers, [Åström and Hägglund, 2006]. One of the approaches was based on selector control and another on ratio control. The advantages of selector control is the way to avoid lack of air flow when increasing burner load. However, these approaches are based on the measurement and control of air flow, whereas in the present setup only fuel flow and oxygen level are measured, and the air flow is not directly controlled. We propose a variant of ratio control presented in Figure 7.
Note that this controller consists of a feedback and a feedforward path. The feedforward from the total fuel flow reference, $r_{\dot{m}_{fu}}$ is functions calculating optimal steady state values for the fuel distribution, $r_{\dot{m}_{fu1}} = f_2(r_{\dot{m}_{fu}})$, $r_{\dot{m}_{fu2}} = r_{\dot{m}_{fu}} - r_{\dot{m}_{fu1}}$, and the corresponding oxygen level, $r_{x_{fn,O_2}} = f_1(r_{\dot{m}_{fu}})$. Note that no compensation is made for disturbances. The feedforward functions are calculated by inverting the steady state version of the model presented in this paper. The functions can be approximated by piecewise quadratic functions consisting of three pieces. The dynamic lag filter, $\frac{k_2\tau_2 s+1}{\tau_2 s+1}$, introduced after the nonlinear feedforward function for $r_{\dot{m}_{fu2}}$ is introduced to accommodate the non-minimum phase behaviour to x_{fn,O_2} when changing $\dot{m}_{fu1}$. The "min" block ensures that air lack never occurs. The other filter, $\frac{1}{\tau_1 s+1}$, has a time constant close to that of the closed loop oxygen response. The feedback, a PI

Table 1: Steady state gains from fuel input to oxygen level and power output for changing burner load along the optimal fuel distribution curve.

Load$[\frac{\text{kg}}{\text{h}}]$	98.00	180.71	228.05	275.39	290.00
$\frac{x^{ss}_{fn,O_2}}{\dot{m}^{ss}_{fu1}}$	17.99	34.29	14.90	7.02	2.75
$\frac{x^{ss}_{fn,O_2}}{\dot{m}^{ss}_{fu2}}$	-15.90	-15.02	-11.90	-9.84	-8.58
$\frac{\dot{Q}^{ss}}{\dot{m}^{ss}_{fu1}}$	1.50	-4.95	2.87	7.20	10.72
$\frac{\dot{Q}^{ss}}{\dot{m}^{ss}_{fu2}}$	73.58	73.25	71.66	70.11	68.85

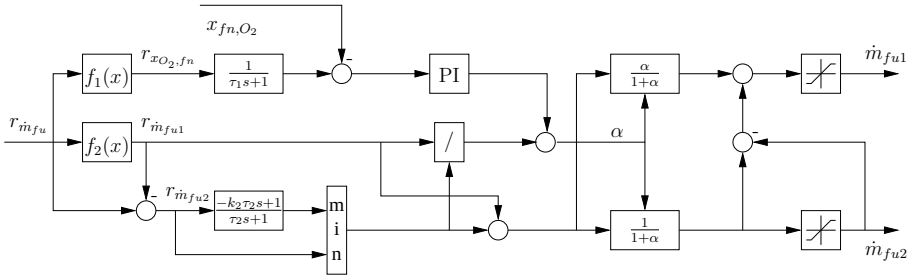

Figure 7: Control structure for the burner unit. A nonlinear feedforward is combined with some dynamic compensation to take into account the dynamics of the process. A feedback around the oxygen is closed to handle disturbances and model uncertainty.

controller, adjusts the ratio, $\alpha = \frac{\dot{m}_{fu1}}{\dot{m}_{fu2}}$, between the two fuel flows to correct the oxygen level if the feedforward compensation is not accurate due to disturbances or model uncertainty. Note that the reference for the oxygen level might also be incorrect. Anti-windup compensation, not shown, is made for the PI controller. The input saturation configuration to the right in the diagram ensures that the reference can be achieved even though $\dot{m}_{fu2}$ has saturated.

4 Simulation Results

In this section we show some simulation result, applying the controller presented in the previous section to the nonlinear model of the burner unit. We show two simulations. The first illustrates the ability of the controller to track the reference. The second shows the ability to suppress disturbances (which to some degree can also be seen as model uncertainty). All simulation plots contain four curves. One curve shows the effect of the nonlinear feedforward (blue), the second the effect of the lag filter (green), the third the effect of the feedback (black) and the fourth is the reference values and feedforward signals (red). The plot showing total fuel flow contains seven curves. The lower ones correspond to the power delivered to the metal in the boiler divided by the specific enthalpy of the fuel, $h_{fu} = c_{p,fu}(T_{fu} - T_0) + H_{fu}$.

In Figure 8 the setpoint for the fuel flow/power output from the burner is ramped up and down.

Note that the feedback and the dynamic term in the feedforward have slowed the response down. However, a more accurate oxygen control is achieved. The burner unit control will normally be in an inner cascade configuration with an outer boiler pressure controller, and even though the response has been slowed down it is still considerably faster than can be expected of the response of any boiler pressure loop.

In Figure 9 changes in input disturbances, compressor inlet air pressure and temperature

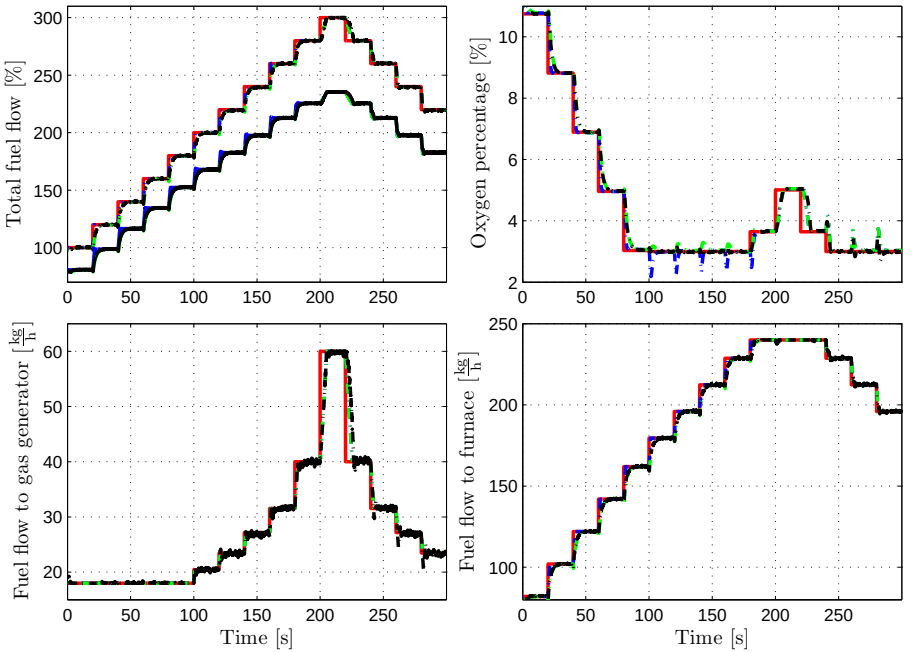

Figure 8: Simulation results with a staircase reference change to the total fuel flow. The total fuel flow is shown in the top left plot, upper curves, along with the power delivered to the metal divided by the fuel enthalpy, lower curves. The oxygen percentage is shown in the top right plot. The fuel flow to the gas generator is shown in the bottom left plot and the fuel flow to the furnace in the bottom right plot. The red lines in the top plots are reference curves. The red lines in the bottom plots are feedforward signals. The blue curves are the uncontrolled system with pure feedforward. The green curves have feedforward and the lag filter in the feedforward path. The black curves have both feedforward and feedback.

corresponding to changing conditions in the engine room are made.
Note that both the pressure and temperature disturbances have a large impact on the burner process. Especially a much higher fuel flow for the gas generator is needed to keep a clean combustion when both inlet air pressure drops and the temperature rises. This might in the worst case limit the maximum possible power from the burner. As these disturbances have not been included in the steady state feedforward calculations the effect will be the same as model uncertainty. This indicates that robustness can be achieved with a rather simple controller. However, as the controller adjusts oxygen to a predetermined reference curve, the performance cannot be optimal in case of disturbances and uncertainty as the current oxygen reference curve does not match the operating conditions.

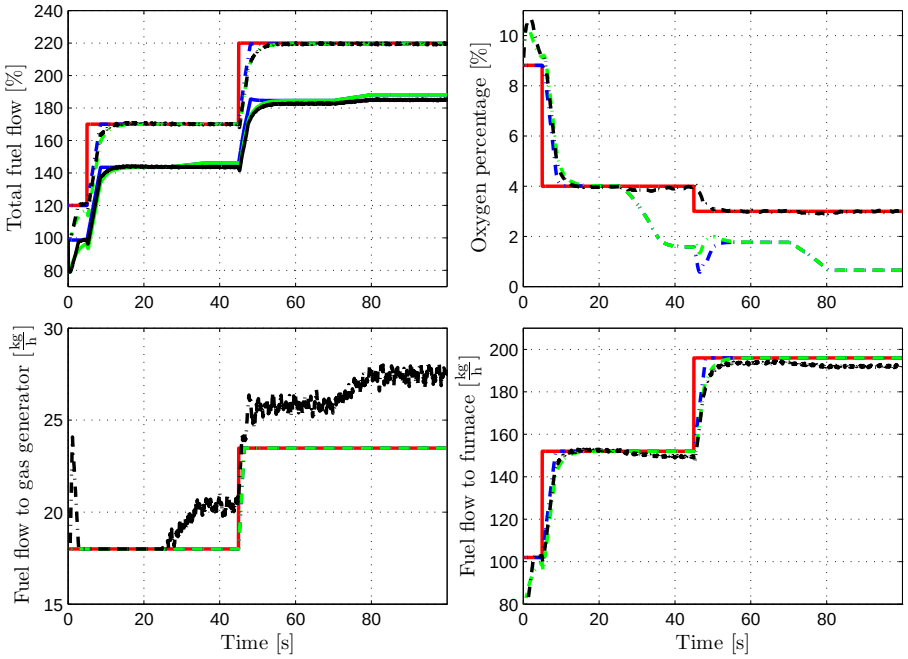

Figure 9: Simulation results with a ramp disturbance in engine room pressure of $-500\frac{\mathrm{Pa}}{\mathrm{s}}$ over 10s, from 25s to 35s. Further, a ramp disturbance occurs in the engine room temperature of $3\frac{^\circ\mathrm{C}}{\mathrm{s}}$ over 10s from 70s to 80s. The total fuel flow is shown in the top left plot; upper curves, along with the power delivered to the metal divided by the fuel enthalpy; lower curves. The oxygen percentage is shown in the top right plot. The fuel flow to the gas generator is shown in the bottom left plot and the fuel flow to the furnace in the bottom right plot. The red lines in the top plots are reference curves. The red lines in the bottom plots are feedforward signals. The blue curves are the uncontrolled system with pure feedforward. The green curves have feedforward and lag filter in the feedforward path. The black curves have both feedforward and feedback.

5 Conclusion

In this paper we have developed a model of a turbocharged burner unit for boiler applications. This model is based on first principles. Dynamically the model performs well, however, the static gains have offsets and increase with load. Further, measurements are required to determine the source of the discrepancies.

The control properties of the derived model were discussed, and both the dynamics and gains of the model proved to be highly nonlinear. Further, it was noted that there is an optimal distribution between the gas generator and furnace fuel flows.

Though nonlinear, a simple controller proved to be able to control the burner in the presence of reference changes and disturbances. This controller was based on a nonlinear

feedforward from the calculated optimal fuel distribution accompanied by a feedback on oxygen to ensure a clean combustion.
It is argued that when uncertainties and disturbances are present, optimal performance cannot be achieved. A more sophisticated control strategy is needed in these cases to approximate optimality.

5.1 Future Work

Further, measurements from the plant are needed to find the reason for the differences between model and plant data. Also, further analysis is needed to study the sensitivity of the burner performance to disturbance changes as inlet pressure and temperature. Also, does the plant dynamics and gains change remarkably as the disturbance changes?
A simple nonlinear model for the gas generator can be derived by neglecting variations in mass and internal energy – see [Sekhon et al., 2006].
A control strategy that is particularly suited for this type of control problem is MPC. The reason for this is that MPC naturally handles the constraints present on input and process variables. Further, a model of the disturbances can easily be introduced and optimal performance can be approximated. However, application of linear MPC shows poor performance possibly due to the nonlinearities in the plant. This means that one could consider nonlinear MPC or linear MPC with multiple models or perhaps simple multiple nonlinear models. It should here be noted that the feasible input region was found to be convex.

References

K. J. Åström and T. Hägglund. *Advanced PID Control*. ISA - Instrumentation, Systems, and Automation Society, 2006.

A. Amstutz and L. Guzzella. Control of diesel engines. *IEEE Control Systems Magazine*, 18(5):53–71, 1998.

T. D. Eastop and A. McConkey. *Applied Thermodynamics for Engineering Technologists*. Addison Wesley Longman, 1993.

P. U. Hvistendahl and B. Solberg. Modelling and multi variable control of a marine boiler. Master's thesis, Aalborg Universitet, Institute of Electronic Systems, Aalborg, Denmark, 2004.

J. P. Jensen, A. F. Kristensen, S. C. Sorenson, N. Houbak, and E. Hendricks. Mean value modelling of a small turbocharged diesel engine. *SAE Technical Paper Series*, No. 910070, 1991.

M. Jung and K. Glover. Control-oriented linear parameter-varying modelling of a turbocharged diesel engine. In *Proceedings of the IEEE Conference on Control Applications*, June 2003.

I. Kolmanovsky and P. Moraal. Turbocharger modeling for automotive control applications. *SAE Technical Paper Series*, 1999-01-0908, March 1999.

J. M. Maciejowski. *Predictive Control With Constraints*. Harlow: Pearson Education Limited, 2001.

M. Müller, E. Hendricks, and S. C. Sorenson. Mean valve modelling of turbocharged spark ignition engines. *SAE Technical Paper Series*, 980784:125–145, February 1998.

R. B. Persson and B. V. Sørensen. Hybrid control of a compact marine boiler system. Master's thesis, Aalborg University, Institute of Electronic Systems, 2006.

S. J. Qin and T. A. Badgwell. A survey of industrial model predictive control technology. *Control Engineering Practice*, 11:733–764, 2003.

J. A. Rossiter. *Model-based Predictive Control: A Practical Approach*. CRC Press LLC, 2003.

H. I. H. Saravanamuttoo, G. F. C. Rogers, and H. Cohen. *Gas Turbine Theory*. Prentice Hall, 5 edition, January 2001.

R. Sekhon, H. Bassily, J. Wagner, and J. Gaddis. Stationary gas turbines – a real time dynamic model with experimental validation. In *American Control Conference*, Minneapolis, Minnesota, USA, 2006.

K. Zhou, J. Doyle, and K. Glover. *Robust and Optimal Control*. New Jersey: Prentice-Hall, Inc, 1996.

Paper B

Model-based Control of a Bottom Fired Marine Boiler

Brian Solberg & Claus M. S. Karstensen & Palle Andersen &
Tom S. Pedersen & Poul U. Hvistendahl

The paper has been published in:
Proceedings of the 16th IFAC World Congress,
July 3-8, 2005, Prague, Czech Republic

Abstract

This paper focuses on applying model based MIMO control to minimize variations in water level for a specific boiler type. A first principles model is put up. The model is linearized and an LQG controller is designed. Furthermore the benefit of using a steam flow measurement is compared to a strategy relying on estimates of the disturbance. Preliminary tests at the boiler system show that the designed controller is able to control the boiler process. Furthermore it can be concluded that relying on estimates of the steam flow in the control strategy does not decrease the controller performance remarkable.

1 Introduction

The control of marine boilers mainly focuses on minimizing the variation of steam pressure and water level in the boiler, keeping both variables around some given set point. Up till now this task has been achieved using classical SISO controllers. One using the fuel flow to control the steam pressure and one using the feed water flow to control the water level.
A more efficient control can allow smaller water and steam volumes in the boiler implying lower production costs and a more attractive product.
The specific boiler concerned in the present work is a MISSION^{TM} OB boiler from AI's product range. The boiler is a bottom fired one pass smoke tube boiler. The boiler consists of a furnace and flue gas pipes surrounded by water. In the top of the boiler steam is led out and feed water is injected. This boiler differs from other boiler designs in two ways: it is bottom fired and the flue gas passes straight through.
The challenge in this work is to minimize the variation of water level to allow smaller boiler geometry without compromising pressure performance. The control problem is complicated by the shrink-and-swell phenomenon which introduces non-minimum phase characteristics in the system. This phenomenon is seen when the steam flow or the feed water flow is abruptly increased or decreased.
The purpose of this paper is to verify if MIMO control is suitable for bottom fired one pass smoke tube boilers. Furthermore the benefit of using the expensive and uncertain steam flow measurement compared to an estimate of this disturbance in the control strategy is investigated. The steam flow influence the shrink-and-swell phenomenon which makes knowledge of this quantity crucial in the control problem.
Tests are performed at a full scale MISSION^{TM} OB boiler.

2 Boiler Model

The boiler model is put up using first principles as was done in [Åström and Bell, 2000] for a drum boiler (for detailed information about the model derivation refer to [Hvistendahl and Solberg, 2004]).
The model consists of two parts, a boiler model and a model of the actuators. Only the boiler model is derived in this paper.

2.1 System Decomposition

The boiler consists of two logically separated parts. One containing the heating part and one containing the water and steam part. The heating part consists of the furnace and the flue gas pipes. The water and steam part consists of all water and steam in the boiler. The two parts are interconnected by the metal separating them i.e. the furnace jacket and the flue gas pipe jackets.

Sub-system models

The boiler is divided into four sub-systems for the purpose of modelling. A block diagram of the boiler using these sub-systems is shown in 1. In the paper $\dot{m}$ denotes mass flow, $\dot{q}$ denotes heat flow, P is pressure, L is level and T is temperature. The subscript a denotes air, fu is fuel, fw is feed water, w is water, s is steam, m is metal, fn is furnace and fp is flue gas pipes.

2.2 The Model Derivation

The derivation is divided into subsections corresponding to the four sub-systems.
The heating part has been divided into four control volumes two in the furnace (one radiation and one convection part) and two in the flue gas pipes (both convection parts). This is done to get a more accurate estimate of the temperature distribution throughout the heating part and to be able to better describe the heat transfer from the flue gas to the metal.
The mean temperature, T_f, in a control volume is set equal to the outlet temperature. The reason for this is that using for instance a bilinear place discretizing method introduces unwanted right half plane zeros in a linear model. Furthermore the mass flow, $\dot{m}_f$, in a control volume is set equal to the input mass flow. Variations in pressure, P, and specific heat capacity $c_{p,f}$ of the flue gas in the heating part are disregarded whereas the density, ρ_f, variations are considered as these are much larger than variations in pressure and heat capacity in the boiler operating range.
The models of the control volumes in the heating part can be found from the mass and

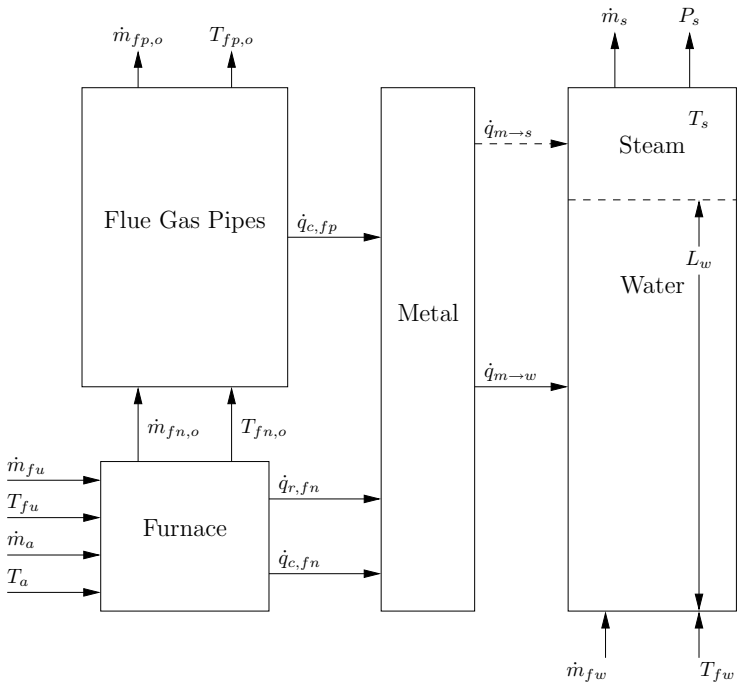

Figure 1: Block diagram of the four sub-systems in the boiler model. Inputs and outputs are shown in the figure as well as flows and variables connecting the sub-systems.

energy balances of each control volume given as:

$$\frac{d\rho_f V}{dt} = \dot{m}_i - \dot{m}_o \tag{1}$$

$$\frac{d}{dt}\left(\rho_f V c_{p,f} T_o\right) = \dot{m}_i c_{p,f} T_i - \dot{m}_o c_{p,f} T_o - Q \tag{2}$$

respectively, where Q is the heat delivered to the metal jackets. The subscripts i and o refer to input and output respectively and V is the volume. Combining the two balance equations gives the following equation for the change in output temperature:

$$\frac{dT_o}{dt} = \underbrace{\frac{\dot{m}_i c_{p,f}(T_i - T_o) - Q}{\rho_f V c_{p,f}}}_{h_{\{1,2,3,4\}}} \tag{3}$$

Before finding the output mass flow $\dot{m}_o$ the change in density ρ_f of the flue gas must

be found. The density can be described using the ideal gas equation and is given as:

$$\rho_f = \frac{PM_f}{R(T_o + K)}$$

where the M_f is the molar mass of the flue gas, R is the gas constant and $K = 273.15\text{K}$, see e.g. [Serway and Beichner, 2000]. This gives the following equation for the change in density:

$$\frac{d\rho_f}{dt} = \frac{d}{dt}\frac{PM_f}{R(T_o + K)} = -\frac{\rho_f}{T_o + K}\frac{dT_o}{dt}$$

which together with (1) and (3) gives the mass flow:

$$\dot{m}_o = \frac{1}{(T_o + K)c_{p,f}}\left(\dot{m}_i c_{p,f}(T_i + K) - Q\right) \tag{4}$$

Furnace and flue gas pipes

The models of the four control volumes in the heating part are almost identical and can be described by two equations for each control volume. One for expressing the change in temperature (3) and one for expressing the outlet mass flow being input to the next control volume (4).
For each of the control volumes the heat flow Q of Equation 3 is either radiation or convection heat marked $\dot{q}_r$ and $\dot{q}_c$ respectively. Radiation heat $\dot{q}_{r,f1}$ from control volume one is calculated as:

$$\dot{q}_{r,f1} \quad = \quad A_{f1}\alpha_{r,f1}((T_{f1} + K)^4 - (T_m + K)^4)$$

where T_m is the metal temperature, A_{f1} is the volume surface area and $\alpha_{r,f1}$ is the radiation heat transfer constant. Convection heat $\dot{q}_{c,f2}$ from control volume two is calculated as:

$$\dot{q}_{c,f2} = A_{f2}\dot{m}_{f1}^{0.8}\alpha_{c,f2}(T_{f2} - T_m)$$

where $\alpha_{c,f2}$ is the convection heat transfer constant.

Metal

The dynamics of accumulated energy in the metal jackets separating flue gas and water/steam can be captured by means of the energy balance. The metal is assumed to have the same temperature in the entire volume as dynamics of thermal conduction for metal are fast. This gives the following model of the metal part:

$$\frac{dT_m}{dt} = \underbrace{\frac{Q_{f\to m} - Q_{m\to w}}{\rho_m V_{m,fj} c_{p,m}}}_{h_5} \tag{5}$$

where $Q_{f\to m} = \dot{q}_{r,f1} + \dot{q}_{c,f2} + \dot{q}_{c,f3} + \dot{q}_{c,f4}$ is the energy flow supplied from the flue gas to the metal and $Q_{m\to w} = A_{mw}(L_w)\alpha_{mw}(T_m - T_s)$ is the energy supplied to the water from the metal. $A_{mw}(L_w)$ is the metal surface area covered by water. Energy supplied to the water steam part above the water surface is considered negligible.

Water/steam

This model has the purpose of describing the steam pressure in the boiler P_s and the water level L_w. The modelling is complicated by the shrink-and-swell phenomenon which is caused by the distribution of steam bubbles under the water surface (this volume is abbreviated V_b). Further the water and steam are assumed only to appear in saturated form.
For the modelling purpose a model of the water and steam part of the boiler as illustrated in Figure 2 is used.

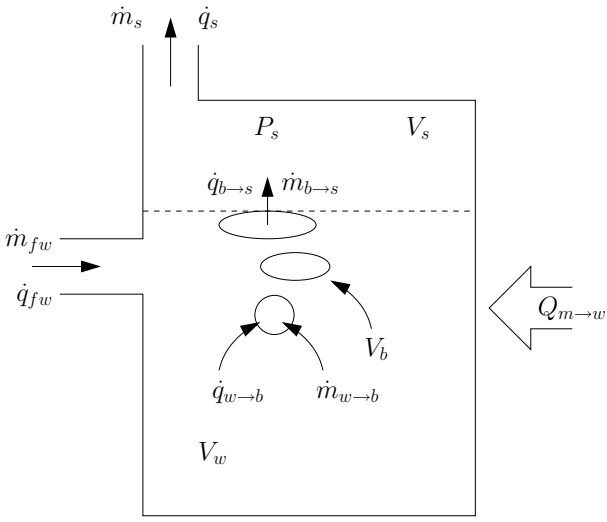

Figure 2: Model for describing the water and steam part.

The total volume of water and steam in the boiler is given as: $V_t = V_w + V_s + V_b$, where V_w is the water volume, V_s is the volume of the steam space above the water surface and V_b is the volume of the steam bubbles below the water surface.
To capture the dynamics of the water/steam part the total mass and energy balances for the water/steam part are considered. The total mass balance for the water/steam part is

given as:

$$\frac{d}{dt}(\rho_s(V_t - V_w) + \rho_w V_w) = \dot{m}_{fw} - \dot{m}_s$$

from which the following expression is found:

$$\underbrace{\left((V_t - V_w)\frac{d\rho_s}{dP_s} + V_w\frac{d\rho_w}{dP_s}\right)}_{f_{66}}\frac{dP_s}{dt} + \underbrace{(\rho_w - \rho_s)}_{f_{67}}\frac{dV_w}{dt} = \underbrace{\dot{m}_{fw} - \dot{m}_s}_{h_6} \tag{6}$$

The total energy balance for the water/steam part is given as:

$$\frac{d}{dt}(\rho_w V_w(h_w - P_s\nu_w) + \rho_s(V_t - V_w)(h_s - P_s\nu_s) + \rho_m V_{m,bj}c_{p,m}T_s) = Q_{m\to w} + \dot{q}_{fw} - \dot{q}_s$$

where h is specific enthalpy and ν is specific volume. This leads to the following differential equation:

$$\underbrace{\left(\begin{array}{c}\rho_w V_w\frac{dh_w}{dP_s} + h_w V_w\frac{d\rho_w}{dP_s} + \rho_s(V_t - V_w)\frac{dh_s}{dP_s} + \\ h_s(V_t - V_w)\frac{d\rho_s}{dP_s} - V_t + \rho_m V_{m,bj}c_{p,m}\frac{dT_s}{dP_s}\end{array}\right)}_{f_{76}}\frac{dP_s}{dt} +$$

$$+\underbrace{(h_w\rho_w - h_s\rho_s)}_{f_{77}}\frac{dV_w}{dt} = \underbrace{\dot{q}_{m\to w} + h_{fw}\dot{m}_{fw} - h_s\dot{m}_s}_{h_7} \tag{7}$$

It should be noticed that the energy in the boiler metal jacket is included in the balance for the water/steam part.

The two equations above only express the pressure and the water volume in the boiler. As the water level of interest in the control problem is given as: $L_w = (V_w + V_b - V_o)/A_{ws}$, another equation is needed for describing the volume of steam bubbles V_b in the water (the water level is measured from the furnace top and V_o is the volume surrounding the furnace and A_{ws} is the water surface area). To do this the mass balances for the steam bubbles and the water are put up as:

$$\frac{d(\rho_s V_b)}{dt} = \dot{m}_{w\to b} - \dot{m}_{b\to s} \tag{8}$$

$$\frac{d(\rho_w V_w)}{dt} = \dot{m}_{fw} - \dot{m}_{w\to b} \tag{9}$$

respectively. The two flows $\dot{m}_{b\to s}$ and $\dot{m}_{w\to b}$ are undetermined. Therefore an empirical equation is introduced. It expresses the amount of steam escaping the water surface as:

$$\dot{m}_{b\to s} = \gamma\frac{V_b}{V_w} + \beta\dot{m}_{w\to b} \tag{10}$$

where β and γ are constants to be estimated. By combining Equations 8, 9 and 10 the final differential equation describing the water/steam part can be written as:

$$\underbrace{\left((1-\beta)V_w\frac{d\rho_w}{dP_s}+V_b\frac{d\rho_s}{dP_s}\right)}_{f_{86}}\frac{dP_s}{dt}+\underbrace{(1-\beta)\rho_w}_{f_{87}}\frac{dV_w}{dt}+$$
$$+\underbrace{\rho_s}_{f_{88}}\frac{dV_b}{dt}=\underbrace{(1-\beta)\dot{m}_{fw}-\gamma\frac{V_b}{V_w}}_{h_8} \tag{11}$$

This equation introduces V_b in the model and hereby the shrink-and-swell phenomenon.

The nonlinear model

The resulting overall nonlinear model of the boiler can be presented as below.

$$\underbrace{\begin{bmatrix} 1 & 0 & 0 & 0 & 0 & 0 & 0 & 0 & 0 \\ 0 & 1 & 0 & 0 & 0 & 0 & 0 & 0 & 0 \\ 0 & 0 & 1 & 0 & 0 & 0 & 0 & 0 & 0 \\ 0 & 0 & 0 & 1 & 0 & 0 & 0 & 0 & 0 \\ 0 & 0 & 0 & 0 & 1 & 0 & 0 & 0 & 0 \\ 0 & 0 & 0 & 0 & 0 & f_{66} & f_{67} & 0 & 0 \\ 0 & 0 & 0 & 0 & 0 & f_{76} & f_{77} & 0 & 0 \\ 0 & 0 & 0 & 0 & 0 & f_{86} & f_{87} & f_{88} & 0 \\ 0 & 0 & 0 & 0 & 0 & 0 & 0 & 0 & 1 \end{bmatrix}}_{\mathbf{F}(x)}\underbrace{\begin{bmatrix} \dot{T}_{f1} \\ \dot{T}_{f2} \\ \dot{T}_{f3} \\ \dot{T}_{f4} \\ \dot{T}_m \\ \dot{P}_s \\ \dot{V}_w \\ \dot{V}_b \\ \dot{T}'_{f4} \end{bmatrix}}_{\dot{\mathbf{x}}}=\underbrace{\begin{bmatrix} h_1 \\ h_2 \\ h_3 \\ h_4 \\ h_5 \\ h_6 \\ h_7 \\ h_8 \\ h_9 \end{bmatrix}}_{\mathbf{h}(x,u,d)} \tag{12}$$

where the first order sensor dynamics of the funnel temperature measurement T'_{f4} are included. The different matrix and vector entries can be found in the equations derived earlier in this section, that is Equations 3, 5, 6, 7 and 11.
In practice the steam flow is governed by several valves combined with pipe resistance. Therefore a variable $k(t)$ expressing pipe resistance and valve strokes is introduced. $\dot{m}_s$ is then given as:

$$\dot{m}_s(t)=k(t)\sqrt{P_s(t)-P_{atm}}$$

where P_{atm} is the atmospheric pressure and $P_s(t)-P_{atm}$ is the differential pressure over the valve. A parameter estimation has been made to find estimates of the critical parameters in the model such that it reflects the physical boiler as well as possible.

3 Controller Design

3.1 Strategy

Scheme

The control strategy consists of two separate control problems. One main controller, concerned in this paper, in a cascade configuration with two actuator flow controllers for fuel and feed water flow respectively.

Compensator

The control strategy is based upon an LQG design. The choice of an LQG design was inspired from a future goal of attempting to implement an MPC (Model-based predictive control) strategy capable of handling limitations in control signals and states. The LQ strategy is comparable to an MPC strategy without constraints. The design is carried out in discrete time. Part of the goal in this control strategy is to compare the benefit of using a steam flow measurement with that of a control strategy relying on estimates of the disturbance. This means that the steam flow disturbance (which is equivalent to the valve stroke k introduced in the model) has to be estimated along with process states. The valve stroke k is the variable determining the load situation of the boiler. A step in k has great influence on the system pressure and water level due to shrink-and-swell effect. A feed-forward in the controller from the valve stroke is presumed to decrease the effects originated from the shrink-and-swell phenomenon. To reconstruct the effect of this feed-forward a good estimate of the valve stroke is needed.

3.2 Model

The model describing the boiler system (12) has the form: $\mathbf{F}(\mathbf{x})\dot{\mathbf{x}} = \mathbf{h}(\mathbf{x}, \mathbf{u}, \mathbf{d})$ where $\mathbf{x}$ is the state vector, $\mathbf{u} = [\dot{m}_{fu}, \dot{m}_{fw}]^T$ is the input vector and $\mathbf{d} = [k, T_{fu}, T_{fw}]^T$ is the disturbance vector. The reason why the air flow $\dot{m}_a$ is not included as an input is that the boiler is constructed with a fixed fuel/air ratio.
Preceding the controller design the model is linearized and the model order is reduced from nine to three leaving the state vector: $\mathbf{x} = [P_s, V_w, V_{sw}]^T$. This new model was found to describe the system sufficiently precisely. The discrete equivalent of the linear model is found and augmented by a model of the actuator controller dynamics resulting in the equation system:

$$\begin{aligned} \mathbf{x}_s(k+1) &= \mathbf{\Phi}_s\mathbf{x}_s(k) + \mathbf{\Gamma}_s\mathbf{u}(k) + \mathbf{G}_s\mathbf{d}(k) \\ \mathbf{y}_s(k) &= \begin{bmatrix} \mathbf{y}(k) \\ \mathbf{y}_a(k) \end{bmatrix} = \begin{bmatrix} \mathbf{H}_y & \mathbf{0} \\ \mathbf{0} & \mathbf{H}_a \end{bmatrix} \mathbf{x}_s(k) = \mathbf{H}_s\mathbf{x}_s(k) \end{aligned}$$

where $\mathbf{y} = [P_s, L_w]$ and $\mathbf{y}_a(k)$ corresponds to outputs from the actuator models.

3.3 Control Law

The goal of the controller is to minimize the variations in the water level L_w and the steam pressure P_s from given set-points. The set-points are constants in normal operation of the boiler hence the purpose is to reject the influence of the disturbances on the two parameters.
The design of the control law follows the principles outlined in [Sørensen, 1995]. The goal is to include disturbances in the controller to reject especially the influence of changes in the steam flow valve position k. Furthermore integral action is required to give offset free tracking of the reference. As both disturbances, references and integral action are included in the performance index, the method requires definition of a disturbance model, a reference model and an integral model.

Augmented system model

The original system state vector is now augmented as
$\mathbf{x}(k) = [\mathbf{x}_s^T(k), \mathbf{x}_d^T(k), \mathbf{x}_r^T(k), \mathbf{x}_i^T(k)]^T$ giving the model:

$$\begin{aligned}
\mathbf{x}(k+1) &= \begin{bmatrix} \mathbf{\Phi}_s & G_s\mathbf{H}_d & \mathbf{0} & \mathbf{0} \\ \mathbf{0} & \mathbf{\Phi}_d & \mathbf{0} & \mathbf{0} \\ \mathbf{0} & \mathbf{0} & \mathbf{\Phi}_r & \mathbf{0} \\ -\mathbf{H}_y & \mathbf{0} & \mathbf{H}_r & \mathbf{I} \end{bmatrix} \mathbf{x}(k) + \begin{bmatrix} \mathbf{\Gamma}_s \\ \mathbf{0} \\ \mathbf{0} \\ \mathbf{0} \end{bmatrix} \mathbf{u}(k) \\
&= \mathbf{\Phi}\mathbf{x}(k) + \mathbf{\Gamma}\mathbf{u}(k) \qquad (13) \\
\mathbf{y}(k) &= \begin{bmatrix} \mathbf{H}_y & \mathbf{0} & \mathbf{0} & \mathbf{0} \end{bmatrix} \mathbf{x}(k) = \mathbf{H}\mathbf{x}(k) \qquad (14) \\
\mathbf{e}(k) &= \begin{bmatrix} -\mathbf{H}_y & \mathbf{0} & \mathbf{H}_r & \mathbf{0} \end{bmatrix} \mathbf{x}(k) = \mathbf{H}_e\mathbf{x}(k) \\
\mathbf{x}_i(k) &= \begin{bmatrix} \mathbf{0} & \mathbf{0} & \mathbf{0} & \mathbf{I} \end{bmatrix} \mathbf{x}(k) = \mathbf{H}_i\mathbf{x}(k)
\end{aligned}$$

A performance index with the purpose of minimizing the errors between reference and output, the integral states and the control signals can be set up as follows:

$$\mathcal{I} = \sum_{k=0}^{\infty} \left(\mathbf{e}^T(k)\mathbf{Q}_{1e}\mathbf{e}(k) + \mathbf{x}_i^T(k)\mathbf{Q}_{1i}\mathbf{x}_i(k) + \mathbf{u}^T(k)\mathbf{Q}_2\mathbf{u}(k) \right)$$

State feedback

Minimizing the performance index results in the well known control law:

$$\mathbf{u}(k) = -\begin{bmatrix} \mathbf{L}_s & \mathbf{L}_d & \mathbf{L}_r & \mathbf{L}_i \end{bmatrix} \mathbf{x}(k) = -\mathbf{L}\mathbf{x}(k)$$

3.4 Estimator

The estimator must reconstruct states not measurable and give a current estimate $\hat{\mathbf{x}}$ of the state vector $\mathbf{x}$. This state estimate will be input to the control law, which becomes $\mathbf{u}(k) = -\mathbf{L}\hat{\mathbf{x}}(k)$.

In the estimator design the two first components ($\mathbf{x_s}(k)$, $\mathbf{x_d}(k)$) of the augmented state vector from Equations 13 and 14 are of interest. In the real boiler system both process and sensor noise are present. Including these noise terms a stochastic state space model of system can be presented as:

$$\begin{aligned}\begin{bmatrix} \mathbf{x}_s(k+1) \\ \mathbf{x}_d(k+1) \end{bmatrix} &= \begin{bmatrix} \mathbf{\Phi}_s & \mathbf{G}_s\mathbf{H}_d \\ \mathbf{0} & \mathbf{\Phi}_d \end{bmatrix} \begin{bmatrix} \mathbf{x}_s(k) \\ \mathbf{x}_d(k) \end{bmatrix} + \\ &\quad + \begin{bmatrix} \mathbf{\Gamma}_s \\ \mathbf{0} \end{bmatrix} \mathbf{u}(k) + \begin{bmatrix} \mathbf{w}_s(k) \\ \mathbf{w}_d(k) \end{bmatrix} \qquad (15) \\ \begin{bmatrix} \mathbf{y}_s(k) \\ \mathbf{y}_d(k) \end{bmatrix} &= \begin{bmatrix} \mathbf{H}_s & \mathbf{0} \\ \mathbf{0} & \mathbf{H}_{dy} \end{bmatrix} \begin{bmatrix} \mathbf{x}_s(k) \\ \mathbf{x}_d(k) \end{bmatrix} + \begin{bmatrix} \mathbf{v}_s(k) \\ \mathbf{v}_d(k) \end{bmatrix} \qquad (16)\end{aligned}$$

where $\mathbf{w}_s(k)$ and $\mathbf{v}_s(k)$ are process noise and measurement noise respectively. Both process and measurement noise are assumed to be uncorrelated zero-mean Gaussian distributed "white" noise sequences. $\mathbf{H}_{dy}$ is a matrix only selecting the temperature disturbances as the steam flow and hence the valve stroke measurement is not available (these temperatures are included in the estimator only to achieve measurement filtering).

3.5 Estimator Gain Design

For derivation of the optimal estimator gain $\mathbf{K}$ see e.g. [Franklin et al., 1998]. Here just note that the problem of finding the optimal estimator requires knowledge of the process and sensor noise covariance matrices, $\mathbf{Q}$ and $\mathbf{R}$ respectively.
Here the system described by Equations 15 and 16 is considered. Assuming knowledge of $\mathbf{Q}$ and $\mathbf{R}$ the estimator gain can be found.

Covariance matrices

As discussed in [Franklin et al., 1998] knowledge of $\mathbf{R}$ is often given from previous measurements and sensor accuracy whereas $\mathbf{Q}$ is a term accounting for unknown disturbances. The assumption of the process noise being white is often used because it simplifies the resulting optimization problem. Physically the process noise can have any characteristics.
In the present work measurements are available for determining the sensor noise and the covariance matrix $\mathbf{R}$ is designed diagonal containing the variances from the different measurements on the diagonal.

$$\mathbf{R} = \mathrm{diag}([\sigma_z^2(1), ..., \sigma_z^2(p)])$$

where $[\sigma_z^2(1), ..., \sigma_z^2(p)]$ is a vector containing the specific sensor noise variances, where p is the dimension of the measurement vector.
The process noise in the boiler system is regarded as the disturbances, k the steam flow valve stroke, T_{fu} fuel temperature and T_{fw} the feed water temperature. But also

unknown disturbances might be present and have to be considered in the design. $\mathbf{w}_d$ is treated as "known" process noise which is changes in the disturbances known to occur. That leaves $\mathbf{w}_s$ regarded as unknown disturbances on the system states. This seems like a reasonable assumption as changes in the disturbance inputs enter the system through the disturbance states.
Of course the variance of $\mathbf{w}_d$ can only be estimated and the problem of the noise being regarded as white still exists. The problem is that changes in the steam flow corresponding to steps from middle load to maximum load are known to occur but these changes can for obvious reasons not be modelled as white noise.
The process noise covariance matrix $\mathbf{Q}$ can now be constructed diagonal with unknown process noise elements corresponding to the system states and reasonable variance expressing disturbance changes corresponding to the disturbance states.
Because of the under determined covariance matrix $\mathbf{Q}$ this is used as a design parameter to achieve the best estimator performance. The matrix is formed as:

$$\mathbf{Q} = \mathrm{diag}([\sigma^2_{ud}(1), ..., \sigma^2_{ud}(n), \sigma^2_d(1), ..., \sigma^2_d(l)])$$

where $[\sigma^2_{ud}(1), ..., \sigma^2_{ud}(n), \sigma^2_d(1), ..., \sigma^2_d(l)]$ is a vector containing variances of the unknown disturbances and the known disturbances respectively. n is the system state dimension and l is the dimension of the disturbance state vector.

3.6 Closed Loop Structure

The closed loop structure of the LQG controller in the form used here is presented in Figure 3. Apart from the model matrices the figure contains the estimator gain matrix $\mathbf{K}$ and the feedback gain matrices $\mathbf{L}$'s. $\mathbf{L}_{sd} = [\mathbf{L}_s, \mathbf{L}_d]$ and $\mathbf{I}_y$ is a matrix selecting the outputs P_s and L_w.
The structure of the controller can be found in e.g. [Sørensen, 1995]. In this closed loop structure the integral action in the compensator is included in the controller directly on the difference between reference and output signal. Another approach to incorporate the integral action through the estimator is discussed in e.g. [Hvistendahl and Solberg, 2004].
Including the measurement of the steam flow in the controller design is assumed a practicable task and is not illustrated here.

3.7 Stability

It is well known that an observer reduces the good stability margins exhibited by the LQ controller. For that reason the stability of the designed controllers (with measured steam flow and estimated steam flow) is investigated to insure robustness of the close-loop system and find out if it is necessary to apply LTR (loop transfer recovery).

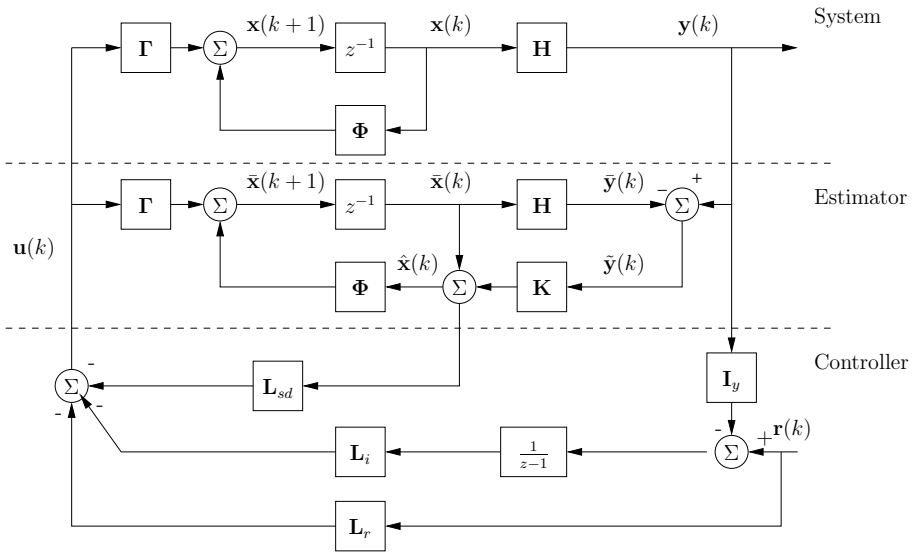

Figure 3: Closed loop structure of LQG controller.

In Figure 4 Nyquist plots of the open-loop system for both controller are shown. From the plots it can be seen that both controllers exhibits good stability margins even with the observer introduced.
Both controllers showed through simulations to behave and control the system well.

4 Results

Two tests were performed on AI's MISSION^{TM} OB boiler - one for each design. The tests consist of making step changes in the steam valve stroke corresponding to a certain steam flow assuming a pressure of 8bar in the boiler. The changes are applied with three minutes interval starting at $1700\frac{\text{kg}}{\text{h}}$. The sequence is: 1700-2100-1300-2100-1700$\frac{\text{kg}}{\text{h}}$. The test results are shown in Figure 5.
From the plots it can be seen that both controllers are able to keep the water level and pressure around the set point. Furthermore it can be seen that there is no remarkable decrease in variations of water level when measuring the steam flow. Whereas performance regarding pressure variations is decreased.

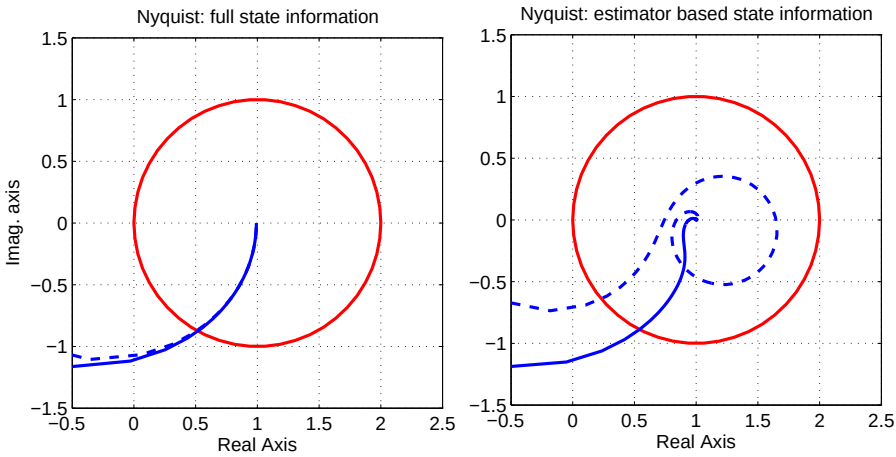

Figure 4: Nyquist plots of open-loop controlled system based on full state information (left) and estimated state information (right). The solid line represent the controller with measured steam flow and the dashed line the controller with estimated steam flow.

5 Discussion and Future Work

It has been verified that model based MIMO control is suitable for control of one specific class of marine boilers (the bottom fired one pass smoke tube boiler). When relying on estimates of the steam flow it was noted that there was no remarkable difference regarding level variations whereas regarding pressure the disturbance is eliminated more slowly. The measurement signals are contaminated by lots of measurement noise corrupting estimates. It is expected that introduction of additional measurement filtering and generation of a better estimate of the disturbance will reduce the influence of the disturbance on the pressure.

Much work still remains in the field of control of marine boilers. The results presented in this paper can be seen as preliminary results. The final goal is to minimize the steam space and water volume in the boiler. To achieve this the final result is expected to use an MPC control strategy as this can handle limitation on states and control signals.

References

K. J. Åström and R. D. Bell. Drum boiler dynamics. *Automatica*, 36:363–378, 2000.

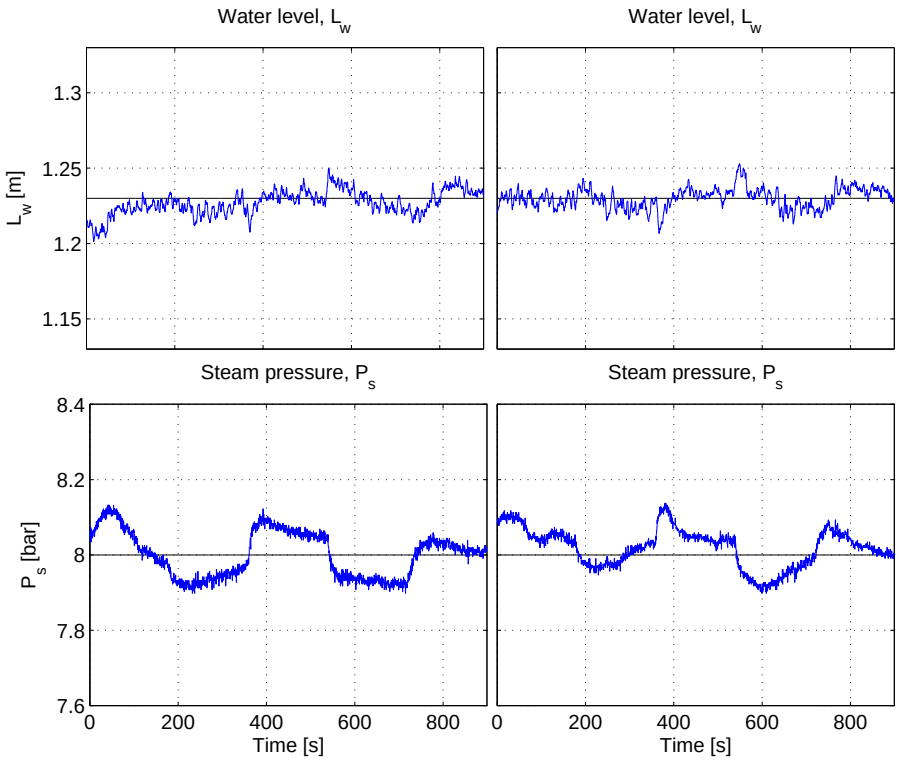

Figure 5: Verification of controllers and evaluation of estimate of valve stroke k. The plots on the left represent the compensator with estimated k and the plots on the right the compensator with measured k. The top plots show the water level and the bottom plots the steam pressure.

G. F. Franklin, J. D. Powell, and M. L. Workman. *Digital Control of Dynamic Systems*. Addison Wesley Longman, 1998.

P. U. Hvistendahl and B. Solberg. Modelling and multi variable control of a marine boiler. Master's thesis, Aalborg Universitet, Institute of Electronic Systems, Aalborg, Denmark, 2004.

R. A. Serway and R. J. Beichner. *Physics for Scientists and Engineers with Modern Physics*. Saunders College Publishing, 2000.

O. Sørensen. Optimal regulering. Technical report, Aalborg Universitet, Institute of Electronic Systems, Aalborg, Denmark, 1995.

Paper C

Control Properties of Bottom Fired Marine Boilers

Brian Solberg & Palle Andersen & Claus M. S. Karstensen

The paper has been published in:
Energy, Volume 32, Issue 4,
ECOS 05. 18th International Conference on Efficiency, Cost, Optimization, Simulation, and Environmental Impact of Energy Systems - ECOS 05,
April, 2007

Nomenclature

Symbol	Description
d, $\mathbf{d}$	disturbance (scalar/vector)
D, $\mathbf{D}$	scaling factor (scalar/matrix)
e, $\mathbf{e}$	error (scalar/vector)
$\mathbf{E}$	output multiplicative perturbation
$\mathbf{G}$, G_{ij}	plant transfer matrix/plant transfer function from input j to output i
$\mathbf{G_a}$	actuator dynamics
$\mathbf{G_d}$, G_{dik}	transfer matrix from disturbance to output/transfer function from disturbance k to output i
$\mathbf{G_u}$	plant without actuator dynamics
$\mathbf{I}$	the identity matrix
k	valve conductance $[\mathrm{kg}/(\mathrm{s}\sqrt{\mathrm{Pa}})]$
$\mathbf{K}$	controller transfer matrix
L	level $[\mathrm{m}]$
$\dot{m}$	mass flow $[\mathrm{kg/s}]$
$\mathbf{M}$	control sensitivity function
P	pressure $[\mathrm{Pa}]$
$\mathbf{P}$	general plant transfer matrix
PM	phase margin
r, $\mathbf{r}$	reference (scalar/vector)
$\mathbf{S}$	sensitivity function
T	temperature $[^{\circ}\mathrm{C}]$
$\mathbf{T}$	complementary sensitivity function
u, $\mathbf{u}$	input (scalar/vector)
$\mathbf{W}$	decoupling transfer matrix
x, $\mathbf{x}$	state (scalar/vector)
y, $\mathbf{y}$	output (scalar/vector)
κ	RIM
$\mathbf{\Lambda}$	RGA
ω	radian frequency $[\mathrm{rad/s}]$

Subscripts	Description
amb	ambient
b	bubbles
bw	bandwidth
c	crossover frequency
f	flue gas
fw	feed water
fu	fuel
i, j, k	indices in vectors and matrices
m	metal
s	steam
w	water

Abbreviations	Description
MIMO	multiple input multiple output
MPC	model predictive control
PI	proportional and integral
RGA	relative gain array
RHP	right half plane
RIM	Rijnsdorp interaction measure
SISO	single input single output

Abstract

This paper focuses on model analysis of a dynamic model of a bottom fired one-pass smoke tube boiler. Linearized versions of the model are analyzed and show large variations in system gains at steady state as function of load whereas gain variations near the desired bandwidth are small. An analysis of the potential benefit from using a multivariable control strategy in favor of the current strategy based on single loop theory is carried out and proves that the interactions in the system are not negligible and a subsequent controller design should take this into account. A design using dynamical decoupling showed substantial improvement compared to a decentralized scheme based on sequential loop closing. Similar or better result is expected to be obtainable using a full Multiple input Multiple output scheme. Furthermore closed loop simulations, applying a linear controller to the nonlinear plant model, prove that the model does not call for nonlinear control. However the results indicate that input constraints will become active when the controller responds to transient behavior from the steam flow disturbance. For this reason an MPC (model predictive control) strategy capable of handling constraints on states and control signals should be considered.

1 Introduction

Traditionally, marine boilers have been controlled using classical SISO controllers. Lately, the focus has been on optimizing the boiler performance through a more comprehensive and coherent control strategy. This includes model-based MIMO control to minimize the variation in drum water level and pressure.
Prior to setting up a control strategy it is important to understand the process to be controlled and the model describing it. The dynamics of the boiler system are described by means of first principles resulting in a model based on nonlinear differential Eq., see e.g. [Sørensen et al., 2004] and [Solberg et al., 2005]. This model has a MIMO structure meaning that all process inputs affect all the outputs. The size of the interactions in the MIMO system are of interest, as are the degree of nonlinearities in the model and whether any of these properties will affect the controlled boiler system.
The model which is analyzed in this paper is based on the bottom fired one-pass smoke tube boiler (MISSION^{TM} OB) from Aalborg Industries A/S product range. The largest of these has a maximum steam load of $3000\mathrm{kg/h}$.
In this paper we start by introducing the boiler model and derive linear versions of this depending on the operating point. Then we analyze this model using primarily linear systems theory and concepts including decentralized control and decoupling to derive stability and performance properties imposed by interaction and nonlinearities.

2 Boiler Model

A diagram of the bottom fired one-pass smoke tube boiler is shown in Figure 1 with model variables indicated. A model of this boiler was presented in [Solberg et al., 2005]. The model has the structure:

$$\frac{d}{dt}(\mathbf{x}) = \mathbf{f}(\mathbf{x},\mathbf{u},\mathbf{d}) \quad (1)$$

$$\mathbf{y} = \mathbf{h}(\mathbf{x}) \quad (2)$$

where $\mathbf{u} = [\dot{m}_{fu}, \dot{m}_{fw}]^T$ (fuel flow and feed water flow), $\mathbf{y} = [P_s, L_w]^T$ (steam pressure and water level), $\mathbf{d} = [k, T_{fu}, T_{fw}]^T$ ("steam flow", fuel temperature and feed water temperature) and $\mathbf{x} = [T_{f1}, T_{f2}, T_{f3}, T_{f4}, T_m, P_s, V_w, V_b]^T$ ($T_{f(i)},\ i = 1, ..., 4$, being temperatures at four different levels in the furnace and convection parts, T_m is the temperature of the metal separating the heating part and the liquid part and V_w and V_b are volumes of water and steam bubbles under the surface in the drum).
Notice that the disturbance k is related to the actual steam flow as $\dot{m}_s = k\sqrt{P_s - P_{amb}}$, and can be interpreted as an overall steam valve and pipe system conductance. k will also be referred to as the steam flow disturbance. P_{amb} is the ambient pressure at the pipe outlet.

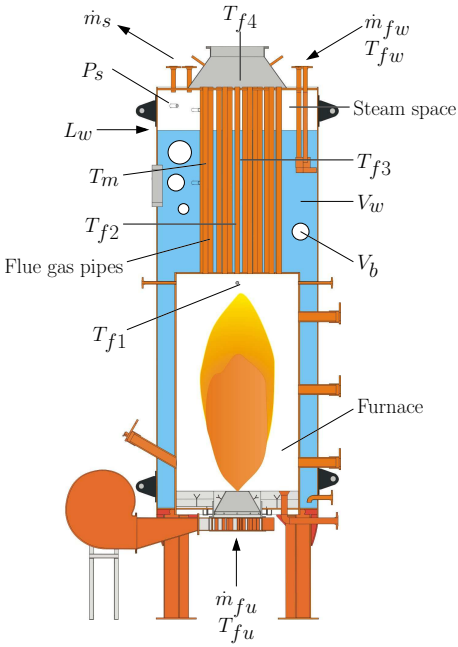

Figure 1: Drawing of the bottom fired one-pass smoke tube boiler.

Parameter estimation was conducted to find the critical parameters in the model in such a way that it reflects the physical boiler system as accurately as possible.

2.1 Linear Model

Linearized versions of the plant are introduced as most of the model analysis and controllers designed will be based on these. The linearization is based on a first order Taylor series expansion. Scaling of the models is introduced (according to Skogestad and Postlethwaite [Skogestad and Postlethwaite, 1996]) since it makes both model analysis and controller design simpler.
Let the unscaled linear small signal valued plant model including tracking error in the Laplace domain be given as:

$$\check{\mathbf{y}}(s) = \check{\mathbf{G}}_u(s)\check{\mathbf{u}}(s) + \check{\mathbf{G}}_d(s)\check{\mathbf{d}}(s) \quad (3)$$

$$\check{\mathbf{e}}(s) = \check{\mathbf{r}}(s) - \check{\mathbf{y}}(s) \quad (4)$$

Introduce scaling factors derived from system demands: allowable control error, knowledge of disturbance variations and allowable input change e.g. due to valve opening

constraints or maximal flow rate etc.:

$$D_{e,i} = \check{e}_{max,i}, \quad D_{u,j} = \check{u}_{max,j}, \quad D_{d,k} = \check{d}_{max,k} \tag{5}$$

where the subscripts $i = 1, 2$, $j = 1, 2$ and $k = 1, 2, 3$ represent the different numbers of entries in the error, input and disturbance vector respectively. The specific values are listed below:

	$\check{e}_{max}$	$\check{u}_{max}$	$\check{d}_{max}$
1	0.5bar	$160\frac{\text{kg}}{\text{h}}$	$6.0 \cdot 10^{-4}\frac{\text{kg}}{\text{s}\sqrt{\text{Pa}}}$
2	0.1m	$4500\frac{\text{kg}}{\text{h}}$	$5°\text{C}$
3			$5°\text{C}$

(6)

The value of $\check{d}_{max,1} = k_{max}$ is determined from assuming a maximal steam flow of 3000kg/h, a steam flow range of 40-100% and assuming that steps in the flow from maximum to minimum and the opposite can occur.
Using vector notation, putting the scaling element on the diagonal of a scaling matrix, the scaled output, input, disturbance and reference vectors are given as:

$$\mathbf{y} = \mathbf{D}_e^{-1}\check{\mathbf{y}}, \quad \mathbf{u} = \mathbf{D}_u^{-1}\check{\mathbf{u}} \tag{7}$$

$$\mathbf{d} = \mathbf{D}_d^{-1}\check{\mathbf{d}}, \quad \mathbf{r} = \mathbf{D}_e^{-1}\check{\mathbf{r}} \tag{8}$$

Substituting these scaled vector representations into Eqs. 3 and 4 gives the scaled model:

$$\begin{aligned} \mathbf{y}(s) &= \mathbf{G}_u(s)\mathbf{u}(s) + \mathbf{G}_d(s)\mathbf{d}(s) \\ \mathbf{e}(s) &= \mathbf{r}(s) - \mathbf{y}(s) \end{aligned} \tag{9}$$

where $\mathbf{G}_u(s) = \mathbf{D}_e^{-1}\check{\mathbf{G}}_u(s)\mathbf{D}_u$ and $\mathbf{G}_d(s) = \mathbf{D}_e^{-1}\check{\mathbf{G}}_d(s)\mathbf{D}_d$.
Now $|\mathbf{d}(t)|_\infty \leq 1$ and the objective is to keep $|\mathbf{e}(t)|_\infty \leq 1$ while obeying $|\mathbf{u}(t)|_\infty \leq 1$. If needed additional scaling can be applied to the references to keep $|\mathbf{r}(t)|_\infty \leq 1$ during reference changes. Here $|\cdot|_\infty$ denotes the vector infinity norm.

2.2 Actuator Models

In the aforementioned boiler model the actuator dynamics were omitted. The actuators will enter in the closed loop strategy in a cascade configuration. The actuators used for both the fuel and feed water flows are valves with a pneumatic actuation. Measurements show that these have a rise time from control signal to flow of $t_r < 10\text{s}$. It is assumed that cascade controllers linearizing the actuator dynamics can be designed with a dynamic behavior equal to or faster than the open loop actuator dynamics.
Models of the controlled actuators with reference flows as input and actual flows as output can be put in a matrix form as:

$$\mathbf{G}_a(s) = \begin{bmatrix} G_{a11}(s) & 0 \\ 0 & G_{a22}(s) \end{bmatrix} \tag{10}$$

Both controlled actuators are assumed to be well described by second order systems. Introducing this model in the total linear model gives a new transfer function from input to output: $\mathbf{G}(s) = \mathbf{G}_u(s)\mathbf{G}_a(s)$.

3 Model Analysis

During this analysis especially three operating points will be considered; minimum load: 40%, middle load: 70% and maximum load 100%. Expanding the notation of $\mathbf{G}(s)$ and $\mathbf{G_d}(s)$ introduced above, including the actuator dynamics, illustrates the transfer functions of the model:

$$\begin{bmatrix} y_1 \\ y_2 \end{bmatrix} = \begin{bmatrix} G_{11} & G_{12} \\ G_{21} & G_{22} \end{bmatrix} \begin{bmatrix} u_1 \\ u_2 \end{bmatrix} + \begin{bmatrix} G_{d11} & G_{d12} & G_{d13} \\ G_{d21} & G_{d22} & G_{d23} \end{bmatrix} \begin{bmatrix} d_1 \\ d_2 \\ d_3 \end{bmatrix} \tag{11}$$

where the dependency of s is omitted. This will be done throughout the analysis, to simplify expressions, where this dependency is obvious. A block diagram illustration of the system is shown in Figure 2.

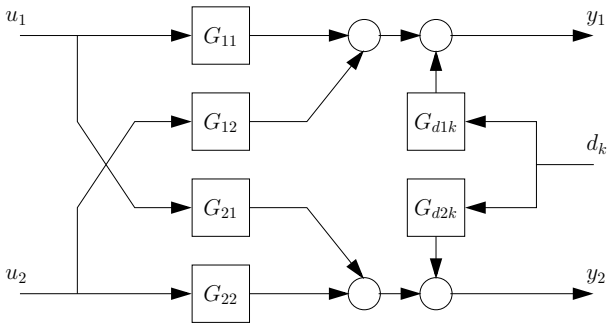

Figure 2: Block diagram of linear boiler model. Where $k \in \{1, 2, 3\}$ represents the three disturbances.

In Figure 3 a magnitude plot of the transfer functions of $\mathbf{G}(s)$ is presented for each of the three mentioned operating points. The actual differences in model dynamics can not be well visualized in these plots. In Figure 4 magnitude plots of $G_{ij,70}/G_{ij,100}$ and $G_{ij,40}/G_{ij,100}$, the ratios between the transfer functions at 70%, 40% load and 100% load are shown. From the plots it can be seen that the main differences between the model dynamics at the different operating points are at low frequencies where gain increases at lower load. On the other hand at frequencies above $10^{-3}\mathrm{rad/s}$ for output one, P_s, and above $10^{-6}\mathrm{rad/s}$ for output two, L_w, the behaviors are similar at least up to about $10\mathrm{rad/s}$ where the ratios associated with the fuel flow input break off. It

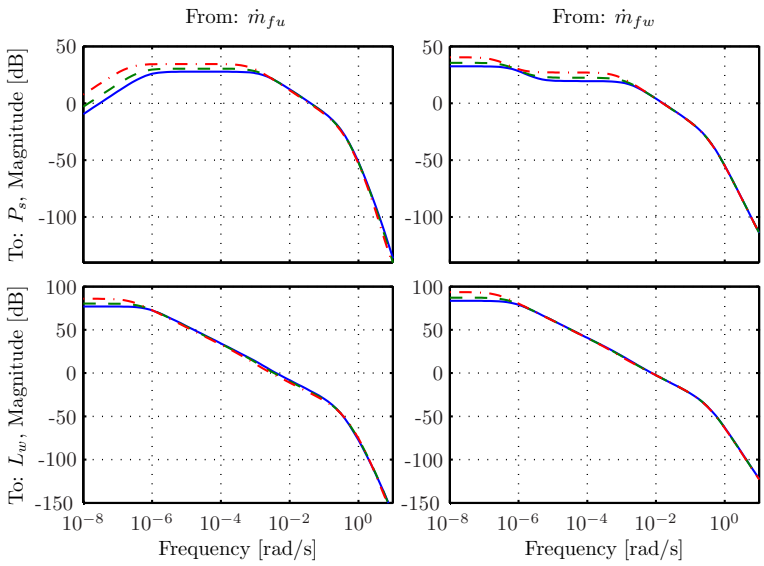

Figure 3: Magnitude plots of transfer functions in $\mathbf{G}(s)$ at three different loads; 100% solid, 70% dashed and 40% dashed-dotted.

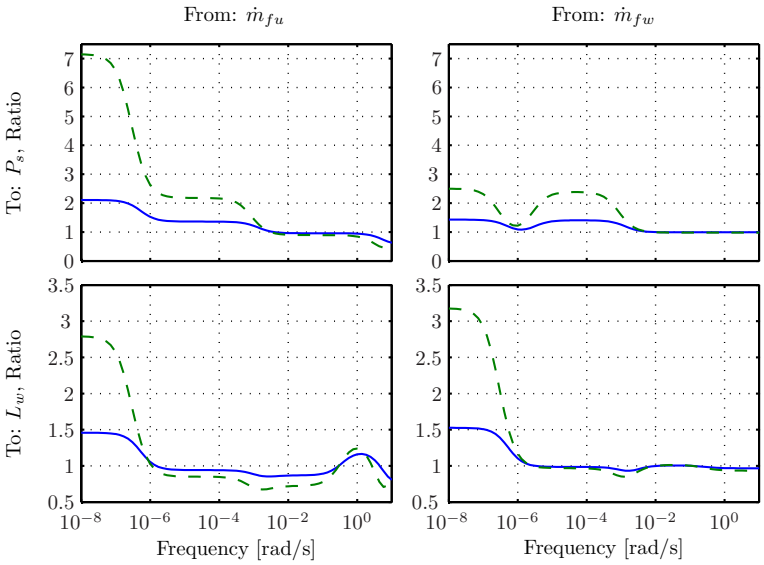

Figure 4: Magnitude plot of $G_{ij,70}/G_{ij,100}$ (solid line) and $G_{ij,40}/G_{ij,100}$ (dashed line).

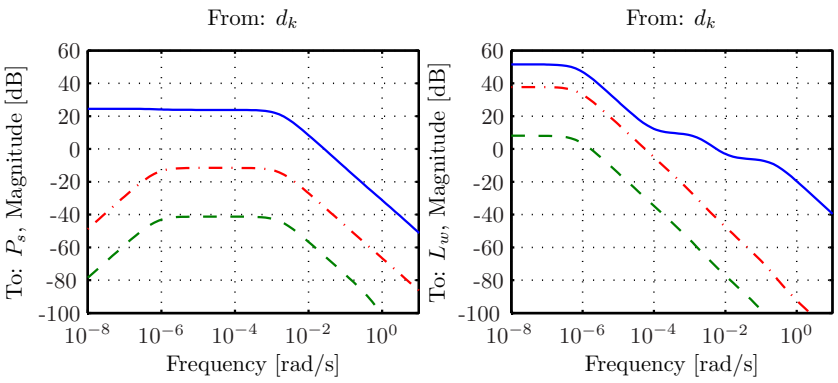

Figure 5: The left plot shows the magnitude plot from $\mathbf{d}$ to y_1 and the right plot the magnitude plot from $\mathbf{d}$ to y_2. The solid line is associated with d_1, the dashed line with d_2 and the dashed-dotted line with d_3.

is of interest to find out whether these differences have any practical implication in a controller design and furthermore whether interactions in the system should be handled by a MIMO control strategy.
It is obvious from the magnitude plots that they do not give any useful information regarding gains and time constants as both quantities are unreasonable high due to a pole in the left half plane close to the origin. Furthermore it can be seen that the magnitude of $G_{11}(s)$ has a low frequency slope of $20\mathrm{dB}/\mathrm{decade}$ indicating a zero in the origin.
Instead of looking at gains at steady state and at the usual definition of time constants another approach is taken. Focus is directed at the desired crossover frequency ω_c, which is closely related to how fast disturbances are rejected. Assuming knowledge of this quantity at the operating point of 100% a suitable controller for this specific load can be designed. Now the system gain variations can be seen as gain variations of the plant at the crossover frequency when the operating point is changed. Furthermore, instead of considering the actual time constants, the variations of the crossover frequency when the operating point is changed are investigated.
This approach gives insight to the stability properties of the nonlinear boiler system.

3.1 Decentralized Control

The controller designed is a simple decentralized controller using SISO PI controllers. An estimate of the bandwidth requirements without taking MIMO interaction into account are investigated from a plot of the magnitudes of the transfer functions from the disturbances to the output, $\mathbf{G}_d(s)$, shown in Figure 5. Control is needed at frequencies where $|G_{dik}(j\omega)| > 1$, $|G_{dik}|$ being the disturbance gain from disturbance k to output i. From the plots it can be seen that for both the pressure, y_1 and water level, y_2, the worst

disturbance is the change in the steam flow; disturbance d_1. The two temperature disturbances have been proven to play a minor role in a closed loop configuration and will not be addressed further in this paper. G_{d11} crosses the zero axis at $\omega_{bw1} \approx 0.027\mathrm{rad/s}$ and G_{d21} crosses the zero axis at $\omega_{bw2} \approx 0.006\mathrm{rad/s}$, setting an estimated bandwidth requirement for the pressure and level loop, respectively.

Stability conditions imposed by interaction

Of interest when performing model analysis and designing decentralized controllers are the stability conditions imposed by interactions in the MIMO model when using the diagonal controller.
Let $\mathbf{P}$ be a square $n \times n$ plant and let $\tilde{\mathbf{P}}$ ("nominal plant") be given as:

$$\tilde{\mathbf{P}} = \begin{bmatrix} P_{11} & 0 & \\ 0 & \ddots & 0 \\ & 0 & P_{nn} \end{bmatrix} \tag{12}$$

Then the closed loop system can be presented as in Figure 6.

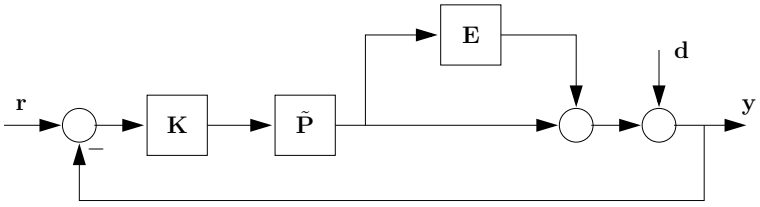

Figure 6: Block diagram of closed loop with the plant $\mathbf{P}$ represented as the diagonal plant $\tilde{\mathbf{P}}$ and an output multiplicative perturbation $\mathbf{E}$. $\mathbf{K}$ is the diagonal controller, $\mathbf{r}$ is the reference signal and $\mathbf{d}$ a disturbance acting on the output $\mathbf{y}$.

$\mathbf{K}$ is the diagonal controller and $\mathbf{E}$ is an output multiplicative perturbation given as:

$$\mathbf{E} = (\mathbf{P} - \tilde{\mathbf{P}})\tilde{\mathbf{P}}^{-1} \tag{13}$$

compensating for the true plant, $\mathbf{P} = (\mathbf{I} + \mathbf{E})\tilde{\mathbf{P}}$, not being diagonal. This means that the problem of designing a controller for the plant $\mathbf{P}$ has been reduced to designing a stabilizing controller with a particular structure (diagonal $\mathbf{K} = \mathrm{diag}(K_{11}, ..., K_{nn})$) for the diagonal plant $\tilde{\mathbf{P}}$ that achieves some performance specifications despite the "uncertainty" $\mathbf{E}$.
By Skogestad and Postlethwaite [Skogestad and Postlethwaite, 1996] the overall output sensitivity function for this system (that is the transfer function from $\mathbf{d}$ to $\mathbf{y}$ in Figure 6) can be factored as:

$$\mathbf{S} = \tilde{\mathbf{S}}(\mathbf{I} + \mathbf{E}\tilde{\mathbf{T}})^{-1} \tag{14}$$

where $\tilde{\mathbf{S}} = (\mathbf{I} + \tilde{\mathbf{P}}\mathbf{K})^{-1}$ is the output sensitivity function of the nominal system and $\tilde{\mathbf{T}} = \mathbf{I} - \tilde{\mathbf{S}}$ is the output complementary sensitivity function of the nominal system, that is the transfer functions from $\mathbf{d}$ to $\mathbf{y}$ and from $\mathbf{r}$ to $\mathbf{y}$ respectively, in Figure 6, ignoring the perturbation $\mathbf{E}$.
Now assume that $\mathbf{P}$ is stable and furthermore that the individual loops are stable ($\tilde{\mathbf{S}}$ and $\tilde{\mathbf{T}}$ stable), then for stability of the overall system it suffices to look at

$$\det(\mathbf{I} + \mathbf{E}\tilde{\mathbf{T}}(s)) \tag{15}$$

as s traverses the Nyquist D-contour and ensure it does not encircle the origin. This follows from lemma A.5 in [Skogestad and Postlethwaite, 1996]. The spectral radius stability condition then yields stability of the overall system if:

$$\rho(\mathbf{E}\tilde{\mathbf{T}}(j\omega)) < 1 \ \ \forall\, \omega \tag{16}$$

At this point it is worth remembering that this condition is only sufficient and necessary condition when we deal with unstructured uncertainty [Skogestad and Postlethwaite, 1996]. As our uncertainty here is fixed in a structure depending on a known plant, we would expect this test to be conservative in general.

2×2 *systems:* For these systems the condition becomes especially simple. This will be illustrated with the system addressed in this paper.

$$\mathbf{E} = \begin{bmatrix} 0 & \frac{G_{12}}{G_{22}} \\ \frac{G_{21}}{G_{11}} & 0 \end{bmatrix}, \ \tilde{\mathbf{T}} = \begin{bmatrix} \tilde{T}_{11} & 0 \\ 0 & \tilde{T}_{22} \end{bmatrix} \tag{17}$$

The spectral radius of $\mathbf{E}\tilde{\mathbf{T}}(j\omega)$ is given by:

$$\rho(\mathbf{E}\tilde{\mathbf{T}}(j\omega)) = \left| \sqrt{\tilde{T}_{11}\tilde{T}_{22}\kappa(j\omega)} \right| \tag{18}$$

where $\kappa = \frac{G_{12}G_{21}}{G_{11}G_{22}}$ is the RIM (Rijnsdorp interaction measure) introduced by Rijnsdorp [Rijnsdorp, 1965]. Now the sufficient condition for stability of the overall system is:

$$|\tilde{T}_{11}\tilde{T}_{22}(j\omega)| < \frac{1}{|\kappa(j\omega)|} \ \ \forall\, \omega \tag{19}$$

or the more conservative condition:

$$\max_{i \in \{1,2\}} |\tilde{T}_{ii}(j\omega)|^2 < \frac{1}{|\kappa(j\omega)|} \ \ \forall\, \omega \tag{20}$$

Bounds can be set on the sizes of $\tilde{T}_{11}(j\omega)$ and $\tilde{T}_{22}(j\omega)$ corresponding to their resonant peaks which again are related to the stability margins of the individual loops. This gives the more conservative condition:

$$\|\tilde{\mathbf{T}}\|_\infty^2 < \frac{1}{\|\kappa\|_\infty} \tag{21}$$

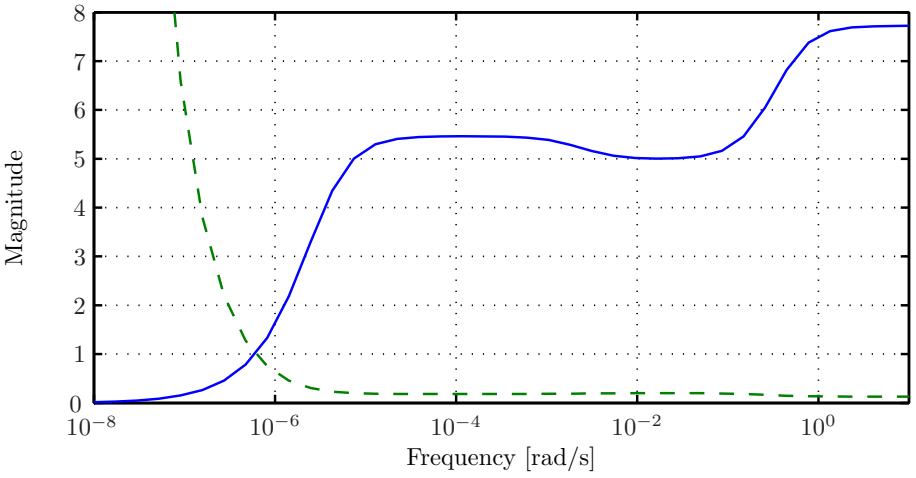

Figure 7: Plot of $1/|\kappa(j\omega)|$ for $\mathbf{G}$ (solid line) and the alternative input/output pairing (dashed line).

For example to ensure stability of a system with offset-free tracking ($T_{ii}(0) = 1$) assuming no resonant peaks the condition becomes $1 < 1/|\kappa(j\omega)| \ \forall\, \omega$. From Eq. 21 it follows that the interactions in the system pose no limit on the achievable closed loop system bandwidth if $\|\kappa\|_\infty < 1$.

It is obvious that systems with $|\kappa(j\omega)| \ll 1 \ \forall\, \omega$ are preferable. The degree to which $|\kappa(j\omega)| < 1 \ \forall\, \omega$ could be interpreted as an insurance of a good stability margin, of the decentralized controlled system, against ignored cross couplings.

In Figure 7 $1/|\kappa(j\omega)|$ for $\mathbf{G}$ and the alternative input/output pairing (where $\kappa = \frac{G_{11}G_{22}}{G_{12}G_{21}}$) are plotted. In the following we work with the pairing corresponding to $\mathbf{G}$ and elaborate on this choice in the next section. Now assume that $\tilde{T}_{ii}$ for all i is designed with no resonant peak such that $\|\tilde{T}_{ii}\|_\infty \leq 1$ given the sufficient condition for stability: $1 < 1/|\kappa(j\omega)| \ \forall\, \omega$ then it is obvious from Figure 7 that stability is not guaranteed in the low frequency band. This is due to the zero in the origin of G_{11}. However the spectral radius stability condition is conservative meaning that this does not necessarily imply that the system is unstable.

To investigate whether the conditions in the low frequency band cause any stability problems for the overall loop again look at Eq. 15. Notice that at low frequencies $\tilde{\mathbf{T}} \approx \mathbf{I}$. This means that for overall stability it suffices to ensure that $\det(\mathbf{I} + \mathbf{E}(j\omega))$ behaves well at low frequencies (does not encircle the origin). Given this, overall stability is guaranteed by (21) for radian frequencies above $10^{-5}\mathrm{rad/s}$. The Nyquist plot of $\det(\mathbf{I} + \mathbf{E}(j\omega))$ is shown in Figure 8. As can be seen the curve indeed behaves well at low frequencies and there are no encirclements of the origin. From the analysis it can be concluded looking at Figure 7 (assuming $\tilde{\mathbf{T}}(j\omega) \approx \mathbf{I} \ \forall\, \omega < 10^{-5}$ for the previous

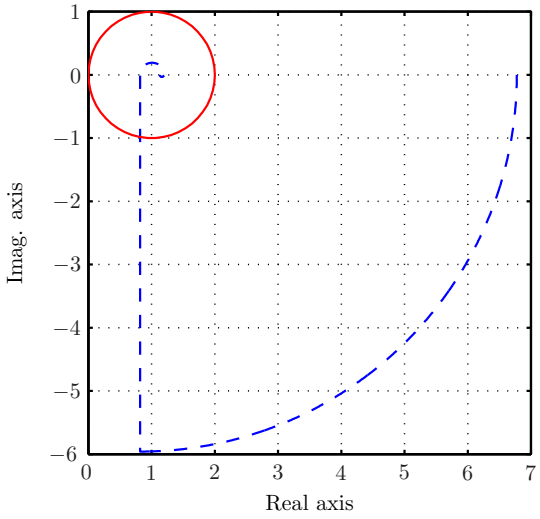

Figure 8: Nyquist plot of $\det(\mathbf{I} + \mathbf{E}(j\omega))$.

analysis to hold) that to ensure stability of the overall system the condition is according to (21); $\|\tilde{T}_{ii}\|_\infty < \sqrt{5}$ that is a resonant peak less than $\sqrt{5}$.
The resonant peak of the closed loop complementary sensitivity function can be related to the achievable phase margins of $\tilde{T}_{ii}$ [Franklin et al., 1994]. A resonant peak of $\sqrt{5} \approx 2.236$ for example ensures a phase margin of $\mathrm{PM} \geq 26°$.

Pairing

The relative gain array (RGA) is another measure of interaction, first introduced by Bristol [Bristol, 1966], and is often used as a measure for pairing control inputs to outputs as the structure of the RGA is dependent on this pairing. The RGA is given as:

$$\mathbf{\Lambda}(\mathbf{G}(s)) = \mathbf{G}(s) \circ (\mathbf{G}^{-1}(s))^T \tag{22}$$

where $\circ$ is the element wise product (also known as the Schur or Hadamard product). In the following $\mathbf{\Lambda}(\mathbf{G}(s))$ is abbreviated as $\mathbf{\Lambda}(s)$. An element of the RGA, $\Lambda_{ij}(s)$, is the ratio between the gain of G_{ij} assuming all other loops open and the gain of G_{ij} assuming all other loops closed by perfect control. Both the RIM and the RGA are independent of the particular plant input and output scaling. For 2×2 systems the RGA can be expressed as:

$$\mathbf{\Lambda}(s) = \begin{bmatrix} \frac{1}{1-\kappa(s)} & \frac{-\kappa(s)}{1-\kappa(s)} \\ \frac{-\kappa(s)}{1-\kappa(s)} & \frac{1}{1-\kappa(s)} \end{bmatrix} \tag{23}$$

In most cases, for stability of the overall system using diagonal decentralized control it is sufficient to require $\mathbf{\Lambda}(j\omega_c) \approx \mathbf{I}$ at the crossover frequencies [Skogestad and Postlethwaite, 1996], which is equivalent to $|\kappa(j\omega_c)| \ll 1$. $\mathbf{\Lambda}(j\omega_c) = \mathbf{I}$ implies that the individual loops are independent of the closings of the other loops meaning that the stability margins from the individual loops are preserved. Furthermore, a unity RGA implies that interaction is zero or only works one way. One way interaction can be interpreted and treated as a disturbance acting from one loop to the other. Hence one seeks to find the input/output coupling that renders the RGA close to unity at the crossover frequency or equivalently the coupling that results in the smallest RIM at this frequency. From the discussion regarding the required bandwidth the crossover frequencies can be expected to be $\omega_{c1} > 0.027\mathrm{rad/s}$ and $\omega_{c2} > 0.006\mathrm{rad/s}$. It can be seen from Figure 7 that the current pairing corresponding to $\mathbf{G}$ (controlling pressure with fuel flow and water level with feed water flow) is the best choice, as would be expected. Intuitively pairing inputs j and outputs i for which $\Lambda_{ij} = 1$ also makes sense since this implies that the gain seen from input j to output i is unaffected by the closing of the other loops. However focusing on the low frequency range Figure 7 shows that the chosen pairing results in small RGA elements indicating control problems if one loop breaks. The problem here is a zero in the origin of the transfer function $G_{11}(s)$ from fuel to pressure discussed below.

RHP-zeros

In SISO controller design and for process understanding it is of interest to determine possible non-minimum phase zeros in the process (zeros in the right half plane). Furthermore, as discussed above, zeros in the origin play a dominant role in the controller design. Processes with RHP-zeros in the transfer function from input to controlled output are difficult to control. The reason for this is that these plants exhibit inverse response behavior. This means that the response initially goes in the opposite direction of that expected. These zeros limit the achievable controller bandwidth.
A list of the transfer functions with a zero in the RHP or in the origin is shown below.

zero in RHP	G_{12}	G_{21}	G_{d21}	G_{d22}	G_{d23}
zero in origin	G_{11}	G_{d12}	G_{d13}		

(24)

In the following only the zeros most important for control will be discussed.
The zero in the origin of $G_{11}(s)$ arises from the fact that with the boiler in steady state, an increase in fuel input, keeping feed water flow constant, causes the steam flow to increase and the water level to drop. But as the water level drops, the efficiency drops. At some point the water level will become sufficiently low so as to reduce the efficiency to a level where steam outlet is equal to the feed water input. This results in a new equilibrium found at the same pressure.
In reality this new equilibrium will not appear due to the large system steady state gains meaning that the boiler will dry out. The zero may be removed by closing the

water level loop. This means that if for some reason the level loop should break then difficulties in controlling the pressure could be expected. This was also the conclusion from the RGA analysis in the previous section.
Regarding the RHP-zeros the most interesting are the ones in the cross connections G_{12} and G_{21} and the one from steam flow to water level in G_{d21} which describes the shrink-and-swell phenomenon in the process. In fact the zero in G_{21} is closer to the origin than the zero in G_{d21}, and furthermore it is associated with a larger gain.
As the operating load drops all the RHP-zeros zeros move closer to the origin. Together with the increasing gain this makes the effect of these zeros most pronounced at low loads. It was expected that the zero in G_{d21} from steam flow to water level would follow these trends more than has been observed. However the load range under consideration in this paper is 40-100% and this phenomenon is mainly pronounced in low load operation as reported in e.g. [Åström and Bell, 2000].
Seen from a control point of view the RHP-zeros do not pose any limits on performance as they are not present in $G_{11}(s)$ and $G_{22}(s)$. However it should be mentioned that a RHP-zero was expected in the transfer function $G_{22}(s)$ from feed water to water level but in the boiler considered no measurement have indicated this.

Loop closing

As was noted previously, the transfer function $G_{11}(s)$ has a zero in the origin, indicating that u_1, fuel flow, can not be used to control y_1, the pressure. However the RGA analysis showed a different result which calls for design via sequential loop closing. This technique has also the advantage of ensuring stability, though the performance of the inner loop might be disturbed when closing the outer loop [Skogestad and Postlethwaite, 1996].
PI controllers are used in both loops. These are designed to achieve the largest possible bandwidth in both loops having resonant peaks $\|T_{ii}\|_\infty = 1.3$, well below the limit found previously, ensuring a phase margin of $\mathrm{PM} \geq 45^\circ$.
First the level loop is closed using K_{22} as illustrated in Figure 9. The new transfer function from u_1 to y_1 is given as:

$$y_1 = G_{11}\left(1 - \kappa\tilde{T}_{22}\right)u_1 = G'_{11}u_1 \tag{25}$$

Inspecting this Eq. it can be seen that at low frequencies: $G'_{11} \approx G_{11}(1-\kappa)$, as $\tilde{T}_{22}$ approximates unity at frequencies where feedback is effective. At high frequencies κ is small indicating that $G'_{11} \approx G_{11}$. As the controller design focuses on relatively high frequencies a design using G_{11} should be adequate though (25) is used to design K_{11}, due to slight phase differences between this and the approximation.

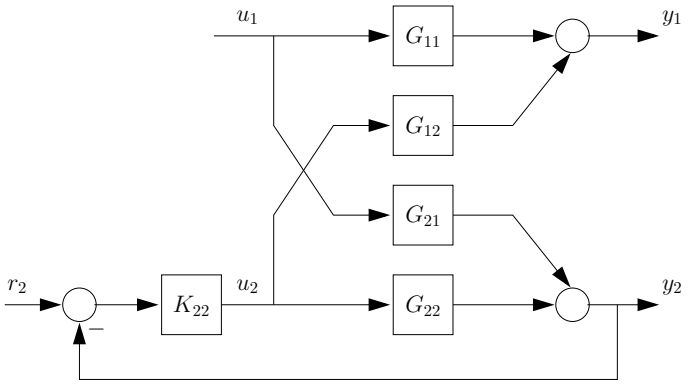

Figure 9: Level loop closed in the sequential design strategy.

3.2 Load Dependency

Above we found two SISO controllers and thereby the crossover frequency for both loops ($\omega_{c1} \approx 0.092\text{rad/s} > \omega_{bw1}$ and $\omega_{c2} \approx 0.131\text{rad/s} > \omega_{bw2}$ where ω_{bw1} and ω_{bw2} were defined in the beginning of Section 3.1). Now the load dependency of gains at the crossover frequencies and the variation of these crossover frequencies can be determined. This is done by applying the controllers found for the 100% load at the remaining two operating points considered, 70% and 40%.

In the following it is assumed that the level loop is closed, meaning that $G'_{11}(s)$ and not $G_{11}(s)$ is in focus. In Figure 10 the mentioned variations as function of load are plotted. Included in the figure are also the variations of the stability margins. The variations in the linearized model are seen to have only a marginal effect on the crossover frequency and the stability margins in the load range considered.

To illustrate that the cross terms in the model do not cause the system to become unstable and to illustrate the little influence the load has on stability, a Nyquist plot of $\det(\mathbf{I}-\mathbf{GK}(s))$ is shown in Figure 11. The plot is shown for the three operating points under consideration given the same controller. From the right plot, which is a zoom close to the unit circle, it can be seen that stability is not effected by load as the three curves cross the unit circle at the same point. The fourth curve shows a Nyquist curve assuming negligible cross terms at 70% load and given the same controller. This curve differs slightly from the other three in the crossing of the unit circle. However the differences are so small that cross terms can be considered not to pose stability problems.

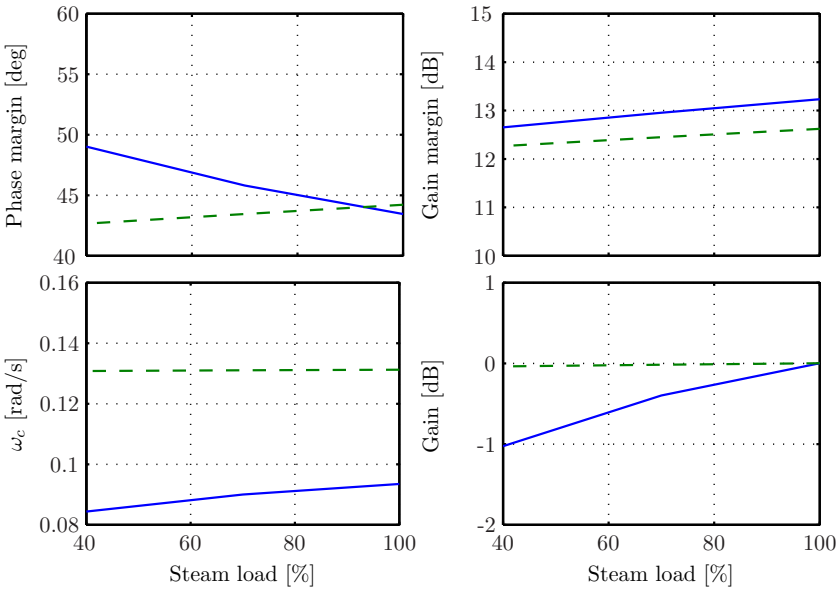

Figure 10: Plots of phase margin variations (top left), gain margin variations (top right), crossover frequency variations (bottom left) and variations of gain at the crossover frequencies for the loop at 100% load (bottom right) all as function of load. The solid line represents the loop associated with G'_{11} (pressure loop) and the dashed line the loop corresponding to G_{22} (level loop).

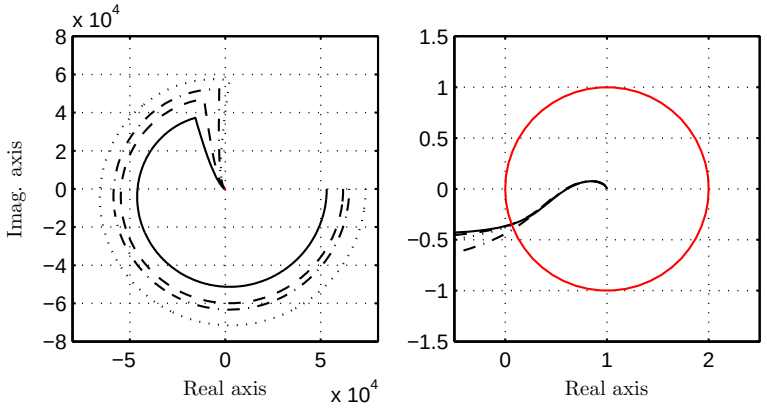

Figure 11: Nyquist plot of open loop system with controller based on sequential loop closing. Left: full plot, right: zoom around the unit circle. The solid line represents a linear model at 100% load, the dashed line a model at 70% load, the dotted line a model at 40% load and the dashed-dotted line a model at 70% load assuming negligible cross terms.

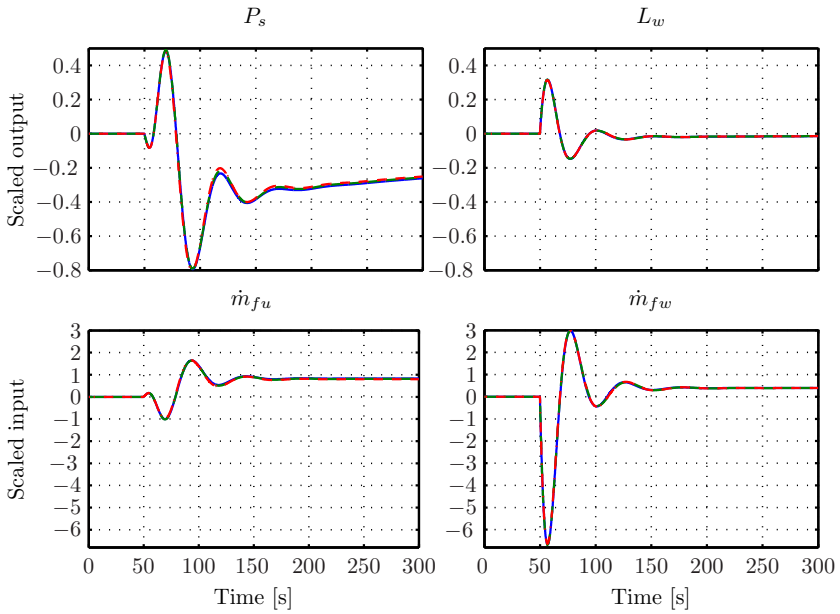

Figure 12: Closed loop response to step disturbance on nonlinear model. Three different step responses are shown; $50\% \rightarrow 75\%$, solid, $50\% \rightarrow 100\%$, dashed and $75\% \rightarrow 100\%$, dashed-dotted.

3.3 Model Nonlinearity

From Figure 3 and the results above it is clear that the nonlinearities are mainly pronounced in the low frequency band as function of load. To investigate whether these low frequency variations should have any influence on the choice of control strategy (linear/nonlinear) the two SISO controllers developed in the last section are simulated together with the nonlinear model to observe the closed loop behavior. Steps in the steam flow disturbance, k, of different sizes are made starting from different operating points. To compare the responses, the outputs from the simulation are first normed with the size of the disturbance step and then scaled according to the discussion in Section 2.1. The result is shown in Figure 12.

From the plots it can be seen that the transient behavior for each step made is approximately the same. The largest differences in the plots are on pressure and fuel flow. This is illustrated in Figure 13 where only the last 200s of Figure 12 is shown. Referring to Figure 4 this makes sense as the largest gain variations over load are associated with the pressure.

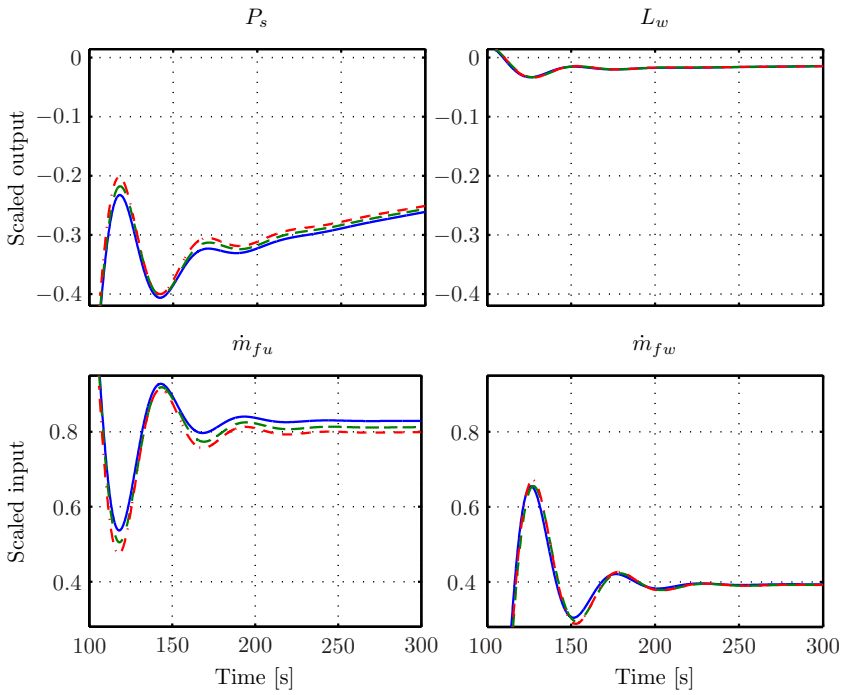

Figure 13: Figure 12 repeated with reduced axes.

3.4 Influence of Interaction on Performance

Having a MIMO system it is of interest to investigate the potential benefit from a MIMO controller design. This can be evaluated by inspecting the influence of the interactions in the model on the achievable controller performance, hereby meaning the ability of the controller to reject the disturbances.

The effect of the cross terms might be positive causing damping of the disturbances, but amplification is also a possibility. To investigate this, the performance of the previously designed controller will be compared to that of a controller designed after decoupling the interactions in the model. The decoupling scheme chosen is referred to as simplified decoupling by Luyben [Luyben, 1970]. This decoupled system is illustrated in Figure 14. This method is chosen as it leads to a simple structure of the decoupling element while still being able to decouple the system fully. However in the paper [Gagnon et al., 1998] they comment on this method as lacking the potential to make the controlled system independent of loop breaking and furthermore it can be troublesome to realize the transfer functions of the decoupled system as they consists of additions and prod-

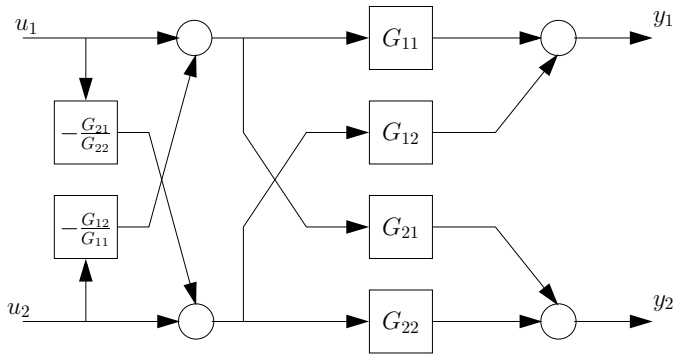

Figure 14: Decoupled system.

ucts of transfer functions. These drawbacks can be overcome by another method, also described in [Gagnon et al., 1998], and referred to as inverted decoupling by Wade in [Wade, 1997]. This has the same transfer functions as the simplified decoupling but furthermore has the benefit of allowing the same decoupled system as the ideal decoupling [Gagnon et al., 1998]. Ideal decoupling consists of recovering the diagonal elements of the plant in the decoupled system. The ideal decoupling is realized by inferring transfer functions in the forward path in Figure 14 (as in the most general decoupling structure) leading to a very complicated decoupling element. In this paper we are not interested in implementation details of the actual decoupling structure, but merely use this technique for analysis. For this reason we are not concerned with loop breaking. Moreover we remark that it will be shown later that ideal- and inverted decoupling is not preferable due to a zero in the origin of the transfer function G_{11}.
The system together with the simplified decoupling can be described as:

$$\mathbf{y} = \mathbf{G}^*\mathbf{u} = \mathbf{GWu} \tag{26}$$

where

$$\mathbf{W} = \begin{bmatrix} 1 & -\frac{G_{12}}{G_{11}} \\ -\frac{G_{21}}{G_{22}} & 1 \end{bmatrix} \tag{27}$$

giving the new system:

$$\begin{bmatrix} y_1 \\ y_2 \end{bmatrix} = \begin{bmatrix} G_{11}(1-\kappa) & 0 \\ 0 & G_{22}(1-\kappa) \end{bmatrix} \begin{bmatrix} u_1 \\ u_2 \end{bmatrix} \tag{28}$$

Note that at low frequencies the transfer function from fuel to pressure is approximately the same as when designing using sequential loop closing, see Eq. 25. Furthermore at high frequencies $\mathbf{G}^* \approx \mathrm{diag}(G_{11}, G_{22})$.

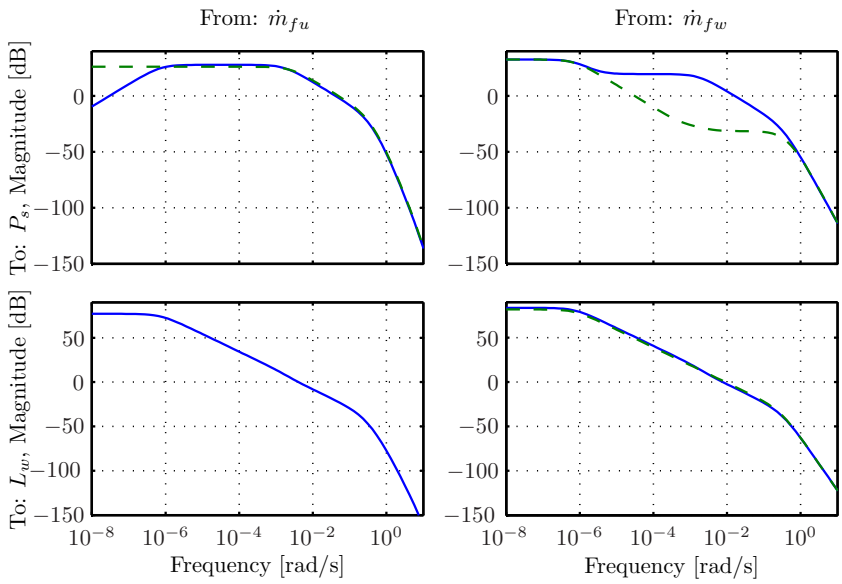

Figure 15: Comparison of open loop model without decoupling, $\mathbf{G}(s)$, solid and with decoupling, $\mathbf{G}^*(s)$, dashed. All four transfer functions in each model are compared.

In practice full decoupling is not possible due to model uncertainties. Decoupling controllers requires accurate process models and are sensitive to modeling errors, particularly when the RGA elements are large [Skogestad and Postlethwaite, 1996]. However theoretically the decoupling from u_1 (fuel flow) to y_2 (water level) can be assumed achieved. Regarding decoupling the other way problems arise in realizing $-\frac{G_{12}}{G_{11}}$ due to an improper system and the zero in the origin of G_{11}. In the frequency range of interest around the crossover frequency $-\frac{G_{12}}{G_{11}}$ is nearly constant with zero phase. For this reason $-\frac{G_{12}}{G_{11}}$ is substituted with a constant. The decoupled system is compared with the original system in the magnitude plot in Figure 15. From the figure it can be seen that for G_{11}^* the zero in the origin has disappeared. Furthermore the non zero decoupling from u_2 to y_1 has damped the interaction at frequencies from well below the crossover frequency.

Now PI controllers are designed based on the diagonal elements in the new transfer matrix. Again these are designed to achieve the largest possible bandwidth in both loops having resonant peaks $\|T_{ii}^*\|_\infty = 1.3$. It should be mentioned that controllers with and without decoupling become very much alike. This is because the two transfer functions depicted in Figure 15 are very similar; there is little difference between the graphs of the paired inputs and outputs in the frequency band around the crossover

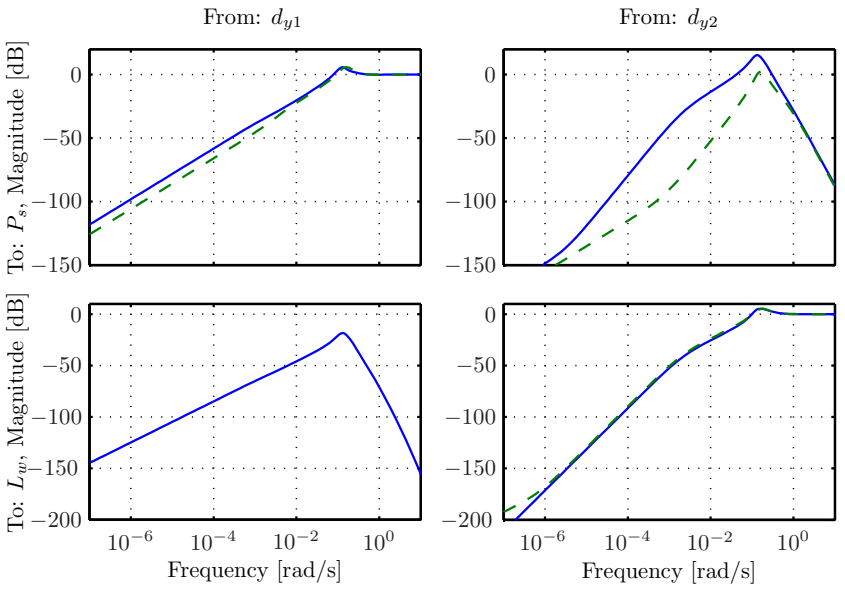

Figure 16: Comparison of sensitivity functions using sequential loop closing, solid, and decoupling design, dashed. d_{y1} and d_{y2} are disturbances acting directly on output 1 and 2 respectively.

frequency. This also means that the only thing that influences whether this decoupling has any positive effect is whether the interaction amplifies the disturbance effect or not. Bode plots of the output sensitivity functions achieved using the decoupling controller and that of the controller designed using sequential loop closing are compared in Figure 16. It can be seen from the figure that the individual sensitivities of the system based on decoupling are more damped than those based on sequential loop closing.

The influence of the interactions can now be evaluated from the two controllers ability to reject disturbances on the output. We look at the transfer function matrix from the disturbance to the output, $\mathbf{SG}_d(s)$, where $\mathbf{S}$ is the output sensitivity transfer matrix. Further, we consider non-simultaneous disturbances and focus on steam flow disturbance. A magnitude plot of the transfer function entries of $\mathbf{SG}_{d1}(s)$ is shown in Figure 17.

The plots show that decoupling have a positive effect on the controller performance especially regarding the pressure loop. Here the resonant top using sequential loop closing is avoided at $10^{-1}\mathrm{rad/s}$.

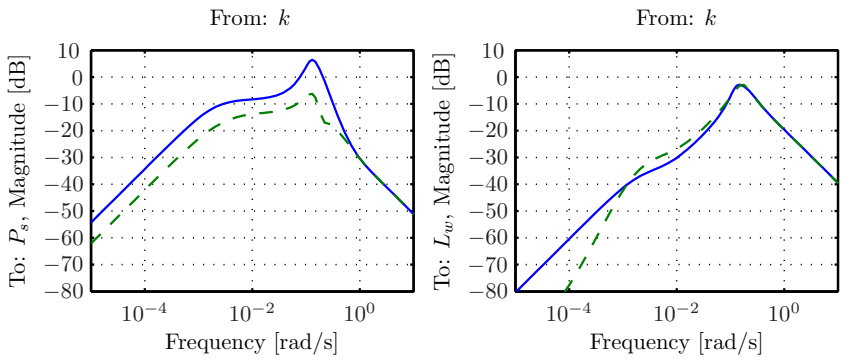

Figure 17: Illustration of effect of interaction. Magnitude plot of transfer functions in $\mathbf{SG}_{d1}(s)$ is shown for two control strategies. Solid line is sequential loop closing and dashed line is design by decoupling.

3.5 Input Constraints

An important issue in controller design is whether input constraints cause any limit on the achievable performance. Constraints can be a problem when rejecting the transients in the disturbance.

Previous results showed that nonlinearities were concentrated in the low frequency band for which reason constraint problems as a consequence of rejecting transients in the disturbances can be carried out using linear model analysis.

This analysis is carried out in the time domain and for non-simultaneous disturbances. Again focus is put on the steam flow disturbance. We limit ourselves to step disturbances as these are the most frequently encountered disturbances in the steam flow. In Figure 18 the step response from the steam flow disturbance to the outputs and control inputs is shown. The plot shows the result of applying two different strategies. The solid lines represent the controller designed by sequential loop closing. The dashed lines represent the same controller but with input constraints on fuel and feed water flow. Further, an anti-windup scheme is implemented in the latter strategy to prevent the integrators from integrating when the inputs are saturated. The step in the steam flow is applied at time 0, is negative and have a magnitude of 1. The constraints on the inputs are calculated from the physical constraints which shifts the band, where the inputs can operate, away from $[-0.5, 0.5]$ on the figure.

From the plot it is easy to see that input constraints become active for both the fuel and feed water supply. The performance requirement for pressure and water level are not exceeded, however the response on the water level is slower when the input saturates. Regarding the pressure the constrained controller seams less aggressive and courses less variations. This is meant to be because the feed water flow does not disturb the pressure loop as much as in the unconstrained case.

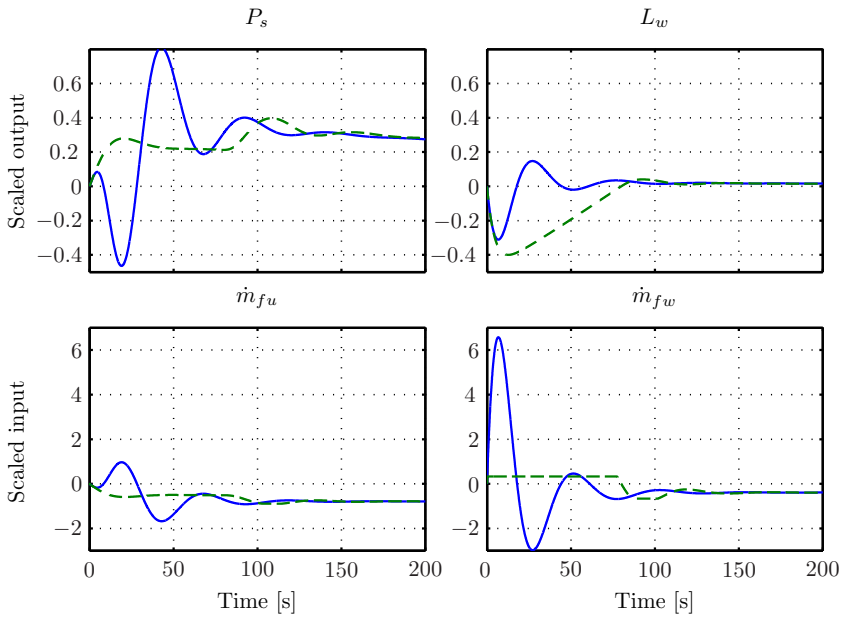

Figure 18: Closed loop response to step in steam flow disturbance on linear model. The solid lines represent an unconstrained controller and the dashed lines a constrained controller.

4 Conclusions

This paper has shown that with use of a MIMO control strategy for the boiler system benefits can be expected. This was a result of improved performance with a decoupled SISO control design compared to a SISO control design based on sequential loop closing.

Linearized boiler models at three different operating points in the load range showed only substantial different behavior at very low frequencies. It was shown that the same linear controller could be used in the entire load range leaving out the need for gain scheduling control or another nonlinear control strategy. This was manifested by inspecting the closed loop performance, using one linear controller, to steps in the steam flow disturbance.

Input constraints were shown to become active when controlling the boiler. However, with the current demands for pressure and water level a constrained SISO controller was shown still to manage to comply with the demands. If we want to tighten the demands to both pressure and water level it is expected that the input constraints will course performance degradation. Also a constrained PI control strategy does not supply

any easily predictable performance. For this reason it would be natural to implement a control strategy explicitly taking actuator limitations into account.

Future work

The fact that input constraints pose limitations on achievable performance, and that hard constraints for level variations are present, could suggest an MPC controller, [Maciejowski, 2001], in which constraints would be incorporated in the optimization. Attempts of successfully applying MPC to boiler systems and thermal power plants are already reported in the literature see e.g. [Kothare et al., 2000] and [Lee et al., 2000]. It is therefore expected that this method should be applicable to the marine boilers.
Furthermore it is of Aalborg Industries A/S' interest to introduce controllers for their boilers that do not require manual tuning and these controllers should work for a whole family of boilers. For this reason work remains in developing a strategy for making the control system self tuning. Also possible problems with model scaling should be investigated as the degree of nonlinearity and interactions in the model for scaled versions of the boiler concerned in this paper are not yet known.

References

K. J. Åström and R. D. Bell. Drum boiler dynamics. *Automatica*, 36:363–378, 2000.

E. H. Bristol. On a new measure of interactions for multivariable process control. *IEEE Transactions on Automatic Control*, AC-II:133–134, 1966.

G. F. Franklin, A. Emami-Naeini, and J. D. Powell. *Feedback Control of Dynamic Systems*. Addison-Wesley, 1994.

E. Gagnon, A. Pomerleau, and A. Desbiens. Simplified, ideal or inverted decoupling? *ISA Transactions*, 37:265–276, 1998.

M. V. Kothare, B. Mettler, M. Morari, P. Bendotti, and C.-M. Falinower. Level control in the steam generator of a nuclear power plant. *IEEE Transactions on control system technology*, 8, No. 1:55–69, 2000.

Y. S. Lee, W. H. Kwon, and O. K. Kwon. A constrained receding horizon control for industrial boiler systems. In G. Hencsey, editor, *IFAC Symposium on Manufacturing, Modeling, Management and Control (MIM 2000)*, pages 411–416, Patras, Greece, 2000.

W. L. Luyben. Distillation decoupling. *AIChE Journal*, 16:198–203, 1970.

J. M. Maciejowski. *Predictive Control With Constraints*. Harlow: Pearson Education Limited, 2001.

J. E. Rijnsdorp. Interaction in two-variable control systems for distillation columns - I. *Automatica,* 1:15–28, 1965.

S. Skogestad and I. Postlethwaite. *Multivariable Feedback Control: Analysis and Design*. Chichester: John Wiley & Sons Ltd, 1996.

B. Solberg, C. M. S. Karstensen, P. Andersen, T. S. Pedersen, and P. U. Hvistendahl. Model-based control of a bottom fired marine boiler. In P. Horacek, editor, *16th IFAC World Congress*, Prague, Czech Republic, 2005.

K. Sørensen, C. M. S. Karstensen, T. Condra, and N. Houbak. Optimizing the integrated design of boilers - simulation. In R. Rivero, editor, *Efficiency, Costs, Optimization, Simulation and Environmental Impact of Energy Systems (ECOS 2004)*, volume 3, pages 1399–1410, Guanajuato, Mexico, 2004.

H. L. Wade. Inverted decoupling: a neglected technique. *ISA Transactions*, 36:3–10, 1997.

Paper D

Advanced Water Level Control in a One-pass Smoke Tube Marine Boiler

Brian Solberg & Palle Andersen & Jakob Stoustrup

The paper has been published as a technical report.
2007, Department of Electronic Systems, Aalborg University, Aalborg, Denmark

The layout has been revised.

Abstract

This paper describes the results of applying model predictive control (MPC) to an oil-fired one-pass smoke tube marine boiler working in cooperation with a waste heat recovery (WHR) boiler. The objective of this controller is to track the water level reference whilst respecting upper and lower bound constraints despite influence from the steam flow and engine load disturbances. Further, the controller must keep an approximate constant pressure to ensure an adequate steam quality. The designed controller is tested on a simulation model verified against data from a stand alone oil-fired boiler present at Aalborg Industries A/S' test centre. The simulations show that model predictive control is applicable to these constructions. The controller for the combined operation of the oil-fired boiler and the WHR boiler is tested on a combination of the aforementioned model and an empirical model of the WHR boiler in simulation study. The results show improvement over a traditional decentralised single loop PI controller design, mainly due to the predictive nature of the MPC algorithm and the use of the process model in the controller.

1 Introduction

In this paper we investigate the applicability of model predictive control, (MPC), to the oil-fired one-pass smoke tube marine boiler working in cooperation with a waste heat recovery (WHR) boiler. MPC is a well proved control method used throughout the process industry [Qin and Badgwell, 2003], and applications to other boiler types are documented in the literature, see e.g. [Kothare et al., 2000; Lee et al., 2000]. The objective is to utilise the ability of MPC to operate closer to constraints than other control strategies and to use knowledge of future disturbances in a feedforward design. Especially, the perspective is to increase the water level close to the upper constraint. The incitement to this is two fold; One: with the level closer to the constraint the efficiency can be increased in current boilers. Two: operating closer to the constraints can allow for smaller steam space geometry reducing production costs.
Previously, it has been shown that a controller design based on a nonlinear process model is not necessary for control of the one-pass smoke tube marine boiler [Solberg et al., 2007]. However, cross couplings in the system play an important role for controller performance. In [Solberg et al., 2005b] an application of linear quadratic Gaussian (LQG) control to the one-pass smoke tube boiler proved that a multivariable control strategy, using a steam flow disturbance estimated, provides satisfactory performance. It is the natural extension of this work to model predictive control this paper documents. The boiler setup is shown in Figure 1. The specific boilers concerned in the present work are the MISSION^{TM} OB oil-fired boiler and the MISSION^{TM} XW WHR boiler, both from Aalborg Industries A/S (AI). The MISSION^{TM} OB boiler is an oil-fired one-pass smoke tube boiler. The boiler consists of a furnace and flue gas pipes surrounded

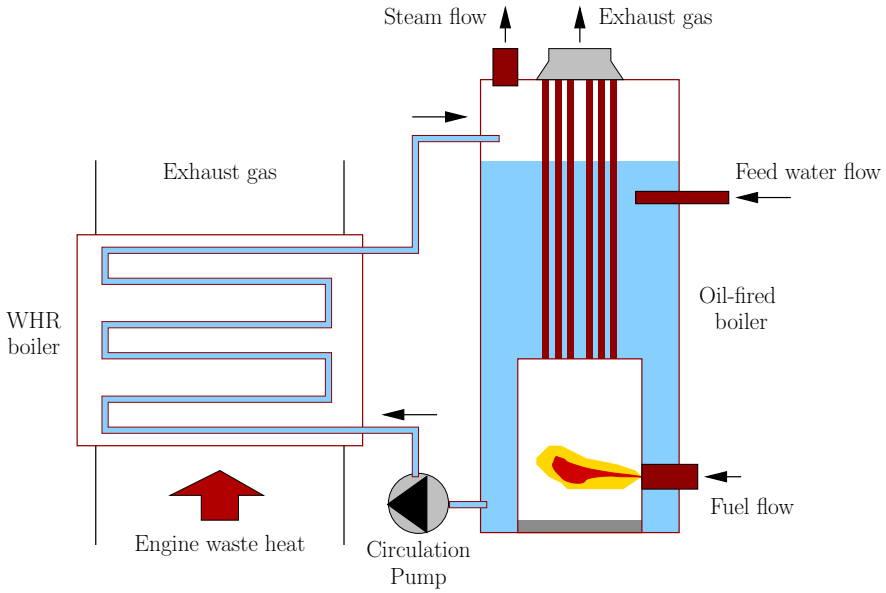

Figure 1: Principle of cooperating an oil-fired one-pass smoke tube boiler and a water tube waste heat fired marine boiler.

by water. In the top of the boiler, steam is led out and feed water is injected. This boiler differs from other boiler designs in two ways: it is side-fired and the flue gas passes straight through. The capacity of the boiler is $1800\frac{\text{kg}}{\text{h}}$ of steam at maximum load at 8bar. The MISSION$^{\text{TM}}$ XW WHR boiler is a water tube boiler with forced circulation and a capacity of $3500\frac{\text{kg}}{\text{h}}$ at maximum engine load. The capacity of the circulation pump is five times the maximum steam production, ensuring sufficiently low steam quality in the WHR boiler tubes to avoid overheating of the tubes and thereby prevent soot fires to occur. This boiler is placed in the engine funnel on the ship.
The interesting feature in this construction is that the WHR boiler uses the same steam space as the oil-fired boiler. This makes the construction very sensitive to changes in engine load and especially start and stop of the engine. The reason for this is the shrink-and-swell phenomenon.

- Swell: Occurs during start of the engine and during positive load changes. When the power delivered to the WHR boiler increases, the mass fraction of steam in the boiler increases. At low pressure steam occupies much more space than water which results in large amounts of water being pushed into the oil-fired boiler, and the water level increases.

- Shrink: Occurs during engine shutdown and negative load changes. When the

power delivered to the WHR boiler decreases, the mass fraction of steam decreases. This allows for more water in the WHR boiler which is pumped from the oil-fired boiler in which the water level decreases.

The worst disturbances occur during start-up and in case of emergency maneuvers when the engine load is abruptly changed. Change in engine load can be as fast as $0 - 80\%$ in 3 min.
The challenge in this work is to minimise the variation of the water level to allow a smaller boiler geometry without compromising pressure performance. The control problem is complicated by the aforementioned shrink-and-swell phenomenon which introduces non-minimum phase characteristics in the system. This phenomenon is not only seen when the engine load is abruptly increased or decreased but also when the steam flow load is changed.
Today, the height of the oil-fired boilers is most often extended in both directions from the normal water level (NWL) to cope with the extra amount of water coming from the WHR boiler. However, by applying setpoint control there is a potential to half this distance. AI is already considering simple versions of such schemes. However, here we illustrate that using such a scheme in combination with MPC has advantages and can lead to a potentially smaller increase in boiler height or increase in efficiency.
We design an MPC controller to deal with the situation when the oil-fired boiler and the WHR boiler are operating together. An objective in this preliminary analysis is to compare the strategy with a classical diagonal PI strategy using a traditional tracking antiwindup scheme to illustrate where the benefit from using MPC is achieved. Tuning of the MPC controller is done using the LTR procedure. Notes on LTR can be found in e.g. [Doyle and Stein, 1981; Maciejowski, 1985, 2001, 1989; Saberi et al., 1993]. As an example of application to MPC, see [Rowe and Maciejowski, 1999].
The designed controller is tested on a simulation model verified against a full-scale oil-fired boiler situated in AI's test centre, and the performance is compared to that achieved using traditional single loop controllers. No verified model of the cooperating boiler setup is available. For this reason the controller performance is evaluated from simulation results obtained using an empirical model of the WHR boiler combined with the verified model of the oil-fired boiler.
Finally, it is suggested to augment the predictive controller with an outer loop handling setpoint optimisation for the water level. This optimisation uses knowledge of future engine load changes and an estimate of the steam volume below the water surface together with a prediction of this proportional to the steam flow to calculate current worst case level variations.

2 Model

It is possible to derive a first principles model describing the combined operation of the oil-fired and WHR boiler. This could easily be done by e.g. using the same principles

for the WHR boiler as were used to model the riser section in a drum boiler in [Åström and Bell, 2000]. In fact the only difference would be that this boiler has forced circulation. However, no measuring data for such a boiler in operation have been available for which reason we shall take a somewhat less model-based approach and treat the interaction with the WHR boiler as disturbances acting directly on the water volume and the heat input respectively. We do this by introducing the new disturbance, the engine load $L_e \in [0, 1]$, and the two transfer functions describing its effect:

$$\dot{Q}_{ex}(s) = \frac{K_{\dot{Q}}}{\tau_{\dot{Q}} s + 1} L_e(s) \tag{1}$$

where $\dot{Q}_{ex}$ is the extra amount of heat recovered from the exhaust gas. The first order filter is set to have a time constant of 3 min.

$$\dot{m}_{ex}(s) = \frac{K_{\dot{m}} s}{\tau_{\dot{m}} s + 1} L_e(s) \tag{2}$$

where $\dot{m}_{ex}$ is the excess water from the WHR boiler replaced by steam.
We are aware that this is a much simplified model of the WHR boiler behaviour where we have neglected disturbances due to varying weather conditions which will change the engine exhaust gas temperature at the same load. Further, all uncertainty in the estimate of the power delivered to the WHR boiler has been neglected. In a real plant, sooting of the water tubes introduces an uncertainty in the amount of heat recovered by the WHR boiler.
The model of the oil-fired boiler is based on first principles. The version we present here is a slight modification of the work presented in [Solberg et al., 2005b] including WHR disturbances. Studies have shown that both the flue gas part (furnace and convection tubes) and the metal separating the water/steam part (pressure part) from the flue gas have considerably faster dynamics than the desired closed loop bandwidth. Due to this fact the power delivered to the water/steam part is modelled as:

$$\dot{Q} = \eta(\dot{m}_{fu}) = \eta_2 \dot{m}_{fu}^2 + \eta_1 \dot{m}_{fu} + \eta_0 \tag{3}$$

where η is a function describing a combination of energy released in the combustion plus furnace and convection tubes heat transfer efficiency. Both steady state versions of the model presented in [Solberg et al., 2005b] and measurement of the temperature at the funnel of the boiler suggest this structure.
The purpose of the model of the water/steam part is to describe the steam pressure in the boiler p_s and the water level L_w. The modelling is complicated by the shrink-and-swell phenomenon due to steam load changes caused by the distribution of steam bubbles under the water surface.
The total volume of water and steam in the oil-fired boiler is given as: $V_t = V_w + V_s + V_b$, where V_w is the water volume, V_s is the volume of the steam space above the water surface, and V_b is the volume of the steam bubbles below the water surface.

To capture the dynamics of the water/steam part, the total mass and energy balances are considered. The total mass balance for the water/steam part leads to the following expression:

$$\left[(V_t - V_w)\frac{d\varrho_s}{dp_s} + V_w\frac{d\varrho_w}{dp_s}\right]\frac{dp_s}{dt} + (\varrho_w - \varrho_s)\frac{dV_w}{dt} = \dot{m}_{fw} + \dot{m}_{ex} - \dot{m}_s, \quad (4)$$

and the total energy balance for the water/steam part leads to:

$$\left(\begin{array}{c} \varrho_w V_w \frac{dh_w}{dp_s} + h_w V_w \frac{d\varrho_w}{dp_s} + \varrho_s(V_t - V_w)\frac{dh_s}{dp_s} + \\ h_s(V_t - V_w)\frac{d\varrho_s}{dp_s} - V_t + \varrho_m V_m c_{p,m}\frac{dT_s}{dp_s} \end{array}\right)\frac{dp_s}{dt} + (h_w\varrho_w - h_s\varrho_s)\frac{dV_w}{dt} = \dot{Q} + \dot{Q}_{ex} + h_{fw}\dot{m}_{fw} + h_w\dot{m}_{ex} - h_s\dot{m}_s \quad (5)$$

where $\dot{m}_{fw}$ is the feed water flow, $\dot{m}_s$ is the steam flow, ϱ is density, h is enthalpy and T is temperature, c_p is specific heat capacity and subscript m stands for metal. It should be noticed that energy accumulated in the boiler, furnace and convection tubes metal jackets is included in the balance for the water/steam part.

The two equations above only express the pressure and the water volume in the boiler. As the water level of interest in the control problem is given as: $L_w = (V_w + V_b - V_o)/A_{ws}$, another equation is needed to describe the volume of steam bubbles V_b in the water (the water level is measured from the furnace top, and V_o is the volume surrounding the furnace, and A_{ws} is the water surface area). To do this, the mass balance for the steam bubbles and the water is put up and combined with an empirical equation (first used by [Andersen and Jørgensen, 2007] for the marine boiler):

$$\dot{m}_{b\to s} = \frac{\varrho_s}{T_d}V_b \quad (6)$$

which expresses the amount of steam escaping the water surface, $\dot{m}_{b\to s}$ as a function of the steam bubble volume and density of the steam, the constant T_d expresses the average rise time of bubbles in the water. A similar expression can be found in [Åström and Bell, 2000]. This leads to the final differential equation describing the water/steam part:

$$\left(V_w\frac{d\varrho_w}{dp_s} + V_b\frac{d\varrho_s}{dp_s}\right)\frac{dp_s}{dt} + \varrho_w\frac{dV_w}{dt} + \varrho_s\frac{dV_b}{dt} = \dot{m}_{fw} + \dot{m}_{ex} - \frac{\varrho_s}{T_d}V_b \quad (7)$$

This equation introduces V_b in the model and hereby the shrink-and-swell phenomenon. In practice the water/steam circuit is closed, and the steam flow is governed by several valves combined with pipe resistance. Therefore, a variable $k(t)$ expressing pipe conductance and valve strokes is introduced. $\dot{m}_s$ is then given as:

$$\dot{m}_s(t) = k(t)\sqrt{p_s(t) - p_{dws}} \quad (8)$$

where the downstream pressure, p_{dws}, is the pressure in the feed water tank which is open and hence has ambient pressure, $p_{dws} = p_a$. $p_s(t) - p_{dws}$ is the differential pressure over the steam supply line.
The final model has the form:

$$F(x)\dot{x} = h(x,u,d) \tag{9a}$$
$$y = g(x) \tag{9b}$$

where $x = [p_s, V_w, V_b, x_{ex,1}, x_{ex,2}]^T$, $u = [\dot{m}_{fu}, \dot{m}_{fw}]$ and $d = [k, L_e]^T$ where the $x_{ex,i}$s are states describing the WHR boiler dynamics (1) and (2). The temperature of the feed water is assumed to be constant and therefore not included in d. The output is $y = g(x) = [p_s, L_w]^T$.
A linear approximation of (9) can be generated for controller design. In [Solberg et al., 2005a] it was shown that the dynamics, of the one-pass smoke tube boilers from AI, around the crossover frequency has little dependency on the steam load. For this reason it suffices to focus on a controller design derived from one linear model hence leaving out any gain scheduling. Hence the sampled linear approximation of the marine boiler takes the form:

$$x(k+1) = Ax(k) + Bu(k) + B_d d(k) \tag{10a}$$
$$y(k) = Cx(k) \tag{10b}$$
$$x \in \mathcal{X},\ u \in \mathcal{U} \tag{10c}$$

where $y = [p_s, L_w]^T$, $\mathcal{X} \subset \mathbb{R}^n$ and $\mathcal{U} \subset \mathbb{R}^m$ are compact sets describing constraints on states and inputs respectively. The matrices extracted at the operating point $p_s^0 = 8 \times 10^5 \text{Pa}$, $L_w^0 = 1.23\text{m}$ and $\dot{m}_s^0 = 1500/3600 \frac{\text{kg}}{\text{s}}$ and sampling time $T_s = 2\text{s}$ (8 times in the rise time of the fastest closed loop) are:

$$A = \begin{bmatrix} 0.998 & 0 & 0 & 1.80\times10^{4} & 4.99\times10^{3} \\ -9.82\times10^{-10} & 1 & 0 & 1.68 & 9.81\times10^{-4} \\ -4.06\times10^{-8} & 0 & 0.132 & -0.692 & 1.40\times10^{-3} \\ 0 & 0 & 0 & 0.819 & 0 \\ 0 & 0 & 0 & 0 & 0.989 \end{bmatrix}, \quad B = \begin{bmatrix} 7.60\times10^{4} & -1.27\times10^{3} \\ 1.49\times10^{-2} & 1.99\times10^{-3} \\ 2.13\times10^{-2} & 1.31\times10^{-3} \\ 0 & 0 \\ 0 & 0 \end{bmatrix},$$

$$B_d = \begin{bmatrix} -4.33\times10^{6} & 1.83\times10^{3} \\ -2.72 & 0.168 \\ 172 & 6.92\times10^{-2} \\ 0 & 1.81\times10^{-2} \\ 0 & 1.10\times10^{-2} \end{bmatrix}, \quad C = \begin{bmatrix} 1 & 0 & 0 & 0 & 0 \\ 0 & 0.610 & 0.610 & 0 & 0 \end{bmatrix}$$

2.1 Actuators

In practice the feed water and fuel flows are governed by complex nonlinear systems combined of pipes, valves and pumps. However, for the boiler control purpose, inner control loops around these systems can be used to linearise the gains, reduce uncertainty and suppress disturbances at the input of the plant.

This is achieved in case of the feed water by design of a gain scheduled flow controller having a closed loop time constant of $\approx 4\mathrm{s}$. Further, the feed water flow is limited by $\dot{m}_{fw} \in [0, 2100/3600]\frac{\mathrm{kg}}{\mathrm{s}}$. In fact, the upper bound is a function of the boiler pressure, however, with adequate pressure control this dependency can be neglected.
The fuel system is handled in a different way. First of all, the gain from valve position to flow in a large part of the operating range of the fuel system was found linear in [Andersen and Jørgensen, 2007]. Also fuel flow sensors are generally not mounted on boilers of the size presented in this paper. For this reason only a position controller for the fuel flow valve is used and a linear characteristic from position to flow is assumed known. This position is adjusted by an electric motor which is controlled using pulse width modulation (PWM). The fuel flow is limited by $\dot{m}_{fu} \in [30/3600, 155.5/3600]\frac{\mathrm{kg}}{\mathrm{s}}$. Further, the rate of change is limited by $|\frac{d\dot{m}_{fu}}{dt}| \leq \frac{37}{3600}\frac{\mathrm{kg}}{\mathrm{s}^2}$. The dynamics of the fuel systems is so fast that stationary conditions can be assumed.
The structure of the total nonlinear model of the boiler system (feed water supply system, fuel supply system and boiler) is shown in Figure 2. This is the simulation model used later for controller performance validation.

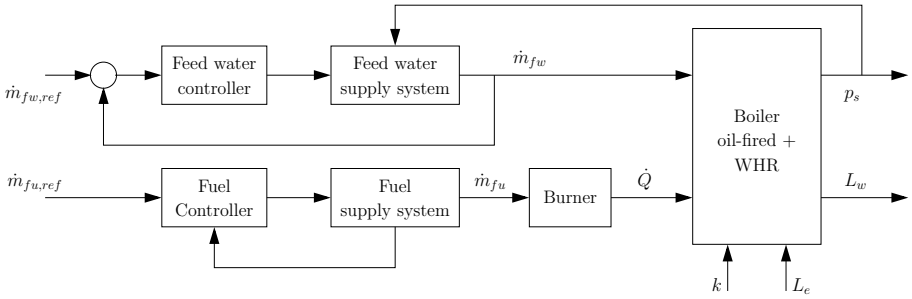

Figure 2: Structure of total nonlinear model used for simulation purposes. This structure includes flow controllers for the feed water and oil input.

3 Controller

The MPC controller designed in this section will be based on standard linear techniques [Maciejowski, 2001; Rossiter, 2003]. Our goal is to compare the MPC strategy to the standard diagonal PI controller to illustrate where performance improvements can be expected. The PI controllers are designed from the diagonal plant $\tilde{G}(s) = \begin{bmatrix} G_{11}(s) & 0 \\ 0 & G_{22}(s) \end{bmatrix}$ where $G(s) = \begin{bmatrix} G_{11}(s) & G_{12}(s) \\ G21(s) & G_{22}(s) \end{bmatrix} = C(sI - A)^{-1}B$. We define the design return ratio as the return ratio achieved by the PI controller on the diagonal plant: $\tilde{H}_{PI}(s) = \tilde{G}K_{PI}(s)$ with $K_{PI}(s) = \begin{bmatrix} K_{PI,11}(s) & 0 \\ 0 & K_{PI,22}(s) \end{bmatrix}$. The PI controller has the

following specifications:

$$K_{PI,jj} = k_{p,j}\left(1 + \frac{1}{T_{i,j}s}\right) \tag{11}$$

with $k_{p,1} = 1.88 \times 10^{-6}$, $T_{i,1} = 47.9$, $k_{p,1} = 9.4$ and $T_{i,1} = 426$. The controllers have been designed to achieve a phase margin of $\approx 71^\circ$ from simplified first order approximations of the plant. The pressure loop with a crossover frequency of $\omega_{c,1} = 0.073$ and the level loop with one at $\omega_{c,1} = 0.0063$. In the design the neglected dynamics of the actuators and furnace have been considered through selection of the phase margin. The reason for the large separation in bandwidth is that the level loop is limited by measurement noise.

The goal of the MPC controller design, besides including a feedforward from the engine load disturbance, is to recover the design return ratio $\tilde{H}_{PI}(s)$ of the diagonal plant on the full plant to be able to compare the PI and MPC designs. This means that the multiple input/multiple output nature of the MPC controller is used to achieve decoupling of the pressure and water level loop. In this way the design of the MPC controller consists of matching the singular values of the return ratio $H(z) = GK(z)$ (where $K(z)$ is the MPC controller) to those of the diagonal design $\tilde{H}_{PI}(s)$. In the design one must be careful to make sure that the singular values correspond to the directions of the correct outputs.

3.1 Model Predictive Controller

As mentioned above the predictive controller must be designed as to achieve a certain return ratio. MPC is a nonlinear controller. However, when the constraints are not active, it behaves as the finite horizon LQ controller. It is this linear part of the controller combined with an estimator to achieve output feedback that we shall match to the design return ratio.

To achieve this goal, we shall use the loop transfer recovery (LTR) procedure to design LQG controllers. Especially, we shall design the estimator to match the singular values of the return ratio when the loop is broken at the output and following use LTR to recover the properties of this design for the combined estimator and state feedback. For the use of LTR for tuning MPC controllers, see e.g. [Maciejowski, 2001; Rowe and Maciejowski, 1999]

A standard quadratic performance index is used in the predictive controller:

$$\begin{aligned} J^N(x_0, \mathbf{u}) = &\left[r(N) - y(N)\right]^T P \left[r(N) - y(N)\right] + \\ &+ \sum_{i=0}^{N-1} \left[r(i) - y(i)\right]^T Q \left[r(i) - y(i)\right] + \Delta u^T(i) R \Delta u(i) \end{aligned} \tag{12}$$

where Q includes weights on the pressure and water level deviations from the references r, R includes weights on the rate of input changes and P is a terminal error penalty.

The performance (12) might be recast as a regulation problem by augmenting the state vector by a reference model, see e.g. [Bitmead et al., 1990] or by shifting the origin of the system, see e.g. [Muske and Rawlings, 1993].
The estimator is designed as to achieve off-set free tracking of the pressure and water level. This is done by adding integrating disturbances to the process model in the direction Γ, see also [Muske and Rawlings, 1993; Pannocchia and Rawlings, 2003].

$$\begin{bmatrix} x(k+1) \\ \nu(k+1) \end{bmatrix} = \begin{bmatrix} A & \Gamma \\ 0 & I \end{bmatrix} \begin{bmatrix} x(k) \\ \nu(k) \end{bmatrix} + \begin{bmatrix} B \\ 0 \end{bmatrix} u(k) + \begin{bmatrix} 0 \\ I \end{bmatrix} w(k) \tag{13}$$

where ν is the integrating disturbance, $w(k)$ is a zero-mean white Gaussian noise process with covariance matrix W, and 0 and I are the zero matrix and identity matrix respectively of appropriate dimensions. In (13) d can be included through ν by choosing $\Gamma = B_d$. Using input increments as in the MPC performance index this becomes:

$$\begin{bmatrix} x(k+1) \\ \nu(k+1) \\ u(k) \end{bmatrix} = \begin{bmatrix} A & \Gamma & B \\ 0 & I & 0 \\ 0 & 0 & I \end{bmatrix} \begin{bmatrix} x(k) \\ \nu(k) \\ u(k-1) \end{bmatrix} + \begin{bmatrix} B \\ 0 \\ I \end{bmatrix} \Delta u(k) + \begin{bmatrix} 0 \\ I \\ 0 \end{bmatrix} w(k) \tag{14}$$

Let us start by setting the integrating disturbance in the direction of the inputs $\Gamma = B$ (this is similar to what was done in [Kothare et al., 2000]) and define the new state variable $\mu(k) = \nu(k) + u(k-1)$ which means that the model can be presented in the following form:

$$\begin{bmatrix} x(k+1) \\ \mu(k+1) \end{bmatrix} = \underbrace{\begin{bmatrix} A & B \\ 0 & I \end{bmatrix}}_{\tilde{A}} \begin{bmatrix} x(k) \\ \mu(k) \end{bmatrix} + \underbrace{\begin{bmatrix} B \\ I \end{bmatrix}}_{\tilde{B}} \Delta u(k) + \underbrace{\begin{bmatrix} 0 \\ I \end{bmatrix}}_{\tilde{B}_w} w(k) \tag{15}$$

which has the corresponding output equation:

$$y(k) = \underbrace{\begin{bmatrix} C & 0 \end{bmatrix}}_{\tilde{C}} \begin{bmatrix} x(k) \\ \mu(k) \end{bmatrix} + v(k) \tag{16}$$

where $v(k)$ is process measurement noise assumed to be zero-mean white Gaussian noise with covariance matrix V. The representation (15), (16) has the advantage of being both controllable and observable. If the disturbance is not put in the direction of the control inputs, (14) is neither stabilisable nor detectable. This is not a problem. There are many ways to handle this issue. One solution is to choose another model representation, including a state vector consisting of the change in state increments, $\Delta x(k) = x(k) - x(k-1)$, and the output, $y(k)$, see [Maciejowski, 2001] for details. A second solution is to move the integrator poles in (14) slightly inside the unit circle to achieve stabilisability and detectability. Also one can do as in [Bitmead et al., 1990] and calculate the gains associated with the state $x(k)$ first and then use this result to obtain

the gain associated with the disturbance by iterating a Riccati type difference equation. Finally, one might observe that for estimation purpose $u(k)$ is known and need not be estimated which means that when calculating estimator gains, (13) can be used. Further, to find the regulator gain, we can treat the unmeasured disturbance as known (given from the estimator). This way a matrix, relating the disturbances to steady state values of state and input, x_{ss}, u_{ss}, necessary for rejecting the disturbance (if possible) can be calculated. By shifting the origin of the original model to $(x(k) - x_{ss}), (u(k) - u_{ss})$, the regulator gain can be found. Using this gain and x_{ss}, u_{ss}, the regulator gain from the unmeasured disturbances can be found.

References and measured disturbances are handled in the same way when calculating regulator gains. However, it should be mentioned that the last-mentioned approach is only possible if the disturbance and reference are steps. If they are not steps but their dynamics are stable, they can be included in the state vector as above. If they are unstable, this does not work. It is noted in [Muske and Rawlings, 1993] that most unstable reference vectors (e.g. a ramp) are not realistic over an infinite horizon, meaning that for MPC purposes it might be more realistic to put the reference or disturbance constant at the end of the prediction horizon.

The estimator is implemented in the filter form which has the return ratio:

$$H_e(z) = \tilde{C}[zI - \tilde{A}]^{-1}\tilde{A}F \tag{17}$$

where F is the filter gain found by solving the filter algebraic Riccati equation. By defining $\left[\begin{smallmatrix} F_x \\ F_\mu \end{smallmatrix}\right] = \tilde{A}F$, a few algebraic manipulation leads to:

$$H_e(z) = C[zI - A]^{-1}\left(\frac{(z-1)F_x + BF_\mu}{z-1}\right) \tag{18}$$

From this representation, integral action in the controller is visible. The full controller is given by:

$$K = \begin{cases} x_c(k+1) = & (\tilde{A} - \tilde{B}L)(I - F\tilde{C})x_c(k) + (\tilde{A} - \tilde{B}L)Fy(k) \\ \hat{x}_c(k) = & (I - F\tilde{C})x_c(k) + Fy(k) \\ u_c(k) = & L\hat{x}_c(k) + L_r r(k) \end{cases} \tag{19}$$

where $\Delta u(k) = -u_c(k)$ and L, L_r are the stationary gains of the unconstrained LQR controller defined by (12) when $N \to \infty$ and $P = 0$. By setting the measurement noise covariance matrix equal to the identity matrix, $V = I$, the singular value of the return ratio can be shaped by changing the covariance matrix W describing the integrated noise.

We shall refer to the controller resulting from choosing $\Gamma_1 = B$ above as Design 1. A second design is considered, Design 2, which differs from Design 1 in the choice of disturbance model. Instead of focusing the unmeasured disturbances solely in the

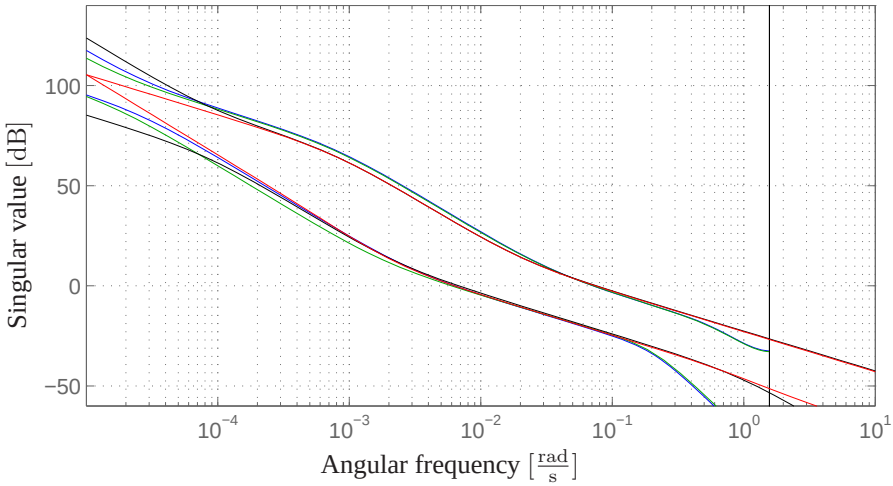

Figure 3: Singular value plot of the return ratios: $H_1(z)$ blue, $H_2(z)$ green, $\tilde{H}_{PI}(s)$ red and $H_{PI}(s)$ black. The black line at $\frac{\pi}{2}$ corresponds to the Nyquist frequency for the sampled plant. Notice the small difference between $H_{PI}(s)$, $H_1(z)$ and $H_2(z)$ over a large frequency band including the crossover frequency.

direction of the inputs, we set some in the direction of the unmeasured steam flow. More precisely, we choose $\Gamma_2 = \left[\frac{1}{2}B\left[\begin{smallmatrix}1\\1\end{smallmatrix}\right]\ B_d\left[\begin{smallmatrix}1\\0\end{smallmatrix}\right]\right]$. Subscripts 1, 2 will be used to denote each design.

One goal is to match the singular values of $\tilde{H}_{PI}$ precisely at the crossover frequencies and as good as possible elsewhere. In Figure 3 the singular values for $H_1(s)$, $H_2(s)$, $\tilde{H}_{PI}(s)$ and $H_{PI}(s)$ are shown. The last-mentioned being the return ratio achieved with the PI controller on the full plant.

The gains L, L_r are found in the recovery step of the LTR procedure which consists of setting $Q = I$ and $R = \rho I$ in (12) and then gradually decrease ρ until sufficient recovery has been achieved over a sufficiently large frequency range. Here we set $\rho = 10^{-2}$. $H_{e,1}(z)$ and $H_{e,2}(z)$, not shown in Figure 3 does not break off from the PI design at frequencies above $0.1\frac{\text{rad}}{\text{s}}$. The reason why $H_1(z)$ and $H_2(z)$ break off is that we have only sought recovery up to frequencies above the crossover frequency. The benefit from this is a high frequency roll off which helps damping measurement noise.

In Figure 3 the largest singular value corresponds to the pressure loop and the smallest singular value corresponds to the level loop. From Figure 3 it can be seen that cross couplings in the plant do not have a large influence on return ratio over a large frequency range, including the crossover frequency as $H_{PI}(j\omega) \approx \tilde{H}_{PI}(j\omega)$ for $\omega \in [5 \times 10^{-4}, 1]$. In Figure 4 the singular values of the output sensitivities $S_1(z) = (I + H_1(z))^{-1}$, $S_2(z) = (I + H_2(z))^{-1}$, $\tilde{S}_{PI}(s) = (I + \tilde{H}_{PI}(s))^{-1}$, $S_{PI}(s) = (I + H_{PI}(s))^{-1}$ and complementary output sensitivities $T_1(z) = I - S_1(z)$, $T_2(z) =$

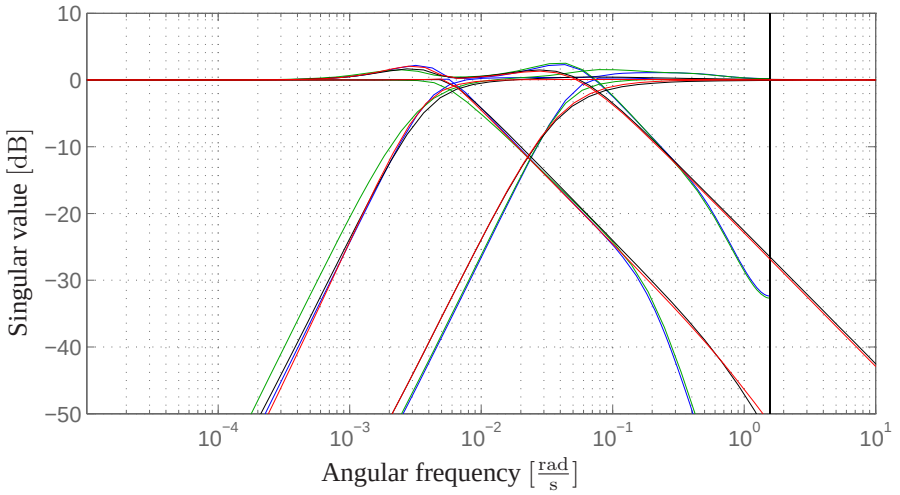

Figure 4: Singular value plot of the output sensitivities and complementary output sensitivities: $S_1(z)$, $T_1(z)$ blue, $S_2(z)$, $T_2(z)$ green, $\tilde{S}_{PI}(s)$, $\tilde{T}_{PI}(s)$ red and $S_{PI}(s)$, $T_{PI}(s)$ black. The black line at $\frac{\pi}{2}$ corresponds to the Nyquist frequency for the sampled plant.

$I - S_2(z), \tilde{T}_{PI}(s) = I - \tilde{S}_{PI}(s), T_{PI}(s) = I - S_{PI}(s)$ are plotted.
From this figure we see that the controllers have good stability margins. As can be seen there is not much apparent benefit in performance using a controller exploring the full information of the MIMO model. This is due to the large separation in bandwidth of the pressure and level loop. If there had been less noise on the water level measurement so that the bandwidth of this loop could be increased to near the pressure loop, the level loop would start to influence the pressure loop as was illustrated in [Solberg et al., 2007].
Look instead at the controller's ability to reject disturbances in the direction of Γ_2 which partly corresponds to the steam flow. The magnitude plot of the individual transfer functions of $S_1(z)G_{\Gamma_2}(z)$, $S_2(z)G_{\Gamma_2}(z)$, $\tilde{S}_{PI}(s)G_{\Gamma_2}(s)$ and $S_{PI}(s)G_{\Gamma_2}(s)$, with $G_{\Gamma_2}(s) = C(sI - A)^{-1}\Gamma_2$, are shown in Figure 5. These plots reveal that there is a potential for improvement of the response to steam load disturbances by using the MIMO control and appropriate disturbance modelling. In fact, Design 2 achieves similar bandwidths for the pressure and level seen from the steam flow disturbance.
Now the MPC controller consists of solving the following optimisation problem at each controller update:

$$\mathbf{u}^* = \arg\min_{\mathbf{u}} J^{\infty}(x_0, \mathbf{u}) \tag{20a}$$

$$\text{subj. to : (14)},\ x_0 = \hat{x}_c,\ x \in \mathcal{X},\ u \in \mathcal{U},\ \Delta u \in \Delta\mathcal{U} \tag{20b}$$

where u is the vector of future control inputs, of which only the first is used and ap-

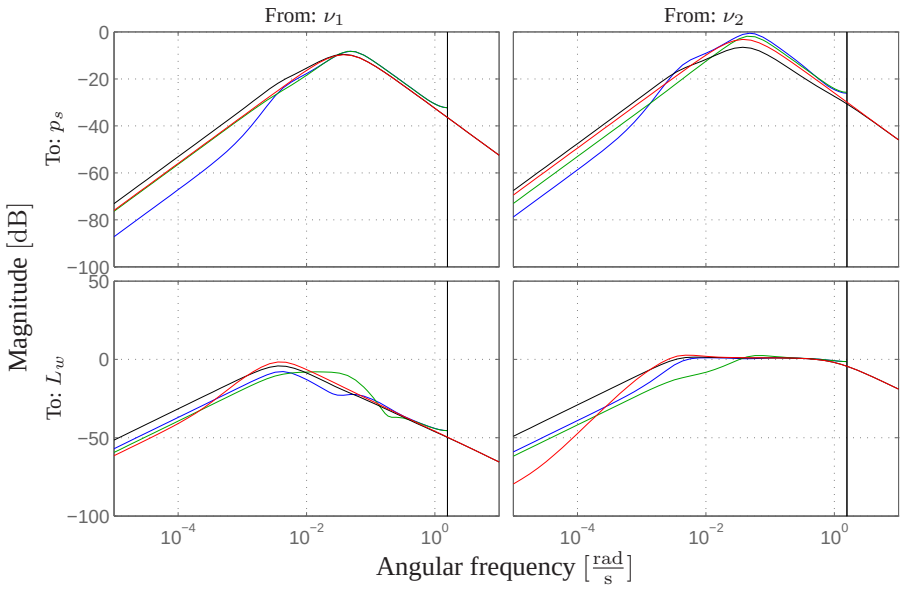

Figure 5: Magnitude plots of the individual transfer functions in the response from disturbances in direction of Γ_2 to the output: $S_1(z)G_{\Gamma_2}(z)$ blue, $S_2(z)G_{\Gamma_2}(z)$ green, $\tilde{S}_{PI}(s)G_{\Gamma_2}(s)$ red and $S_{PI}(s)G_{\Gamma_2}(s)$ black. The black line at $\frac{\pi}{2}$ corresponds to the Nyquist frequency for the sampled plant.

plied to the plant. This is in fact the infinite horizon constrained LQR problem where the initial state is set equal to the filter estimate, see (19). It is shown in [Scokaert and Rawlings, 1998] that there exists a finite N such that the finite horizon constrained regulator associated with (12) is identical to the infinite horizon controller. This requires definition of a terminal constraint set and cost defined by the unconstrained LQR control law. Definition of terminal sets and costs is one of the standard methods used in predictive control to ensure stability of the constrained nominal MPC controller [Mayne et al., 2000]. The problem with using this method for the boiler example is that it will require very long prediction horizons to ensure that at the end of the horizon $i = N$, the states enter a set where the autonomous system defined by the plant and unconstrained LQR controller satisfies both input and state constraints for all future time.

Alternatively, the method suggested in [Rawlings and Muske, 1993] also provide infinite horizon and stability. However, in this method the number of free control moves is adjusted by introducing a control horizon $N_c \leq N$. This method requires all unstable mode to be driven to zero in $i < N_c$ steps. This will lead to a long control horizon and thereby a large number of decision variables increasing computational complexity.

To have the solution correspond to the infinite horizon LQR controller at least when constraints are inactive, we could choose to include a terminal weight equal to the so-

lution to the algebraic Riccati equation associated with the LQR [Chmielewski and Manousiouthakis, 1996]. However, the controller was intended to be implemented using the MPC toolbox v. 2.2.3 and Real-Time Workshop® v. 6.5 from The MathWorks which do not support definition of such a weight (nondiagonal weights) for which reason we omit this here.
Instead the horizon N in (12) for the MPC controller will be chosen so that the gain of the unconstrained MPC is approximately equal to the LQR gain which can be verified by how well the return ratio achieved by the MPC controller approximated that of the LQG controller. In fact, our design is not particularly sensitive to the choice of horizon. However, a reasonable choice of horizon would be the longest time constant for the full state LQR controller which is $\approx 10\text{s}$ leading to $N = 5$. Please note that the horizon needed here is strongly dependent on the degree of recovery obtained in the LTR design or equivalently the weight factor ρ on the manipulated variables. The larger, the penalty the longer the horizon.

3.2 Robustness and Uncertainty

Application of MPC Design 2 to the full-scale boiler situated at AI's test center revealed problems with robustness of the design. This was seen as oscillations in the feed water flow and a poorly controlled water level. The controlled pressure and fuel flow showed acceptable behaviour.
The robustness issues are not a result of the differences in phase at different steam loads spotted in Bode plots in [Solberg et al., 2008], as generalised Nyquist plots show only a small variation in stability margins for varying loads. In [Solberg et al., 2007] it was noted that the nonlinear model also used in this paper does not have a non-minimum phase zero from changes in the feed water flow to the water level due to the shrink-and-swell phenomenon. The reason for accepting this was that it had not been observed in any measurements. New measurements from the failed controller test still do not give any conclusion whether this non-minimum phase zero is present. However, including this in the simulation model does not explain the oscillations observed.
Instead the problem is thought to be caused by model uncertainty. In particular, this uncertainty seems to be in the cross coupling from feed water to the pressure. The problem with uncertainty in the cross couplings is that we try to use these to speed up the disturbance rejection with a hard-tuned controller. In particular, we do not put a large penalty on the feed water flow which will cause the controller to manipulate the feed water flow when observing pressure changes. This can be seen from a Bode plot of the control sensitivity which has a high gain (> 1, with 1 being large with the scaling used) from pressure to feed water in a frequency range from just above the bandwidth for the water level control to just above the bandwidth of the pressure loop. The oscillations observed are in this frequency range.
Now, we might be able to fix this robustness problem by returning to the recovery step of the LTR design. Instead of setting $R = I$, we set $R = \text{diag}([1,\ 1000])$. This causes

the roll off of the singular value related to the water level loop to be moved just above the bandwidth of the level loop. This will have the benefit of keeping a more steady feed water supply operation while reducing sensitivity to measurement noise and increasing robustness towards uncertainty in the cross couplings. This new design does still allow for speeding up the disturbance rejection on the water level.
Remember that if we do not include a terminal weight in the performance index corresponding to the solution to infinite horizon LQR problem detuning, the regulator requires a longer prediction horizon. However, so far only simulations of the retuned controller are considered, and offline there are lots of resources available for controller computation. Also the desktop computer is much faster than the dedicated hardware used in the AI control platform.
To improve the sensitivity of the designed PI controller to measurement noise, we have designed second order filters in such a way that the open-loop singular value plots of the PI and MPC controller are approximately equal despite that full recovery is not achieved in the LTR design.

3.3 Disturbance Feedforward

If a measurement of the steam flow had been available, this could have been used in a feedforward. However, it is possible, as shown in [Hvistendahl and Solberg, 2004] and attempted above, to generate an estimate of this flow.
Accounting for shrink-and-swell introduced by the steam flow would need a prediction horizon of above 150 s. The reason is that e.g. the swell lasts this long before the water level drops (according to the integrator) due to insufficient water volume if more feed water has not been added.
Instead a feedforward from the engine load is possible as such a measurement is available. In fact information about when the engine is about to start or stop is assumed known 3 min. beforehand. This information can be naturally incorporated in the MPC algorithm from the previous section. Such information can of course also be handled in a more ad hoc way using a supervisory controller above a classical control scheme. The engine load is monitored by measuring the torque applied to the ship's propeller.
Further, the design from the previous section can easily be extended with this feedforward as it does not effect the stability and the designed controller. Hence the only thing needed is to include the engine load L_e in the model of the plant used in the estimator and internal model in the MPC algorithm.
In fact, one extra control variable is available when a WHR boiler is present, the steam dump valve, to be able to control the pressure in the common supply line. But unless there is an overproduction of steam from the WHR boiler it is not intentional to use this valve as at least in steady state this would mean that too much fuel has been consumed. Here we will not consider this extra degree of freedom, but considering standalone WHR boiler operation this is necessary.

4 Simulation Results

This section presents the simulation results gathered with a model verified with measurements from a full-scale MISSION^{TM} OB marine boiler from AI's test centre. The simulations focus on showing that MPC is applicable to the marine boilers and a comparison between the MPC and PI performance is made.
Four simulations are made. The simulations contain: a small step in the steam load, a large step in steam load, and as a preliminary study of the setpoint controller, a step in the water level reference is made, and finally the use of disturbance feedforward is illustrated when the engine starts.
All simulations start from the same operating point at a steam load of $1500\frac{\mathrm{kg}}{\mathrm{h}}$. In all the plots the colors have the same interpretation: the blue curves correspond to the PI controller, the green curves to MPC controller of Design 1, and the orange curves to MPC controller of Design 2. The figures have four plots where the top left plot shows the pressure and its setpoint red. The top right plot shows the water level and its setpoint red. The bottom left plot shows the fuel flow and the red line here illustrates the initial steady state fuel flow. The bottom right plot shows the feed water flow, the red line here illustrates the initial steady state feed water flow, and the black line is the disturbance in the steam valve converted to a requested steam flow at $8\mathrm{bar}$. Low-pass filtered white noise estimated from plant data has been added to the simulation outputs used for feedback.

4.1 Small Step

In this test a pulse of $-200\frac{\mathrm{kg}}{\mathrm{h}}$ lasting for $400\mathrm{s}$ is made at time $100\mathrm{s}$. The results are shown in Figure 6.
It is obvious from this plot why it is difficult to increase the bandwidth of the water level loop using the current measurement due to noise. PI and MPC do equally well in this test.

4.2 Large Step

In this test a pulse of $-900\frac{\mathrm{kg}}{\mathrm{h}}$ lasting for $400\mathrm{s}$ is made at time $100\mathrm{s}$. The results are shown in Figure 7.
In this test we see that PI does a little better regarding the pressure than MPC Design 1, whereas MPC Design 2 is best. However, both MPC designs do better regarding the water level. Further, there is a large difference between MPC Design 1 and Design 2. Design 2 is much better at bringing the water level back to its reference after the disturbance has changed. Also the pressure regulation is better. The reason is the disturbance model which has proved to play a large role in the performance of the MPC algorithm for the boiler application. Design 2 includes an estimate of the steam flow and is capable of generating better estimates of the outputs as well.

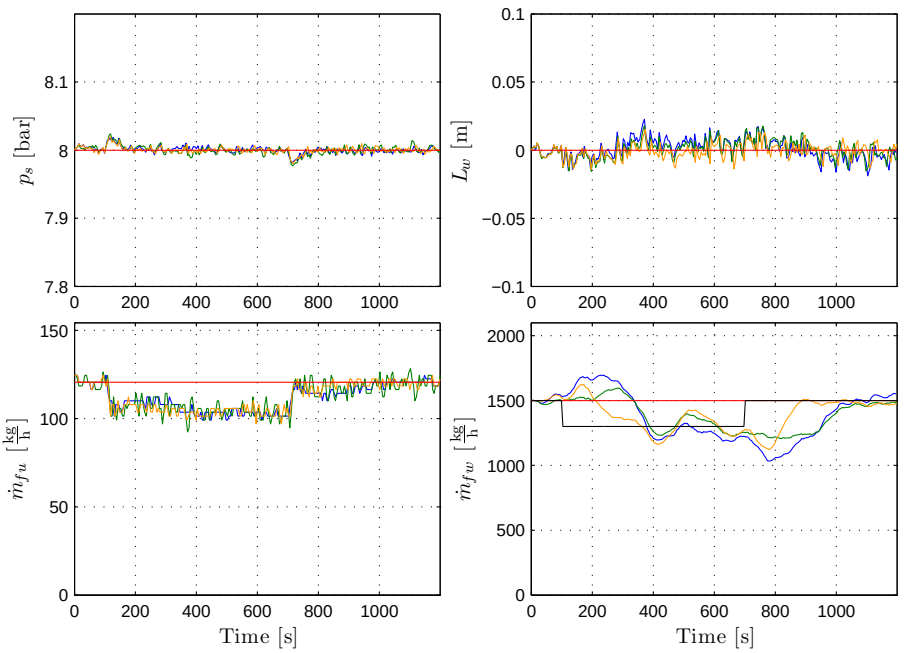

Figure 6: Plot of simulation results with a pulse in steam flow of $-200\frac{\text{kg}}{\text{h}}$ shown as the black line in the bottom right plot. The pressure is shown in the top left plot, the water level in the top right plot, the fuel flow in the bottom left plot, and the feed water flow in the bottom right plot. The red lines in the top plots are the references, and the red lines in the bottom plots are the initial steady state value of the inputs. The blue curves represent the PI controller, the green curves represent the MPC controller of Design 1, and the orange curves represent the MPC controller of Design 2.

4.3 Level Setpoint Change

In this test a step of -0.1m is made in the water level reference at time 100s. The results are shown in Figure 8.
As can be seen from the figure, the MPC controllers perform better than the PI controller when the setpoint is changed. Further, the MPC designs perform equally well. The reason is that in this case the model of the process is well known and no disturbances are acting on the system.

4.4 Disturbance Feedforward

This section has the purpose of illustrating the potential benefit of using MPC to incorporate a feedforward from a disturbance of which there is prior knowledge. In the simulation setup the boiler is started at the steady state where the engine load $L_e = 0$

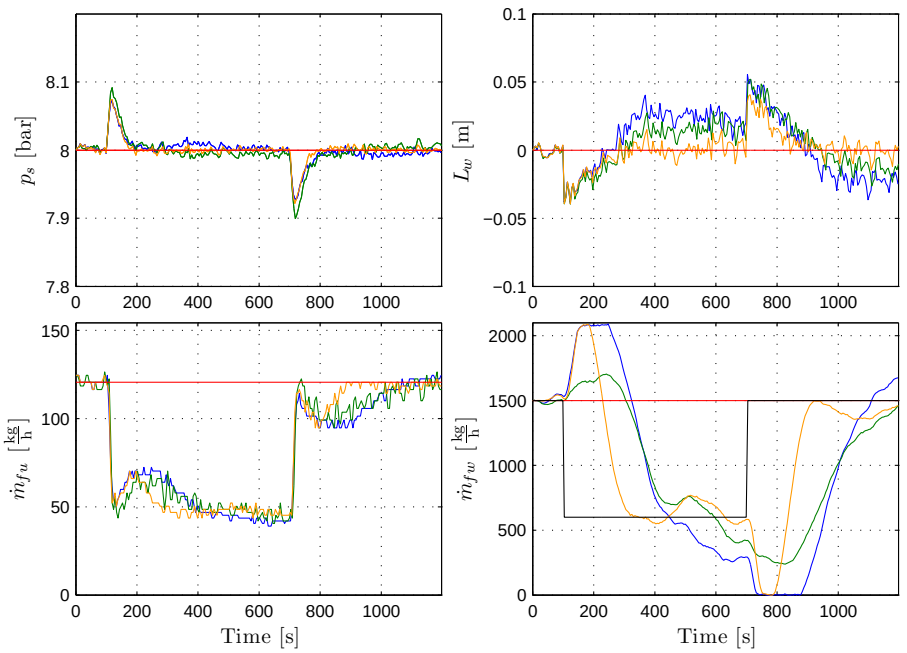

Figure 7: Plot of simulation results with a pulse in steam flow of $-900\frac{\text{kg}}{\text{h}}$ shown as the black line in the bottom right plot. The pressure is shown in the top left plot, the water level in the top right plot, the fuel flow in the bottom left plot, and the feed water flow in the bottom right plot. The red lines in the top plots are the references, and the red lines in the bottom plots are the initial steady state value of the inputs. The blue curves represent the PI controller, the green curves represent the MPC controller of Design 1, and the orange curves represent the MPC controller of Design 2.

and the steam load is $1800\frac{\text{kg}}{\text{h}}$. The engine is started at time 200s, $L_e = 0.35$ and knowledge of this change is assumed known 3min beforehand. The simulation results are shown in Figure 9. Only MPC Design 1 is considered. The reason is that no changes are made in the steam flow disturbance, and referring to Figure 8 this implies similar response from Designs 1 and 2. Further, the controller is modified. The prediction horizon has been increased to show the benefit from the predictive nature. It is set equal to $N = 75$ corresponding to 150 s. The blue curves in the figure correspond to the PI controller and the green curves to the MPC controller.

As expected it can be seen that having prior knowledge of the engine load disturbance can improve the performance of rejecting this disturbance. Also it can be seen that in this particular situation, the improvement is a water level maximum deviation from the setpoint of 0.05m less than when not using this information. Such a result could be used directly to reduce the steam space.

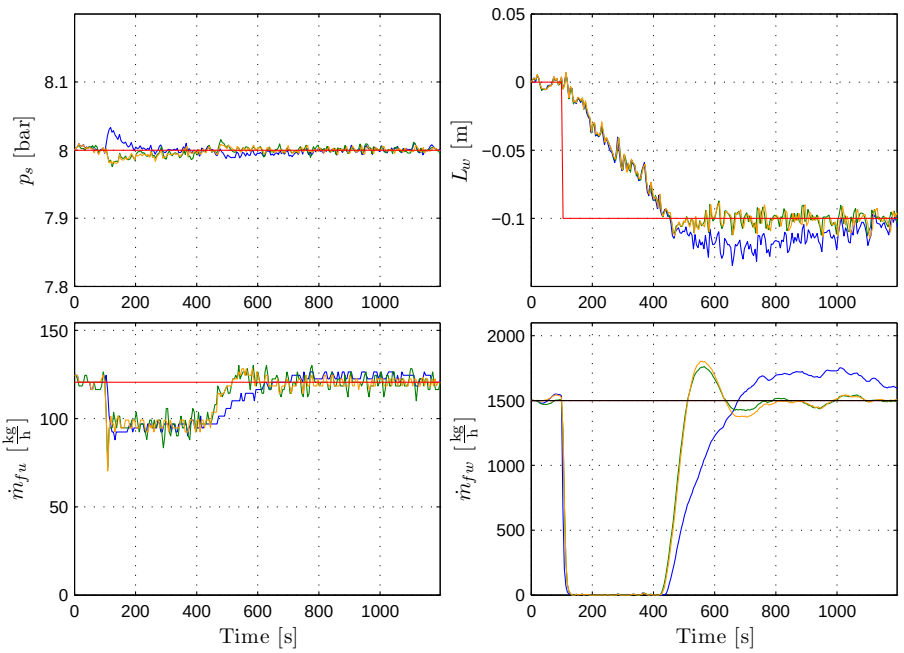

Figure 8: Plot of simulation results with a step change in the water level reference of -0.1m. The pressure is shown in the top left plot, the water level in the top right plot, the fuel flow in the bottom left plot, and the feed water flow in the bottom right plot. The red lines in the top plots are the references, and the red lines in the bottom plots are the initial steady state value of the inputs. The blue curves represent the PI controller, the green curves represent the MPC controller of Design 1, and the orange curves represent the MPC controller of Design 2. Notice that the MPC controllers have less overshoot.

5 Discussion

5.1 Setpoint Control

The setup of the setpoint control scheme is shown in Figure 10.
There are numerous reasons why a water level setpoint control loop is attractive in boiler control. Here we will briefly discuss this topic and propose the overall idea which could be converted into such a scheme. For the marine boiler we find the following three reasons for implementing an outer loop to handle setpoint changes in the water level:

- Knowledge of the current steam load can be converted into a current worst case shrink or swell level variation. At high load the maximum possible swell is small, meaning that one can operate at a higher water level than at low load.
- Knowledge of start/stop and large changes in the engine load can be converted

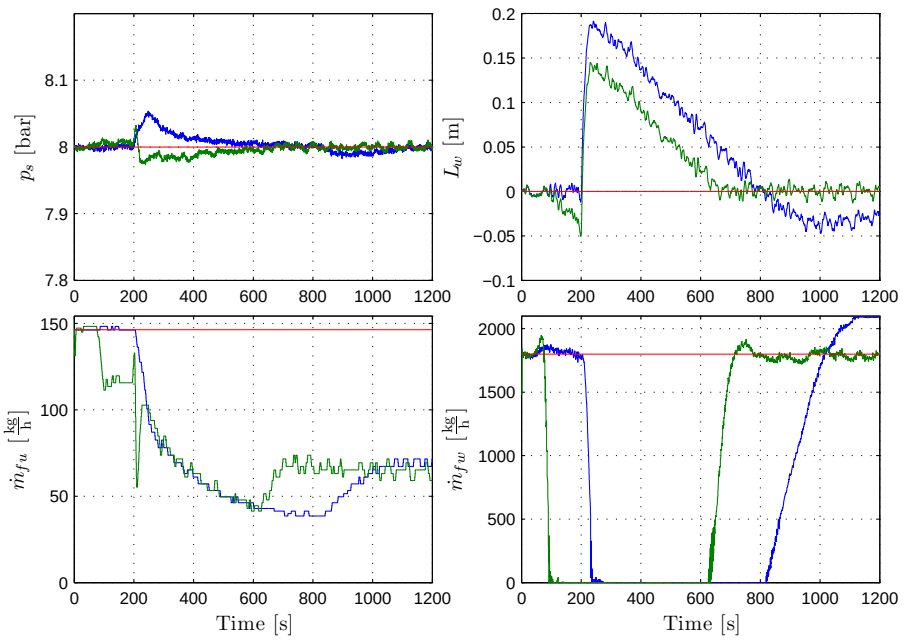

Figure 9: Plot of simulation results with a step change in the engine load from $L_e = 0$ to $L_e = 0.35$. The pressure is shown in the top left plot, the water level in the top right plot, the fuel flow in the bottom left plot, and the feed water flow in the bottom right plot. The red lines in the top plots are the references, and the red lines in the bottom plots are the initial steady state value of the inputs. The blue curves represent the PI controller and the green curves represent the MPC controller of Design 1. Notice that the MPC controller acts before the disturbance occurs.

into a water level setpoint at which a possible shrink or swell can be handled. E.g. the setpoint at sea with the engine running can be higher than when in harbour and the engine is stopped.

- The variance of fluctuation of the water level is increasing with the steam load. This means that at high load there is a larger probability for carrying water drops into the steam supply line. However, in the specific boiler a mechanical installation makes this phenomenon less pronounced.

All of these reasons have the same purpose: to minimise the steam space or equivalently raise the water level to improve boiler efficiency or reduce the physical boiler dimensions. AI has already implemented a simple version of setpoint control in their control system. This controller monitors the engine state (a digital signal). If the engine is running, the setpoint is set at a high level, and if the engine is stopped, the setpoint is set at a low level. These setpoints are calculated from the worst case engine load change

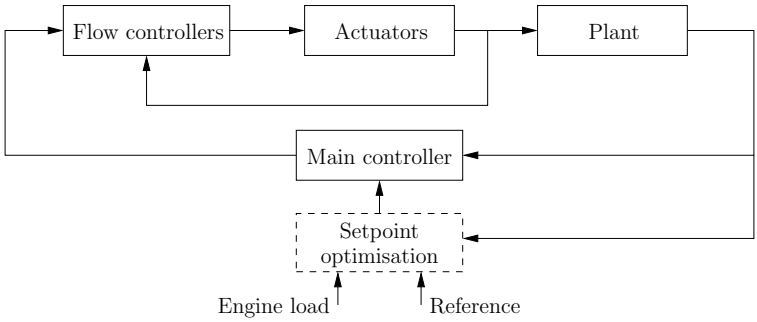

Figure 10: Principle of setpoint control scheme.

which occurs during start/stop. The lower setpoint when the engine is off is difficult to change. However, the upper setpoint needs not be constant. When there is only one upper setpoint, the distance to high water level alarm needs to be capable of still handling swell occurring due to changes from slow ahead operation to maximum engine load. Making the setpoint dependent on the current load can allow for minimising the required distance between the maximum upper setpoint and high water level alarm. Also using prior knowledge of the engine load changes can minimise the distance between the minimum and maximum setpoint.

We will focus on the first two bullet points above. Notice first that having an outer loop setting setpoints for the level controller would, if there were large couplings between the level and pressure loop, definitely comes at the expense of good pressure performance. However, as long as the gap between the bandwidths of the two loops is large this is less severe.

It is possible to generate predictions of the shrink-and-swell phenomenon. This can be achieved using knowledge of future engine load changes, a possible estimate of the steam load and steam bubble content beneath the water surface. Notice that the average rise time of the bubbles T_d is small compared to the pressure and water volume dynamics, see (7). So for the setpoint controller we might make the assumption that $V_b = \frac{T_d}{\varrho_s}\dot{m}_s$. Simulations and frequency analysis show that this assumption is approximately valid in the frequency range important for controller design. Using this assumption and the model of the engine load disturbance describing the amount of water shifted between the boilers during load changes (2) together with a simple model of the level closed loop P_{cl}, it is possible at each sample time to calculate a setpoint for the water level which is safe while maximising the level. Safe, here meaning that the upper and lower bound constraint on the water level can be respected.

This can be formulated as an optimisation problem of the form:

$$r_{L_w}(x_0, \hat{\dot{m}}_s, \mathbf{L}_e) = \arg\max L_w \tag{21a}$$

subj. to

$$L_w(t) = P_{cl}(t, r_{L_w}, \dot{m}_s, L_e),\ \overline{L}_w \geq L_w \geq \underline{L}_w \tag{21b}$$

$$\dot{m}_s \in W(\hat{\dot{m}}_s) \tag{21c}$$

where $\mathbf{L}_e$ is the vector of future known engine load disturbances, and $W(\hat{\dot{m}}_s)$ is the set of possible steam load disturbances given an estimate of the current steam load.

5.2 Alternatives to Setpoint Control

An alternative to the setpoint control is to simply include a maximisation of the water level in the cost function, subject to varying constraints or static constraints. If varying, finding these constraints will be a lot like finding the optimal setpoint in the setpoint control. If the constraints are kept fixed at a predefined minimum interval for the water level, the optimisation problem concerned with finding the manipulated variables must be overall possible disturbances in such a way that a proper distance is always kept to the hard constraint.

5.3 MPC vs. Clipped-LQG

One could wonder whether MPC $\approx$ clipped-LQG as long as only input constraints become active. To answer this question, we make the simulation with a large step in the steam flow disturbance again but now with only MPC Design 2 and clipped-LQG. Results are shown in Figure 11.
From this figure it is obvious that the benefits from using the more complex implementation of the MPC controller compared to clipped-LQG are small, when only input constraints become active. Further, the LQG controller might be approximated by low order transfer functions implemented as a decoupling and SISO controllers, delivering similar performance.

6 Conclusion

This paper has presented the preliminary application of MPC to an oil-fired one-pass smoke tube boiler operating together with a WHR boiler. MPC was shown applicable for controlling the standalone oil-fired boiler, using simulations on a model of a full-scale marine boiler where it performed just as good as the state-of-the-art PI controller. In fact, out of two MPC designs, one including an estimate of the steam flow disturbance outperformed PI control for large disturbance changes. Further, simulation results showed the benefit of using the predictive nature of MPC and its ability to use prior knowledge of disturbance changes for controlling the water level in the oil-fired boiler when the engine load is changed, resulting in shrink or swell in the level as water is pushed from or carried over to the WHR boiler. It should be mentioned that the

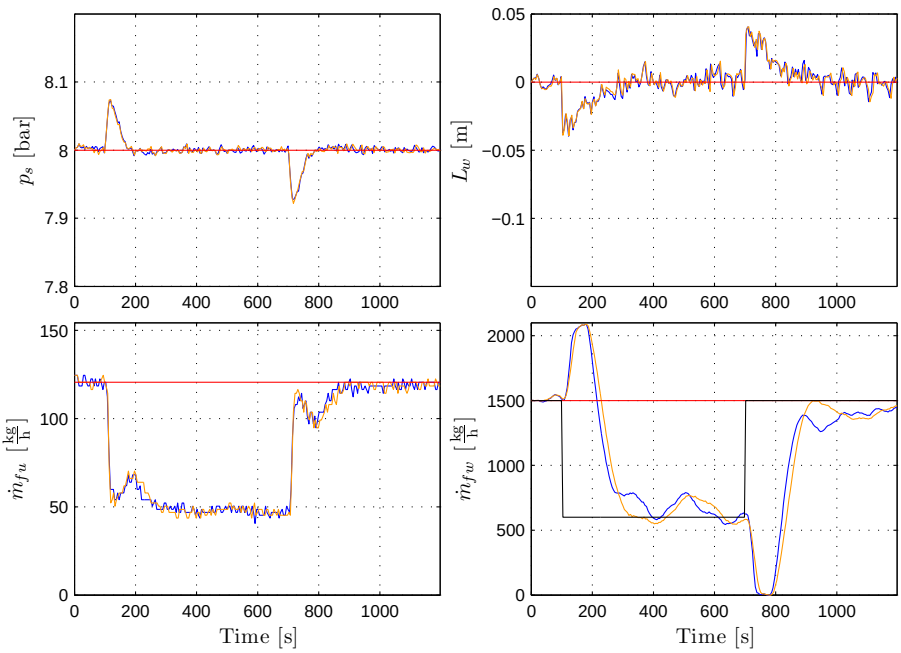

Figure 11: Plot of closed-loop response to a large step in the steam flow with blue the MPC of Design 2 and orange the clipped-LQG design. Note that apart from the small difference in feed water flow, the pressure and water level responses are almost coinciding.

success of the MPC controller regarding the steam load changes was not so much a consequence of the improved constraint handling but rather due to the internal model and state estimate.

The LTR procedure was chosen to match the singular values of the return ratio of the MPC controller to that of the diagonal PI controller. Further, using LTR makes the choice of controller and estimator gains more systematic. However, the drawback of using LTR to recover the return ratio at the output of the plant is that it makes it necessary to make the estimator slow to avoid amplifying measurement noise (remember that the recovery step consists of decreasing the weight on the control signal until sufficient recovery has been achieved). It seems that such a procedure will cause prediction mismatches between the plant and internal model used in MPC when steps are made in the steam flow disturbance which is due to the estimator dynamics.

The MIMO nature of the MPC controller improved the performance over the diagonal PI strategy. This was seen as an improved response to steam flow disturbances. Also the bandwidth of the level loop was so low that settling time for the PI controller and MPC Design 1 when responding to steps in the steam flow was very long. This would not

be acceptable if more steps occur just after each other or if the disturbance is changed according to a ramp. The benefit from using an estimate of the steam flow in Design 2 proved to improve this settling time by increasing the bandwidth of the sensitivity from the steam flow disturbance.
Further, a setpoint optimisation augmented to the MPC strategy for water level regulation was discussed to allow for operating closer to the high water level constraints.

6.1 Future Work

It would be possible to reduce the effect of the shrink-and-swell phenomenon coming from the WHR boiler using different mechanical installations and extra actuators. However, for economic and safety reasons, such solutions are not feasible for which reason research should be directed towards extending the present work.
First of all, a first principle model of the WHR boiler verified against measuring data is required. Secondly, an implementation of a variant of the setpoint optimisation scheme suggested should be tried. Also the extra degree of freedom available in the form of the steam dump valve should be included in the control scheme and standalone WHR boiler operation addressed.
Focus should also be put in the direction of improving an estimate of the steam flow disturbance for use in a feedforward scheme. This way level performance needs not be improved through speeding up the feedback. Also as the measurements are corrupted by noise and the model behave linearly with known structure, system identification techniques could be considered to obtain a state space model and an estimate of the process noise covariance to be used in a Kalman filter design. Alternative to system identification techniques the autocovariance least-squares (ALS) method [Odelson et al., 2006a,b] could be used to tune the Kalman filter. To speed up the feedback, other measuring techniques must be used.
As long as the bandwidth of the level loop cannot be increased due to noise on the level, there will be a large gap between the pressure and level loop bandwidths. This also means that we could design a fast pressure loop using any control strategy and then using MPC in a SISO scheme for the water level meaning that we can allow for a much longer sample time and hence longer prediction horizon. Even in the SISO case, MPC is preferred over PID as the computational demands of the SISO MPC controller are similar to those of PID control, and further the MPC controller in general outperforms the PID controller regarding setpoint changes, disturbance rejecting and constraint handling [Pannocchia et al., 2005].

References

K. J. Åström and R. D. Bell. Drum boiler dynamics. *Automatica*, 36:363–378, 2000.

S. Andersen and L. Jørgensen. Scheme for auto tuning control of marine boilers. Master's thesis, Aalborg University, June 2007.

R. Bitmead, M. Gevers, and V. Wertz. *Adaptive Optimal Control: The Thinking Man's GPC*. Prentice Hall International, 1990.

D. Chmielewski and V. Manousiouthakis. On constrained infinite-time linear quadratic optimal control. *Systems & Control Letters*, 29:121–129, 1996.

J. Doyle and G. Stein. Multivariable feedback design: Concepts for a classical/modern synthesis. *IEEE Transactions on Automatic Control*, 26:4–16, 1981.

P. U. Hvistendahl and B. Solberg. Modelling and multi variable control of a marine boiler. Master's thesis, Aalborg Universitet, Institute of Electronic Systems, Aalborg, Denmark, 2004.

M. V. Kothare, B. Mettler, M. Morari, P. Bendotti, and C.-M. Falinower. Level control in the steam generator of a nuclear power plant. *IEEE Transactions on control system technology*, 8, No. 1:55–69, 2000.

Y. S. Lee, W. H. Kwon, and O. K. Kwon. A constrained receding horizon control for industrial boiler systems. In G. Hencsey, editor, *IFAC Symposium on Manufacturing, Modeling, Management and Control (MIM 2000)*, pages 411–416, Patras, Greece, 2000.

J. M. Maciejowski. Asymptotic recovery for discrete-time systems. *IEEE Transactions on Automatic Control*, 30:602–605, 1985.

J. M. Maciejowski. *Predictive Control With Constraints*. Harlow: Pearson Education Limited, 2001.

J. M. Maciejowski. *Multivariable Feedback Design*. Addison-Wesley, 1989.

D. Q. Mayne, J. B. Rawlings, C. V. Rao, and P. O. M. Scokaert. Constrained model predictive control: Stability and optimality. *Automatica*, 36(6):789–814, June 2000.

K. R. Muske and J. B. Rawlings. Model predictive control with linear models. *AIChE Journal*, 39:262–287, 1993.

B. J. Odelson, A. Lutz, and J. B. Rawlings. The autocovariance least-squares method for estimating covariances: Application to model-based control of chemical reactors. *IEEE Transactions on Control Systems Technology*, 14:532–540, 2006a.

B. J. Odelson, M. R. Rajamani, and J. B. Rawlings. A new autocovariance least-squares method for estimating noise covariances. *Automatica*, 42:303–308, 2006b.

G. Pannocchia and J. B. Rawlings. Disturbance models for offset-free model-predictive control. *American Institute of Chemical Engineers, AIChE*, 49:426–437, 2003.

G. Pannocchia, N. Laachi, and J. B. Rawlings. A candidate to replace PID control: SISO-constrained LQ control. *American Institute of Chemical Engineers, AIChE*, 51:1178–1189, 2005.

S. J. Qin and T. A. Badgwell. A survey of industrial model predictive control technology. *Control Engineering Practice*, 11:733–764, 2003.

J. B. Rawlings and K. R. Muske. The stability of constrained receding horizon control. *IEEE Transactions on Automatic Control*, 38:1512–1516, 1993.

J. A. Rossiter. *Model-based Predictive Control: A Practical Approach*. CRC Press LLC, 2003.

C. Rowe and J. M. Maciejowski. Tuning robust model predictive controllers using LQG/LTR. In *14th IFAC World Congress*, Beijing, P.R. China, 1999.

A. Saberi, B. M. Chen, and P. Sannuti. *Loop Transfer Recovery: Analysis and Design*. Springer-Verlag, London, 1993.

P. O. M. Scokaert and J. B. Rawlings. Constrained linear quadratic regulation. *IEEE Transactions on Automatic Control*, 43(8):7, August 1998.

B. Solberg, C. M. S. Karstensen, and P. Andersen. Control properties of bottom fired marine boilers. In T. Gundersen, editor, *ECOS 2005 Conference*, volume 2, pages 669–678, Trondhjem, Norway, 2005a.

B. Solberg, C. M. S. Karstensen, P. Andersen, T. S. Pedersen, and P. U. Hvistendahl. Model-based control of a bottom fired marine boiler. In P. Horacek, editor, *16th IFAC World Congress*, Prague, Czech Republic, 2005b.

B. Solberg, C. M. S. Karstensen, and P. Andersen. Control properties of bottom fired marine boilers. *Energy*, 32:508–520, 2007.

B. Solberg, P. Andersen, and J. Stoustrup. The one-pass smoke tube marine boiler - limits of performance. In *ECOS 2008 Conference*, volume 2, pages 867–885, Kraków, Poland, 2008.

Paper E

The One-pass Smoke Tube Marine Boiler - Limits of Performance

Brian Solberg & Palle Andersen & Jakob Stoustrup

The paper has been published in:
Proceedings of the 21st International Conference on Efficiency, Cost, Optimization, Simulation and Environmental Impact of Energy Systems (ECOS 2008),
June 24–27, 2008, Kraków, Poland

Abstract

This paper summarises a number of results gathered over the past few years regarding modelling and control of the one-pass smoke tube marine boiler. The purpose is to communicate our state of knowledge regarding the limits of performance in these processes. The standpoint of the paper is limits with respect to the current standard configured boiler. We present a simple second order control model for the boiler capturing also cross couplings and disturbance influence. This model is accurate over a large frequency range including the crossover frequencies. Performance limitations imposed by the actuator systems, sensor noise and neglected model dynamics are treated. Also control design guidelines are presented and suggestions for pushing the limits by new equipment presented.

1 Introduction

Over the past few years much research has been directed towards the modelling and control of the one-pass smoke tube marine boiler reported in e.g. [Solberg et al., 2005, 2007a,b, 2008; Sørensen et al., 2004] along with numerous student projects conducted at Aalborg University in co-operation with Aalborg Industries A/S.

In this paper the results gathered from these works will be used to setup control design guidelines and specify limits of performance for the boiler process. The boiler setup is shown in Figure 1. The boiler family concerned in the present work is the oil-fired one-pass smoke tube boiler from Aalborg Industries A/S (AI). The boiler consists of a furnace and flue gas pipes surrounded by water. In the top of the boiler steam is led out and feed water is injected. This boiler differs from other boiler designs in two ways: it is side-fired and the flue gas passes straight through. As an example one of these boilers is designed for a maximum steam load of $1800\frac{\mathrm{kg}}{\mathrm{h}}$ at operating pressure $8\mathrm{bar}$. The minimum steam load is obviously $0\frac{\mathrm{kg}}{\mathrm{h}}$ whereas the minimum capacity of the burner unit corresponds to a steam flow of approximately $400\frac{\mathrm{kg}}{\mathrm{h}}$.

The initial interest in the one-pass smoke tube boiler was to obtain a control strategy which was able to minimise the fluctuations in the water level without compromising pressure performance in such a way that the physical geometry of the boiler could be reduced. It was the conviction that such initiatives would require accurate detailed nonlinear first principle models of the boiler and a controller design taking into account the multiple input multiple output and nonlinear characteristics of the process. However, in this paper we will more or less argue the opposite. If the boiler dimensions are to be minimised and hence the process pushed to the limits it is important to know what set these limits. Likewise studying these limits might help engineers manually tuning controller during commissioning. However, it is also obvious that if simple control design guide lines can be put up, the current relatively long time spent by the engineer tuning the controllers can be reduced remarkably.

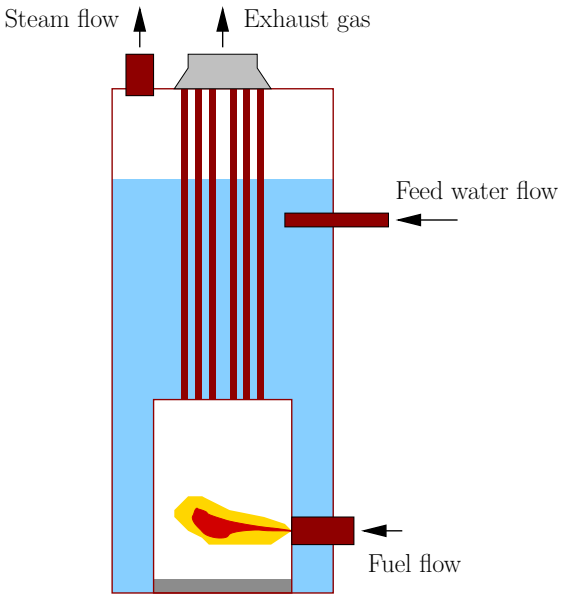

Figure 1: Principle of the oil-fired one-pass smoke tube marine boiler.

Much published work on boiler modelling and control is available, [Åström and Bell, 2000; Chien et al., 1958; Kim and Choi, 2005; Lee et al., 2000; Pellegrinetti and Bentsman, 1996]. Both models based on first principles of varying complexity and models based on system identification techniques to specify a black box model based on e.g. linear parametric models have been proposed. Setting up control guide lines can be done using any of the existing control design techniques as: Linear Quadratic Control, [Athans and Falb, 1966], Model predictive control [Maciejowski, 2001; Rossiter, 2003], Robust control [Dullerud and Paganini, 2000; Zhou et al., 1996] and PID control [Åström and Hägglund, 2006]. Regarding limits of performance tools for analysing linear systems can be found in almost any text book on control theory e.g. [Boyd and Barratt, 1991; Skogestad and Postlethwaite, 1996]. However, for nonlinear systems there are less systematic analysis procedures available.

The focus is on nonlinear model reduction to create a simple second order model including cross terms and disturbance influences. The important nonlinearities will be shown to persist at the input of the plant due to the actuator systems. Regarding performance the constraint on the actuator absolute values together with sensor noise will be shown to be the limiting factor. Simple controller design guidelines are presented. For these controllers to be easy to understand and tune by any service engineer the control theory used is based on classical PID control.

The paper is organised as follows. Firstly the simple nonlinear model is described along with simple linearised versions. Secondly the limits of performance are discussed, treating the actuator systems, shrink-and-swell, disturbances, nonlinearities, interaction measurements noise and constraints. In the subsequent section control design guidelines for the actuator systems and the boiler are put up. Lastly concluding remarks are presented.

2 Model

Here we briefly discuss the nonlinear model of the boiler with one purpose only: how to find a suitable model for controller design. Many dynamical models of varying complexity for the drum boiler have been proposed in the literature – see e.g. [Åström and Bell, 2000; Andersen and Jørgensen, 2007; Kothare et al., 2000; Solberg et al., 2005; Sørensen et al., 2004]. However, already in [Hvistendahl and Solberg, 2004] it was pointed out that a high order linear model was not necessary for describing the dynamics of the boiler important to controller design and further step response analysis showed good agreement between responses from a nonlinear model and linear model. The simple control model does not account for precise stationary gains and further does not provide information on many internal variable. However, when constraints are not present for the internal variables these thing are not important to the control. In particular, a controller will usually include integral action which among others account for model stationary gain mismatches.
Studies have shown that both the flue gas part (furnace and convection tubes) and the metal separating the water/steam part from the flue gas have considerably faster dynamics than the desired closed loop bandwidth with time constants $< 2\mathrm{s}$. Due to this fact the power delivered to the water/steam part is modelled as:

$$Q = \eta \dot{m}_{fu} \tag{1}$$

where η is a constant describing a combination of energy released in the combustion plus furnace and convection tubes heat transfer efficiency. η is in fact a function of the burner load and water level in the boiler drum, but for control purposes it is sufficiently accurate to consider η constant. First of all modelling the dependency on the water level was shown in [Solberg et al., 2007b] to give rise to some special low frequency phenomena. This was seen as a zero in the origin from fuel flow to pressure and the integrator from feed water to water level was moved slightly into the left half plane. These phenomena are seen at frequencies far below the interesting bandwidth and since water level will always be controlled, which removes the zero in the origin, there is no further need to include this in a control model. Also it turns out that in the boiler family treated here η is approximately invariant to the burner load.
The model of the water/steam part has the purpose of describing the steam pressure in the boiler p_s and the water level L_w. The modelling is complicated by the shrink-and-

swell phenomenon due to steam load changes which is caused by the distribution of steam bubbles under the water surface.
The total volume of water and steam in the boiler is given as: $V_t = V_w + V_s + V_b$, where V_w is the water volume, V_s is the volume of the steam space above the water surface and V_b is the volume of the steam bubbles below the water surface.
To capture the dynamics of the water/steam part the total mass and energy balances are considered. The total mass balance for the water/steam part is:

$$\frac{d}{dt}(\varrho_s(V_t - V_w) + \varrho_w V_w) = \dot{m}_{fw} - \dot{m}_s \tag{2}$$

and the energy balance is:

$$\frac{d}{dt}\Big[\varrho_w V_w h_w + \varrho_s(V_t - V_w)h_s - V_t p_s + \varrho_m V_m c_{p,m} T_s\Big] = Q + h_{fw}\dot{m}_{fw} - h_s \dot{m}_s \tag{3}$$

where $\dot{m}_{fw}$ is the feed water flow, $\dot{m}_s$ is the steam flow, ϱ is density, h is enthalpy and T is temperature, c_p is specific heat capacity and subscript m stands for metal. It should be noticed that energy accumulated in metal of the boiler jacket, furnace and convection tubes is included in the balance for the water/steam part.
The mass balance can be written as:

$$\left[(V_t - V_w)\frac{d\varrho_s}{dp_s} + V_w \frac{d\varrho_w}{dp_s}\right]\frac{dp_s}{dt} + (\varrho_w - \varrho_s)\frac{dV_w}{dt} = \dot{m}_{fw} - \dot{m}_s \tag{4}$$

and as $\frac{d\varrho_s}{dp_s}$ is ≈ 10 times smaller than $\frac{d\varrho_w}{dp_s}$ we make the following approximation of (4):

$$V_w \frac{d\varrho_w}{dp_s}\frac{dp_s}{dt} + (\varrho_w - \varrho_s)\frac{dV_w}{dt} \approx \dot{m}_{fw} - \dot{m}_s \tag{5}$$

Now following [Åström and Bell, 2000] another simple expression for the pressure can be derived. Multiplying (2) by h_w and subtracting the result from (3) gives:

$$\left[\begin{array}{c} h_c(V_t - V_w)\frac{d\varrho_s}{dp_s} + \varrho_w V_w \frac{dh_w}{dp_s} + \\ \varrho_s(V_t - V_w)\frac{dh_s}{dp_s} - V_t + \varrho_m V_m c_{p,m}\frac{dT_s}{dp_s} \end{array}\right]\frac{dp_s}{dt} + - h_c \varrho_s \frac{dV_w}{dt} = Q - (h_w - h_{fw})\dot{m}_{fw} - h_c \dot{m}_s \tag{6}$$

where $h_c = h_s - h_w$ is the vaporisation enthalpy. (5) could be inserted in (6). However, the ratio $\frac{\varrho_s}{\varrho_w - \varrho_s} = 0.0047$ is small for which reason we neglect the $\frac{dV_w}{dt}$ term in (6). The term multiplying $\frac{dp_s}{dt}$ has large differences in numerical size and a good approximation of the pressure dynamics is due to the large water volume in the boiler given by:

$$\frac{dp_s}{dt} \approx \frac{1}{\varrho_w V_w \frac{dh_w}{dp_s}}(Q - (h_w - h_{fw})\dot{m}_{fw} - h_c \dot{m}_s) \tag{7}$$

Equations (5) and (7) above only express the pressure and the water volume in the boiler. As the water level of interest in the control problem is given as: $L_w = (V_w + V_b - V_o)/A_{ws}$, another equation is needed for describing the volume of steam bubbles V_b in the water (the water level is measured from the furnace top and V_o is the volume surrounding the furnace and A_{ws} is the water surface area). Many proposals describing the distribution of steam bubbles under the water surface have been made – see e.g. [Åström and Bell, 2000; Andersen and Jørgensen, 2007; Kim and Choi, 2005; Solberg et al., 2005]. Most of these are based on assumptions and all end up including empirical constants to be estimated to fit the model to process data. In [Kothare et al., 2000] an approach was taken to model the boiler as a collection of linear models in which a non-minimum phase zero is easily inserted.
The difficult part of the modelling is to describe the amount of steam escaping the water surface, $\dot{m}_{b\to s}$. Here we take the approach of [Andersen and Jørgensen, 2007] which is similar to the expression in [Åström and Bell, 2000]:

$$\dot{m}_{b\to s} = \frac{\varrho_s}{T_d} V_b \tag{8}$$

where $\dot{m}_{b\to s}$ is expressed as a function of the steam bubble volume and density of the steam, the constant T_d expresses the average rise time of bubbles in the water. This flow can be used to set up a mass balance for the water and steam below the water surface. However, the dynamics of this extra mode is very fast with a time constant of about $1\mathrm{s}$. Therefore it is reasonable to assume a stationary relationship between the steam load and bubble volume as:

$$V_b = \frac{T_d}{\varrho_s} \dot{m}_s \tag{9}$$

This equation introduces V_b in the model and hereby the shrink-and-swell phenomenon. In practice the water/steam circuit is closed and the steam flow is governed by several valves combined with pipe resistance. Therefore a variable $k(t)$ expressing pipe conductance and valve strokes is introduced. $\dot{m}_s$ is then given as:

$$\dot{m}_s(t) = k(t)\sqrt{p_s(t) - p_{dws}} \tag{10}$$

where the downstream pressure, p_{dws}, is the pressure in the feed water tank which is open and hence has ambient pressure, $p_{dws} = p_a$. $p_s(t) - p_{dws}$ is the differential pressure over the steam supply line.
The final second order model has the form:

$$\dot{x} = f(x, u, d) \tag{11a}$$

$$y = c(x, u, d) \tag{11b}$$

where $y = [p_s, L_w]^T$, $x = [p_s, V_w]^T$, $u = [\dot{m}_{fu}, \dot{m}_{fw}]$ and $d = k$. As the temperature of the feed water is controlled it can be assumed constant and therefore not included in d.

The linearised version of this model is:

$$\dot{x}(t) = Ax(t) + Bu(t) + B_d d(t) \tag{12a}$$
$$y(t) = Cx(t) + Du(t) + D_d d(t) \tag{12b}$$

where we note the direct term from the disturbance to the water level output, due to the shrink-and-swell phenomenon. The matrices are given as:

$$A = \begin{bmatrix} \frac{-\dot{m}_s^0}{\varrho_w^0 V_w^0 \left\{\frac{dh_w}{dp_s}\right\}^0} \left(\frac{h_c^0 + 2(p_s^0 - p_a)\left\{\frac{dh_s}{dp_s}\right\}^0}{2(p_s^0 - p_a)} \right) & 0 \\ \frac{-\dot{m}_s^0}{2(p_s^0 - p_a)(\varrho_w^0 - \varrho_s^0)} \left(1 - \frac{\left[h_c^0 + 2(p_s^0 - p_a)\left\{\frac{dh_s}{dp_s}\right\}^0\right]\left\{\frac{d\varrho_w}{dp_s}\right\}^0}{\varrho_w \left\{\frac{dh_w}{dp_s}\right\}^0} \right) & 0 \end{bmatrix} \tag{13a}$$

$$B = \begin{bmatrix} \frac{\eta}{\varrho_w^0 V_w^0 \left\{\frac{dh_w}{dp_s}\right\}^0} & -\frac{(h_w^0 - h_{fw})}{\varrho_w^0 V_w^0 \left\{\frac{dh_w}{dp_s}\right\}^0} \\ -\frac{\eta \left\{\frac{d\varrho_w}{dp_s}\right\}^0}{\varrho_w^0 (\varrho_w^0 - \varrho_s^0)\left\{\frac{dh_w}{dp_s}\right\}^0} & \frac{1}{\varrho_w^0 - \varrho_s^0} \left(1 + \frac{(h_w^0 - h_{fw})\left\{\frac{d\varrho_w}{dp_s}\right\}^0}{\varrho_w^0 \left\{\frac{dh_w}{dp_s}\right\}^0} \right) \end{bmatrix} \tag{13b}$$

$$B_d = \begin{bmatrix} -\frac{h_c^0 \sqrt{p_s^0 - p_a}}{\varrho_w^0 V_w^0 \left\{\frac{dh_w}{dp_s}\right\}^0} \\ -\frac{\sqrt{p_s^0 - p_a}}{\varrho_w^0 - \varrho_s^0} \left(1 - \frac{h_c^0 \left\{\frac{d\varrho_w}{dp_s}\right\}^0}{\varrho_w^0 \left\{\frac{dh_w}{dp_s}\right\}^0} \right) \end{bmatrix} \tag{13c}$$

$$C = \begin{bmatrix} 1 & 0 \\ \frac{\dot{m}_s^0 T_d}{A_{ws}\{\varrho_s^0\}^2} \left(\frac{\varrho_s^0 - 2(p_s^0 - p_a)\left\{\frac{d\varrho_s}{dp_s}\right\}^0}{2(p_s^0 - p_a)} \right) & \frac{1}{A_{ws}} \end{bmatrix} \tag{13d}$$

$$D = \begin{bmatrix} 0 & 0 \\ 0 & 0 \end{bmatrix}, \; D_d = \begin{bmatrix} 0 \\ \frac{T_d \sqrt{p_s^0 - p_a}}{A_{ws} \varrho_s^0} \end{bmatrix} \tag{13e}$$

where we have used $\dot{m}_{fw}^0 = \dot{m}_s^0$. Remember also that $V_w^0 = A_{ws} L_w^0 + V_o - \frac{T_d}{\varrho_s^0} \dot{m}_s^0$. We see that the linear model matrices depend only on the pressure, the water level and the steam load. In particular, we see that the matrices are linearly dependent on $\dot{m}_s^0$ if variations in V_w^0 can be ignored. For reference the Laplace transform of the model is:

$$y(s) = G(s)u(s) + G_d(s)d(s) \tag{14}$$

with $G(s) = C(sI - A)^{-1}B$ and $G_d(s) = C(sI - A)^{-1}B_d + D_d$. The complexity in this model is introduced because we insist on modelling the cross terms as well. However, a very good approximation using only direct terms can be given as:

$$p_s(s) = \hat{G}_{11}(s)\dot{m}_{fu}(s) + \hat{G}_{d,11}(s)k(s) \tag{15a}$$
$$L_w(s) = \hat{G}_{22}(s)\dot{m}_{fw}(s) + \hat{G}_{d,21}(s)k(s) \tag{15b}$$

with

$$\hat{G}_{11}(s) = \left(\frac{\eta}{\varrho_w^0 V_w^0 \left\{ \frac{dh_w}{dp_s} \right\}^0} \right) \frac{1}{s} \tag{16a}$$

$$\hat{G}_{22}(s) = \left(\frac{1}{A_{ws}(\varrho_w^0 - \varrho_s^0)} \right) \frac{1}{s} \tag{16b}$$

$$\hat{G}_{d,11}(s) = \left(\frac{-h_c^0 \sqrt{p_s^0 - p_a}}{\varrho_w^0 V_w^0 \left\{ \frac{dh_w}{dp_s} \right\}^0} \right) \frac{1}{s} \tag{16c}$$

$$\hat{G}_{d,21}(s) = \left(\frac{T_d \sqrt{p_s^0 - p_a}}{A_{ws} \varrho_s^0} \right) \frac{s - \frac{\varrho_s}{T_d(\varrho_w - \varrho_s)}}{s} \tag{16d}$$

The only unknown parameters in the presented model are the efficiency η and the residence time of the steam bubbles in the drum T_d. Normally when finding these one has a good idea about the size of the efficiency whereas regarding T_d one must rely on experience from previous boiler designs.

3 Limits of Performance

This section discusses in detail the properties of the marine boiler system and what sets the limit of how good performance can be achieved.

3.1 Boiler Nonlinearities

In [Solberg et al., 2007b] the MISSION^{TM} OB boiler was shown to behave linearly over a large frequency range when varying the steam load. The nonlinearities present were mainly pronounced at low frequencies. This was seen as higher gains at lower steam load and variation of certain dynamics. The model used was of eighth order. The variation closest to the desired crossover frequency is that induced by the energy balance. This is also captured by the derived second order model. In particular, we refer to the pole presented in (13a) entry A_{11}. This corresponds to dynamics with a time constant that can vary between ≈ 1000s (maximum load) to ≈ 3500s (minimum load). Also the right half plane zero from fuel to water level varies in this frequency range from $s \approx 0.0006$ (low load) to $s \approx 0.003$ at high load. Also above these frequencies the gains both from inputs and disturbance to the outputs in the different load situation are coinciding. These properties are easily identified from the Bode plot of the derived second order model presented in Figure 2 for three different steam loads. We note that these variations of gain and dynamics are not present in the coupling from feed water to water level.

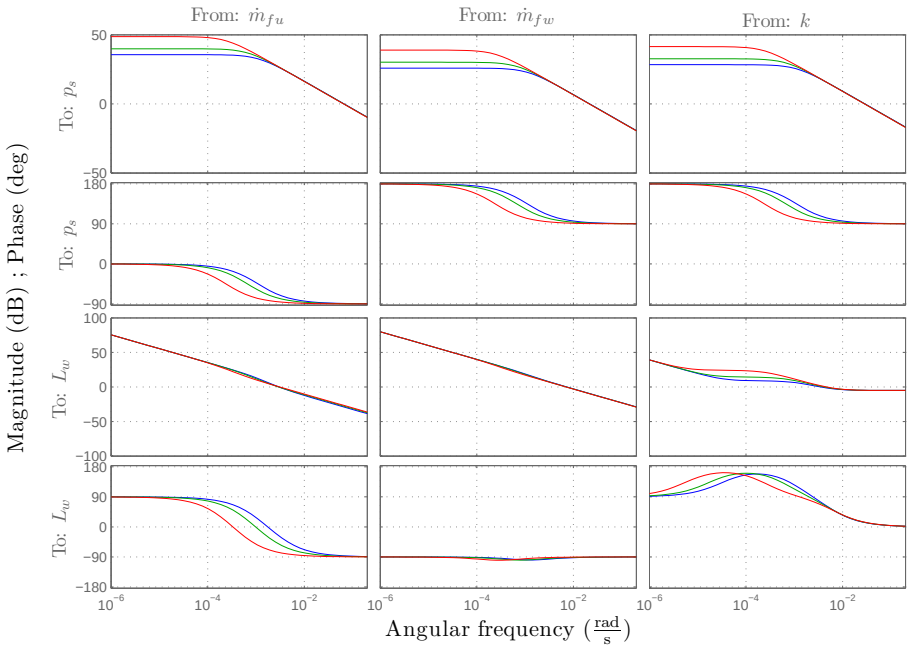

Figure 2: Bode plot of scaled $[G(s)\ G_d(s)]$ for three different steam loads. Blue: $\dot{m}_s = 1800\frac{\text{kg}}{\text{h}}$, green: $\dot{m}_s = 1100\frac{\text{kg}}{\text{h}}$ and red: $\dot{m}_s = 400\frac{\text{kg}}{\text{h}}$. Note the variation of gain at low frequencies to the pressure output and the change in system bandwidth.

Regarding the singular values the linear range is at angular frequencies $> 0.003\frac{\text{rad}}{\text{s}}$ which includes the desired crossover also one linear controller has proved to behave similar over the entire load range. For these reasons it was concluded in [Solberg et al., 2007b] that a controller design could rely on one linear model if the controller had integral action. If attention is directed at the phase of the different transfer functions in the model this range starts at a higher frequency $\approx 0.01\frac{\text{rad}}{\text{s}}$ except for the transfer function from fuel to water level where phase differences over a large frequency range still persist, see Figure 2. This means that when designing diagonal controllers the nonlinearities of the plant pose no limit on the performance. When designing multiple input multiple output controllers one must keep in mind that the phase response of the transfer function from fuel to water level is inaccurate when relying on one linear model for design.

In [Solberg et al., 2008] it was pointed out that in certain situations, e.g. when using hysteresis control where the system state never reaches a steady state but rather converges to a limit cycle, then the low frequency nonlinearities can cause problems. First of all the limit cycle which the state converges to will be dependent on the low

frequency parts of the model if the switching does not occur too frequent, and further an estimate of the steam flow is difficult to derive and is very slowly converging when using only one linear model.
This indicates that dependent on the controller strategy, the nonlinearities are more or less important. However, hysteresis control is only applied in very special cases, and normally the low frequency gain variations can be ignored when designing controllers.
In the above we have suggested that the boiler system is described sufficiently using a linear model. However, this model does not include the actuator systems generating the fuel and feedwater flows. These actuator systems are nonlinear and will be considered next.

3.2 Actuator Systems

Feed water supply system

The feed water system is well known and a diagram of it is shown in Figure 3.

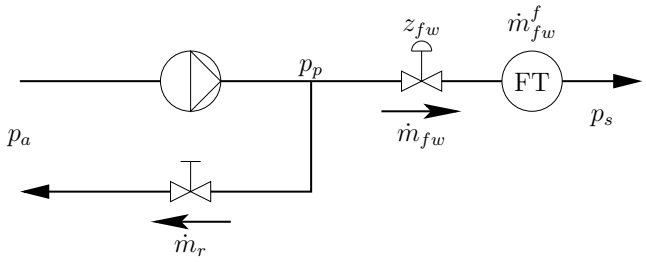

Figure 3: Diagram of feed water system. Water pumped from the feed water tank is injected into the boiler in the forward path, and in the return path the water is led back to the feed water tank.

The valve in the forward path is a pneumatic control globe valve which has an equal percentage characteristic (chosen over the linear characteristics as it in this setup helps linearising the gain from stroke to flow). The flow through the valve can be expressed as [Haugen, 1994]:

$$\dot{m}_{fw} = k_f f(z_{fw}) \sqrt{p_p - p_s} \tag{17}$$

where

$$f(z_{fw}) = \frac{1}{R}(R^{z_{fw}} - e^{-R_0 z_{fw}}) \tag{18}$$

is the function describing the valve characteristic and relating the valve stroke, z_{fw}, to the flow. k_f is the valve gain, which in the valve data sheet is usually given for water at $20^\circ\mathrm{C}$ and expresses the flow through a fully open valve with a pressure drop of $1\mathrm{bar}$ over the valve. Finally p_p is the pressure after the pump and p_s is the steam pressure in the boiler. In most cases the dynamics that govern the feed water supply system is

that of the flow sensor as the pneumatic control valve and flow dynamics are fast when pipes are not too long. The sensor may adequately be described with dynamics of first order given as:

$$\dot{m}_{fw}^{f}(s) = G_{fw}(s)\dot{m}_{fw}(s) = \frac{1}{\tau_{fw}s + 1}\dot{m}_{fw}(s) \tag{19}$$

The valve in the return path is a manually adjustable valve which should not be adjusted during plant operation. The flow through this valve is expressed as:

$$\dot{m}_r = k_r\sqrt{p_p - p_{fwt}} \tag{20}$$

where k_r is the return valve conductance and p_{fwt} is the pressure in the feed water tank assumed equal to the ambient pressure $p_{fwt} = p_a$. The function of this valve is to change the characteristics of the pump which is running at fixed speed. The flow delivered by the pump is:

$$\dot{m}_p = \dot{m}_r + \dot{m}_{fw} \tag{21}$$

and the pressure after the pump and before both the forward and the return valves is:

$$p_p = \Delta p_p + p_a \tag{22}$$

where Δp_p is the pressure rise over the pump which again can be found as:

$$\Delta p_p = \rho g \Delta H_p \tag{23}$$

where H_p is the lifting height. This height is often approximated in the literature, see e.g. [Eastop and McConkey, 1993], by:

$$\Delta H_p = H_{p,max}\left(\left(\frac{n_p}{n_{p,max}}\right)^2 - \left(\frac{Q_p}{Q_{p,max}}\right)^2\right) \tag{24}$$

where $H_{p,max}$ is the maximum lift height occurring at a zero throughput. n_p and $n_{p,max}$ is the current and maximal pump speed, respectively, and Q_p and $Q_{p,max}$ is the current and maximal flows. Note that $Q_p = Av_p$ and $\dot{m}_p = \rho_w A v_p$, where A is effective flow area and v_p is the fluid velocity. This together with (23) leads to:

$$\Delta p_p = p_{p,max}\left(\left(\frac{n_p}{n_{p,max}}\right)^2 - \left(\frac{\dot{m}_p}{\dot{m}_{p,max}}\right)^2\right) \tag{25}$$

The pump always runs at maximum speed meaning that we can simplify the expression by using: $n_p = n_{p,max} \Leftrightarrow n_p/n_{p,max} = 1$.

We want a model of the feed water supply system that gives us a feed water flow when we send a certain voltage to the control valve. The equations above, however, do not allow to put up such a model in a straight forward manner, (insertion of (17) and (20) into (25) and isolating for $\dot{m}_{fw}$ requires solving a quadratic equation), this is treated next.

Explicit expression for feed water flow

First we notice that the feed water flow to the boiler, $\dot{m}_{fw}$, is dependent on three parameters; the control variable, z_{fw} (the valve stroke), the steam pressure, p_s, which acts as a disturbance and finally the stroke position of the manual valve in the return path which together with the valve characteristics is described by k_r.
The explicit expression for the feed water flow as function of the valve stroke and boiler pressure is now found as

$$\dot{m}_{fw} = g(z_{fw}, p_s) = k_f f(z_{fw}) \sqrt{\Delta p_p + p_a - p_s} \tag{26}$$

where Δp_p is given as the solution to a quadratic equation: $\Delta p_p = \frac{-a_1 - \sqrt{a_1^2 - 4a_2 a_0}}{2a_2}$ with:

$$a_2 = \left\{ \begin{array}{c} \left[1 + \frac{p_{p,max}}{\dot{m}^2_{p,max}} \left(k_r^2 + k_f^2 f(z_{fw})^2\right)\right]^2 + \\ -4 \frac{p^2_{p,max}}{\dot{m}^4_{p,max}} k_r^2 k_f^2 f(z_{fw})^2 \end{array} \right\} \tag{27a}$$

$$a_1 = \left\{ \begin{array}{c} 2\left[1 + \frac{p_{p,max}}{\dot{m}^2_{p,max}} \left(k_r^2 + k_f^2 f(z_{fw})^2\right)\right] \times \\ \left(\frac{p_{p,max}}{\dot{m}^2_{p,max}} k_f^2 f(z_{fw})^2 (p_a - p_s) - p_{p,max}\right) + \\ -4 \frac{p^2_{p,max}}{\dot{m}^4_{p,max}} k_r^2 k_f^2 f(z_{fw})^2 (p_a - p_s) \end{array} \right\} \tag{27b}$$

$$a_0 = \left(\frac{p_{p,max}}{\dot{m}^2_{p,max}} k_f^2 f(z_{fw})^2 (p_a - p_s) - p_{p,max} \right)^2 \tag{27c}$$

This model provides a good fit to measurement data and the sensor time constant is about $\tau_{fw} = 4\mathrm{s}$ modelled by the first order system $G_{fw}(s)$ (19). Note that the pipe resistance from the valve to the boiler has been ignored. The only unknown parameter in this model is the positioning of the return valve k_r. It is obvious that the system is very nonlinear which is illustrated in Figure 4.
From the figure it can be seen that for the example boiler pressure the small gain (top right plot) can vary worst case up to a factor of 35 and at nominal pressure $8\mathrm{bar}$ up to a factor of 22.
Unfortunately, the flow is dependent on the boiler steam pressure. One implication from this is that the upper achievable flow is dependent on this disturbance $\dot{m}_{fw} \in [0, \overline{\dot{m}}_{fw}(p_s)]$. This means that if one uses flow as control variable in an outer loop together with a flow controller the input constraints are not constant which might cause problems in e.g. model predictive controller (MPC) configurations.
As always there are two possibilities regarding control. Either try to linearise the actuator dynamics by flow feedback or gain scheduling or use the valve stroke directly as a control variable in the outer loop. Using the valve stroke directly in the outer loop has two major disadvantages.

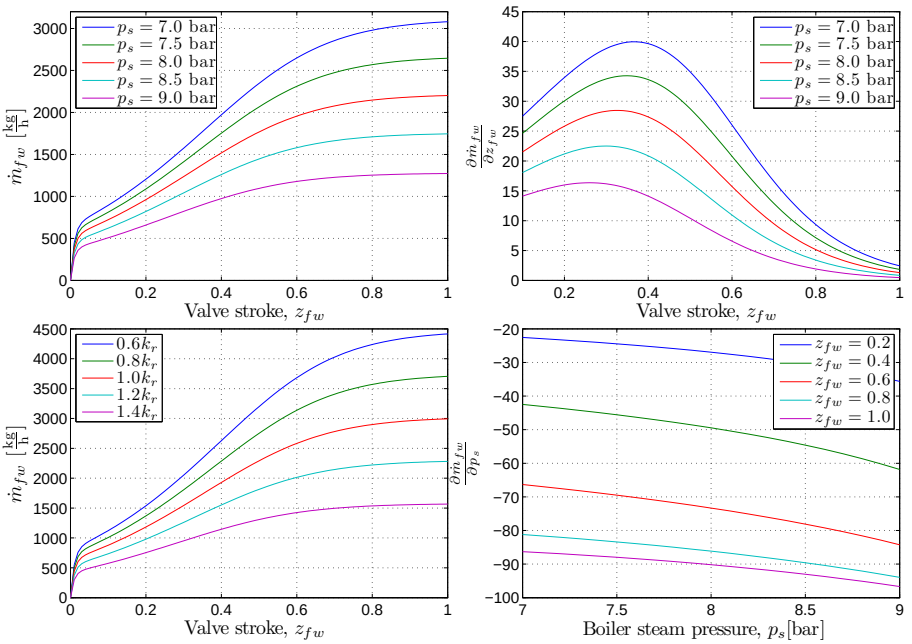

Figure 4: Feed water system characteristics. In the top left corner the feed water flow is shown as a function of the valve stroke for different boiler pressures. In the top right corner the partial derivative of the feed water flow with respect to the valve stroke is shown for different boiler pressures. Notice that only valve strokes $z_{fw} \geq 0.1$ are included as the valve positioning is unreliable below this level. In the bottom left corner the feed water flow is shown as a function of the valve stroke for different return valve strokes, and in the bottom right corner the partial derivative of the feed water flow with respect to the boiler pressure is shown for different valve strokes.

First of all the disturbance from varying boiler steam pressure is not compensated for. Worst case this can result in an unintentional coupling as e.g. an increase in pressure causes the feed water flow to decrease. This will cause a level controller to open the feed water valve more which will increase the feed water inlet but at the same time the extra water causes the pressure to drop and hence the feed water flow to increase even more. This phenomenon is especially pronounced if the gap between level and pressure loop bandwidth is small.

The other disadvantage is that when using such a strategy it is custom to design the feedback controller according to the largest gain (see Figure 4 top right). However, with such large gain variations this means that the actually achieved bandwidth may vary more that one decade. Here we have assumed a slope $20 - 40\frac{\text{dB}}{\text{dec}}$ around the crossover frequency, which is consistent with what would be achieved by PI control on (16b). If a flow sensor is available this is an unnecessary restriction as the valve gain

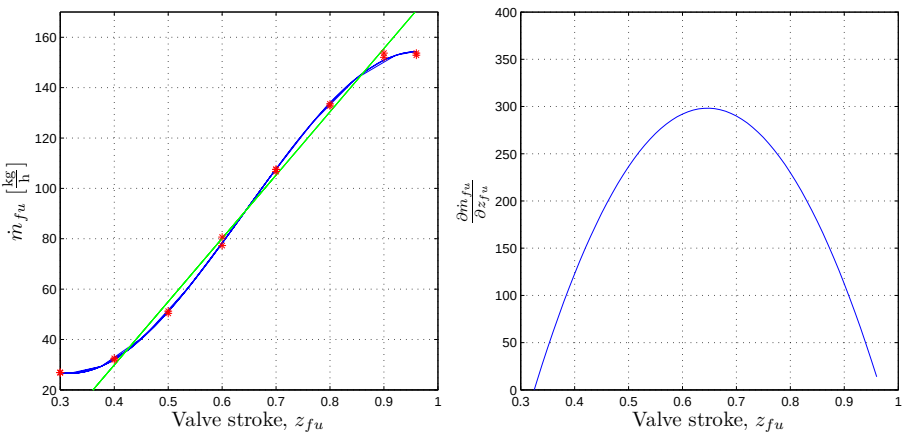

Figure 5: Fuel system characteristic. The red dots are measurement points, the blue curve is a third order polynomial fitted to the measurements and the green line is a first order fit to the data set truncated to valve strokes $z_{fu} \in [0.4, 0.9]$.

can be linearised by feedback or gain scheduling. Using only feedback the bandwidth of the flow dynamics will vary just as much as those for the outer controller in the above example. However, this might be acceptable as this inner loop can be made very fast, meaning that if the outer level loop bandwidth is not too high the effort of designing a gain scheduling to linearise the flow dynamics is not worthwhile. Pure gain scheduling and no feedback is not preferable as this still leaves the problem of compensating for the boiler pressure disturbance and it requires a very accurate model of the system gain. The feed water system is designed in such a way that the maximal flow is higher than the maximal steam production at nominal pressure. This insures that instability of the water level is avoided due to constraint limitations in the flow.

Burner

The burner must deliver the requested power while keeping a clean combustion. The dynamics of combustion is very fast and we saw earlier that the heat released in the combustion is treated stationary and proportionally to the fuel flow (1). The burner systems is not as well known as the feed water system and it has not been possible to acquire information on the functionality of the nozzle-lance/atomiser system. For this reason no first principle model has been derived of this unit. However, data-sheets of the atomiser and measurements suggest a third order characteristic between valve position, z_{fu}, and flow $\dot{m}_{fu}$. In Figure 5 left a third order fit, blue, to measurement data, the red dots, is shown together with a linear fit to the region $z_{fu} \in [0.40, 0.90]$.
In the right plot of the figure the derivative of the flow with respect to the valve stroke is

shown. From the plot it can be seen that in the region $z_{fu} \in [0.4, 0.9]$ the gain varies up to a factor of 2.5. Designing a robust controller with reasonable stability margins such a gain variation is not a problem. Small boilers like the one treated in this paper are never shipped with fuel flow sensors as this is too expensive. For this reason no feedback can be closed around the fuel system to linearise the gain. However, as can be seen from Figure 5 the linear approximation is good in a large operating range and represents a gain not far from the maximal. It is assumed that such a relationship can be found by simple experiments. This leaves the fuel system controller as a pure feedforward control of the flow, and slow controller response has to be accepted when in the low flow range below a valve stroke of 0.4 and in the high flow range above a valve stroke of 0.9. The valve position is adjusted by an electric motor using pulse width modulation (PWM) of the electric control signals. The behaviour of this controller is dead beat.
Keeping a clean combustion is a matter of having the correct fuel to air ratio. In boilers treated here the combustion air flow is controlled by letting the air damper position be directly dependent on the fuel control valve position.
The dynamics between fuel flow and position are negligible. However, the electric motor controlling the position only has one speed which sets a rate constraint on the change in fuel flow.

Input constraints

Both the feed water and fuel system are subject to constraints and these constraints are likely to be active during disturbance rejection and reference tracking. These constraints set the limit for how fast the disturbances can be rejected or how fast the setpoint can be changed. The constraints are never active during normal steady state operation unless the steam flow is so low that on/off burner control is necessary.
Regarding reference changes the limit on the rate of change depends on the steam load, e.g. if close to the maximum steam consumption there will not be much excess feed water or fuel to fast increase the water level or pressure.
Regarding disturbance rejection the same holds. However, here the nonlinearities introduced by the constraints will become important. This is due to the non-minimum phase zero in the response from steam flow to water level, shrink-and-swell. These issues are discussed in the following section.
Due to the frequent activation of constraints during disturbance and reference changes and the need for integral action to avoid steady state offsets it is important to include an appropriate anti-windup scheme in the controller design.

3.3 Shrink-and-swell

The worst shrink-and-swell behaviour is a consequence of changes in the steam load disturbance. As illustrated in Section 2 the bandwidth of this disturbance is very high and we neglected the dynamics of the bubble volume. To fully cancel the transients

in the water level during step changes in the disturbance input one can look at the change in volume of the water and steam bubble mixture. Then for any disturbance we need $Q \geq \frac{d(V_w+V_b)}{dt}$ where Q is a volume flow added to the process. When a steam flow disturbance occurs the short term changes are spotted in the steam bubble volume according to (9). For instance a step in steam flow of $\Delta\dot{m}_s$ causes a change in bubble volume of $\Delta V_b \approx 0.63\frac{T_d}{\varrho_s}\Delta\dot{m}_s$ in T_d seconds. This would require $Q \geq 0.63\frac{1}{\varrho_s}\Delta\dot{m}_s$ which depends only on steam data and hence the pressure and the size of the step in steam flow. A small step in steam flow of $\Delta\dot{m}_s = 100\frac{\mathrm{kg}}{\mathrm{h}}$ requires Q to be higher than $15\frac{\mathrm{m}^3}{\mathrm{h}}$ with a very high rate of change. It is of course not possible to generate such flow rates to or from the boiler. Further we did not specify that this flow must be water or steam at saturated conditions as the response from feed water to water level has a right half plane zero at high frequencies. Also attempts to generate such flow rate would compromise pressure performance.

This means that one has to accept the shrink or swell as a consequence of disturbance changes. However, the rate of recovery from these can be tuned. Our model (9), (16d) gives us a rough estimate of the shrink-and-swell occurring as $\Delta L_w = \frac{T_d}{A_{ws}\varrho_s}\Delta\dot{m}_s$ if we assume that the reference is reached between steps in the disturbance. For the worst case step from 400-1800$\frac{\mathrm{kg}}{\mathrm{h}}$ of steam this corresponds to a swell of $5.6\mathrm{cm}$.

As mentioned we cannot cancel the effect of the steam flow disturbance completely. Even so any linear feedback regulator will try. E.g. for a large positive disturbance step the swell will cause the controller to lower the feed water input. Often it will reach the lower zero flow constraint. However, the swell is followed by the negative integrating response from the disturbance. This response is fast making it difficult for the controller to avoid undershoot in the response. To avoid such problems a feedforward or fast estimate of the steam flow is necessary.

As mentioned above there is a right half plane zero in the response from feed water to water level which is also a consequence of shrink-and-swell. This zero was not included in the model in Section 2. The reason is that higher order models place this zero at a frequency much higher than the desired crossover frequency. Further this zero has been difficult to spot in measurement performed on the full-scale boiler.

3.4 Disturbances

The most important disturbance to the pressure and level is the steam flow which was treated above. Other disturbances as feed water temperature, fuel temperature, combustion air temperature and ambient pressure do not affect these outputs much. This was shown in [Solberg et al., 2007b] for the feed water and fuel temperatures. These two are also controlled in the plant. All these disturbances enter at the plant input and can be seen as unmeasured disturbances in the firing rate/fuel flow.

3.5 Neglected Dynamics

As mentioned in Section 2 much of the plant high frequency dynamics have been neglected and also some of the low frequency dynamics have been neglected in the second order control model. The low frequency dynamics came from the dependency of the efficiency on the water level, which we already pointed out only moved the integrator for the water level slightly into the left half plane and added a zero in the origin from fuel flow to pressure. Regarding the zero in the origin for the pressure this is removed when the level is controlled and the pole moved into the left half plane is still close to the origin so that the dynamics behave as an integrator close to the crossover frequency. The high frequency dynamics were actuator dynamics, flue gas dynamics, metal dynamics and bubble volume dynamics. Obviously these could be included in the control model reducing uncertainty, however, at the expense of higher model and controller order when using a model-based approach. If the desired crossover frequency is close to the bandwidth of the neglected dynamics the controller must exhibit appropriate stability margins or the model expanded. However, as long as the bandwidth is kept below $0.1\frac{\mathrm{rad}}{\mathrm{s}}$ and a reasonable stability margin is attained the models (12) or (15) can be used for controller design.

3.6 Decentralised Control and Interaction

In [Solberg et al., 2007b] it was shown that the interaction in the system does not cause any stability problems for a diagonally designed controller. Also it was shown that benefits especially in pressure performance could be expected by applying a multiple input multiple output (MIMO) control to the process. However, in practise these benefits were shown in [Solberg et al., 2007a] not to be the main advantage of MIMO control. It was shown that due to noise on the water level measurement the bandwidth of the response from the steam flow disturbance to the water level using SISO control was limited. However, using a model-based MIMO controller improvements were shown. This was seen as an improved steam flow disturbance rejection on the water level compared with SISO PI controllers.

3.7 Uncertainty

In [Solberg et al., 2007a] it was mentioned that test had exposed unexpected uncertainty in the cross couplings of the presented model. This led to a poor controller performance when the feed water actuator was assigned a low weight in the performance index of an optimising controller. However, simulations have shown that this is less severe as increasing the weight on the feed water flow did not make any visible deterioration compared to the desired performance and at the same time increased robustness.

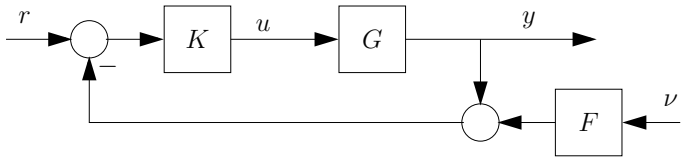

Figure 6: Block diagram of closed loop system with measurement noise input filter.

3.8 Measurement Noise

The measurement noise in the system is what really set the limit of the achievable performance. Especially the water level, which is measured by a device using a capacitive measurement principle, is subject to much noise caused by turbulence in the water surface. Analysing measurement data collected from the full-scale boiler shows that the measurement noise for both pressure and water level can be modelled as unit variance zero-mean white Gaussian low pass filtered noise processes where the actual noise variances have been moved into the filters. Such filters are found by identifying autoregressive models for each noise channel. For the steam pressure this results in the first order filter $F_{p_s}(s)$ and for the water level the second order filter $F_{L_w}(s)$. The noise input is $\nu = [\nu_1, \nu_2]^T$ with $E\{\nu(t)\} = 0$, $E\{\nu(t_1)\nu^T(t_2)\} = \delta(t_2 - t_1)I$. See Figure 6 for reference on where the noise enters the system.

Figure 7 illustrates the problems introduced by the noise. The figure shows the control sensitivity function $M(s) = K(s)(I + G(s)K(s))^{-1}$ achieved by the diagonal PI controller $K(s)$ for two different settings of proportional and integral terms. The controllers were designed from (16) to achieve a phase margin of 71° and certain crossover frequencies. Particularly, the crossover frequency for the pressure loop is in both designs $\omega_{c,p_s} = 0.075\frac{\text{rad}}{\text{s}}$ whereas it for the level loop in design $K_1(s)$ was $\omega_{c_1,L_w} = 0.0068\frac{\text{rad}}{\text{s}}$ and in design $K_2(s)$ was $\omega_{c_2,L_w} = 0.021\frac{\text{rad}}{\text{s}}$.

The figure further displays the noise filters $F(s) = \text{diag}(F_{p_s}(s), F_{L_w}(s))$ and product of the filters and control sensitivity $M(s)F(s)$. It is important to remember that neither of the displayed transfer functions are scaling independent for which reason appropriate scaling of input and noise must be applied. The noise was already scaled and the input is scaled according to allowed input variation.

From the figure it can be seen that the noise on the water level causes problems for the controller. It can also be seen that increasing the crossover frequency of the level controller from $\omega_{c_1,L_w} = 0.0068\frac{\text{rad}}{\text{s}}$ the measurement noise will cause large control signal action.

This is a problem as the bandwidth of the disturbance response is high and as a result we get a slow regulation and long settling between disturbances changes.

In fact it is very difficult to push the bandwidth of the level loop above $\omega_{c,L_w} = 0.0068\frac{\text{rad}}{\text{s}}$ and still keep a reasonable control signal. However, by careful design of

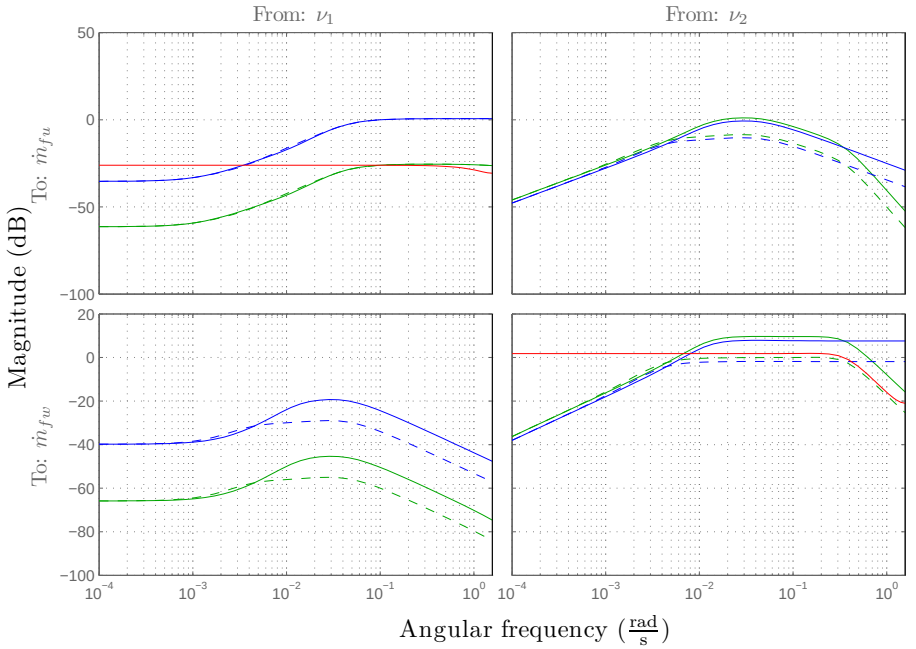

Figure 7: Magnitude plot of noise shaping filters $F(s)$, red, control sensitivity function $M(s)$, blue, and product between control sensitivity function and shaping filters $M(s)F(s)$, green. The dashed lines corresponds to design $K_1(s)$ and the solid lines design $K_2(s)$. Notice the high gains in the bottom right plot from $\omega \approx 0.007$ to $\omega \approx 0.7$.

measurement filters small improvements can be achieved. In particular, an LQG design has shown capable of achieving a $40\frac{\text{dB}}{\text{dec}}$ slope just above the chosen crossover frequency and reasonable control signals can be achieved with the crossover frequency at $\omega_{c,L_w} = 0.01\frac{\text{rad}}{\text{s}}$. This can be done by keeping an appropriate stability margin without adding extra model states apart from those introduced to achieve integral action. Similar performance can be achieved by designing a second order filter in combination with a PI design. However, pushing the crossover frequency has a negative effect on the pressure performance when using a diagonal controller, and further this controller will be of approximately the same order as an LQG compensator.

3.9 Output Constraints

Hard constraints are present on both the water level and pressure for the marine boiler. The high pressure constraint is important but not likely to become active unless a fault has occurred in the system. Regarding the water level both upper and lower alarms can

be present on the boiler. There is a demand from the classification societies that the flue gas pipes must be under water up to the point at which the flue gas drops below $600^{\circ}\mathrm{C}$. This sets requirements for the fluctuation on the water level in the drum. Of course, this bound must in any case be somewhat conservative as it is at a constant level whereas the point would in reality change with load. The boiler is equipped with a low water level alarm to indicate when the water level is within a certain range from this point (typically 45-60mm). In some cases the boiler is also equipped with a high water level alarm to prevent water from entering the steam supply line and keep a good steam quality. This is especially important when the downstream equipment is turbines.
These constraints must not become active for which reason the distances to the high and low alarms from normal water level operation are designed somewhat conservative today. In the introduction we mentioned that there is a desire to reduce the physical geometry of the boiler. This can be achieved by reducing the distances between the high and low water level alarms. We postulate that this cannot be achieved by feedback alone but must be accompanied by a water level setpoint controller. The reason is the shrink-and-swell phenomenon and the fact that the steam flow disturbance is not known in advance. As was illustrated in Section 3.3 the level variation caused by shrink-and-swell has to be accepted. But by appropriate feedback (and possible feedforward) the recovery time from a step can be reduced and especially the overshoot/undershoot when rejecting the disturbance can be eliminated such that the maximum variation is not increased if a step in the disturbance is applied in the opposite direction before the level has settled again. By augmenting the feedback structure by a setpoint algorithm maximising the level at all time by estimating the current worst case disturbance there is a possibility to reduce the distance between the high and low water level alarms. However, remember that the worst shrink or swell caused a level variation of approximately $5.6\mathrm{cm}$ (Section 3.3) meaning that under perfect control the potential maximal level variation could be reduced to $5.6\mathrm{cm}$. More precise we can write water level constraints equations based on the current worst case disturbance. Define HWL as the water level at which the high water level alarm is activated and LWL as the water level at which the low water level alarm is activated. Then the maximum allowable water level, $L_{w,max}$, at any instant is given by:

$$L_{w,max} = HWL - \frac{\Delta V_{b,max}(\dot{m}_s)}{A_{ws}} \tag{28a}$$

$$= HWL - \frac{T_d}{A_{ws}\varrho_s}\Delta\dot{m}_{s,max}(\dot{m}_s) \tag{28b}$$

$$= HWL - \frac{T_d}{A_{ws}\varrho_s}(\dot{m}_{s,max}(\dot{m}_s) - \dot{m}_s) \tag{28c}$$

$$= HWL - \frac{1}{A_{ws}}(V_{b,max}(p_s) - V_b) \tag{28d}$$

where $\Delta V_{b,max}(\dot{m}_s)$ denotes the maximum positive change in bubble volume given the current disturbance. Likewise $\Delta\dot{m}_s$ denotes the maximum possible positive change in

disturbance at current time. Also $V_{b,max}(p_s)$ denotes the maximum volume of steam below the water surface given the maximum disturbance $\dot{m}_{s,max}$. V_b here denotes the current bubble volume. This relationship is only possible due to linearity of the steam bubble volume in the load assumed in (9). This leads to the following water volume constraint:

$$L_w \leq HWL - \frac{1}{A_{ws}}(V_{b,max}(p_s) - V_b) \tag{29a}$$

$$\frac{V_w + V_b}{A_{ws}} \leq HWL - \frac{1}{A_{ws}}(V_{b,max}(p_s) - V_b) \tag{29b}$$

$$V_w \leq A_{ws}HWL - V_{b,max}(p_s) \tag{29c}$$

Likewise for the low water level constraint we get:

$$L_{w,min} = LWL + \frac{1}{A_{ws}}(V_b - V_{b,min}(p_s)) \tag{30}$$

leading to the water volume constraint:

$$V_w \geq A_{ws}LWL - V_{b,min}(p_s) \tag{31}$$

more compact this gives the water volume constraint

$$A_{ws}LWL - V_{b,min}(p_s) \leq V_w \leq A_{ws}HWL - V_{b,max}(p_s) \tag{32}$$

For perfect control of the water volume the minimum distance between the HWL and LWL is then:

$$HWL - LWL \geq \frac{1}{A_{ws}}(V_{b,max}(p_s) - V_{b,min}(p_s)) \tag{33a}$$

$$\geq \frac{\Delta V_{b,max}(\dot{m}_s)}{A_{ws}} = \frac{T_d}{A_{ws}\varrho_s}\Delta\dot{m}_{s,max}(\dot{m}_s) \tag{33b}$$

This essentially means that we should control the water volume in the boiler and not the actual water level. In [Kothare et al., 2000] the authors define a narrow range water level as the water level which includes the bubble volume and a wide range water level as one that only measures the water in the drum. A measurement of the wide range water level can be generated by a differential pressure measurement as suggested in [Hvistendahl and Solberg, 2004; Kothare et al., 2000]. In [Kothare et al., 2000] they end up controlling the narrow range water level which must be kept within pre-calculated alarm levels to ensure that the wide range water level is high enough. For the one-pass smoke tube boiler it seems more appropriate to control the wide range water level as this can be done without any fast feedback. However, due to model uncertainties it is still important to have constraints on the narrow range water level to ensure good steam quality and avoid violation of low water level constraints.

4 Controller Design Guidelines

This section is devoted to present simple control design guidelines for the one-pass smoke tube boiler. The control scheme suggested uses a cascade configuration with actuator flow controllers in an inner loop and outer controllers handling pressure and level control.
There are two reasons for choosing such a configuration; first of all the feed water valve system is difficult to describe and highly nonlinear and closing the loop will partly linearise the map from feed water reference to actual flow, secondly this approach helps minimising uncertainties at the boiler plant input. However, the upper feed water flow bound is still dependent on the boiler pressure which might cause trouble if designing e.g. an MPC controller in which the constraints are assumed to be known.

4.1 Actuators

The fuel flow controller is based on pure feedforward. As described in Section 3.2 this feedforward is based on a linear map which is a good approximation of the actual map from fuel flow reference to valve position.
Regarding the feed water it was partly illustrated in [Andersen and Jørgensen, 2007] that closing a loop around the feed water flow can limit the variance of the controlled water level and pressure. The reason for this observation is most likely the coupling from the boiler steam pressure to the feed water flow discussed in Section 3.2.
The general structure of the feed water controller we consider here is shown in Figure 8.

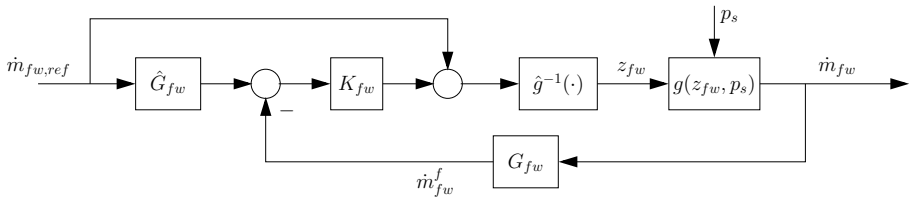

Figure 8: Feed water control scheme including both feedforward and feedback. K_{fw} is the feedback controller (a PI controller), $\hat{g}^{-1}$ is a model of the feed water system gain and $\hat{G}_{fw}$ is a model of the feed water sensor dynamics. Notice for $\hat{G}_{fw} = G_{fw}$ and $\hat{g} = g$ we have $\dot{m}^f_{fw} = G_{fw}\dot{m}_{fw,ref}$.

When using neither feedback or gain scheduling for flow control we have to design the controller somewhat conservative to be able to handle the large gain variations. This could maybe be excepted if it had not been for the large influence of the measurement noise which set an upper bound for the bandwidth. Already this bandwidth is very low meaning that the level loop bandwidth will become extremely low.

For these reasons it will be advantageous to include a feedback to linearise the gain and provide robustness against the pressure disturbance. Now as the measurement noise set a low achievable bandwidth feedback will in most cases provide adequate performance as the variations in time constant for the closed loop feed water system is such that the lowest time constant still corresponds to dynamics faster than the level loop. However, if another level measurement becomes available, gain scheduling will become necessary to be able to raise the bandwidth. For this reason we shortly discuss the inverse of the map from feed water control valve to feed water flow.
Dividing the control system into different modules also makes the design more flexible as the outer controller becomes somewhat independent on the burner and feed water system configuration and the other way around. Hence breaking the system into modules allows changing modules without influencing the complete control system.

Inverse mapping

For control purpose we are interested in finding the inverse mapping of $g(z_{fw}, p_s)$ which is a function mapping a reference flow and a particular boiler pressure to a valve stroke, $g^{-1} : \mathbb{R}^2 \mapsto \mathbb{R}$.
From (17) we immediately get:

$$z_{fw,ref} = f^{-1}\left(\frac{\dot{m}_{fw,ref}}{k_f\sqrt{p_{p,ref} - p_s}}\right) \tag{34}$$

which gives:

$$z_{fw,ref} = \frac{1}{\log(R)}\log\left(\frac{\dot{m}_{fw,ref}}{k_f\sqrt{\Delta p_{p,ref} + p_a - p_s}}\right) + 1 \tag{35}$$

Now we need to find $\Delta p_{p,ref}$ as a function of $\dot{m}_{fw,ref}$. To do so we proceed with the following version of (25):

$$\Delta p_{p,ref} = p_{p,max}\left[1 - \left(\frac{k_r\sqrt{\Delta p_{p,ref}} + \dot{m}_{fw,ref}}{\dot{m}_{p,max}}\right)^2\right] \tag{36}$$

then $\Delta p_{p,ref}$ is the solution to a quadratic equation: $\Delta p_{p,ref} = \frac{-b_1 - \sqrt{b_1^2 - 4b_2b_0}}{2b_2}$ where:

$$b_2 = \left[\left(1 + \tfrac{p_{p,max}}{\dot{m}^2_{p,max}}k_r^2\right)^2\right] \tag{37a}$$

$$b_1 = \begin{bmatrix} 2\left(1 + \tfrac{p_{p,max}}{\dot{m}^2_{p,max}}k_r^2\right)\left(\tfrac{p_{p,max}}{\dot{m}^2_{p,max}}\dot{m}^2_{fw,ref} - p_{p,max}\right) + \\ -4\tfrac{p^2_{p,max}}{\dot{m}^4_{p,max}}k_r^2\dot{m}^2_{fw,ref} \end{bmatrix} \tag{37b}$$

$$b_0 = \left(\tfrac{p_{p,max}}{\dot{m}^2_{p,max}}\dot{m}^2_{fw,ref} - p_{p,max}\right)^2 \tag{37c}$$

In [Andersen and Jørgensen, 2007] the inverse (34) was approximated by the solution to a quadratic equation in $\dot{m}_{fw,ref}$ which proved to give satisfactory results in practice. The pressure dependency was omitted but treated as an unmeasured disturbance handled by feedback.

4.2 Boiler

The performance specifications for the oil-fired one-pass smoke tube boiler are vague. The actual steam consumption pattern on the ships is unknown but known to vary dependent on the type of vessel. Regarding the water level there are no consumer requirements but as discussed in Section 3.9 there is a wish from AI to minimise the level fluctuations which means that fast damping of the disturbance is needed and no overshoot can be tolerated. Regarding the pressure the same holds that there are no consumer specified performance demands. However, setting high demands for the water level performance one has to expect that this will come at the expense of the pressure performance. This does not mean that the pressure is allowed to vary arbitrarily. When the boiler is bought for heating in various application the steam output from the boiler is expected to have a certain temperature which is directly equivalent to boiler pressure as it operates under saturated conditions. Further large fluctuations in the pressure and here by boiler construction temperature cause stress in material and a reduced product lifetime. Despite this lack of knowledge AI assumes that steps in the disturbance can occur every tenth minute.

The model (16) serves as a good candidate for designing classical controllers as PI controllers. This is also a consequence of the weak nonlinear behaviour of the plant around the crossover frequency as was discussed in Section 3.1. From this model it is easy to derive analytic expressions for the proportional and integral terms of the PI controller specifying design parameters such as desired crossover frequency and phase margin. Especially the phase margin can be chosen to account for neglected actuator and measurement filter dynamics. It would also be possible to use single input single output (SISO) model predictive controllers which handle the input constraints in a natural way. In [Pannocchia et al., 2005] it was shown that such controllers have approximately the same computational burden as classical PID controllers.

It is advisable to include measurement filter of at least second order with a bandwidth not much over the desired crossover frequency to limit the large influence of the noise and keep adequate control signals.

If it is possible to create an estimate of the steam flow this is strongly advisable as this can be used in a feedforward to the level control especially to avoid overshoot and speed up rejection of the steam flow disturbance. A Kalman filter was shown in [Solberg et al., 2005] to be able to generate such an estimate. But simpler estimates can be generated by considering the much faster pressure loop. The fuel flow must to some degree together with the current feed water flow give an estimate of the current steam flow (e.g. by considering a steady state version of (7)).

4.3 Controller Tuning

It is of interest to reduce installation time of new boilers by making the control system auto tuning. This will further limit the time spent by service personal during commissioning. Further this makes it possible to make the performance invariant to the environment into which the boiler is placed. During the boiler lifetime it is also likely that sensors or actuators are replaced, adjustment can be made to e.g. the return valve position k_r of the feed water system and different films might build up on both the water and flue gas sides of the heating surface. These things can change the boiler dynamics, and to keep appropriate controller performance a retuning might be necessary.
In [Andersen and Jørgensen, 2007] the first attempts to make the marine boiler control system tune automatically was made. In fact such a tuning can be made by just identifying a few model parameters. The reason here being the simple structure of $\hat{G}_{11}$ and $\hat{G}_{22}$ in (16) suggested to be used for controller design. There are no unknowns in $\hat{G}_{22}$ which depend on construction data and operating conditions alone whereas $\hat{G}_{11}$ has the unknown parameter η. However, η can be chosen arbitrarily (preferable according to nominal conditions) as the fuel flow is not measured and instead the linear gain from fuel valve stroke z_{fu} to fuel flow $\dot{m}_{fu}$ can be estimated.
Regarding the feed water system the unknowns were the sensor time constant and the gain whether this is considered linear or produced by the solution to a quadratic equation.
All the unknown parameters can be identified by simple experiment such as steps in the fuel flow and staircase sequence in the feed water flow. Further these experiments can be performed during the boiler start up sequence not disturbing the availability of the boiler.
Of course, if other level sensors with less noise is available and a controller design based on a multivariable process model is used, more sophisticated experiments must be considered. This could be closed loop experiments to avoid disturbing normal operation too much having an initial PI controller installed and tuned as above.

5 Conclusion

In this paper we discussed performance limitations, system characteristics and simple control guidelines for the one-pass smoke tube marine boiler.
It was found that the measurement noise on the water level is what limits the achievable bandwidth. This led to the conclusion that benefits could be gained by a multivariable control structure as this allowed for speeding up the response from steam flow disturbance to water level through a disturbance estimate.
The control structure suggested was a cascade configuration where feedback and possible gain scheduling were applied to the feed water system whereas the fuel system was controlled by pure feedforward. The simple model used for the controller design makes controller auto-tuning relatively simple.

To improve performance it would be necessary to reduce the noise on the water level measurement. An opportunity could also be to use a differential pressure sensor to measure the amount of water in the boiler and control this instead of the actual level. Such a measurement is assumed to be less prone to noise. The idea is to combine this with a level setpoint controller which makes an estimate of the steam bubble volume to ensure that the actual water level does not violate the upper level constraints.
If other level measurements become available so that the bandwidth of the level loop can be moved closer to that of the pressure loop, then a multivariable control strategy should be applied to suppress the influence of interaction.
Given the hard constraints on the water level and the actuator limitations, MPC seems to be the natural choice from the control literature for marine boiler control. MPC has the advantage of allowing operation closer to the limits of the system, and further handle actuator constraints in a natural way. However, as the boiler only operates close to these limits when disturbances occur it seems reasonable to use another strategy and incorporate anti-windup to handle the few cases when constraint bounds are active. Other advantages of MPC are the ease at which feedforward from the measured disturbance and future reference changes and disturbance changes can be incorporated in the design. However, neither of such information is available in case of the stand alone oil-fired marine boiler.
Instead it seams more appropriate to use a H_∞/loop-shaping approach as such design methods have a natural way of including uncertainty and noise filters in the design through weight functions.

References

K. J. Åström and R. D. Bell. Drum boiler dynamics. *Automatica*, 36:363–378, 2000.

K. J. Åström and T. Hägglund. *Advanced PID Control*. ISA - Instrumentation, Systems, and Automation Society, 2006.

S. Andersen and L. Jørgensen. Scheme for auto tuning control of marine boilers. Master's thesis, Aalborg University, June 2007.

M. Athans and P. L. Falb. *Optimal control : an introduction to the theory and its applications*. New York McGraw-Hill, 1966.

S. Boyd and C. Barratt. *Linear Controller Design: Limits of Performance*. Prentice-Hall Inc., 1991.

K. L. Chien, E. I. Ergin, C. Ling, and A. Lee. Dynamics analysis of a boiler. *ASME Transactions*, 80:1809–1819, 1958.

G. E. Dullerud and F. Paganini. *A Course in Robust Control Theory: A Convex Approach*. Springer, 2000.

T. D. Eastop and A. McConkey. *Applied Thermodynamics for Engineering Technologists*. Addison Wesley Longman, 1993.

F. Haugen. *Regulering av Dynamiske Systemer*. Tapir Forlag, 1994.

P. U. Hvistendahl and B. Solberg. Modelling and multi variable control of a marine boiler. Master's thesis, Aalborg Universitet, Institute of Electronic Systems, Aalborg, Denmark, 2004.

H. Kim and S. Choi. A model on water level dynamics in natural circulation drum-type boilers. *International Communications in Heat Transfer*, 32:786–796, 2005.

M. V. Kothare, B. Mettler, M. Morari, P. Bendotti, and C.-M. Falinower. Level control in the steam generator of a nuclear power plant. *IEEE Transactions on control system technology*, 8, No. 1:55–69, 2000.

Y. S. Lee, W. H. Kwon, and O. K. Kwon. A constrained receding horizon control for industrial boiler systems. In G. Hencsey, editor, *IFAC Symposium on Manufacturing, Modeling, Management and Control (MIM 2000)*, pages 411–416, Patras, Greece, 2000.

J. M. Maciejowski. *Predictive Control With Constraints*. Harlow: Pearson Education Limited, 2001.

G. Pannocchia, N. Laachi, and J. B. Rawlings. A candidate to replace PID control: SISO-constrained LQ control. *American Institute of Chemical Engineers, AIChE*, 51:1178–1189, 2005.

G. Pellegrinetti and J. Bentsman. Nonlinear control oriented boiler modeling - a benchmark problem for controller design. *IEEE Transactions on Control Systems Technology*, 4:57–64, 1996.

J. A. Rossiter. *Model-based Predictive Control: A Practical Approach*. CRC Press LLC, 2003.

S. Skogestad and I. Postlethwaite. *Multivariable Feedback Control: Analysis and Design*. Chichester: John Wiley & Sons Ltd, 1996.

B. Solberg, C. M. S. Karstensen, P. Andersen, T. S. Pedersen, and P. U. Hvistendahl. Model-based control of a bottom fired marine boiler. In P. Horacek, editor, *16th IFAC World Congress*, Prague, Czech Republic, 2005.

B. Solberg, P. Andersen, and J. Stoustrup. Advanced water level control in a one-pass smoke tube marine boiler. Technical report, Department of Electronic Systems, Aalborg University, Aalborg, Denmark, 2007a.

B. Solberg, C. M. S. Karstensen, and P. Andersen. Control properties of bottom fired marine boilers. *Energy*, 32:508–520, 2007b.

B. Solberg, P. Andersen, J. M. Maciejowski, and J. Stoustrup. Optimal switching control of burner setting for a compact marine boiler design. Submitted March 2008 for journal publication, 2008.

K. Sørensen, C. M. S. Karstensen, T. Condra, and N. Houbak. Optimizing the integrated design of boilers - simulation. In R. Rivero, editor, *Efficiency, Costs, Optimization, Simulation and Environmental Impact of Energy Systems (ECOS 2004)*, volume 3, pages 1399–1410, Guanajuato, Mexico, 2004.

K. Zhou, J. Doyle, and K. Glover. *Robust and Optimal Control*. New Jersey: Prentice-Hall, Inc, 1996.

Paper F

Hybrid Model Predictive Control Applied to Switching Control of Burner Load for a Compact Marine Boiler Design

Brian Solberg & Palle Andersen & Jan M. Maciejowski &
Jakob Stoustrup

The paper has been published in:
Proceedings of the 17th IFAC World Congress,
July 6-11, 2008, Seoul, Korea

Abstract

This paper discusses the application of hybrid model predictive control to control switching between different burner modes in a novel compact marine boiler design. A further purpose of the present work is to point out problems with finite horizon model predictive control applied to systems for which the optimal solution is a limit cycle. Regarding the marine boiler control the aim is to find an optimal control strategy which minimizes a trade-off between deviations in boiler pressure and water level from their respective setpoints while limiting burner switches. The approach taken is based on the Mixed Logic Dynamical framework. The whole boiler systems is modelled in this framework and a model predictive controller is designed. However to facilitate on-line implementation only a small part of the search tree in the mixed integer optimization is evaluated to find out whether a switch should occur or not. The strategy is verified on a simulation model of the compact marine boiler for control of low/high burner load switches. It is shown that even though performance is adequate for some disturbance levels it becomes deteriorated when the optimal solution is a limit cycle.

1 Introduction

The control of marine boilers mainly focuses on minimizing the variation of steam pressure and water level in the boiler, keeping both variables around some given setpoint. Up till now this task has been achieved using classical SISO controllers, one using the fuel flow to control the steam pressure and one using the feed water flow to control the water level.

A more efficient control can allow smaller water and steam volumes in the boiler implying lower production and running costs and a more attractive product. In [Solberg et al., 2005] a successful application of LQG control to the MISSION^{TM} OB boiler from Aalborg Industries A/S (AI) product range was shown.

The specific boiler concerned in the present work is a novel compact marine boiler from AI. The boiler is a side fired one-pass smoke tube boiler. The boiler consists of a furnace and convection tubes surrounded by water. At the top of the boiler steam is led out and feed water is injected. The compact boiler is equipped with a two-stage burner unit with two pressure atomizer nozzles of different size. With slight abuse of notation we refer to these nozzles as Burner 1 (the small nozzle) and Burner 2 (the large nozzle). This means that there are two burners and designing an appropriate switching strategy between these can allow for a high turndown ratio, defined as the ratio between the largest and lowest possible fuel flow, or equivalently burner load. However too much switching will increase actuator wear and decrease performance due to non-optimal combustion during burner start-up.

Unfortunately the maximum power generated by Burner 1, $\overline{Q}_l$, alone is lower than the minimum power generated by the combined operation of the burners, $\underline{Q}_h$. There are two

power gaps. This means that, for a steam flow that corresponds to a steady state power consumption in one of these gaps, the burners have to follow some on/off switching scheme to keep the pressure around its reference value. The gaps will be defined as: *Gap-region 1* $Q_{ss} \in [0; \underline{Q}_1] := G_1 \subset \mathbb{R}$ and *Gap-region 2* $Q_{ss} \in [\overline{Q}_l; \underline{Q}_h] := G_2 \subset \mathbb{R}$. In the sequel we shall refer to these gap-regions a bit loosely using statements such as 'the disturbance-', 'the required fuel flow-', 'the energy request belong to a gap-region', which all translate into the equivalent formulation that the steady state power consumption can not be met exactly by any available fuel flow.

The challenge in this work is to design an appropriate burner switching strategy that minimizes pressure variations and hence fluctuations in steam quality without compromising water level performance to still allow the smaller boiler geometry. Such a task would normally have been approached using heuristic rules combined with hysteresis control, however we seek a more systematic design procedure. The control problem is complicated by the shrink-and-swell phenomenon which introduces non-minimum phase characteristics in the system, [Åström and Bell, 2000]. This phenomenon is seen when e.g. the steam flow is abruptly increased. This causes the pressure to drop instantly, which in turn causes an expansion of steam bubbles below the water surface and further lowers the boiling point causing even more bubbles to be generated leading to an almost instant increase in the water level. However mass is removed from the boiler so eventually the water level will decrease. Similar behaviors can be observed when the feed water or fuel flow is changed.

The boiler system belongs to the special class of systems integrating logic and dynamics. Many methods along with traditional hysteresis and pulse width modulation (PWM) have been proposed for controlling these systems – see e.g. [Bemporad and Morari, 1999; Hedlund and Rantzer, 1999; Sarabia et al., 2005; Solberg et al., 2008]. If we do not accept large persistent deviations in pressure from the setpoint or if a goal is to bring the integrated pressure error to zero then for some steam loads the burners must switch on and off according to some pattern to compensate for the gap-regions. In particular this will introduce a limit cycle in the state trajectory.

Let us define the optimal solution as the solution achieved by using an integral cost functional taking the average over an infinite horizon.

The optimal solution will then be dependent on the current disturbance and states and can be a limit cycle. The period and amplitude of the pressure oscillation corresponding to the limit cycle will change with operating conditions. Therefore this solution can not be found by traditional hysteresis control which operates with fixed bounds on the pressure to switch the burners. Traditional PWM suffers from similar shortcomings as the switching period for such schemes are fixed and only the duty-cycle can vary. Further, normally PWM is seen in connection with a cascade control configuration where the inner loop, PWM, runs much faster than the outer process. Neither hysteresis control nor PWM explicitly consider that a cost is assigned to switching the burners which is essential in this problem setup. The method we describe in this paper does not suffer from these limited degrees of freedom. This method is based on Model Predictive

Control (MPC) in combination with the Mixed Logic Dynamical (MLD) framework, which is an approach which allows standard tools to be applied to obtain an optimizing control law [Bemporad and Morari, 1999].
We show through simulations that this new method indeed does change behavior for different choices of the steam load.
The paper is organized as follows. First the marine boiler system is introduced and its control properties are discussed. Secondly the hybrid MPC controller is described. In the subsequent section the controller is validated in a simulation study where prediction mismatches are illustrated as consequence of a finite horizon cost. Further a comparison with traditional hysteresis control is made. Finally conclusion and future works are presented.

2 System Description

The boiler consists of two logically separated parts, one containing the heating system and one containing the water-steam system. The heating system consists of the furnace and the convection tubes. The water-steam system consists of all water and steam in the boiler. These two systems are interconnected by the metal separating them i.e. the furnace jacket and the convection tube jackets.
The boiler is equipped with two actuator systems for feed water and burner control, respectively. The feed water flow dynamics are linearized in an inner cascade controller which allows the reference to the feed water flow to be used as a manipulated variable. The corresponding inner loop can easily be designed to be faster than the outer loop. The burner system is more complicated. It can operate in three modes; Mode 0: both burners off; Mode 1: Burner 1 on and Burner 2 off; Mode 2: both burners on.
The function of the burner unit can be described by a finite state machine. The state machine consists of six states: three representing the modes described above and another three describing transitions between these, see Figure 1.
The function of each state is summarized in Table 1.
States n_1, n_2 are characterised by the continuous input variable, fuel, being controllable. In contrast transition states $n_{0,1}, n_{1,2}, n_{1,0}$ are governed by predetermined control sequences. To initiate a switch between modes, certain guards have to be satisfied, as shown in Figure 1. In most cases this is just a matter of setting the Boolean variable corresponding to the specific burner being on or off. However, to initiate a switch from Mode 1 to Mode 2, $n_1 \rightarrow n_{1,2}$, the combustion air flow and hence the fuel flow to Burner 1 has to be below a certain level, in order to be able to fire Burner 2.

2.1 Modeling

A detailed model of the boiler system can be found in [Solberg et al., 2005] and a thorough model analysis was presented in [Solberg et al., 2007]. In this section we

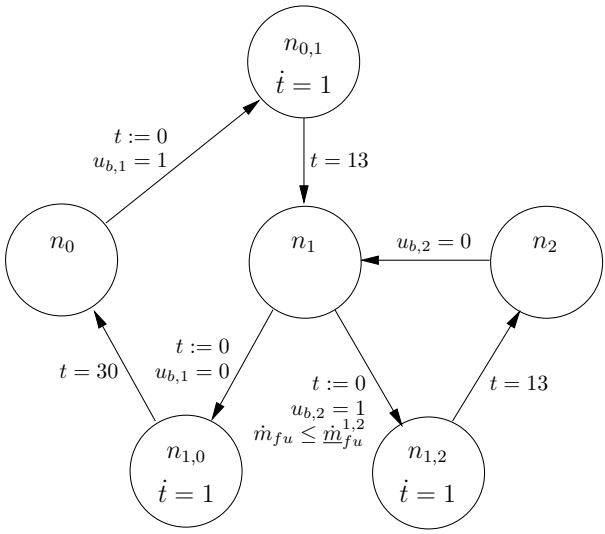

Figure 1: Finite state machine describing burner operation.

shall not repeat these results but only summarize the details important to the current work.

The simplified model will consist of the state machine shown in Figure 1. The model should describe the total fuel supply to the burners $\dot{m}_{fu} = \dot{m}_{fu,1} + \dot{m}_{fu,2}$ as this is assumed equivalent to the total power delivered from the burner unit. This model is different for each state in the finite state machine. In the transition states $n_{0,1}, n_{1,2}, n_{1,0}$ the fuel flow is constrained to move according to certain patterns. In n_0 there is no flow. In n_1 the fuel flow is equal to the flow to Burner 1. Finally in n_2 an underlying controller distributes the flow reference to the two burners in order to maximize efficiency. The total fuel flow can be assumed to be equal to the reference due to the much faster dynamics of the combustion process than that of the boiler water/steam part. We note here that the fuel flow rate constraints are different in n_1 and n_2. When the burners are on, an underlying controller adjusts the combustion air flow keeping a clean combustion with an oxygen percentage of the exhaust gas above three percent.

The model of the boiler presented in [Solberg et al., 2005] is presented here in a simplified version as studies have shown that both the flue gas part (furnace and convection tubes) and the metal separating the water/steam part from the flue gas have considerably faster dynamics than the desired closed loop bandwidth. Due to this fact the power delivered to the water/steam part is modelled as:

$$Q = \eta \dot{m}_{fu} \tag{1}$$

where η is a constant describing a combination of energy released in the combustion

n_0	*Idle*: both burners are off and Burner 1 is ready to enter start-up sequence.
$n_{0,1}$	*Burner 1 start-up*: this state contains a sequence of events split into three time intervals. It takes 3 second from the electrode is ignited to the solenoid valve opens. Then the flame scanner must detect a flame within the next 5 seconds and finally the flame has 5 seconds to stabilize before release for modulation.
n_1	*Low load*: Burner 1 is on and Burner 2 is off.
$n_{1,2}$	*Burner 2 start-up*: this state is analogous to $n_{0,1}$.
n_2	*High load*: both burners are on.
$n_{1,0}$	*Shut down*: in this state Burner 1 is shut off followed by 30 seconds of purging.

Table 1: Function of states in the finite state machine describing the burner unit.

plus furnace and convection tubes heat transfer efficiency. η is in fact a function of the boiler load. However it turns out that in the specific boiler treated here η is approximately constant leading to (1).

The model of the water/steam part has the purpose of describing the steam pressure in the boiler p_s and the water level L_w. The modeling is complicated by the shrink-and-swell phenomenon, [Åström and Bell, 2000], which is caused by the distribution of steam bubbles under the water surface.

The total volume of water and steam in the boiler is given as: $V_t = V_w + V_s + V_b$, where V_w is the water volume, V_s is the volume of the steam space above the water surface and V_b is the volume of the steam bubbles below the water surface.

To capture the dynamics of the water/steam part the total mass and energy balances are considered. The total mass balance for the water/steam part leads to the following expression:

$$\left[(V_t - V_w)\frac{d\rho_s}{dp_s} + V_w\frac{d\rho_w}{dp_s}\right]\frac{dp_s}{dt} + (\rho_w - \rho_s)\frac{dV_w}{dt} = \dot{m}_{fw} - \dot{m}_s, \tag{2}$$

and the total energy balance for the water/steam part leads to:

$$\begin{pmatrix} \rho_w V_w \frac{dh_w}{dp_s} + h_w V_w \frac{d\rho_w}{dp_s} + \rho_s (V_t - V_w)\frac{dh_s}{dp_s} + \\ h_s (V_t - V_w)\frac{d\rho_s}{dp_s} - V_t + \rho_m V_m c_{p,m}\frac{dT_s}{dp_s} \end{pmatrix}\frac{dp_s}{dt} +$$
$$+ (h_w\rho_w - h_s\rho_s)\frac{dV_w}{dt} = Q + h_{fw}\dot{m}_{fw} - h_s\dot{m}_s \tag{3}$$

where $\dot{m}_{fw}$ is the feed water flow, $\dot{m}_s$ is the steam flow,ρ is density, h is enthalpy and T is temperature, c_p is specific heat capacity and subscript m stands for metal. It should be noticed that energy accumulated in the boiler, furnace and convection tubes metal jackets are included in the balance for the water/steam part.

The two equations above only express the pressure and the water volume in the boiler. As the water level of interest in the control problem is given as: $L_w = (V_w + V_b - V_o)/A_{ws}$, another equation is needed for describing the volume of steam bubbles V_b in the water. (The water level is measured from the furnace top, V_o is the volume surrounding the furnace, and A_{ws} is the water surface area). To do this the mass balances for the steam bubbles and the water are combined with the empirical equation:

$$\dot{m}_{b\to s} = \gamma \frac{V_b}{V_w} + \beta \dot{m}_{w\to b}, \tag{4}$$

which expresses the amount of steam escaping the water surface, $\dot{m}_{b\to s}$ as function of the water volume, steam bubble volume and vaporization flow from water to bubbles $\dot{m}_{w\to b}$. This leads to the final differential equation describing the water/steam part:

$$\left((1-\beta)V_w \frac{d\rho_w}{dp_s} + V_b \frac{d\rho_s}{dp_s}\right)\frac{dp_s}{dt} + (1-\beta)\rho_w \frac{dV_w}{dt} + \\ + \rho_s \frac{dV_b}{dt} = (1-\beta)\dot{m}_{fw} - \gamma \frac{V_b}{V_w} \tag{5}$$

This equation introduces V_b in the model and thereby the shrink-and-swell phenomenon. The shrink-and-swell phenomenon is only introduced through the variable V_b. From a physical point of view this seems natural as it is the steam bubbles that experience the non-minimum phase behavior and transfer this to the output water level, whereas the water volume/mass in the boiler does not exhibit the inverse response behavior.
In practice the water/steam circuit is closed and the steam flow is governed by several valves combined with pipe resistance. Therefore a variable $k(t)$ expressing pipe conductance and valve strokes is introduced. $\dot{m}_s$ is then given as:

$$\dot{m}_s(t) = k(t)\sqrt{p_s(t) - p_{dws}} \tag{6}$$

where the downstream pressure, p_{dws}, is the pressure in the feed water tank which is open and hence has ambient pressure, $p_{dws} = p_a$. $p_s(t) - p_{dws}$ is the differential pressure over the steam supply line.
The final model has the form:

$$F(\check{x})\dot{\check{x}} = h(\check{x}, \check{u}, \check{d}) \tag{7}$$

where $\check{x} = [p_s, V_w, V_b]^T$, $\check{u} = [\dot{m}_{fu}, \dot{m}_{fw}]$ and $\check{d} = k$. The temperature of the feed water is assumed constant and therefore not included in $\check{d}$.
A linear approximation of (7) can be generated for controller design. In [Solberg et al., 2007] it was shown that the dynamics of the one-pass smoke tube boilers from AI, around the cross-over frequency has little dependency of the steam load. For this reason it suffices to focus on a controller design derived from one linear model hence leaving

out any gain scheduling. Thus the sampled linear approximation of the marine boiler takes the form:

$$\check{x}(k+1) = \check{A}\check{x}(k) + \check{B}\check{u}(k) + \check{B}_d\check{d}(k) \tag{8a}$$

$$\check{y}(k) = \check{C}\check{x}(k) + \check{D}\check{u}(k) + \check{D}_d\check{d}(k) \tag{8b}$$

$$\check{x} \in \mathcal{X},\ \check{u} \in \mathcal{U}_{i(k)} \quad i(k) \in \{0,1,2\} \tag{8c}$$

where i is the current burner mode, $\check{y} = [p_s, L_w]^T$, $\mathcal{X} \subset \mathbb{R}^n$ and $\mathcal{U}_i \subset \mathbb{R}^m$ are compact sets describing constraints on state and inputs respectively.

2.2 Control Properties

For the marine boilers concerned the well known shrink-and-swell phenomenon from feed water flow to water level, [Åström and Bell, 2000], has not been observed in measurements. This means that this loop, in principle, is limited in bandwidth only by actuators and sensors (and model uncertainty).
Another property of the system is the high bandwidth in the response from the steam flow disturbance to the outputs. This complicates the controller design as it sets a requirement for a high closed loop bandwidth in order to suppress the effect of the disturbance. This means that the controller update frequency should be high limiting the time available between updates for on-line controller computations. In particular the controller sampling time is set to $T_s = 1$ second.
It is preferred to avoid the use of a flow sensor for steam flow measurement as such equipment is expensive. In [Solberg et al., 2005] it was shown that relying on an estimate of this flow provides satisfactory performance.
Regarding the control structure, it would be preferred to leave the burner switching to an underlying burner control system which delivers the requested fuel flow. However due to the long sequences associated with burner stop/start both pressure and level control are disturbed making this approach less suitable. This requires the burner switches to be handled by the pressure and water level controller.
One drawback of this strategy is that when switching from high to low load the total fuel flow becomes uncertain, as the distribution of fuel between the two burners is not modelled. Burner 2 is constrained only to turn off when the fuel flow is at a minimum, in order to avoid cutting off an unknown fuel flow in future predictions.
The control problem is formulated as follows:

Problem 2.1. *At every sample instant k, given the current state $\check{x}(k)$, minimize the*

following performance index over $\check{\mathbf{u}} = [\check{u}(k), \check{u}(k+1|k), \dots]$*:*

$$J(\check{x}(k), \check{\mathbf{u}}) = \lim_{T\to\infty} \frac{1}{T}\Big\{ \sum_{j=1}^{M(T)} h_{m_{j-1},m_j} + \\ + T_s \sum_{i=0}^{T} \left[\check{z}^T(i+k|k)\check{Q}(i)\check{z}(i+k|k) + \Delta\check{u}^T(i+k|k)\check{R}(i)\Delta\check{u}(i+k|k)\right]\Big\} \quad (9)$$

where $\Delta\check{u}(i) = \check{u}(i) - \check{u}(i-1)$*,* $\check{z}(i) = \check{r}(i) - \check{y}(i)$ *with the reference vector* $\check{r}(i)$*,* $m \in \{0, 1, 2\}$*,* $M(T)$ *is the total number of burner switches and* h_{m_{j-1},m_j} *is the cost associated with a switch from burner mode* m_{j-1} *to mode* m_j*. Also* $\check{x}(i)$ *and* $\check{y}(i)$ *evolves according to* (8)*.* $\check{Q}$ *and* $\check{R}$ *are quadratic penalties on error and input changes.*

Hence the control problem poses a trade-off between output (pressure and level) setpoint deviations and control input action including costs for burner switches. It would seem natural to include a cost on the accumulated fuel use; however this is not implemented. The reason is that the performance criterion is to achieve zero steady state errors for both pressure and water level. A weight on the accumulated fuel use will urge the system to save fuel at the expense of inferior pressure performance. Further the disturbance appears as infrequent steps in the load, meaning that the fuel used in the transient response is small compared to the steady state fuel use.

An important property of the performance (9) is that, dependent on the choice of weights, there may exist constant steam flows corresponding to the gap-regions, for which the cost of allowing a constant offset in the output is larger than that of introducing a limit cycle through switching the input. This would always be the case if $\check{z}$ included the integral error of the pressure, as any possible constant input would result in the pressure approaching a constant value different from the setpoint, meaning that (9) would be infinite. When $\check{z}$ does not include the integral error there still exist steam flows and choices of weights for which the integral over one cycle of period T_p, corresponding to a switching input, will be smaller than the corresponding integral over T_p with any possible constant input and converged output. Finding the optimal limit cycle which the state trajectory converges to can be achieved by posing a relatively simple optimization problem. The period of this limit cycle is dependent on the steam flow disturbance. The reason for this is that the steady state fuel flow required to achieve zero pressure error is dependent on the steam flow. When the required steady state fuel flow is in a gap-region and close to where the steady state solution is optimal, the limit cycle period is long because the pressure error only slowly grows to a level where the cost is comparable to the cost of switching Burner 1 or Burner 2 on and off. In the middle of the gap-region the pressure error will increase and decrease faster and the limit cycle period will be shorter.

3 Methods

In this section we describe a method for solving control problem 2.1. The burner switch decisions will be made at the same level as the pressure and level control. This method incorporates both the finite state automaton and the dynamical system into one mixed integer optimization problem (MIP), which is solved repeatedly in a receding horizon manner.

3.1 Finite Horizon Model Predictive Control

Recently discrete time finite horizon MPC has become a tractable tool for the control of hybrid systems [Bemporad and Morari, 1999]. The reason is that the method offers a systematic design procedure for these systems. Modeling tools such as HYSDEL (hybrid system description language) [Torrisi and Bemporad, 2004] make it easy to generate MLD models suitable for implementation with an MPC control law. This is done by describing the system to be controlled as a discrete time hybrid automaton. In [Heemels et al., 2001] the equivalence between a number of classes of hybrid systems was shown. This is important since it gives methods to identify which set of equivalent classes you should use for a particular control problem. Using this framework a hybrid model of the boiler system can be put up.

Hybrid control model

The boiler system (8) including the state machine of the burner described in HYSDEL can be put together in the MLD form using tools from the MPT-toolbox [Kvasnica et al., 2004]:

$$x(k+1) = Ax(k) + B_1u(k) + B_2\delta(k) + B_3z(k) \tag{10a}$$

$$y(k) = Cx(k) + D_1u(k) + D_2\delta(k) + D_3z(k) \tag{10b}$$

$$E_2\delta(k) + E_3z(k) \leq E_1u(k) + E_4x(k) + E_5 \tag{10c}$$

where $x \in \mathbb{R}^{n_{x_r}} \times \{0,1\}^{n_{x_b}}$, $u \in \mathbb{R}^{n_{u_r}} \times \{0,1\}^{n_{u_b}}$ and $y \in \mathbb{R}^{n_y}$. $\delta \in \{0,1\}^{n_\delta}$ and $z \in \mathbb{R}^{n_z}$ represent Boolean and continuous auxiliary variables respectively. There are many possible realizations of the boiler system using this modeling tool depending e.g. on how burner switches are described. One possibility is to use the Boolean input to set a flag signaling that the burner should switch when the conditions for a switch are satisfied. Another possibility is to let the Boolean input indicate when to initiate a sequence (maneuver) which will lead to a switch. However the most general realisation is to let the Boolean input indicate a switch, hence to be able to set this input certain conditions must be satisfied. Using this realisation a state update sequence for the model is constructed as (borrowing notation from [Torrisi and Bemporad, 2004]):

Pseudo code for state update: Given old states $x(k)$ and input $u(k)$ complete the following updates to find $x(k+1)$:

Event generator: First events are logged. These are generated according to the satisfaction of linear affine constraints

$$\delta_e(k) = f_H(x_r(k), u_r(k), k) \tag{11}$$

where $f_H : \mathcal{X}_r \times \mathcal{U}_r \times \mathbb{Z}_{\geq 0} \to \mathcal{D} \subset \{0,1\}^{n_e}$. x_r is the real part of the state vector composed of $x_r(k) = [p_s(k), V_w(k), V_b(k), \dot{m}_{fu}(k-1), \dot{m}_{fw}(k-1), d_{um,1}(k), d_{um,2}(k), t(k), m(k)]^T$ where $d_{um,1}(k)$ is an unmeasured disturbance in the direction of the steam flow and $d_{um,2}(k)$ is an unmeasured disturbance in the direction of the feed water flow. Both disturbances are modelled as integrated white noise and included to achieve offset free tracking. t is a timing variable used during burner switches, and $m \in \{0,1,2\}$ is the current burner mode — but implemented as a continuous variable. u_r is the real part of the input vector given as $u_r(k) = [\Delta\dot{m}_{fu}(k), \Delta\dot{m}_{fw}(k)]^T$.

5 events are observed: 3 time events for operating the burner sequences during start and shut down, and 2 for detecting that fuel flow constraints are satisfied such that a burner switch may occur.

Finite state machine: The update of the state machine is done according to the deterministic logic function

$$x_b(k+1) = f_B(x_b(k), u_b(k), \delta_e(k)) \tag{12}$$

where $f_B : \mathcal{X}_b \times \mathcal{U}_b \times \mathcal{D} \to \mathcal{X}_b$. x_b is the Boolean part of the state vector describing the burner finite state machine: $x_b(k) = [n_0, n_{0,1}, n_1, n_{1,2}, n_2, n_{1,0}]^T$ (Figure 1) and u_b is the Boolean part of the input vector denoting Burner 1 and 2 on and off respectively given as $u_b(k) = [u_{b,1}, u_{b,2}]^T$.

The i-th row of the function generally has the form

$$x_b^i(k+1) = (\text{stay}_i) \vee (\text{switch}_{1i}) \vee (\text{switch}_{2i}) \vee \cdots$$

where $\vee$ is the logical *OR* operator, stay_i is a logical expression returning 1 if the next Boolean state is equal to the current and switch_{ji} is a Boolean expression returning 1 if a switch from state j to state i should occur.

Mode selector: The mode selector is usually designed to determine which dynamics govern the system at current time k. However as mentioned in section 2.2 the model dynamics do not change much with the steam load; for this reason only one set of system matrices is implemented. Here the Mode selector is used to determine when the clock (state t) should be reset and start counting. This clock requires the introduction of one auxiliary continuous variable, z.

Continuous dynamics: With appropriate A_r, B_r, C_r and D_r the update of the continuous state dynamics and the output are done according to:

$$x_r(k+1) = A_r x_r(k) + B_r u_r(k) \tag{13a}$$
$$y(k) = C_r x_r(k) + D_r u_r(k) \tag{13b}$$
$$h(k) = m(k) - m(k-1) \tag{13c}$$

where $y(k) = [p_s(k), L_w(k)]^T$ and $h(k) \neq 0$ denotes a change in burner mode. Note that this is a slight abuse of the h notation from (9).

Constraint verification: Finally constraints are added to the update to describe allowed input combinations, changing constraints as a function of burner mode and fuel constraints during switches.

The vector of auxiliary Boolean variables $\delta(k)$ is composed of the 5 variables of δ_e mentioned above and 5 variables to determine statements related to the clock reset and fuel constraints and finally 6 variables for the logic statement in the update equation for the Boolean states.

□

Summarizing, this update scheme has been implemented in HYSDEL and the dimensions in the resulting MLD model are: $n_{x_r} = 9$, $n_{x_b} = 6$, $n_{u_r} = 2$, $n_{u_b} = 2$, $n_\delta = 16$, $n_z = 1$ and $n_y = 3$. Further the number of constraints is $N_c = 109$.
It should be mentioned that this model formulation is non-unique. For instance there are numerous ways to describe the logic associated with a burner switch. Furthermore, in this framework switches can only occur at sample time instants, which restricts the choice of sample time if the burner sequences must be implemented accurately.

Predictive control setup

As mentioned in [Bemporad and Morari, 1999], solving a problem like *Problem* 2.1 subject to the MLD model (10) is not computationally feasible, because of the infinite horizon. Hence the criterion (9) in *Problem* 2.1 will be approximated by a finite horizon cost:

$$J(x(0), \mathbf{v}) = (r - y(T))^T P (r - y(T)) + \sum_{i=0}^{T-1} \left[(r - y(i))^T Q (r - y(i)) + u^T(i) R u(i) + h^T(i) H h(i) \right] \tag{14}$$

where the current time $k = 0$, $\mathbf{v} = [\mathbf{u}^T, \boldsymbol{\delta}^T, \mathbf{z}^T]^T$ with $\mathbf{u} = [u(0), \ldots, u(T-1)]^T$, $\boldsymbol{\delta} = [\delta(0), \ldots, \delta(T)]^T$, $\mathbf{z} = [z(0), \ldots, z(T)]^T$, $Q = \text{diag}([q_1, q_2])$, $R = \text{diag}([r_1, r_2, 0, 0])$, and the switching cost is equal to $H = \frac{h_{0,1}}{T_s} = \frac{h_{1,0}}{T_s} = \frac{h_{1,2}}{T_s} = \frac{h_{2,1}}{T_s}$. The terminal cost P is set equal to Q.

There is a lower bound on the horizon length T. This due to the fact that the fuel flow to Burner 1 needs to be reduced to its minimum before Burner 2 can be fired. The bound can be found by the integral inequality which says that the average energy supplied to the system over the finite horizon starting from the maximal fuel flow in state n_1 making a transition to state n_2 must be greater than what one would get had one stayed in n_1, else a switch will never occur. This also depends on the weight on the switches; however only looking at the supplied energy the bound is $T > 22$. Furthermore, it is preferable to have the horizon at least as long as the limit cycle period, in case the disturbance corresponds to a gap-region. However for disturbances close to the boundary of the gap-region the period gets very long, suggesting a long T. This is not feasible and a trade-off between performance and computational resources has to be made. To predict the fastest possible cycle in both gap-regions we need $T > 43$, and a practical limit cycle needs an even longer horizon. Here we set $T = 45$.
The weight H in the performance index is important as it expresses the cost for a switch. There are many reasons for including such a weight. The first was discussed in the introduction: too many switches can cause wear on the supply system and degrade overall combustion performance. Also too frequent burner on/off switching can cause high frequency oscillation of boiler pressure and water level. However there is also a period after a burner switch in which the system is vulnerable to disturbances. The reason for this is due to the nature of the disturbance, which is unknown but appears as steps in the load (worst case from almost 0 to 100% load). The problem is that if a step load change is applied just after a burner is shut down, it takes time to turn the burner on again due to the burner start-up sequence. For Burner 1 shut-down purging is also necessary. Increasing the weight H reduces this problem.

Controller implementation

The problem of minimizing (14) can be solved using a mixed integer quadratic programing solver. There are many such solvers available, of which some of the most popular have been tested, with mixed success. The problem becomes very dependent on the available optimization software. However due to the problem size, (horizon, constraints and number of Boolean variables) solving this optimization problem on-line is computationally prohibitive. A few off-line techniques, based on multiparametric programming and dynamic programming, has been suggested in the literature for defining the explicit control law (see e.g. [Bemporad et al., 2002; Borrelli et al., 2005]); however these methods are most suitable for relatively small systems using a relatively short prediction horizon. Instead on-line computational complexity must be reduced somehow.
The obvious way to do so is to restrict the Boolean decision variables to change only a few times in the prediction horizon, hence applying *input blocking* [Qin and Badgwell, 1997]. However doing so introduces another problem. Previously the prediction horizon could be too short. But when using certain blocking schemes it can also be too long. In fact this generally occurs for systems which have interior regions of the

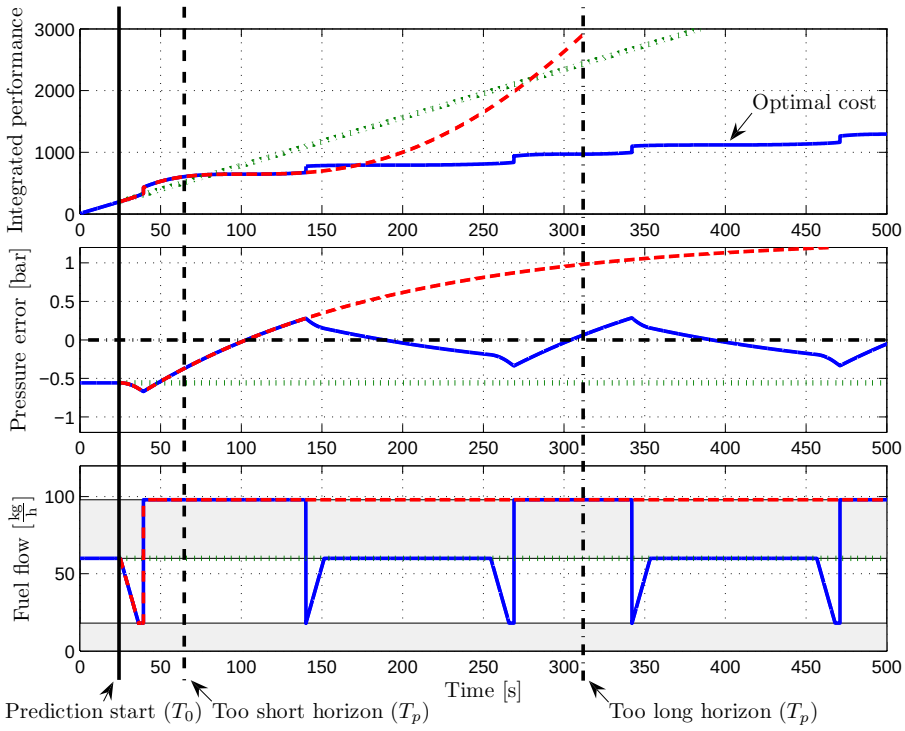

Figure 2: Plot of the optimiser choosing to switch the input at prediction time 0 (T_0) (dash-dotted curves) or not to switch the input (dotted curves). The solid curves represent the optimal strategy according to the cost (9). The top plot shows the integrated cost without division by the time. The middle plot shows the pressure error and the bottom plot the fuel flow. Notice that the dash-dotted integrated cost becomes lower than the dotted one between 80 and 270 seconds.

input space which can not be reached. We shall illustrate this here using the cost (9) for the boiler, where we shall ignore water level and feed water contributions to the cost, and approximate the pressure by a first order system — since the level loop is closed. Suppose the blocking scheme is such that the Boolean input can only change at time 0; then the situation shown in Figure 2 might occur.

From the figure it is easy to see how one can choose not only a too short, but also a too long prediction horizon. In the depicted situation what happens is that Burner 1 is *on* and Burner 2 is *off*; predicting far enough ahead, the benefit from switching Burner 2 *on*, causing the pressure to rise, will not be apparent, since the pressure will continue to rise, as Burner 2 can not be turned off again. This issue makes it very difficult to tune such algorithms and the prediction horizon must be chosen carefully considering several load disturbances.

One way to apply blocking is by introducing two new continuous input variables which represents times, T_1, T_2, at which a sequence to turn on or off Burner 1 or 2 should be initiated. Besides two new input variables, this method requires a new state variable describing absolute time over the prediction horizon, and an additional 4 mixed integer inequalities to be introduced. However this method has proven not to reduce the computational time enough to allow on-line computation.
The blocking scheme used in the final setup has full horizon for the continuous variables, whereas the Boolean variables are only allowed to change at times 0 and 1. Furthermore, the Boolean variables are defined to represent initiation of the sequence which will lead to a burner switch.
Instead of actually using model (10) as constraints in the optimization problem, and using an MIP solver, we simply implement the few optimization problems of the search tree and solve all of them at each sample time. This is necessary as introducing sequenced switches increases the model complexity to a degree where even a blocked strategy is not computationally feasible.
Regarding the feedback, a state estimator has been constructed. This estimator can operate in all modes and is hence independent of the control strategy discussed. The estimator is designed to achieve offset-free tracking of the pressure and water level. This is done by adding integrated disturbances to the process model in the direction of the steam load disturbance and the feed water flow — see e.g. [Pannocchia and Rawlings, 2003].

Remark 3.1. *The above proposed method is suboptimal in two ways: first it solves a relaxed version of the original MIQP. Secondly the method has the inherent problem of operating over a finite horizon, which according to [Solberg et al., 2008] is never optimal when the optimal state trajectory converges to a limit cycle, which is the case for the boiler system for certain energy requests corresponding to the gap-regions.*

4 Simulation Results

This section presents simulation results applying the controller presented in section 3 to the nonlinear simulation model of the marine boiler. Let us call this controller Design 1. The focus is directed to Gap-region 2 as this is the most interesting case regarding the sequences required to carry out a switch in Burner 2.
The simulation results are shown in Figure 3 to the right. The figure also shows the results of applying traditional hysteresis control in combination with standard MPC, Design 2. The pressure setpoint is 8bar. The hysteresis control is given as:

$$u_{b,1} = \begin{cases} 0 \text{ for } p_s \geq 8.30\text{bar} \\ 1 \text{ for } p_s \leq 7.76\text{bar} \\ u_{b,1} \text{ otherwise} \end{cases}, u_{b,2} = \begin{cases} 0 \text{ for } p_s \geq 8.24\text{bar} \\ 1 \text{ for } p_s \leq 7.70\text{bar} \\ u_{b,2} \text{ otherwise} \end{cases} \tag{15}$$

The hysteresis bounds are asymmetric. Note that this could be avoided by e.g. defining a rule stating that a certain burner can not switch unless the estimated steady state fuel input (shown in the bottom left plot) is in a certain region of the input space. The MPC controller has the same weight matrices as the hybrid MPC controller. During burner switches the fuel flow is simply constrained to move along a predetermined trajectory.
The disturbance profile used in the simulations is converted to represent the requested steam flow and is shown in the third row plots as dash-dotted curves. In the same plots the dotted curves represent the estimated disturbance also converted into a presumed requested steam flow.
There are a few things to notice in this figure regarding Design 1. The spikes in the fuel flow just after a burner switch from Mode 1 to Mode 2 are due to prediction mismatches. The horizon is not long enough, meaning that the algorithm cannot see the damage the choice of such a switch causes until it is too late. One could try adjusting the horizon length taking care not to make the horizon too long. In fact this method is very difficult to tune to achieve both good pressure and level control using reasonable control signals. Also it is worth noticing the asymmetry in the pressure oscillations when the disturbance corresponds to the gap-region. This stems from the maneuver which has to be performed during switches. When in Mode 1 and the maximum fuel input is injected, a switch to Mode 2 requires the fuel input first to reach the minimum level for Mode 1. As weights are put on both the pressure and input changes during these maneuvers it will naturally cost more to switch from Mode 1 to Mode 2 than the other way around. As the final performance criterion included a weight on pressure deviations and no weight on accumulated fuel use, this is not the desired performance. However this could be compensated e.g. by using a cost for the integrated pressure error, or by having asymmetric weights dependent on the current mode. However such implementations are not standard and quite cumbersome, for which reason we settle for the result presented above.
When comparing Design 1 and Design 2 there is an obvious difference in pressure behavior and hence burner switching. Design 1 can be viewed as a hysteresis controller which for some disturbances will act similar to Design 2. However, Design 1 can vary the hysteresis bounds to adapt to the current disturbance. The spikes in the fuel flow are present for both Designs (Design 2 as Design 1 does not know any better than to bring the pressure error to zero fast). Further evaluation of the performance (9) during the simulation period, for both designs, shows only small numerical differences. Also this difference is alternating in favour of Design 1 and Design 2.
Regarding the level control, only small oscillations are detected during burner on/off switching for both designs. This was consistent with an original objective, not to improve pressure performance at the expense of level regulation.

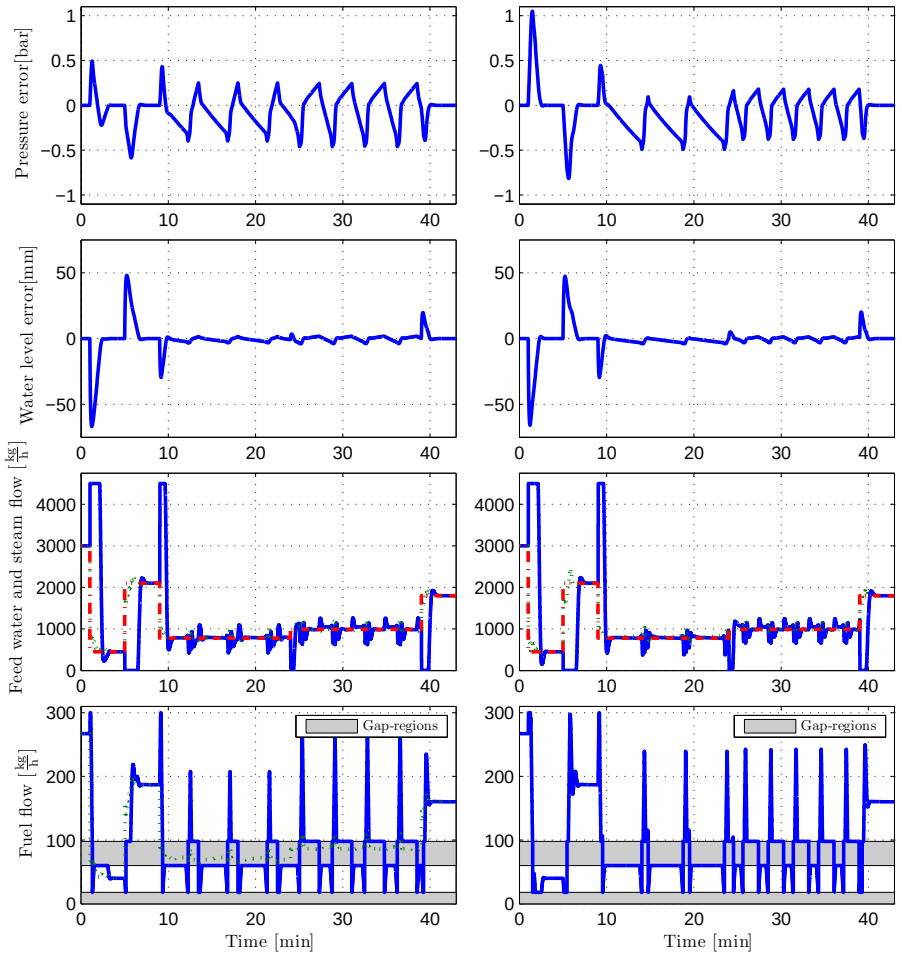

Figure 3: Simulation results for Design 1 right and Design 2 left. From the top: the first row shows the pressure, the second row shows water level, the third row shows the feed water flow (solid), estimated (dotted) and measured (dash-dotted) disturbance both converted to represent requested steam flow, the last row shows the fuel flow and the gray fields correspond to the gap-regions, the plot on the left includes the estimated steady state fuel input. Notice the spikes in the fuel flow from 12 to 38 min. and the change in asymmetry in the pressure error oscillations in the same period for Design 1.

5 Conclusion

In this paper we described the application of the MPC/ MLD method for hybrid model predictive control [Bemporad and Morari, 1999] to control of burner on/off switching in

a marine boiler application. Simulation results proved adequate performance whilst indicating potential problems with the chosen strategy. The problem was seen as spikes in fuel flow after a burner switch indicating prediction mismatches in the receding horizon implementation.
This is a general shortcoming of hybrid model predictive control using a finite horizon when the state converges to a limit cycle — as was discussed in [Solberg et al., 2008]. This paper states that such systems are not rare in the industry. In particular systems including actuators which can be described as continuous in one region and discrete in another often have such properties. A well known example is valves (linear or exponential) which, to provide predictable performance, must run in on/off mode for low openings. These systems can sometimes be treated using PWM in the discrete region. However, when the on/off control has noticeable impact on the performance outputs (the switches are not filtered out by the system dynamics) or weights are assigned to switches other strategies must be applied, like the one described in the present paper.
The improvement over traditional PWM and hysteresis control is that the period and amplitude of the pressure oscillations during limit cycle behavior can adapt to the current disturbance to fulfill a desired performance criteria. The PWM and hysteresis controller can only be optimal for one disturbance and one operating point. Further the discussed method offers a systematic control design procedure though difficult to tune.

5.1 Future Work

Generally focus should be directed towards developing infinite horizon predictive control strategies for hybrid systems.
In the context of marine boiler control it would be preferable to search for algorithms requiring less on-line computation. This could be some variant of hysteresis control.

References

K. J. Åström and R. D. Bell. Drum boiler dynamics. *Automatica*, 36:363–378, 2000.

A. Bemporad and M. Morari. Control of systems integrating logic, dynamics, and constraints. *Automatica*, 35:407–427, 1999.

A. Bemporad, M. Morari, V. Dua, and E. N. Pistikopoulos. The explicit linear quadratic regulator for constrained systems. *Automatica*, 38:3–20, 2002.

F. Borrelli, M. Baotic, A. Bemporad, and M. Morari. Dynamic programming for constrained optimal control discrete-time linear hybrid systems. *Automatica*, 41:1709–1721, 2005.

S. Hedlund and A. Rantzer. Optimal control of hybrid systems. In *Proceedings of the 38th IEEE Conference on Decision and Control*, volume 4, pages 3972–3977, 1999.

W. P. M. H. Heemels, B. D. Schutter, and A. Bemporad. On the equivalence of classes of hybrid dynamical models. In *Proceedings of the 40th IEEE Conference on Decision and Control*, 2001.

M. Kvasnica, P. Grieder, and M. Baotić. Multi-parametric toolbox (MPT), 2004. URL `http://control.ee.ethz.ch/~mpt/`.

G. Pannocchia and J. B. Rawlings. Disturbance models for offset-free model-predictive control. *American Institute of Chemical Engineers, AIChE*, 49:426–437, 2003.

S. J. Qin and T. A. Badgwell. An overview of industrial model predictive control technology. *AIChE Symposium Series*, 93:232–256, 1997.

D. Sarabia, C. de Prada, S. Cristea, and R. Mazaeda. Hybrid model predictive control of a sugar end section. In *European Symposium on Computer Aided Process Engineering, ESCAPE 16*, 2005.

B. Solberg, C. M. S. Karstensen, P. Andersen, T. S. Pedersen, and P. U. Hvistendahl. Model-based control of a bottom fired marine boiler. In P. Horacek, editor, *16th IFAC World Congress*, Prague, Czech Republic, 2005.

B. Solberg, C. M. S. Karstensen, and P. Andersen. Control properties of bottom fired marine boilers. *Energy*, 32:508–520, 2007.

B. Solberg, P. Andersen, and J. Stoustrup. Optimal switching strategy for systems with discrete inputs using a discontinuous cost functional. Submitted March 2008 for publication in International Journal of Control, 2008.

F. D. Torrisi and A. Bemporad. Hysdel - a tool for generating computational hybrid models for analysis and synthesis problems. *IEEE Transactions on Control Systems Technology*, 12:235–249, 2004.

Paper G

Optimal Switching Control of Burner Setting for a Compact Marine Boiler Design

Brian Solberg & Palle Andersen & Jakob Stoustrup

The paper has been submitted for journal publication.
March, 2008

The layout has been revised.

Abstract

This paper discusses optimal control strategies for switching between different burner modes in a novel compact marine boiler design. The aim is to find an optimal control strategy which minimises a trade-off between deviations in boiler pressure and water level from their respective setpoints while limiting burner switches. Two different sub-optimal strategies have been considered. The first one is based on the Mixed Logical Dynamical framework. The second approach is based on a generalisation of hysteresis control. The strategies are verified on a simulation model of the compact marine boiler for control of low/high burner load switches.

1 Introduction

The control of marine boilers mainly focuses on minimising the variation of steam pressure and water level in the boiler, keeping both variables around some given setpoint. Up till now this task has been achieved using classical SISO controllers, one using the fuel flow to control the steam pressure and one using the feed water flow to control the water level.

A more efficient control can allow smaller water and steam volumes in the boiler implying lower production and running costs and a more attractive product. In [Solberg et al., 2005] a successful application of LQG control to the MISSION^{TM} OB boiler from Aalborg Industries A/S (AI) product range was shown.

The specific boiler concerned in the present work is a novel compact marine boiler from AI. The boiler is a side-fired one-pass smoke tube boiler. The boiler consists of a furnace and convection tubes surrounded by water. At the top of the boiler steam is led out and feed water is injected. The compact boiler is equipped with a two-stage burner unit with two pressure atomiser nozzles of different size. With slight abuse of notation these nozzles are referred to as Burner 1 (the small nozzle) and Burner 2 (the large nozzle). This means that there are two burners and designing an appropriate switching strategy between these can allow for a high turndown ratio, defined as the ratio between the largest and lowest possible fuel flow, or equivalently burner load. However, too much switching will increase actuator wear and decrease performance due to non-optimal combustion during burner start-up.

The challenge in this work is to design an appropriate burner switching strategy that minimises pressure variations and hence fluctuations in steam quality without compromising water level performance to still allow the smaller boiler geometry. Such a task would normally have been approached using heuristic rules combined with hysteresis control, however, a more systematic design procedure is sought. The control problem is complicated by the shrink-and-swell phenomenon which introduces non-minimum phase characteristics in the system, [Åström and Bell, 2000]. This phenomenon is seen when e.g. the steam flow is abruptly increased. This causes the pressure to drop in-

stantly, which in turn causes an expansion of steam bubbles below the water surface and further lowers the boiling point causing even more bubbles to be generated leading to an almost instant increase in the water level. However, mass is removed from the boiler so eventually the water level will decrease. Similar behaviours can be observed when changing the feed water or fuel flow.

Many methods have been proposed for control of systems integrating logic and dynamics. Many of these are based on online optimisation schemes, see e.g. [Bemporad and Morari, 1999; Hedlund and Rantzer, 1999; Sarabia et al., 2005]. Others, such as traditional hysteresis control, are based on conditional switching. For systems whose optimal state trajectory converge to a limit cycle, a generalisation of hysteresis control was presented in [Solberg et al., 2008b] given only discrete decision variable. In [Giua et al., 2001; Seatzu et al., 2006; Xuping and Antsaklis, 2003] the authors treat switched linear and affine systems. It is noted that when the switching sequence is predetermined the optimal control reduces to a state feedback. However, the focus is restricted to a finite number of switches.

In this paper two different suboptimal control strategies shall be compared: the first strategy, Method A, described in [Solberg et al., 2008a] uses finite horizon Model Predictive Control (MPC) in combination with the Mixed Logical Dynamical (MLD) framework [Bemporad and Morari, 1999] which is an approach where standard tools can be applied to obtain an optimising control law. The other strategy, Method B, uses a cascade control configuration where a generalised hysteresis controller sends functions describing switching surfaces for the hysteresis, calculated from an infinite horizon optimisation problem, to an inner loop. Method B is the only strategy known to the authors which allows an infinite number of switches while penalising switches in the cost function.

It is shown through simulations that Method B in general produces better responses than Method A. The main reason for this is argued to be due to the infinite horizon used in Method B reducing prediction mismatches. Method B is further found computationally more attractive than Method A for online implementation.

The paper is organised as follows; First the marine boiler system is introduced and control properties of this is discussed. Secondly the two suboptimal control strategies are discussed. In the subsequent section these two methods are compared in a simulation study. Finally conclusion and future works are presented.

2 System Description

The boiler consists of two logically separated parts, one containing the heating system and one containing the water-steam system. The heating system consists of the furnace and the convection tubes. The water-steam system consists of all water and steam in the boiler. These two systems are interconnected by the metal separating them i.e. the furnace jacket and the convection tube jackets.

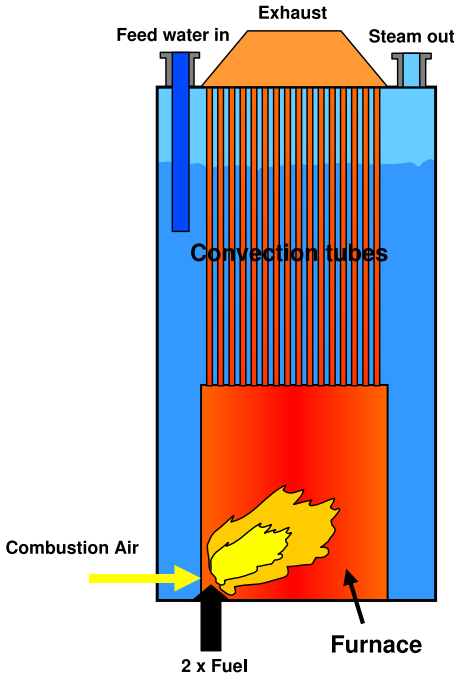

Figure 1: Compact marine boiler principle.

The boiler is equipped with two actuator systems for feed water and burner control, respectively. The feed water flow dynamics are linearised in an inner cascade controller which allows the reference to the feed water flow to be used as a manipulated variable. The corresponding inner loop can easily be designed to be faster than the outer loop. The burner system is more complicated. It can operate in three modes; Mode 0: both burners off; Mode 1: Burner 1 on and Burner 2 off; Mode 2: both burners on. A sketch of the boiler system is shown in Figure 1.
The function of the burner unit can be described by a finite state machine. The state machine consists of six states: three representing the modes described above and another three describing transitions between these, see Figure 2.
The function of each state is summarised in Table 1.
States n_1, n_2 are characterised by the continuous input variable, fuel, being controllable. In contrast transition states $n_{0,1}, n_{1,2}, n_{1,0}$ are governed by predetermined control sequences. To initiate a switch between modes, certain guards have to be satisfied, as shown in Figure 2. In most cases this is just a matter of setting the Boolean variable corresponding to the specific burner being on or off. However, to initiate a switch from Mode 1 to Mode 2, $n_1 \rightarrow n_{1,2}$, the combustion air flow and hence the fuel flow to

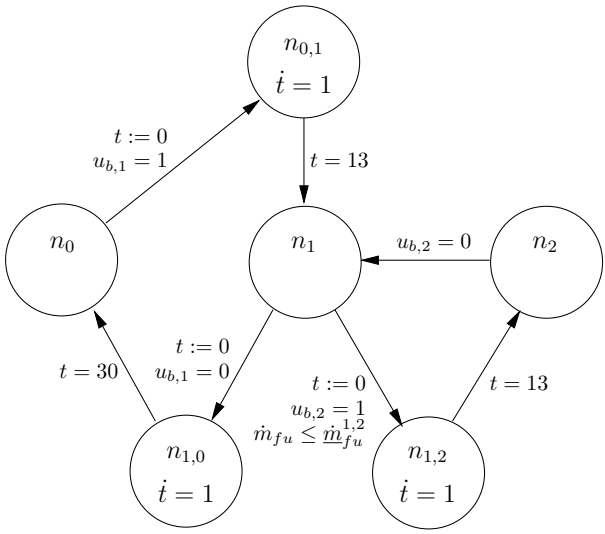

Figure 2: Finite state machine describing burner operation.

Burner 1 has to be below a certain level, in order to be able to fire Burner 2. Unfortunately, the maximum power generated by Burner 1, $\overline{Q}_l$, alone is lower than the minimum power generated by the combined operation of the burners, $\underline{Q}_h$. This is illustrated in Figure 3 where the shaded area corresponds to possible power inputs. There are two power gaps in the figure. This means that, for a steam flow that corresponds to a steady state power consumption in one of these gaps, the burners have to follow some on/off switching scheme to keep the pressure around its reference value. The gaps will be defined as: *Gap-region 1* $Q_{ss} \in [0; \underline{Q}_1] := G_1 \subset \mathbb{R}$ and *Gap-region 2* $Q_{ss} \in [\overline{Q}_l; \underline{Q}_h] := G_2 \subset \mathbb{R}$. In the sequel these gap-regions are referred to a bit loosely using statements such as 'the disturbance-', 'the required fuel flow-', 'the energy request belong to a gap-region', which all translate into the equivalent formulation that the steady state power consumption cannot be met exactly by any available fuel flow.

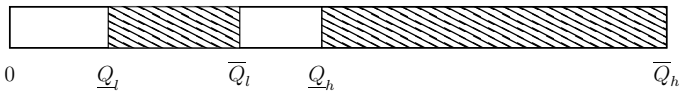

Figure 3: Modes of operation for the two-stage burner module.

n_0	*Idle*: both burners are off and Burner 1 is ready to enter start-up sequence.
$n_{0,1}$	*Burner 1 start-up*: this state contains a sequence of events split into three time intervals. It takes 3 seconds from the electrode is ignited to the solenoid valve opens. Then the flame scanner must detect a flame within the next 5 seconds and finally the flame has 5 seconds to stabilise before release for modulation.
n_1	*Low load*: Burner 1 is on and Burner 2 is off.
$n_{1,2}$	*Burner 2 start-up*: this state is analogous to $n_{0,1}$.
n_2	*High load*: both burners are on.
$n_{1,0}$	*Shut down*: in this state Burner 1 is shut off followed by 30 seconds of purging.

Table 1: Description of states in the finite state machine modelling the burner unit.

2.1 Modelling

A detailed 8th order model of the boiler system can be found in [Solberg et al., 2005]. This model took the two inputs oil flow and feed water flow along with the three disturbances steam flow, feed water temperature and oil temperature to describe the two outputs steam pressure and water level. Two states were used to describe dynamics of temperatures in the furnace and another two states were used to describe dynamics of temperatures in the flue gas pipes. One state was used to describe the temperature dynamics of the metal separating the flue gas from the water and steam. The remaining three states were used to describe the steam pressure, water volume and steam volume below the water surface. A thorough analysis of this model was presented in [Solberg et al., 2007b]. In this section we shall not repeat these results but only summarise the details important to the current work.

The simplified burner model will consist of the state machine shown in Figure 2. The model should describe the total fuel supply to the burners $\dot{m}_{fu} = \dot{m}_{fu,1} + \dot{m}_{fu,2}$ as this is assumed equivalent to the total power delivered from the burner unit. This model is different for each state in the finite state machine. In the transition states $n_{0,1}, n_{1,2}, n_{1,0}$ the fuel flow is constrained to move according to certain patterns. In n_0 there is no flow. In n_1 the fuel flow is equal to the flow to Burner 1. Finally in n_2 an underlying controller distributes the flow reference to the two burners in order to maximise efficiency. The total fuel flow can be assumed to be equal to the reference due to the much faster dynamics of the combustion process than that of the boiler water-steam part. We note here that the fuel flow rate constraints are different in n_1 and n_2. When the burners are on, an underlying controller adjusts the combustion air flow keeping a clean combustion with an oxygen percentage of the exhaust gas above three percent.

The model of the boiler presented in [Solberg et al., 2005] is presented here in a simplified version as studies have shown that both the flue gas part (furnace and convection

tubes) and the metal separating the water-steam part from the flue gas have considerably faster dynamics than the desired closed loop bandwidth. Due to this fact the power delivered to the water-steam part is modelled as:

$$Q = \eta \dot{m}_{fu} \tag{1}$$

where η is a constant describing a combination of energy released in the combustion plus furnace and convection tubes heat transfer efficiency. η is in fact a function of the boiler load. However, it turns out that in the specific boiler treated here η is approximately constant leading to (1).

The model of the water-steam part has the purpose of describing the steam pressure in the boiler p_s and the water level L_w. The modelling is complicated by the shrink-and-swell phenomenon, [Åström and Bell, 2000], which is caused by the distribution of steam bubbles under the water surface.

The total volume of water and steam in the boiler is given as: $V_t = V_w + V_s + V_b$, where V_w is the water volume, V_s is the volume of the steam space above the water surface and V_b is the volume of the steam bubbles below the water surface.

To capture the dynamics of the water-steam part the total mass and energy balances are considered. The total mass balance for the water-steam part leads to the following expression:

$$\left[(V_t - V_w)\frac{d\rho_s}{dp_s} + V_w\frac{d\rho_w}{dp_s}\right]\frac{dp_s}{dt} + (\rho_w - \rho_s)\frac{dV_w}{dt} = \dot{m}_{fw} - \dot{m}_s, \tag{2}$$

and the total energy balance for the water-steam part leads to:

$$\begin{pmatrix} \rho_w V_w \frac{dh_w}{dp_s} + h_w V_w \frac{d\rho_w}{dp_s} + \rho_s (V_t - V_w)\frac{dh_s}{dp_s} + \\ h_s (V_t - V_w)\frac{d\rho_s}{dp_s} - V_t + \rho_m V_m c_{p,m}\frac{dT_s}{dp_s} \end{pmatrix}\frac{dp_s}{dt} + \\ + (h_w\rho_w - h_s\rho_s)\frac{dV_w}{dt} = Q + h_{fw}\dot{m}_{fw} - h_s\dot{m}_s \tag{3}$$

where $\dot{m}_{fw}$ is the feed water flow, $\dot{m}_s$ is the steam flow, ρ is density, h is enthalpy and T is temperature, c_p is specific heat capacity and subscript m stands for metal. It should be noticed that energy accumulated in the boiler, furnace and convection tubes metal jackets are included in the balance for the water-steam part.

The two equations above only express the pressure and the water volume in the boiler. As the water level of interest in the control problem is given as: $L_w = (V_w + V_b - V_o)/A_{ws}$, another equation is needed for describing the volume of steam bubbles V_b in the water. (The water level is measured from the furnace top, V_o is the volume surrounding the furnace, and A_{ws} is the water surface area). To do this the mass balances for the steam bubbles and the water are combined with the empirical equation:

$$\dot{m}_{b\to s} = \gamma\frac{V_b}{V_w} + \beta\dot{m}_{w\to b}, \tag{4}$$

which expresses the amount of steam escaping the water surface, $\dot{m}_{b\to s}$ as function of the water volume, steam bubble volume and vaporisation flow from water to bubbles $\dot{m}_{w\to b}$. This leads to the final differential equation describing the water-steam part:

$$\left((1-\beta)V_w\frac{d\rho_w}{dp_s}+V_b\frac{d\rho_s}{dp_s}\right)\frac{dp_s}{dt}+(1-\beta)\rho_w\frac{dV_w}{dt}+ \\ +\rho_s\frac{dV_b}{dt}=(1-\beta)\dot{m}_{fw}-\gamma\frac{V_b}{V_w} \tag{5}$$

This equation introduces V_b in the model and thereby the shrink-and-swell phenomenon. The shrink-and-swell phenomenon is only introduced through the variable V_b. From a physical point of view this seems natural as it is the steam bubbles that experience the non-minimum phase behaviour and transfer this to the output water level, whereas the water volume/mass in the boiler does not exhibit the inverse response behaviour.
In practice the water/steam circuit is closed and the steam flow is governed by several valves combined with pipe resistance. Therefore, a variable $k(t)$ expressing pipe conductance and valve strokes is introduced. $\dot{m}_s$ is then given as:

$$\dot{m}_s(t)=k(t)\sqrt{p_s(t)-p_{dws}} \tag{6}$$

where the downstream pressure, p_{dws}, is the pressure in the feed water tank which is open and hence has ambient pressure, $p_{dws}=p_a$. $p_s(t)-p_{dws}$ is the differential pressure over the steam supply line.
The final model has the form:

$$F(\check{x})\dot{\check{x}}=h(\check{x},\check{u},\check{d}) \tag{7}$$

where $\check{x}=[p_s,V_w,V_b]^T$, $\check{u}=[\dot{m}_{fu},\dot{m}_{fw}]$ and $\check{d}=k$. The temperature of the feed water is assumed constant and therefore not included in $\check{d}$.
A linear approximation of (7) can be generated for controller design. In [Solberg et al., 2007b] it was shown that the dynamics of the one-pass smoke tube boilers from AI, around the crossover frequency has little dependency of the steam load. For this reason it suffices to focus on a controller design derived from one linear model hence leaving out any gain scheduling. Thus the sampled linear approximation of the marine boiler takes the form:

$$\check{x}(k+1)=\check{A}\check{x}(k)+\check{B}\check{u}(k)+\check{B}_d\check{d}(k) \tag{8a}$$

$$\check{y}(k)=\check{C}\check{x}(k) \tag{8b}$$

$$\check{x}\in\mathcal{X},\ \check{u}\in\mathcal{U}_{i(k)}\quad i(k)\in\{0,1,2\} \tag{8c}$$

where i is the current burner mode, $\check{y}=[p_s,L_w]^T$, $\mathcal{X}\subset\mathbb{R}^n$ and $\mathcal{U}_i\subset\mathbb{R}^m$ are compact sets describing constraints on state and inputs respectively.

2.2 Control Properties

For the marine boilers concerned the well-known shrink-and-swell phenomenon from feed water flow to water level, [Åström and Bell, 2000], has not been observed in measurements. This means that this loop, in principle, is limited in bandwidth only by actuators and sensors (and model uncertainty).
Another property of the system is the high bandwidth in the response from the steam flow disturbance to the outputs. This complicates the controller design as it sets a requirement for a high closed loop bandwidth in order to suppress the effect of the disturbance. This means that the controller update frequency should be high limiting the time available between updates for online controller computations. In particular, the controller sampling time is set to $T_s = 1$ second.
It is preferred to avoid the use of a flow sensor for steam flow measurement as such equipment is expensive. In [Solberg et al., 2005] it was shown that relying on an estimate of this flow provides satisfactory performance.
Regarding the control structure, it would be preferred to leave the burner switching to an underlying burner control system which delivers the requested fuel flow. However, due to the long sequences associated with burner stop/start both pressure and level control are disturbed making this approach less suitable. This requires the burner switches to be handled by the pressure and water level controller.
One drawback of this strategy is that when switching from high to low load the total fuel flow becomes uncertain, as the distribution of fuel between the two burners is not modelled. Burner 2 is constrained only to turn off when the fuel flow is at a minimum, in order to avoid cutting off an unknown fuel flow in future predictions.
The control problem is formulated as follows:

Problem 2.1. *At every sample instant k, given the current state $\check{x}(k)$, minimise the following performance index over $\check{\mathbf{u}} = [\check{u}(k), \check{u}(k+1|k), \dots]$:*

$$J(\check{x}(k), \check{\mathbf{u}}) = \lim_{T\to\infty} \frac{1}{T}\Big\{ \sum_{j=1}^{M(T)} h_{i_{j-1},i_j} + \\ + T_s \sum_{j=0}^{T} \left[\check{z}^T(j+k|k)\check{Q}(j)\check{z}(j+k|k) + +\Delta\check{u}^T(j+k|k)\check{R}(j)\Delta\check{u}(j+k|k)\right]\Big\} \quad (9)$$

where $\Delta\check{u}(j) = \check{u}(j) - \check{u}(j-1)$, $\check{z}(j) = \check{r}(j) - \check{y}(j)$ with the reference vector $\check{r}(j)$, $i \in \{0,1,2\}$, $M(T)$ is the total number of burner switches and h_{i_{j-1},i_j} is the cost associated with a switch from burner mode i_{j-1} to mode i_j. Also $\check{x}(j)$ and $\check{y}(j)$ evolve according to (8)*. $\check{Q}$ and $\check{R}$ are quadratic penalties on error and input changes.*

Hence the control problem poses a trade-off between output (pressure and level) set-point deviations and control input action including costs for burner switches. It would

seem natural to include a cost on the accumulated fuel use. This, however, is not implemented. The reason is that one performance criterion is to achieve zero steady state errors for both water level and pressure, when possible. A weight on the accumulated fuel use will urge the system to save fuel at the expense of inferior pressure performance. Further the disturbance appears as infrequent steps in the load, meaning that the fuel used in the transient response is small compared to the steady state fuel use.
An important property of the performance (9) is that, dependent on the choice of weights, there may exist constant steam flows corresponding to the gap-regions shown in Figure 3, for which the cost of allowing a constant offset in the output is larger than that of introducing a limit cycle through switching the input. This would always be the case if $\check{z}$ included the integral error of the pressure, as any possible constant input would result in the pressure approaching a constant value different from the setpoint, meaning that (9) would be infinite. When $\check{z}$ does not include the integral error steam flows and choices of weights still exist for which the integral over one cycle of period T_p, corresponding to a switching input, will be smaller than the corresponding integral over T_p with any possible constant input and converged output. Finding the optimal limit cycle which the state trajectory converges to can be achieved by posing a relatively simple optimisation problem. The period of this limit cycle is dependent on the steam flow disturbance. The reason for this is that the steady state fuel flow required to achieve zero pressure error is dependent on the steam flow. When the required steady state fuel flow is in a gap-region and close to where the steady state solution is optimal, the limit cycle period is long because the pressure error only slowly grows to a level where the cost is comparable to the cost of switching Burner 1 or Burner 2 on and off. In the middle of the gap-region the pressure error will increase and decrease faster and the limit cycle period will be shorter.

3 Methods

In this section two suboptimal methods for solving control problem 2.1 are described. The two methods are based on different control configurations. In the first method the burner switch decisions are made at the same level as the pressure and level control. This method incorporates both the finite state automaton and the dynamical system into one mixed integer optimisation problem (MIP) solved in a receding horizon manner. The second method exploits a strategy where an inner controller optimises over the continuous variables controlling pressure and level. The inner controller further switches the burners when the states hit switching surfaces and an outer controller optimises over these switching surfaces. It is important to notice here that the strategy of the second approach is only possible if the outer loop runs at a relatively high sample frequency due to the need for fast disturbance rejection or as here if the outer loop is sending functions describing switching surfaces to the inner loop.

3.1 Method A: Finite Horizon Model Predictive Control

Recently discrete time finite horizon MPC has become a tractable tool for the control of hybrid systems [Bemporad and Morari, 1999]. The reason is that the method offers a systematic design procedure for these systems. Modelling tools such as HYSDEL (hybrid system description language) [Torrisi and Bemporad, 2004] make it easy to generate MLD models suitable for implementation with an MPC control law. This is done by describing the system to be controlled as a discrete time hybrid automaton. Such a procedure was in [Solberg et al., 2008a] applied to the same setup as described in this paper.

Referring to this work a model of the boiler system (8) including the state machine of the burner described in HYSDEL can be put together in the MLD form using tools from the MPT-toolbox [Kvasnica et al., 2004]:

$$x(k+1) = Ax(k) + B_1u(k) + B_2\delta(k) + B_3z(k) \tag{10a}$$

$$y(k) = Cx(k) + D_1u(k) + D_2\delta(k) + D_3z(k) \tag{10b}$$

$$E_2\delta(k) + E_3z(k) \leq E_1u(k) + E_4x(k) + E_5 \tag{10c}$$

where $x \in \mathbb{R}^{n_{x_r}} \times \{0,1\}^{n_{x_b}}$, $u \in \mathbb{R}^{n_{u_r}} \times \{0,1\}^{n_{u_b}}$, $\delta \in \{0,1\}^{n_\delta}$, $z \in \mathbb{R}^{n_z}$ and $y \in \mathbb{R}^{n_y}$. The real part of the state vector is composed of $x_r(k) =$

$$[p_s(k), V_w(k), V_b(k), \dot{m}_{fu}(k-1), \dot{m}_{fw}(k-1), d_{um,1}(k), d_{um,2}(k), t(k), i(k)]^T$$

where $d_{um,1}(k)$ is an unmeasured disturbance put in the direction of the steam flow and $d_{um,2}(k)$ is an unmeasured disturbance put in the direction of the feed water flow both included to achieve offset free tracking. t is a timing variable used during burner switches, $i \in \{0,1,2\}$ is the current burner mode implemented as a continuous variable. The real part of the input vector is given as $u_r(k) = [\Delta\dot{m}_{fu}(k), \Delta\dot{m}_{fw}(k)]^T$. The Boolean part of the state vector describes the burner finite state machine: $x_b(k) = [n_0, n_{0,1}, n_1, n_{1,2}, n_2, n_{1,0}]^T$ (Figure 2) and the Boolean part of the input vector represents when to initiate a manoeuvre/sequence leading to a burner switch $u_b(k) = [u_{b,1}, u_{b,2}]^T$. Finally $y(k) = [p_s(k), L_w(k)]^T$ and $h(k) = i(k) - i(k-1)$, with $h(k) \neq 0$ denoting a change in burner mode. Note that this is a slight abuse of the h notation from (9). For further details on the model refer to [Solberg et al., 2008a].

As the infinite horizon control problem 2.1 is not computationally feasible in this setup a model predictive controller was designed based on the following finite horizon performance index:

$$\begin{aligned} J(x(0), \mathbf{v}) = {} & (y(N) - r)^T P(y(N) - r) + \\ & \sum_{j=0}^{N-1} \left[(y(j) - r)^T Q(y(j) - r) + u^T(j) R u(j) + h^T(j) H h(j) \right] \end{aligned} \tag{11}$$

where the current time $k = 0$, $T = 45$, $\mathbf{v} = [\mathbf{u}^T, \boldsymbol{\delta}^T, \mathbf{z}^T]^T$ with

$$\mathbf{u} = [u(0), \ldots, u(N)]^T, \boldsymbol{\delta} = [\delta(0), \ldots, \delta(N)]^T, \mathbf{z} = [z(0), \ldots, z(N)]^T,$$

and $Q = \text{diag}([q_1, q_2])$, $R = \text{diag}([r_1, r_2, 0, 0])$, and the switching cost is equal to $H = \frac{h_{0,1}}{T_s} = \frac{h_{1,0}}{T_s} = \frac{h_{1,2}}{T_s} = \frac{h_{2,1}}{T_s}$. The terminal cost P is set equal to Q.
To facilitate online computations blocking was used on the Boolean decision variables allowing these only to change at time 0 and 1. Further instead of actually using model (10) as constraint in the optimisation problem and use an MIP solver, the few optimisation problems of the search tree are simply implemented and all of them solved at each sample time. This is necessary as even a blocked strategy is not computationally feasible.
Regarding the feedback a state estimator has been constructed. This estimator can operate in all modes and is hence independent of the control strategy discussed. The estimator is designed as to achieve off-set free tracking of the pressure and water level. This is done by adding integrating disturbances to the process model in the direction of the steam load disturbance and the feed water flow see e.g. [Pannocchia and Rawlings, 2003].
The above proposed method is suboptimal in two ways: first it solves a relaxed version of the original MIQP. Secondly the method has the inherent problem of operating over a finite horizon, which according to [Solberg et al., 2008b] is never optimal when the optimal state trajectory converges to a limit cycle which is the case for the boiler system for certain energy requests corresponding to the gap-regions.

3.2 Method B: Generalised Hysteresis Control

The second method discussed is based on a method described in [Solberg et al., 2008b] for controlling systems whose optimal state trajectory converge to a limit cycle. The idea is to use this method when in the gap-regions. The strategy is illustrated in the block diagram in Figure 4.

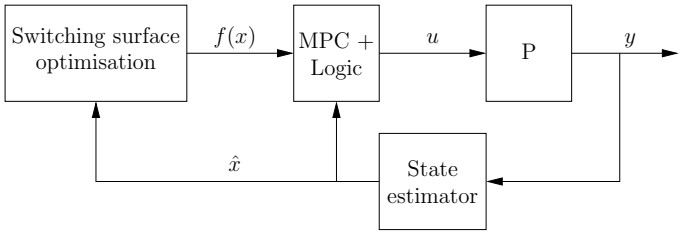

Figure 4: Control structure for Method B.

The idea behind this scheme is that the block named switching surface optimisation (SSO) might consist of setting simple hysteresis bounds for the pressure. This archi-

tecture is especially good for the marine boiler system where the disturbance profile is limited to non-frequent steps.
The SSO block need not run at the same sample frequency as the inner MPC loop which can allow for more computational demanding algorithms to be implemented at this level. Further the SSO needs only be executed when the energy demand corresponds to the gap-regions. This requires an energy estimator to run at the fastest sample time to be able to react fast when a disturbance influences the process and brings it outside the gap-regions.
Determination of when the requested energy belongs to a gap-region is done from an estimate of the steady state input needed to reject the steam flow disturbance.

$$\begin{bmatrix} I-\check{A} & -\check{B} \\ \check{C} & 0 \end{bmatrix} \begin{bmatrix} \check{x}_{ss} \\ \check{u}_{ss} \end{bmatrix} = \begin{bmatrix} \check{B}_{umd} & 0 \\ 0 & I \end{bmatrix} \begin{bmatrix} \check{d}_{um} \\ \check{r} \end{bmatrix} \tag{12}$$

Here $\check{d}_{um}$ are integrating disturbances added to the process model to achieve consistent estimates of the process output. If $\check{B}_{umd} = \check{B}$ the estimated steady state flow would simply be the first component of the $\check{d}_{um}$ vector. It turns out that a better result is achieved with $\check{B}_{umd} = [\check{B}_d \ \check{B}_2]$ corresponding to the direction of the steam flow disturbance and the feed water flow.
In the following each block in Figure 4 are described separately. The P is simply the boiler process, and the state estimator is equivalent to the one used in Section 3.1.

MPC + logic

This is the part of the controller that handles the burner switching and executes the continuous controller. The continuous controller is an MPC controller, [Maciejowski, 2001; Rossiter, 2003] in which the constraints can be adjusted on line to take into account that the fuel flow sequence executed during a switch is known. MPC control for a boiler in the same family as the one treated here is also treated in [Solberg et al., 2007a]. The performance index of the MPC controller takes the form:

$$J(\check{x}(0), \mathbf{\Delta u}) = \check{z}^T(N)\check{P}_i\check{z}(N) + \sum_{j=0}^{N-1}[\check{z}^T(j)\check{Q}_i\check{z}(j) + \Delta\check{u}^T(j)\check{R}_i\Delta\check{u}(j)] \tag{13}$$

where $\check{z} = [p_s, L_w]^T$, $\check{Q}_i = \check{P}_i = \text{diag}([\check{q}_1, \check{q}_2])$, $\check{R}_i = \text{diag}([\check{r}_1, \check{r}_2])$ and the index i on the weight matrices indicates the current burner mode. However, to be able to compare the two methods only one set of weights is included and these are equal to the ones for Method A. If the state belongs to a gap-region then $\check{q}_1 = 0$ and $\check{r}_1 = \infty$. The constraints are changed according to which mode the burner unit is operating in and which sequence is executed. This is easily done by defining appropriate upper and lower bound vectors, $\underline{\mathbf{\Delta u}}, \overline{\mathbf{\Delta u}}, \underline{\mathbf{u}}, \overline{\mathbf{u}}, \underline{\mathbf{z}}, \overline{\mathbf{z}}$, and matrices Λ, Φ such that:

$$\underline{\mathbf{\Delta u}}_i(k) \le \mathbf{\Delta u} \le \overline{\mathbf{\Delta u}}_i(k), \quad \underline{\mathbf{u}}_i(k) \le \Lambda\mathbf{\Delta u} \le \overline{\mathbf{u}}_i(k), \quad \underline{\mathbf{z}} \le \Phi\mathbf{\Delta u} \le \overline{\mathbf{z}} \tag{14}$$

The matrices Λ, Φ are constant whereas the upper and lower bound vectors are changed on line. The model used when minimising (13) over $\mathbf{\Delta u}$ subject to (14) is the same for all modes but could just as well have been different linearisations for the different load situations.
When the state hits a switching surface described in the next section a burner switch is initiated.

Switching surface optimisation

The final block of Figure 4 is supposed to communicate functions describing switching surfaces to the inner MPC controller. The strategy used for this block was proposed in [Solberg et al., 2008b]. In this paper two suboptimal methods for controlling systems with discrete decision variables when the optimal solution converge towards a limit cycle were proposed. One strategy was based on finding switching surface in the state space using time-optimal control related techniques to make the state converge to a predetermined limit cycle which results in a state feedback policy. Note that the approach of this section will use a continuous time linear model of the system.
[Solberg et al., 2008b] does not consider the case when there are mixed continuous and discrete decision variables. However, the authors proposed to use a sequential loop closing strategy by closing the inner loop using the continuous variables. Using sequential closing has the advantage of making the process react more intuitively to the operator, meaning that the level is regulated to zero between switches. Moreover, controlling the water level using burner switches is not of interest. The method of using the LQR state feedback to get an autonomous system was proposed in [Bemporad et al., 2002]. These ideas are used in the structure shown in Figure 4. Closing the inner loop, using the MPC controller for the water level when in the gap-region, a high order linear approximation of the response from fuel to pressure can be derived. In the low frequency band this model is well approximated by the simple first order system:

$$p_s(s) = \frac{K_{p_s}}{\tau_{p_s} s + 1} \dot{m}_{fu}(s) \tag{15}$$

This is the model of the system used in the outer loop for generating switching surfaces. Obvious this is only an approximation of the original setup shown in Figure 4, which contains a constrained inner MPC controller. The performance to be minimised in this outer loop is punishing the pressure error and a continuous time equivalent to input changes. The equivalent to input changes are introduced by filtering the derivative of the input signal: $\tilde{\dot{u}}_f = \frac{1}{as+1}\dot{u} = \frac{s}{as+1}u$ where a can be found by matching discrete time and continuous time costs. Given $z = \frac{1}{a}e^{-\frac{1}{a}t}\Delta u$ resulting from a step change in the input, leads to $\int_0^\infty z^T R z dt = \frac{1}{T_s}\Delta u^T R \Delta u \Rightarrow a = \frac{T_s}{2}$.
As the reference is constant and the model is linearised around the desired pressure

setpoint, the model of interest is:

$$\begin{bmatrix}\dot{p}_s\\ \dot{u}_f\end{bmatrix} = \begin{bmatrix}-\frac{1}{\tau_{p_s}} & 0\\ 0 & -\frac{1}{a}\end{bmatrix}\begin{bmatrix}p_s\\ u_f\end{bmatrix} + \begin{bmatrix}\frac{K_{p_s}}{\tau_{p_s}}\\ 1\end{bmatrix}\dot{m}_{fu} - \begin{bmatrix}\frac{K_{p_s}}{\tau_{p_s}}\\ 0\end{bmatrix}\dot{m}_{fu,ss} \tag{16a}$$

$$\begin{bmatrix}p_s\\ \tilde{u}_f\end{bmatrix} = \begin{bmatrix}1 & 0\\ 0 & -\frac{1}{a^2}\end{bmatrix}\begin{bmatrix}p_s\\ u_f\end{bmatrix} + \begin{bmatrix}0\\ \frac{1}{a}\end{bmatrix}\dot{m}_{fu} \tag{16b}$$

Recall that there are only two levels of inputs to switch between hence for energy requests belonging to either of the gap-regions $\dot{m}_{fu} \in [\underline{\dot{m}}_{fu,i}, \overline{\dot{m}}_{fu,i}]$. That is: either Burner 1 is switched on and off or Burner 2 is switched on and off. However, during switches the input, $\dot{m}_{fu}$, will follow some predetermined trajectory. The cost function takes the form:

$$J(x(0), \mathbf{u}) = \lim_{T\to\infty} \frac{1}{T}\left(\int_0^T q_1 p_s^2 + r_1 \tilde{u}_f^2 d\tau + \sum_{j=1}^{M(T)} h_{i_{j-1},i_j}\right) \tag{17}$$

where M is the number of burner switches and h_{i_{j-1},i_j} is the cost for switching from Mode i_{j-1} to Mode i_j. Before proceeding, recall that the task is to find switching surfaces describing the optimal limit cycle which the state converges to when minimising (17). In the meantime it might happen that no limit cycle is optimal meaning that a smaller cost is associated with allowing a constant off-set compared to tracking a limit-cycle. For this reason a dead band may be defined which redefines the gap-regions in such a way that a limit cycle is always optimal when in the gap-regions. In particular, we introduce a dead band on the pressure stationary value. This dead band is converted to new bounds for the gap-regions. The dead band $D \subset G$ is defined as the subset:

$$D := \{u_{ss} | \exists u \in \{\underline{u}, \overline{u}\} \wedge u_{ss} \in G \text{ s.t. } J_{ss} \leq J_{lc}\} \tag{18}$$

with J_{ss} being the cost for having a constant off-set and J_{lc} is the cost for staying on a limit cycle. Then the new gap is $\tilde{G} = G \setminus D$. However, when choosing an integral cost this is not possible as any constant off-set will cause the cost to become infinite. Instead a traditional dead band can be introduced in such situations:

$$D := \{u_{ss} | \exists u \in \{\underline{u}, \overline{u}\} \wedge u_{ss} \in G \text{ s.t. } K_{p_s}(u - u_{ss}) < \epsilon\} \tag{19}$$

with ϵ being the allowed pressure error. Modifying the gap also has the effect as to provide robustness against uncertainties and noise in the steady state estimates.
The full model used in the outer loop can be described as a piece-wise affine system:

$$\dot{x}(t) = A_{i(t)}x(t) + B_{i(t)}u_{i(t)}(t) - B_{d,i(t)}u_{ss} = A_{i(t)}x(t) + f_{i(t)}(t) \tag{20a}$$

$$y(t) = C_{i(t)}x(t) + D_{i(t)}u_{i(t)}(t), i(t) \in \mathcal{S} \tag{20b}$$

$$x(t^+) = M_{j,k}x(t^-) + g_{j,k}, \text{ if } i(t^-) = j, i(t^+) = k \tag{20c}$$

where $i \in \mathcal{S}$ corresponding to the current burner mode and $\mathcal{S} \triangleq \{0, 1, 2\}$ is the different burner modes each associated with a set of model matrices. Due to the nature of the switches more than one consecutive switch at the same time instance is not allowed. The transition matrices $M_{j,k}, g_{j,k}$ are related to manoeuvres and hence do not represent instantaneous jumps in the state (here lending terminology from [Frazzoli, 2001] and [Frazzoli et al., 1999] where such manoeuvres made up an manoeuvre automaton for shifting between trim trajectories in helicopter flight). Instead the manoeuvres are time intervals in which the state is taken from $x(t^-)$ to $x(t^+)$ in time $\delta T_{j,k}$. Hence:

$$M_{j,k} = e^{\left(\sum_{n=0}^{N-1} A_{i_n} \tau_{n+1}\right)}, \text{ and} \tag{21a}$$

$$g_{j,k} = \sum_{n=0}^{N-1} \left\{ e^{\left(\sum_{h=n}^{N-1} A_{i_h} \tau_{h+1}\right)} \left[\int_0^{\tau_{n+1}} e^{-A_{i_n} \tau} f_{i_n}(\tau) d\tau \right] \right\} \tag{21b}$$

where $i_0 = j$, $i_{N-1} = k$, $\delta T_{j,k} = \sum_{n=0}^{N-1} \tau_{n+1}$, $f_{i_n}(\tau) = B_{i_n} u_{j,k}(\tau) - B_{d,i_n} u_{ss}$ and $u_{j,k}(\tau) = \Delta \in \{u_0, \ldots, u_{N-1}\}$ is a sequence of inputs hence $g_{j,k}$ can be split into a finite number of integrals with the same input profile e.g. a constant $u_n(t) = c$ or a ramp $u_n(t) = at + u_{n-1}$ where $t \in [0, \tau_n)$.
Now define

$$\delta_j = \begin{cases} T & M = 0 \\ T_j & j \leq 1 \wedge M > 0 \\ T - T_{j-1} - \delta T_{i_{j-2}, i_{j-1}} & j \geq M \wedge M > 0 \\ T_j - T_{j-1} - \delta T_{i_{j-2}, i_{j-1}} \geq 0 & \text{otherwise} \end{cases} \tag{22}$$

T_j denotes the time of the j'th input switch and $M = M(T)$ is the number of switches occurring in time T. The optimisation problem associated with minimising the cost (17), using the above notation, having L as the stage cost and H, h as the costs associated with switches, can be written as:

$$J^*(x_0) = \min_{\mathbf{T},\mathbf{I}} \lim_{T \to \infty} \frac{1}{T} \left\{ \sum_{k=0}^{M(T)} \left[L(x_k, \delta_{k+1}) \right] + \sum_{k=1}^{M(T)} \left[H_{i_{k-1}, i_k}(\tilde{x}_k) + h_{i_{k-1}, i_k} \right] \right\} \tag{23a}$$

s.t.

$$k = 0, \ldots, M-1 \tag{23b}$$

$$L(x_k, \delta_{k+1}) = x_k^T \mathbf{Q}_{i_k}(\delta_{k+1}) x_k + x_k^T \mathbf{r}_{i_k}(\delta_{k+1}) + \mathbf{s}_{i_k}(\delta_{k+1}) \tag{23c}$$

$$H_{i_{k-1}, i_k}(\tilde{x}_k) = \tilde{x}_k^T \mathbf{Q}_{i_{k-1}, i_k} \tilde{x}_k + \tilde{x}_k^T \mathbf{r}_{i_{k-1}, i_k} + \mathbf{s}_{i_{k-1}, i_k} \tag{23d}$$

$$\tilde{x}_{k+1} = \mathbf{A}_{i_k}(\delta_{k+1}) x_k + \mathbf{f}_{i_k}(\delta_{k+1}) \tag{23e}$$

$$x_{k+1} = M_{i_k, i_{k+1}} \tilde{x}_{k+1} + g_{i_k, i_{k+1}} \tag{23f}$$

$$0 \leq T_1 < T_2 < \cdots < T_M \tag{23g}$$

$$x_0 = x(0), i_0 = i(0) \tag{23h}$$

where $\mathbf{T} = [T_1, \ldots, T_M]$ and $\mathbf{I} = [i_1, \ldots, i_M]$. This cost looks much like the one in [Xuping and Antsaklis, 2003] and [Seatzu et al., 2006], though here the average over time is taken and the state jump is governed by manoeuvres. It is easy to find symbolic expressions for $\mathbf{Q}_i, \mathbf{r}_i, \mathbf{s}_i, \mathbf{A}_i, \mathbf{f}_i$ as function of the switching times as follows [Seatzu et al., 2006].

$$\mathbf{A}_i(\delta) = e^{A_i\delta} \tag{24a}$$

$$\mathbf{f}_i(\delta) = e^{A_i\delta}\int_0^\delta e^{-A_i\tau} f_i(\tau)d\tau \tag{24b}$$

and allowing a cost on the input $u^T S_i u$ for generality leads to:

$$\mathbf{Q}_i(\delta) = \int_0^\delta e^{A_i^T t} C_i^T Q_i C_i e^{A_i t} dt \tag{25a}$$

$$\mathbf{r}_i(\delta) = 2\int_0^\delta e^{A_i^T t} C_i^T Q_i \left(C_i e^{A_i t}\left(\int_0^t e^{-A_i\tau} f_i(\tau)d\tau\right) + D_i u_i(t)\right) dt \tag{25b}$$

$$\begin{aligned}\mathbf{s}_i(\delta) = \int_0^\delta \Big\{ & u_i^T(t)(D_i^T Q_i D_i + S_i)u_i(t) + \\ & + 2u_i^T(t) D_i^T Q_i C_i e^{A_i t}\left(\int_0^t e^{-A_i\tau} f_i(\tau)d\tau\right) + \\ & + \left(\int_0^t f_i^T(\tau) e^{-A_i^T\tau} d\tau\right) e^{A_i^T t} C_i^T Q_i C_i e^{A_i t}\left(\int_0^t e^{-A_i\tau} f_i(\tau)d\tau\right)\Big\} dt\end{aligned} \tag{25c}$$

If A_i is Hurwitz, $D_i = 0$, $S_i = 0$ and $f_i = 0$:

$$\mathbf{Q}_i(\delta) = Z_i - e^{A_i^T\delta} Z_i e^{A_i\delta},\ \mathbf{r}_i(\delta) = 0,\ \mathbf{s}_i(\delta) = 0 \tag{26}$$

where Z_i is the solution to the Lyapunov equation $A_i^T Z_i + Z_i A_i = -C_i^T Q_i C_i$. Instead if the assumption on A_i is that it is diagonisable, $A_i = V_i \Lambda_i V_i^{-1}$, where $\Lambda_i = \text{diag}(\lambda_1, \ldots, \lambda_n)$, then:

$$\mathbf{Q}_i(\delta) = (V_i^{-1})^T \left(\int_0^\delta e^{\Lambda_i^T t} V_i^T C_i^T Q_i C_i V_i e^{\Lambda_i t} dt\right) V_i^{-1} \tag{27a}$$

$$\begin{aligned}\mathbf{r}_i(\delta) = 2(V_i^{-1})^T \int_0^\delta \Big\{ & e^{\Lambda_i^T t} V_i^T C_i^T Q_i \times \\ & \times \left(C_i V_i e^{\Lambda_i t}\left(\int_0^t e^{-\Lambda_i\tau} V_i^{-1} f_i(\tau)d\tau\right) + D_i u_i(t)\right)\Big\} dt\end{aligned} \tag{27b}$$

$$\mathbf{s}_i(\delta) = \int_0^\delta \Big\{ u_i^T(t)(D_i^T Q_i D_i + S_i)u_i(t) + \tag{27c}$$

$$
\begin{aligned}
&+ 2u_i^T(t) D_i^T Q_i C_i V_i e^{\Lambda_i t} \left(\int_0^t e^{-\Lambda_i \tau} V_i^{-1} f_i(\tau) d\tau \right) + \\
&+ \left(\int_0^t f_i^T(\tau) (V_i^{-1})^T e^{-\Lambda_i^T \tau} d\tau \right) e^{\Lambda_i^T t} V_i^T C_i^T Q_i C_i V_i e^{\Lambda_i t} \times \\
&\times \left(\int_0^t e^{-\Lambda_i \tau} V_i^{-1} f_i(\tau) d\tau \right) \Big\} dt
\end{aligned}
$$

These integrals are easy to calculate symbolically due to the simple form of the matrix exponential of a diagonal matrix. Further,

$$
H_{i,j}(\tilde{x}_k) = \sum_{h=0}^{N-1} \left[x_h^T \mathbf{Q}_{i_h}(\tau_{h+1}) x_h + x_h^T \mathbf{r}_{i_h}(\tau_{h+1}) + \mathbf{s}_{i_h}(\tau_{h+1}) \right], \tag{28}
$$

with

$$
x_{h+1} = e^{A_{i_h} \tau_{h+1}} x_h + e^{A_{i_h} \tau_{h+1}} \int_0^{\tau_{h+1}} e^{-A_{i_h} \tau} f_{i_h}(\tau) d\tau \tag{29a}
$$

$$
x_0 = \tilde{x}_k \tag{29b}
$$

with N being the number of continuous input profiles that make up the manoeuvre and τ_j the time spent with input profile j. By defining $\tilde{\mathbf{Q}}_{i,j} = \mathrm{diag}(\mathbf{Q}_{i_0}(\tau_1), \ldots, \mathbf{Q}_{i_{N-1}}(\tau_N))$, $\tilde{\mathbf{r}}_{i,j} = \left[\mathbf{r}_{i_0}(\tau_1), \ldots, \mathbf{r}_{i_{N-1}}(\tau_N) \right]^T$ and $\tilde{\mathbf{s}}_{i,j} = \mathbf{s}_{i_0}(\tau_1) + \cdots + \mathbf{s}_{i_{N-1}}(\tau_N)$, (28) can be rewritten as a quadratic form in $\tilde{x}_k$

$$
\begin{aligned}
H_{i,j}(\tilde{x}_k) = \tilde{x}_k^T \mathbf{M}_{i,j}^T \tilde{\mathbf{Q}}_{i,j} \mathbf{M}_{i,j} \tilde{x}_k + \tilde{x}_k^T \mathbf{M}_{i,j}^T \left(2 \tilde{\mathbf{Q}}_{i,j} \mathbf{g}_{i,j} + \tilde{\mathbf{r}}_{i,j} \right) + \\
+ \mathbf{g}_{i,j}^T \tilde{\mathbf{Q}}_{i,j} \mathbf{g}_{i,j} + \mathbf{g}_{i,j}^T \tilde{\mathbf{r}}_{i,j} + \tilde{\mathbf{s}}_{i,j}
\end{aligned} \tag{30}
$$

where

$$
\begin{bmatrix} x_0 \\ x_1 \\ x_2 \\ \vdots \\ x_{N-1} \end{bmatrix} = \begin{bmatrix} I \\ e^{(A_1 \tau_1)} \\ e^{(A_1 \tau_1 + A_2 \tau_2)} \\ \vdots \\ e^{\left(\sum_{n=1}^{M-1} A_n \tau_n \right)} \end{bmatrix} \tilde{x}_k + \tag{31a}
$$

$$
+ \begin{bmatrix} 0 & 0 & & \\ e^{A_1 \tau_1} & 0 & & \\ e^{(A_1 \tau_1 + A_2 \tau_2)} & e^{A_2 \tau_2} & & \\ \vdots & & \ddots & \\ e^{\left(\sum_{n=1}^{N-1} A_n \tau_n \right)} & & e^{\left(\sum_{n=2}^{N-1} A_n \tau_n \right)} \ \ldots \ e^{A_{N-1} \tau_{N-1}} & \end{bmatrix} \begin{bmatrix} \int_0^{\tau_1} e^{-A_1 \tau} f_1(\tau) d\tau \\ \int_0^{\tau_2} e^{-A_2 \tau} f_2(\tau) d\tau \\ \vdots \\ \int_0^{\tau_{N-1}} e^{-A_{N-1} \tau} f_{N-1}(\tau) d\tau \end{bmatrix}
$$

$$
\mathbf{x} = \mathbf{M}_{i,j} \tilde{x}_k + \mathbf{g}_{i,j} \tag{31b}
$$

where for simplicity $i_0 = 1, i_1 = 2, \ldots$ have been used. The ultimate goal would be to solve this problem for T approaching infinity while also allowing M to approach

infinity. This is a hard, yet unsolved, problem for which reason the approximative solution described in [Solberg et al., 2008b] will be used. Hence set the number of switches equal to two $M = 2$ and add the constraints $x_2 = x_0$, $T = T_2 + \delta T_{i_1,i_2}$ to find the optimal limit cycle if one exists.

Having found the optimal limit cycle and thereby found the two points (x^+, x^-) representing the state just after each of the two switches, the switching surfaces and their domains can be calculated using techniques from time optimal control. Following [Solberg et al., 2008b] means starting by finding the solution to the system when the input is constant using the notation $x_1 = p_s$, $x_2 = u_f$, $u = \dot{m}_{fu}$, $\lambda_1 = -\frac{1}{\tau_{p_s}}$, $\lambda_2 = -\frac{1}{a}$, $f_1 = \frac{K_{p_s}}{\tau_{p_s}}(\dot{m}_{fu} - \dot{m}_{fu,ss})$, $f_2 = \dot{m}_{fu}$, $x^0 = x^-$, $x = [x_1, x_2]^T$, $x' = [x_1', x_2']^T$ and $\Lambda = \left[\begin{smallmatrix} \lambda_1 & 0 \\ 0 & \lambda_2 \end{smallmatrix}\right]$.

$$\begin{bmatrix} x_1'(t) \\ x_2'(t) \end{bmatrix} = e^{\Lambda t} \begin{bmatrix} x_1^0 \\ x_2^0 \end{bmatrix} + \int_0^t e^{\Lambda(t-\tau)} d\tau \begin{bmatrix} f_1 \\ f_2 \end{bmatrix} \tag{32}$$

Now the switching surface is sought which is a curve in the 2-dimensional system. First find, Γ^-, the curve along which the state approach x^- with negative f_1 after a switch by setting $t = -\tau,\ (\tau > 0)$ in (32) and eliminating τ. This curve is given by the equations:

$$x' = M_{1,2}x + g_{1,2} \tag{33a}$$

$$\tau(x') = -ln\left(\frac{x_1' + f_1/\lambda_1}{x_1^0 + f_1/\lambda_1}\right)/\lambda_1 \tag{33b}$$

$$f^-(x') = \left(\frac{x_1' + f_1/\lambda_1}{x_1^0 + f_1/\lambda_1}\right)^{\frac{\lambda_2}{\lambda_1}} - \left(\frac{x_2' + f_2/\lambda_2}{x_2^0 + f_2/\lambda_2}\right) = 0 \tag{33c}$$

over the domain $X_{\Gamma^-} = \{x | \tau(x') > 0\}$. The curve Γ^+ and domain X_{Γ^+} can be found in a similar manner starting from the point x^+. Now a new function describing the surface dividing the state space $E = \Gamma^+ \cup \Gamma^-$ can be defined. This function, defined on $X_{\Gamma^+} \cup X_{\Gamma^-}$, is given as:

$$f(x) = \begin{cases} f^+(x) \text{ for } x(t) \in X_{\Gamma^+} \\ f^-(x) \text{ for } x(t) \in X_{\Gamma^-} \end{cases} \tag{34}$$

Finally define the space above the surface E as E^- and the space below as E^+ being regions of the state space where a negative input or a positive input can take the state to one of the switching surfaces.

Now the switching law steering the state of the reduced order system to the optimal

limit cycle is:

$$u_b(t) = \begin{cases} 1 \text{ for } x(t) \in E^+ \\ 0 \text{ for } x(t) \in E^- \\ 1 \text{ for } x(t) \in \Gamma^+ \\ 0 \text{ for } x(t) \in \Gamma^- \\ u_b(t) \text{ for } x(t) \in \mathbb{R}^2 \setminus (X_{\Gamma^+} \cup X_{\Gamma^-}) \end{cases} \tag{35}$$

u_b can be either of the on signals to the two burners depending on the gap-region the energy reference is belonging to. This law is implemented on the MPC + Logic level in the control structure in Figure 4. It is obvious that the behaviour of this control law is close to that of ordinary hysteresis control, which would have one dimensional switching surfaces dependent on the pressure only. This is due to the system being of second order and the second state being simply a filtered version of the input. If one had chosen a cost where the integral of the pressure was penalised, a third order system would have been the result and a more complicated state trajectory would be the result. Now this switching law is only valid for one particular u_{ss} in practise the calculation in this section has to be done at every sample time of the outer controller to take account for the changing disturbance. However, it is also possible, as will be done here, to construct a lookup table by evaluating the optimal limit cycle off line for as many different disturbance levels as the desired accuracy dictates and then use the switching surfaces which corresponds to the closest disturbance. This is computationally very efficient as evaluating the switching surfaces takes little resources whereas finding the optimal limit cycle is very demanding.

An illustration of the method is shown in Figure 5 where a simulation on the nonlinear model (7) has been carried out and the associate states (pressure and filtered fuel flow) are shown. The blue line is the state evolution while the red lines are the parts of the optimal limit cycle trajectory (for the linear system) between switches and the green lines the part during switches.

From this plot it can be seen that the state converges to a neighbourhood around the limit cycle. This indicates as assumed that the nonlinearities in the system are not pronounced in the fuel/pressure loop. Accurate convergence to the limit cycle can be achieved but it will require far more than two switches in a cycle due to model uncertainties and unmodelled/disregarded dynamics and disturbances and as a cost is assigned to a switch this is not desired.

As the previous method based on finite horizon MPC this method is suboptimal. The suboptimality lies in the use of a reduced order model plus the separate optimisation of discrete and continuous decision variables in the outer and inner loop, respectively. Further, only a finite horizon cost is used when outside the gap-regions. However, this needs not be the case as different methods exist for implementing quasi infinite horizon strategies for linear systems [Mayne et al., 2000]. The horizon is set equal to the one for Method A.

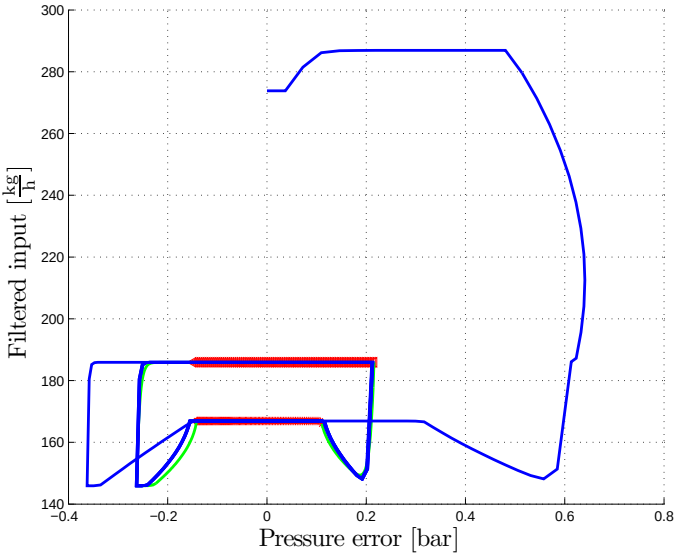

Figure 5: Projection of the state trajectory into the plane containing p_s, u_f after a simulation on (7).

4 Simulation Results

This section presents simulation results applying the two methods discussed in Section 3 to the nonlinear simulation model of the marine boiler. The focus is directed to Gap-region 2 as this is the most interesting case regarding the sequences required to carry out a switch in Burner 2.

The simulation results for Method A are shown in the left column of Figure 6. The disturbance profile used in the simulation is converted to represent the requested steam flow and is shown in the plot in row three column 1 as a red line. In the same plot the green line represents the estimated disturbance also converted into a presumed requested steam flow.

There are a few things to notice in this figure. The spikes in the fuel flow just after a burner switch from Mode 1 to Mode 2 are due to prediction mismatches. The horizon is not long enough meaning that the algorithm cannot see the damage the choice of such input sequence causes until it is too late. One could try adjusting the horizon length taking care not to make the horizon too long. In fact this method is very difficult to tune to achieve both good pressure and level control using reasonable control signals. Also it is worth noticing the asymmetry in the pressure error oscillations when the disturbance corresponds to the gap-region. This stems from the manoeuvre necessary to perform during switches. When in Mode 1 and the maximum fuel input is injected

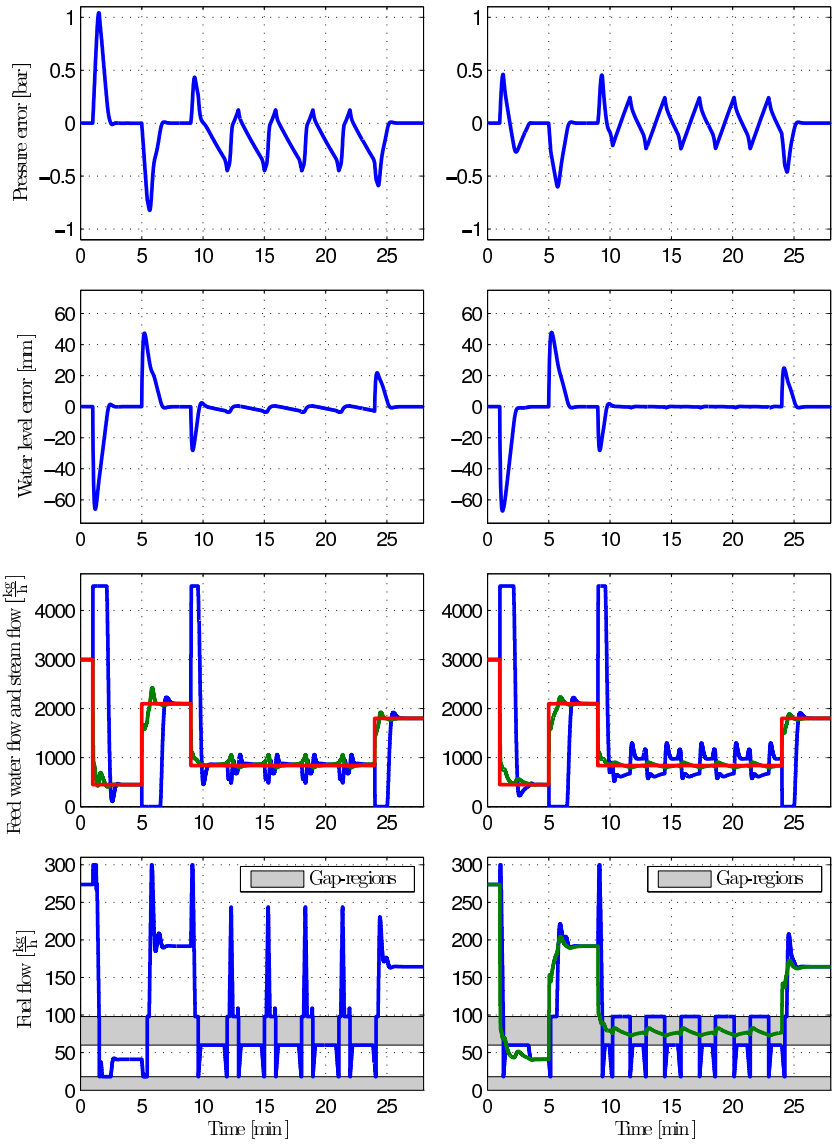

Figure 6: Simulation results using Method A left and Method B right. From the top the first row shows pressure error, the second water level error, the third row shows the feed water flow (blue), estimated (green) and measured (red) disturbance both converted to represent requested steam flow, and the bottom row shows fuel flow. The plot on the right includes the estimated steady state fuel input (green), the grey fields correspond to the gap-regions. Notice the spikes in the fuel flow from 12 to 25 min. bottom left and the asymmetry in the pressure error oscillations in the same period top left for Method A.

a switch to Mode 2 requires the fuel input first to reach the minimum level for Mode 1. As weights are put on both the pressure error and input changes also during these manoeuvres it will naturally cost more to switch from Mode 1 to Mode 2 than the other way around. As the final performance included a weight on the pressure error and no weight on accumulated fuel use, this is not the desired performance. However, this could be compensated by e.g. using a cost for the integrated pressure error or by having asymmetric weights dependent on the current mode. However, such implementations are not standard and quite cumbersome for which reason the result presented above are used.

The simulation results for Method B are shown in the right column of Figure 6. The lines in the plot in row three column two have the same interpretation as in the plot beside it and moreover the extra green line in the bottom right plot represents the estimated required steady state fuel flow.

As opposed to Method A the pressure error oscillations when in the gap-region are close to symmetric around the reference for Method B. The spikes in the fuel flow are also avoided using Method B as prediction mismatches are reduced. As can be seen it would be advantageous to reduce the uncertainty on the steam flow estimate as this is the key component in the method and too large variance on this can deteriorate performance. In particular, when close to the boundary of the gap-region the steady state estimate might switch between being outside and inside the gap-region. One natural possibility for reducing this phenomenon is to simply include a measurement of the steam flow instead of relying on an estimate. However, much of the performance lack for this estimate seems to come from the neglected steady state gain nonlinearities in the low frequency region. The estimate converges when the pressure can reach a steady state but when the input saturates the pressure becomes "unstable" and the estimate seems to converge slowly. It would be simple to use different models dependent on the current load estimate which would be a natural extension to the presented approach. This is not done here in order to be able to compare the results from the two methods.

Regarding the level control, only small oscillations are detected during burner on/off switching for both methods. Part of the original setup was not to improve pressure performance at the expense of level regulation which has been achieved. The variation seems smaller though for Method B which is due to the sequential implementation which ensures that the water level error is regulated to zero between burner switches.

5 Conclusion

Two different approaches to control a marine boiler equipped with a two-stage burner has been discussed: One, Method A, based on finite horizon MPC using a hybrid internal model and another, Method B, based on a generalised hysteresis approach. Both methods were able to provide satisfactory performance keeping both pressure and level around the desired reference values. A direct performance comparison is difficult due

to the heuristics involved in both methods. Even so there are still conclusions to be drawn regarding the choice of method. Further the objective of both methods was to minimise (9) and the performance weights were set equal. This leads to the quantitative performance comparison for the simulation sequence presented in Section 4: $J_A = 7.64 > 7.47 = J_B$.

Method A has problems regarding prediction mismatches which is not the case for method B when in the gap-regions. However, it should be mentioned that one major assumption was made, which was that the optimal solution is periodic. Further only the change between two constant input levels were considered.

Both of the proposed methods are suboptimal solutions of the original control problem. Further both methods requires optimisation solvers to be shipped with the industrial product; Method A for solving multiple optimisation problems at each sample time and Method B for solving one at each sample time. Regarding offline design Method B requires considerably more computations. The original implementation of Method A using a MIP solver requires considerably longer computation time than the proposed solutions.

Method B has the advantage that it can easily be reduced to a simple hysteresis controller. The method is relevant also for normal boilers running on/off burner control and can be used for finding conventional hysteresis bounds. Further the inner controller needs not be MPC type but can be replaced by any suitable controller of designers choice. The method is not limited to burner control but can be applied with advantage in all systems in which the actuator signal is characterised as being continuous over one region and discrete outside this region.

Regarding Method B there is a risk of slow convergence as the ability to switch when the energy request is just outside the gap is not utilised. This is naturally incorporated in Method A.

Finally Method A proved very difficult to tune to achieve both good level and pressure performance which did not seem to be the case for Method B. This means that in fact some kind of decoupling of the performance measures should be considered. This is exactly what have been achieved with Method B even though this was not intended from the beginning.

5.1 Future Work

The future focus should be directed towards Method B. In particular, interest should be directed towards reducing the uncertainty in the steam flow estimate since this quantity determines when we are in a gap-region and determines the switching functions within the gap-region. The obvious extension here is to include more models in the controller design. Further different input function could be tested when in between switches to reduce conservatism of the method.

References

K. J. Åström and R. D. Bell. Drum boiler dynamics. *Automatica*, 36:363–378, 2000.

A. Bemporad and M. Morari. Control of systems integrating logic, dynamics, and constraints. *Automatica*, 35:407–427, 1999.

A. Bemporad, A. Giua, and C. Seatzu. A master-slave algorithm for the optimal control of continuous-time switched affine systems. In *Proceedings of the IEEE Conference on Decision and Control*, volume 2, pages 1976–1981, 2002.

E. Frazzoli. *Robust Hybrid Control for Autonomous Vehicle Motion Planning*. PhD thesis, MIT, June 2001.

E. Frazzoli, M. Dahleh, and E. Feron. A hybrid control architecture for aggressive maneuvering of autonomous helicopters. In *Proceedings of the 38th IEEE Conference on Decision and Control*, volume 3, pages 2471–2476, December 1999.

A. Giua, C. Seatzu, and C. Van der Mee. Optimal control of autonomous linear systems switched with a pre-assigned finite sequence. In *IEEE International Symposium on Intelligent Control - Proceedings*, pages 144–149, 2001.

S. Hedlund and A. Rantzer. Optimal control of hybrid systems. In *Proceedings of the 38th IEEE Conference on Decision and Control*, volume 4, pages 3972–3977, 1999.

M. Kvasnica, P. Grieder, and M. Baotić. Multi-parametric toolbox (MPT), 2004. URL `http://control.ee.ethz.ch/~mpt/`.

J. M. Maciejowski. *Predictive Control With Constraints*. Harlow: Pearson Education Limited, 2001.

D. Q. Mayne, J. B. Rawlings, C. V. Rao, and P. O. M. Scokaert. Constrained model predictive control: Stability and optimality. *Automatica*, 36(6):789–814, June 2000.

G. Pannocchia and J. B. Rawlings. Disturbance models for offset-free model-predictive control. *American Institute of Chemical Engineers, AIChE*, 49:426–437, 2003.

J. A. Rossiter. *Model-based Predictive Control: A Practical Approach*. CRC Press LLC, 2003.

D. Sarabia, C. de Prada, S. Cristea, and R. Mazaeda. Hybrid model predictive control of a sugar end section. In *European Symposium on Computer Aided Process Engineering, ESCAPE 16*, 2005.

C. Seatzu, D. Corona, A. Giua, and A. Bemporad. Optimal control of continuous-time switched affine systems. *IEEE Transactions on Automatic Control*, 51(5):726–741, May 2006.

B. Solberg, C. M. S. Karstensen, P. Andersen, T. S. Pedersen, and P. U. Hvistendahl. Model-based control of a bottom fired marine boiler. In P. Horacek, editor, *16th IFAC World Congress*, Prague, Czech Republic, 2005.

B. Solberg, P. Andersen, and J. Stoustrup. Advanced water level control in a one-pass smoke tube marine boiler. Technical report, Department of Electronic Systems, Aalborg University, Aalborg, Denmark, 2007a.

B. Solberg, C. M. S. Karstensen, and P. Andersen. Control properties of bottom fired marine boilers. *Energy*, 32:508–520, 2007b.

B. Solberg, P. Andersen, J. M. Maciejowski, and J. Stoustrup. Hybrid model predictive control applied to switching control of burner load for a compact marine boiler design. In D. D. Cho, editor, *17th IFAC World Congress*, Seoul, Korea, 2008a.

B. Solberg, P. Andersen, and J. Stoustrup. Optimal switching strategy for systems with discrete inputs using a discontinuous cost functional. Submitted March 2008 for publication in International Journal of Control, 2008b.

F. D. Torrisi and A. Bemporad. Hysdel - a tool for generating computational hybrid models for analysis and synthesis problems. *IEEE Transactions on Control Systems Technology*, 12:235–249, 2004.

X. Xuping and P. Antsaklis. Quadratic optimal control problems for hybrid linear autonomous systems with state jumps. In *Proceedings of the American Control Conference*, volume 4, pages 3393–3398, 2003.

Paper H

Optimal Switching Strategy for Systems with Discrete Inputs using a Discontinuous Cost Functional

Brian Solberg & Palle Andersen & Jakob Stoustrup

The paper has been submitted for publication in International Journal of Control.
March, 2008

The layout has been revised.

Abstract

The aim of this paper is to illustrate optimality problems arising when using receding horizon control laws with a discontinuous cost functional. When the optimal "stationary" condition for such systems is that of a limit cycle, finite horizon control laws fail to provide optimality. This is an inherent property of finite horizon strategies as a consequence of repeated prediction mismatch. The problem is in the choice of cost functional and prediction horizon. Focus is on the problems where changes in discrete inputs are penalised in the cost functional. We provide two solution strategies for handling this problem; one penalising deviations from a predetermined optimal stationary reference trajectory in the cost functional of a receding horizon controller. The other method is a generalisation of hysteresis control taking a geometrical approach looking at hypersurfaces of the state space to determine switches in the input. The methods are illustrated by two simple examples.

1 Introduction

In recent years much research has been directed towards optimal control of hybrid systems. [Bemporad et al., 2002; Egerstedt et al., 2006; Giua et al., 2001a,b; Hedlund and Rantzer, 1999; Riedinger et al., 1999; Seatzu et al., 2006; Verriest et al., 2005; Xuping and Antsaklis, 2003]. One suggested approach, which shall be the focus of this paper, is based on the receding horizon control framework. In this framework a cost functional, penalising future predicted deviations from a setpoint trajectory, is minimised repeatedly, at every controller sample time, subject to various physical and design constraints. Among the class of hybrid systems are those systems which have mixed discrete and continuous decision variables. These systems are common in the industry, e.g. in thermodynamical and chemical processes where a mixture of on/off and continuous valves and heating element might be present. Using receding horizon control for these systems requires definition of a cost functional describing a suitable performance trade-off. Often it is desired to limit the number of switches in the discrete decision variables to limit e.g. actuator wear and save resources. In particular; when a cost in the receding horizon control problem is assigned to changes in the discrete variables, the associated cost functional becomes discontinuous.

This paper describes problems caused exactly by the cost functional becoming discontinuous due to costs assigned to changes in discrete decision variables. The focus is on single input/single output systems. In particular, we assume that the input is piecewise constant and only takes on an upper value and a lower value, $u(t) \in \{\underline{u}, \overline{u}\}$.

We argue that in general; *if the optimal solution is periodic (a limit cycle), optimal performance cannot be achieved using a finite prediction horizon.*

The paper is organised as follows. Firstly, this problem is described in detail and

optimisation-based methods proposed in the literature for control of these systems are reviewed. Secondly, modifications of the existing methods to handle this problem are introduced. The methods are then applied to two simple examples for illustration. Finally, we discuss the extension of the methods for multiple input/multiple output processes with e.g. mixed continuous and discrete decision variables and complexity of the methods.

2 Formulation of the Problem

First, let us make clear what is here meant by optimal performance.

Definition 2.1. *Optimal performance: is the performance achieved using an integral cost functional taking the average over an infinite horizon.*

Physical systems are almost always (excluding batch processes) operating over an "infinite horizon". Hence in optimal control of the nominal system, assuming full information about future disturbances and reference trajectories, the cost functional is naturally looking over an infinite horizon. However, due to computational complexity one most often end up minimising over a finite horizon recursively. In cases where the reference value can be achieved, optimal performance can still be approximated using a semi-infinite horizon strategy, having the appropriate terminal cost and terminal constraint set [Mayne et al., 2000]. The extension of this work to control problems dealing with discontinuous dynamics and cost functional was reported in [Lazar et al., 2006]. The extension does not consider the discrete decision variables. However, these variables are treated in [Cairano et al., 2008] where a hybrid version of the control Lyapunov function notion to ensure convergence and stability is employed. This work considers finite-time convergence of discrete states while asymptotic stability of continuous states are guaranteed. Further the target is considered a point with associated steady state inputs.

In [Bemporad and Morari, 1999; Bemporad et al., 2000], treating control of Mixed Logic Dynamical (MLD) systems, it was further noted that the infinite horizon approach is prohibited due to computational reasons. The cost considered does not include the average over time and it is reasoned that it could happen that no input sequence has a finite cost. This is exactly the case when the state converges to a limit cycle where the cost is well defined only if the average over time is considered.

This means that optimisation-based methods for these systems are limited to the use of finite horizon. However, taking no special precautions, this will not result in optimal performance. The cost functional consists of a continuous and a discontinuous monotonic part. The basic problem is that a finite horizon strategy will constantly keep pushing changes in the discrete variables until at some point it will cost more to let the cost increase over a finite time than to switch the discrete variable which leads to a subsequent decrease in the cost functional and the switch occurs. This leads us to the following proposition.

Proposition 2.2. *Given a control problem described by a cost functional which has discontinuous jumps. If the optimal state trajectory converges to a limit cycle, finite receding horizon control is never optimal.*

Proof. First, assume that we are at the point x_0^* at time $t = t_0$ which is on the optimal trajectory $\varphi^*(\cdot)$. Further, assume that within the finite prediction horizon T_p, the performance associated with the optimal trajectory $J^*(t_0, \tau)$ has a discrete jump at time $T_1 = T_p - \delta\tau$. Then it is possible, for $\delta\tau$ small enough, to find a cost $J^f(t_0, T_p)$ which has no discrete jumps such that $J^f(T_1, T_p) < J^*(T_1, T_p) \Rightarrow J^f(t_0, T_p) \leq J^*(t_0, T_p)$ due to continuity of J^f. □

The concept of the above proposition is illustrated with the following example.

Example 2.3. *Finite horizon control of the double integrator. The system equation is:*

$$\begin{bmatrix} \dot{x}_1 \\ \dot{x}_2 \end{bmatrix} = \begin{bmatrix} 0 & 1 \\ 0 & 0 \end{bmatrix} \begin{bmatrix} x_1 \\ x_2 \end{bmatrix} + \begin{bmatrix} 0 \\ 1 \end{bmatrix} u, \tag{1}$$

where $u \in \{-1, 1\}$. *The optimisation problem is formulated as follows:*

$$J^*(0) = \min_{N_u} \min_{T_1,\ldots,T_{N_u}} \int_0^{T_p} l\left(x(\tau), u(\tau)\right) d\tau \tag{2a}$$

subject to:

$$T_i \leq T_p \qquad i = 1, \ldots, N_u \tag{2b}$$
$$T_i < T_{i+1}, \qquad i = 1, \ldots, N_u \tag{2c}$$
$$u(\tau) = u(0), \qquad T_i \leq \tau < T_{i+1} \text{ for } i = 0, 2, \ldots \tag{2d}$$
$$u(\tau) = -u(0), \qquad T_j \leq \tau < T_{j+1} \text{ for } j = 1, 3, \ldots \tag{2e}$$

where the prediction horizon $T_p = T_p^*$ *is set equal to the period of the optimal limit cycle which we define as the solution to* (19) *defined later.* T_i *is the time of the* i*'th input change, and* $T_0 = 0$. N_u *is the number of free control moves. Further, the cost* l *is chosen as:*

$$\begin{aligned} l(x(\tau), u(\tau)) &= q x_1^2(\tau) + \rho \left| du/d\tau \right| \\ &= q x_1^2(\tau) + \rho \left(\delta\left(\tau - T_1\right) + \delta\left(\tau - T_2\right) + \ldots \right), \end{aligned} \tag{3}$$

for $q, \rho > 0$ *and* $\delta(\cdot)$ *is the Dirac delta function. Unfortunately, the outer minimisation in* (2a) *is over the integer variable* N_u. *For this reason the algorithm is solved iteratively. Figure 1 shows the result of solving the above optimisation problem in a receding horizon manner.*

On the left the value of the cost functional is plotted. The blue line corresponds to the cost associated to the optimal limit cycle. The red line is the achieved cost over a

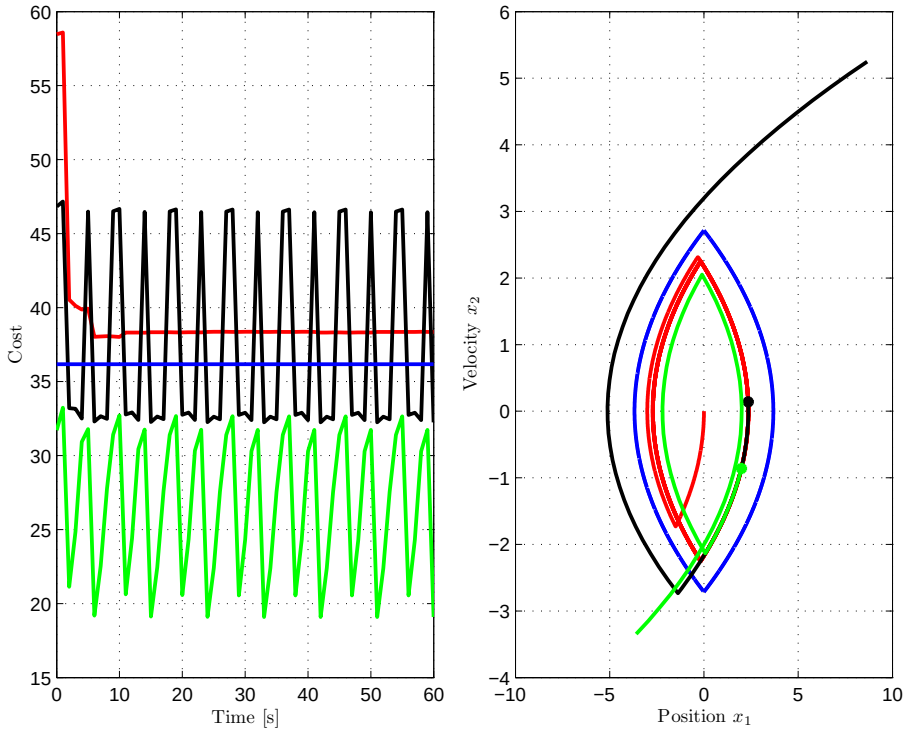

Figure 1: Simulation results for double integrator example. Left: performance plots. Right: state trajectory in the phase plane.

period with the above control law. The green line is the predicted cost divided by the prediction horizon and the black line is the corresponding achieved cost. On the right the trajectory of the closed loop is shown. The red curve is the state evolution, the blue curve is the state trajectory corresponding to the optimal limit cycle. The black and green curves are open loop predictions made by the controller. From these plots it is clear that the state evolution does not converge to the optimal limit cycle and further the prediction mismatches are visible.

The actual performance curve over a period in the above example is evaluated from the following integral:

$$J^a(x,t) = \frac{1}{T_p^a}\Big(\int_t^{T_p^a+t} qx_1^2(\tau)d\tau + 2\rho\Big), \tag{4}$$

where T_p^a, the actual period, is defined as:

$$T_p^a = \min(T_2 + T_0, T_3), \tag{5}$$

with T_0 being the time since the last input change and T_2 and T_3 being the future times at which the second and third input change take place respectively.
A consequence of Proposition 2.2 is that even knowing the optimal period in advance and setting the control horizon equal to a multiple N of the optimal period $T_p = NT_p^*$ and forcing $N_u = 2N$ input changes do not provide a closed loop performance equal to the optimal one. This is exactly the setup in the above example.
Before proceeding we recall that having an infinite horizon, there is a need to take the average over time to ensure a finite cost. The same goes if one uses a variable finite horizon to avoid the discrete variables to switch as fast as constraints allow them to. However, taking the average over time in an infinite horizon strategy makes the optimisation non-unique. In particular, it is possible to find more than one candidate to the optimal input, minimising the cost

$$J(x(0), u(\cdot)) = \frac{1}{T}\int_0^T l(x(\tau), u(\tau))d\tau \tag{6}$$

for $T \to \infty$. However, when the state converges to a limit cycle, this leaves one problem: for any finite T the difference between both the costs and the solution associated with each candidate can oscillate. It can be seen that pointwise convergence is obtained when minimising (6) directly. However, the convergence rate is slow and according to a harmonic series. We return to this issue in Section 3.

2.1 Previous Work

In both [Tsuda et al., 2000] and [Sarabia et al., 2005], methods are proposed for controlling systems of which the state converges to a limit cycle. However, neither of them assign weights to the changes in the discrete decision variables, and in turn both operate with a continuous cost functional. This makes the problem of finding switching times for the discrete variables a matter of scheduling. E.g. finding the appropriate duty cycle. Even though these methods do not directly treat the problem discussed in this paper it is useful to look at the suggested approaches as ideas from these can be applied to the setup treated here.
In [Tsuda et al., 2000], the authors refer to the discrete time MLD systems framework. These systems have the property of allowing a *Cycling Steady State* condition as described in [Tsuda et al., 2000]. To control these systems, the authors suggest finding an entire "steady" state sequence by optimisation and then track this predetermined cycling "steady" state trajectory in a finite horizon control law. However, the optimisation problem has to be solved at every time instance if it is to take changes in disturbances and references into account. The cost functional minimised is penalising large periods to facilitate online computations. Still, however, the calculations are cumbersome, involving mixed integer optimisation, making the method less attractive for online implementation.

The advantages of this method are that it is discrete and hence already handles the sample problem present in continuous time algorithms. Further, as it is discrete, it actually returns the optimal solution of the sampled system instead of an approximation of this when rounding continuous time variables to sampled ones.
In [Sarabia et al., 2005], another approach is taken. A variable horizon model predictive control algorithm for general nonlinear systems with mixed discrete and continuous inputs is introduced. The assumption used is that a limit cycle is reached at the end of the prediction horizon. Further, the discrete nature of the problem is a matter of scheduling batch units.
The internal model is integrated until a full number of periods of the slowest underlying unit have been performed. The optimisation is over switching times for both continuous and discrete variables as well as amplitudes of continuous variables.
The resulting optimisation problem is unfortunately nonlinear and non-convex, however, integer variables are avoided if the method is restricted to a continuous time model in which the switching times are continuous variables. The method does not take the average over time in the performance index which is over a variable horizon. This should lead to the system switching the input variables as fast as the constraints allow. The reason is that the shorter the horizon the lower the cost. This is due to the monotonic increasing nature of the cost function with horizon. For this reason the approach is not directly applicable to our setup where costs are assigned to the input changes. A simple example shows that an algorithm only predicting one period ahead (variable horizon) will never converge to the optimum and also suffers from prediction mismatch.
In [Larsen et al., 2005], the authors use the MLD modelling framework for the control of refrigeration systems and propose a finite horizon cost functional which has a penalty on compressor switches. Hence the cost functional suggested is discontinuous. This method suffers exactly from the lag of optimality explained in Proposition 2.2.
Many authors have focused on switched linear and affine autonomous systems, e.g. [Giua et al., 2001b; Seatzu et al., 2006; Xuping and Antsaklis, 2003]. In particular, it is noticed that when the switching sequence is predetermined, the optimal control reduces to a state feedback. However, the focus is restricted to a finite number of switches. In [Giua et al., 2001a], the stability of these systems, when the number of switches goes to infinity, is studied. However, this is for stable dynamics and no switching cost.
In [Hedlund and Rantzer, 1999], an optimal control example of alternate heating of two furnaces is treated. This control results in a limit cycle behaviour. The cost functional considers only a finite number of switches and to get a bounded cost, the time weight e^{-t} is introduced.
In the next section we propose methods for handling the problems arising using finite horizon.

3 Methods

The methods described in this paper are based on one key assumption; *There exists an optimal infinite horizon periodic solution (limit cycle)*. This is the case for instance when the system cannot be brought to rest at a constant reference value. We focus on linear time invariant continuous time processes of the form:

$$\dot{x}(t) = Ax(t) + Bu(t) \tag{7a}$$
$$y(t) = Cx(t) \tag{7b}$$

where $x \in \mathbb{R}^n$, $y \in \mathbb{R}$ and $u(t) : [0, \infty) \to \{\underline{u}, \overline{u}\}$. The restriction to strictly proper systems is only made to simplify notation. We assume for the sake of notational simplicity that the input is symmetric, $u(t) \in \{-1, 1\}$, and define $\Delta = u(0)$, such that:

$$u(t) = \begin{cases} \Delta \text{ for } 0 \leq t \leq T_1 \\ -\Delta \text{ for } T_1 < t \leq T_2 \\ \Delta \text{ for } T_2 < t \leq T_3 \text{ etc.} \end{cases} \tag{8}$$

The general cost functional treated is:

$$J(x(0), u(\cdot)) = \lim_{T \to \infty} \frac{1}{T} \int_0^T l(e(\tau), u(\tau)) d\tau \tag{9}$$

where $e(\tau) = r(\tau) - y(\tau)$ and the piecewise continuous $l(e(\tau), u(\tau)) : \mathbb{R} \times \{\underline{u}, \overline{u}\} \to \mathbb{R}$ includes a quadratic penalty on the tracking error and a cost for switching the input. Hence:

$$l(e(\tau), u(\tau)) = qe^2(\tau) + \rho \left(\delta \left(\tau - T_1 \right) + \delta \left(\tau - T_2 \right) + \dots \right), \tag{10}$$

where $q > 0$ is the cost associated with output deviations from the reference, and $\rho > 0$ is the cost assigned to the changes in the input signal. $\delta(\cdot)$ is the Dirac delta function, and T_i is the time of the i'th input change.

There exists systems where the optimal strategy has a finite number of switches. For such systems the cost assigned to a constant offset is less than that of following a limit cycle. In case of stable systems where no integral cost is assigned to the tracking error, the state converges asymptotically to the equilibrium $x_{ss} = -A^{-1}Bu_{ss}$ and the optimal cost is:

$$J_{ss}^* = q \left(r - Cx_{ss} \right)^2, \; x(0) \in x_{ss} \tag{11}$$

In this case the solution is simple and can, when treating autonomous stable, systems be found as a state feedback [Giua et al., 2001b].

However, there also exists systems where the optimal strategy contains infinitely many switches. Minimising (9) in an ordinary online receding horizon algorithm for these systems results in a cost converging to:

$$\inf_{u(\cdot)} J(x(0), u(\cdot)) = J_{lc}^* \tag{12}$$

where J_{lc}^* is the cost of staying on the optimal limit cycle $\mathcal{S}^*$ with period T_p^*.

$$J_{lc}^* = \frac{1}{T_p^*} \int_0^{T_p^*} l(e(\tau), u^*(\tau)) d\tau, \; x(0) = x(T_p^*) \in \mathcal{S}^* \tag{13}$$

To find the optimal strategy for these systems we pose the following optimisation problem:

Problem 3.1. *Given the cost:*

$$J(T) = \frac{1}{T} \int_0^T l(e(\tau), u(\tau)) d\tau, \tag{14}$$

find the argument that minimises this cost:

$$\hat{u}(\cdot, T) = \arg \inf_{u(\cdot)} J(T) \tag{15}$$

From this optimisation problem it is possible to define an optimal input minimising (9), which is unique (a.e.).

Theorem 3.2. *The optimal input, $u^*(t)$, defined by*

$$u^*(t) = \lim_{T \to \infty} \hat{u}(t, T), \; \forall \, t \geq 0 \tag{16}$$

is well defined, minimises (9) *and under this input the cost converges to that of the optimal limit cycle, J_{lc}^*.*

Proof. The fact that the input $u^*(t)$ minimises (9) and makes the cost converge to that of the limit cycle, J_{lc}^*, follows by construction. We then need to prove well definedness. Evaluation of (15) as a function of T will cause the time of the first input switch $T_1(T)$ to have the behaviour as in Figure 2 left. In the figure the red open circles illustrates $T_1(T)$ just after a new input switch enters the horizon. The red stars illustrate $T_1(T)$ just before a new switch is introduced. The blue line represents the evolution of $T_1(T)$ between introduction of extra switches. Finally, the green lines are included to visualise convergence.

Now when the first switch converges, we note that under mild conditions the distribution of the remaining switches will occur according to Figure 2 right. The figure shows the integrated cost before (blue) and after (green) a switch occurs. These switches are equally spaced over the remaining time frame, $T_r = T - T_1$ for symmetry reasons.

Now, if the remaining switches are equally spaced, we can look at the time, T_{n+1}^-, just before one particular switching time which relative to T_1 is $T_r = T_{n+1}^- - T_1$. Note that the time between remaining switches will be T_r/n. We then investigate the convergence of the switching times for the number of switches $n \to \infty$. First define

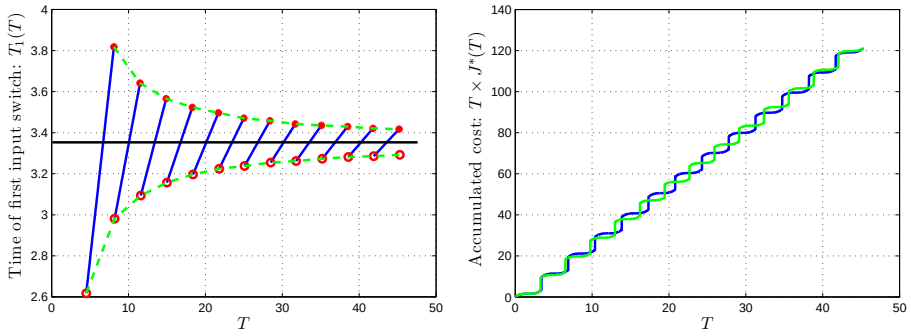

Figure 2: Solving (15) for a particular system. The left plot shows convergence of $T_1(T)$, the red open circles illustrate $T_1(T)$ just after a new input switch enters the horizon. The red stars illustrate $T_1(T)$ just before a new switch is introduced. The blue line represents the evolution of $T_1(T)$ between introduction of extra switches. Finally, the green lines are included to visualise convergence. The right plot shows the integrated cost before (blue) and after (green) a switch occurs.

$0 < \delta_n \leq T_{n+1} - T_n$. Then the difference in time between switches for a case with n and a case with $n+1$ switches will be:

$$\delta T_n = \frac{T_r}{n} - \frac{T_r + \delta_n}{n+1} = \frac{T_r - n\delta_n}{n(n+1)} \tag{17}$$

and

$$\delta T_n = \frac{T_r}{n(n+1)} - \frac{\delta_n}{n+1} \to 0 \text{ for } n \to \infty \tag{18}$$

Hence $f(T) = \hat{u}(t, T)$ has a well defined limit for $T \to \infty$.

□

Note that the convergence is very slow and further there will be a constant error in the last switch $e_{T_\infty} = \lim_{n\to\infty} n\delta T_n = \delta_n$. These aspects can, however, be fixed by sampling the horizon T as $T_k = T_0 + kT_p^*$ (T_p^* the period of the optimal limit cycle). Then there exists $k = N$ independent of T_0 for which the solution in future time will be arbitrarily close to a periodic solution. When this is so, a switch will always occur just after the sample at time T_k^+, meaning that convergence will be fast.
Note that having the optimal solution at each sample time still does not take care of prediction mismatches as varying T_0 results in different input optimal sequences. However, from the above we more or less get the following lemma for free.

Lemma 3.3. *Choosing a fixed time sequence T_k independent of the controller update time, the receding horizon implementation is consistent without prediction mismatch.*

Proof. This follows from the optimality principle. Given the optimal input function, $u^*(\cdot)$ at time t, using the sampling $T_k \in \{T_1, T_2, \dots\}$, then at time $t+\delta$ the same input

function is still optimal, corresponding to the sampling $T_k \in \{T_1 - \delta, T_2 - \delta, \dots\}$. This corresponds to dividing the integral (14) into a part representing the past and another representing the future with the future part being a component of a previously optimal solution. □

Such a sampling always exists. Therefore, in practice the sampling can be defined by first finding this limit cycle and then choosing any T_0 so $T_k = T_0 + nT_p^*$ where T_p^* is the period of the limit cycle, please refer to Section 4 for examples of this. To solve the optimisation problem, one needs to iterate k until some $T_k \in \{T_1, T_2, \dots\} \geq T_N$ to which the state has converged within a user-defined distance to the limit cycle.
This optimisation problem is NP-hard. Even if we set an upper bound on T_N, the number of input switches is still a free variable. In the remainder of this section we present two methods for approximating the above optimisation problem. The idea behind these approximations is that among the solutions minimising (9) are those reaching the limit cycle in finite time or with asymptotic convergence. Therefore, it seems natural to focus on how to approach the limit cycle as this initial behaviour will be important in practical applications. But first we shall find the optimal trajectory.

3.1 Finding the Optimal Reference Trajectory

The system under consideration is assumed to be controllable and further the weights in the cost functional are chosen such that a limit cycle does exist. To find the optimal trajectory, we solve the following optimisation problem which is a continuous time variant of the one in [Tsuda et al., 2000] with a different cost functional.

$$J_{lc}^* = \min_{T_p, x(0), u(\cdot)} \frac{1}{T_p} \int_0^{T_p} l(x(\tau), u(\tau)) d\tau \tag{19a}$$

subj. to:

$$x(T_p) = x(0), u(0) = +1 \tag{19b}$$

$$x(\tau) \neq x(0) \forall \tau < T_p \tag{19c}$$

where two changes in the input are allowed. The last change is constrained to occur at time $\tau = T_p$ meaning that the optimisation can be performed by deciding only when the first change should occur. Note that in this case the constraint (19c) is no special restriction on $x(0)$ for first order systems. The cost functional can be rewritten as:

$$J_{lc}(x(0), u(\cdot)) = \frac{1}{T_p} \left(\int_0^{D_C T_p} l(x(\tau), u(\tau)) d\tau + \int_{D_c T_p}^{T_p} l(x(\tau), u(\tau)) d\tau \right) \tag{20}$$

where D_c is the duty cycle expressing the portion of the period with the input at its high level. The solution of (7a) for constant $u(t) = \Delta$ is given by:

$$x(t) = e^{At} x(0) + \int_0^t e^{A(t-\tau)} d\tau B \Delta \tag{21}$$

If the model is of a high order, the computational complexity can be reduced by approximating the solution by a Taylor series expansion taking as many derivative terms as required for appropriate accuracy see e.g. [Maciejowski, 2001].
The optimal period T_p^*, duty cycle, D_c^* and initial condition $x^*(0)$ define the reference trajectory together with the system (7). The reference trajectory is made up of two curves in $\mathbb{R}^n$ corresponding to each of the input levels and is piecewise continuous with well defined switching points at the intersections. We define two new points $x^+ = x^*(0)$ and $x^- = x^*(D_c T_p) = -x^*(0)$ to be the points on the limit cycle where a switch in input from negative to positive and positive to negative occurs respectively.
It is possible for stable systems to use pure feedforward control to approach the limit cycle by just changing the input level according to the optimal period and duty cycle. However, this method is obviously not very robust. Instead in the following, two different feedback methods are discussed.

3.2 Method A: Reference Tracking

This approach is based on a more or less traditional model predictive control framework. For an overview of conventional MPC, reference is made to [Maciejowski, 2001; Rossiter, 2003]. The method is based on the following finite horizon optimisation problem:

$$J^*(x(0)) = \min_{u(\cdot)} \int_0^{T_p} |Q^{\frac{1}{2}} e(\tau)|_2^2 d\tau \tag{22}$$

where $e(\tau) = x_{lc}(\tau) - x(\tau)$ and $T_p = T_p^*$ the period of the optimal limit cycle to track. Knowing the optimal limit cycle, it can be identified as produced from an autonomous piecewise affine system. In this way, given initial conditions $x_{lc}(0)$ and $x(0)$ the current state, a prediction of the tracking error can be generated from the model:

$$\begin{bmatrix} \dot{x}_{lc}(t) \\ \dot{x}(t) \end{bmatrix} = \begin{bmatrix} A & 0 \\ 0 & A \end{bmatrix} \begin{bmatrix} x_{lc}(t) \\ x(t) \end{bmatrix} + \begin{bmatrix} 0 \\ B \end{bmatrix} u(t) + \begin{bmatrix} B \\ 0 \end{bmatrix} \Delta \tag{23a}$$

$$e(t) = \begin{bmatrix} I & -I \end{bmatrix} \begin{bmatrix} x_{lc}(t) \\ x(t) \end{bmatrix} \tag{23b}$$

$$\Delta = \begin{cases} 1 \text{ for } x_{lc}(t) \in \mathcal{S}^+ \\ -1 \text{ for } x_{lc}(t) \in \mathcal{S}^- \end{cases} \tag{23c}$$

where $\mathcal{S}^+$ and $\mathcal{S}^-$ correspond to components of the limit cycle with positive input and negative input respectively. At each controller update the initial condition of the reference model $x_{lc}(0)$ specifies where to start penalising deviations from. Define the projection map $Pr(x, \dot{x}) : \mathbb{R}^n \times \mathbb{R}^n \to \mathcal{S}$ taking a state in the phase plane and project it onto the optimal limit cycle $\mathcal{S}$. Now take the initial point on the limit cycle as $x_{lc}(0) = Pr(x(0), \dot{x}(0))$ given a suitable projection map. Also note that it is possible to define the unique map between a state belonging to the limit cycle and time as: $(x^*, \dot{x}^*) \mapsto c(x^*, \dot{x}^*) = t,\ t \in [0, T_p]$.

There are many ways to define the projection map. One particularly simple way, which gives reasonable results in the examples treated in this paper, is simply to start at some arbitrary state $x_{lc}(0)$ and then simply use $x_{lc}(s), s = t \mod T_p$ as initial conditions. This implies that the reference trajectory is started at some time $t = 0$ and then the control problem consists of catching up with it.
Examples are presented later in Section 4.

3.3 Method B: A Geometrical Approach to State Feedback

The second approach we apply is a variant of time-optimal control. The performance in (9) is penalising the number of switches and has an increasing cost over time. Time-optimal control seems like a good choice for driving the state to the target set as it represents the fastest way to reach the limit cycle using the fewest possible input changes. Also it is expected that the states, using the original optimisation problem, will get close to the limit cycle in short time and when close, the limit cycle can be reached without a high cost. Furthermore, for linear systems with eigenvalues having negative and zero real parts, the time-optimal controller is known to be an extremal controller (bang-bang) [Athans and Falb, 1966] and hence applies to the subclass of systems treated here. A significant amount of research has been devoted to time-optimal control, especially in the sixties see e.g. [Athans and Falb, 1966; Lee and Markus, 1967] for the time domain approach or [Lim, 1969] for a frequency domain approach or [Sontag, 1998] for a more recent publication focusing on convex problems.
Before proceeding to the controller definition it is important to recall the geometric representation of solution curves and the optimal limit cycle in the phase plane.

Geometric representation of optimal limit cycles

Focus is mainly on systems where the eigenvectors have geometric multiplicity equal to 1. The only exception is when the corresponding eigenvalue is equal to 0. However, this case is treated separately below. The extension to general eigenvalues is possible, but the calculations involved are tedious and it may not be possible to find an analytic expression for the corresponding limit cycle for eigenvalues with multiplicity larger than 4. The system is first put into the Jordan canonical form [Horn and Johnson, 1999]. The transformation $x = Tz$ takes the state (7a) to

$$\dot{z}(t) = \tilde{A}z(t) + \tilde{B}u(t) \tag{24}$$

where $\tilde{B} = T^{-1}B$ and $\tilde{A} = T^{-1}AT$ having the Jordan block structure:

$$\tilde{A} = \begin{bmatrix} R_{n_1}(\lambda_1) & & & & \\ & \ddots & & 0 & \\ & & R_{n_p}(\lambda_p) & & \\ & & & C_{n_q}(\lambda_q) & \\ & 0 & & & \ddots \\ & & & & C_{n_r}(\lambda_r) \end{bmatrix} \tag{25}$$

where $R_{n_i}(\lambda) = \begin{bmatrix} \lambda & & \\ & \ddots & \\ & & \lambda \end{bmatrix}$ is an $n_i \times n_i$ matrix and $C_{n_j}(\lambda) = \begin{bmatrix} C(\lambda) & & \\ & \ddots & \\ & & C(\lambda) \end{bmatrix}$ is a $2n_j \times 2n_j$ matrix with elements $C(\lambda) = \begin{bmatrix} \alpha+i\beta & 0 \\ 0 & \alpha-i\beta \end{bmatrix}$. Furthermore, the eigenvalues are organised such that $\lambda_1 > \cdots > \lambda_p$ and $\alpha_q > \cdots > \alpha_r$.
The solution to (24) for constant $u(t) = \Delta$ is given as:

$$z(t) = e^{\tilde{A}t}\left(z(0) + \int_0^t e^{-\tilde{A}\tau} d\tau \tilde{B}\Delta\right) \tag{26}$$

where $z(0) \in \mathcal{S}$, which can be solved to get:

$$z(t) = e^{\tilde{A}t}(z(0) + \tilde{A}^{-1}\tilde{B}\Delta) - \tilde{A}^{-1}\tilde{B}\Delta \tag{27}$$

Now eliminating time in (27) is done differently depending on the type of eigenvalues. Below the strategy for the three types of systems is shown, assuming $n = 2$ for simplicity:

Real negative eigenvalues Equation (27) can be written as:

$$z(t) = M\begin{bmatrix} e^{\lambda_1 t} \\ e^{\lambda_2 t} \end{bmatrix} - g \tag{28}$$

where $g = \tilde{A}^{-1}\tilde{B}\Delta = -z(\infty)$ and $M = \mathrm{diag}(z(0) + g)$. Assuming that $z(0) \in \mathcal{S}$ is chosen such that $\det(M) \neq 0$ then

$$v(t) = M^{-1}(z(t) + g) = \begin{bmatrix} e^{\lambda_1 t} \\ e^{\lambda_2 t} \end{bmatrix}. \tag{29}$$

Setting $e^{\lambda_2 t} = \left(e^{\lambda_1 t}\right)^{\frac{\lambda_2}{\lambda_1}}$ and $v(t) = \left[v_1(t), v_2(t)\right]^T$ results in:

$$v_2 = v_1^{\frac{\lambda_2}{\lambda_1}} \tag{30}$$

which gives the following representation of the part of the limit cycle corresponding to Δ:

$$\mathcal{S}^{\Delta} = \{(v_1, v_2) | f(v) = v_2 - v_1^{\frac{\lambda_2}{\lambda_1}} = 0\} \tag{31}$$

The full limit cycle is the union of everything between the intersection of the two curves corresponding to Δ and $-\Delta$ respectively.

Complex eigenvalues In this case it is not possible to eliminate time unless we use complex calculation. This was the reason for using the complex Jordan form in (25). The solution to the system is given by:

$$z(t) = M \begin{bmatrix} e^{(\alpha+i\beta)t} \\ e^{(\alpha-i\beta)t} \end{bmatrix} - g \tag{32}$$

which again can be put into the form:

$$v(t) = M^{-1}\left(z(t) + g\right) = \begin{bmatrix} e^{(\alpha+i\beta)t} \\ e^{(\alpha-i\beta)t} \end{bmatrix} \tag{33}$$

with $v(t) = \left[v_1(t), v_2(t)\right]^T$. Then use the following relationships:

$$v_1 v_2 = e^{(\alpha+i\beta)t} e^{(\alpha-i\beta)t} = e^{2\alpha t} = \left(e^{2t}\right)^{\alpha} \tag{34}$$

$$\frac{v_1}{v_2} = e^{(\alpha+i\beta)t} e^{-(\alpha-i\beta)t} = e^{2i\beta t} = \left(e^{2t}\right)^{i\beta} = \left[\left(e^{2t}\right)^{\alpha}\right]^{\frac{i\beta}{\alpha}} \tag{35}$$

to get a representation of each part of the limit cycle:

$$\mathcal{S}^{\Delta} = \{(v_1, v_2) | f(v) = \frac{v_1}{v_2} - (v_1 v_2)^{\frac{i\beta}{\alpha}} = 0\} \tag{36}$$

Double eigenvalue in zero The Jordan form is given as:

$$\dot{z}(t) = \begin{bmatrix} 0 & 1 \\ 0 & 0 \end{bmatrix} z(t) + \begin{bmatrix} \tilde{b}_1 \\ \tilde{b}_2 \end{bmatrix} u(t) \tag{37}$$

taking $z(t) = [z_1(t), z_2(t)]$ the solution is:

$$\begin{bmatrix} z_1(t) \\ z_2(t) \end{bmatrix} = \begin{bmatrix} \frac{1}{2}\tilde{b}_2\Delta & z_2(0) + \tilde{b}_1\Delta & z_1(0) \\ 0 & \tilde{b}_2\Delta & z_2(0) \end{bmatrix} \begin{bmatrix} t^2 \\ t \\ 1 \end{bmatrix} \tag{38}$$

hence with $t = (z_2(t) - z_2(0))/(\tilde{b}_2\Delta)$,

$$z_1(t) = \frac{1}{2\tilde{b}_2\Delta}\left(z_2(t)^2 - z_2(0)^2\right) + \frac{\tilde{b}_1}{\tilde{b}_2}\left(z_2(t) - z_2(0)\right) + z_1(0). \tag{39}$$

This gives the following representation of each part of the limit cycle:

$$\begin{aligned} \mathcal{S}^{\Delta} = \{(x, y) | f(z_1, z_2) = & \frac{1}{2\tilde{b}_2\Delta}\left(z_2(t)^2 - z_2(0)^2\right) + \\ & + \frac{\tilde{b}_1}{\tilde{b}_2}\left(z_2(t) - z_2(0)\right) + z_1(0) - z_1(t) = 0\} \end{aligned} \tag{40}$$

In higher dimensions, $n > 2$, the curves of the limit cycle can be expressed as the intersection of $n - 1$ hypersurfaces. The combination of the three representations is possible even though in case of the complex eigenvalues it is not obvious how and if it is useful.
The limit cycle is a piecewise smooth 1-dimensional embedded manifold being the intersection of $n - 1$ smooth $n - 1$-dimensional embedded manifolds, hypersurfaces.

Controller

We suggest a control strategy that is based on the geometrical representation of the optimal limit cycle. The approach resembles time-optimal control in which the boundary $\partial\mathcal{S}$ of the optimal limit cycle, together with hypersurfaces corresponding to each input level, divides the space into two: one for positive and one for negative input. Optimally, this would be a matter of steering the state in minimum time to the set defined by the limit cycle when outside the limit cycle. However, it is not clear how such a time-optimal controller should be constructed, so instead we could steer the state to one of the points, x^+, x^-, on the limit cycle where a switch in input occurs. This will automatically mean that the total limit cycle would be part of the solution. However, when steering for non-equilibrium points, the switching surfaces are asymmetric, [Athans and Falb, 1966], which complicates matters. Instead, only the switching surface corresponding to the opposite input of the one leading to the switching point along the limit cycle is calculated. This is done for both switching points x^+, x^- to get two hypersurfaces, the union of which divides the state space into three regions: one where the positive input should be applied, and one where the negative input should be applied. Finally there is a region representing the "inside" of the limit cycle where no input is defined so it is left unchanged.
The steps in designing the controller are:

1 Find the optimal limit cycle by solving (19).

2 Calculate switching surfaces and their domains, starting from the points x^+ and x^- respectively, using techniques from time-optimal control.

3 The control law aims to evaluate the functions representing the switching surfaces and to check their sign. Based on this information the control input can be set to either $u(t) = -1$, $u(t) = 1$.

In the next section we illustrate the two methods proposed with a couple of simple examples.

4 Examples

Example 4.1. *Triple integrator: the differential equation is simply* $\dddot{x}_1(t) = u(t)$*, which for constant* $u(t) = \Delta$ *has the solution:*

$$\begin{bmatrix} x_1 \\ x_2 \\ x_3 \end{bmatrix} = \begin{bmatrix} \frac{1}{6}\Delta & \frac{1}{2}x_3(0) & x_2(0) & x_1(0) \\ 0 & \frac{1}{2}\Delta & x_3(0) & x_2(0) \\ 0 & 0 & \Delta & x_3(0) \end{bmatrix} \begin{bmatrix} t^3 \\ t^2 \\ t \end{bmatrix} \tag{41}$$

The input is limited to $u(t) \in \{-1, 1\}$ *and* $y(t) = x_1(t)$ *and* $r(t) = 0$*. The design parameters are:* $q = 1$ *and* $\rho = 50\pi$*. Now find the optimal limit cycle by solving* (19) *to get switching points* x^+*,* x^- *and the optimal period* T_p^**. The limit cycle is symmetric and hence the duty cycle is* $D_c = 1/2$*. Next we seek the switching surfaces. First, find* Γ^-*, the curve along which the state approaches* x^- *with negative input* $u(t) = -1$ *by setting* $t = -\tau$ *(*$\tau > 0$*) in* (41) *and eliminating* τ*. This curve is given by the intersection of the two hypersurfaces:*

$$f_1^-(x) = \frac{1}{6}(x_{32} - x_3^0)^3 + \frac{1}{2}x_3^0(x_{32} - x_3^0)^2 - x_2^0(x_{32} - x_3^0) + x_1^0 - x_{12} = 0 \tag{42}$$

$$f_2^-(x) = -\frac{1}{2}(x_{32} - x_3^0)^2 - x_3^0(x_{32} - x_3^0) + x_2^0 - x_{22} = 0 \tag{43}$$

over the domain $\{x | x_3^0 < x_3\}$*. These curves are equivalent to those discussed in Section 3.3 for second order systems. The next step is to find the surface,* W^+*, on which a positive input can bring the state to the curve* Γ^-*. To do this, set* $t = -s$ *(*$s \geq 0$*) in* (41) *and set the initial condition to the points on* Γ^- *defined by* $f_1^- = 0, f_2^- = 0$*. By eliminating* s *and points on* Γ^- *from the equation, the following expression for the surface can be derived:*

$$g^+(x) = \frac{1}{6}(x_{32} - x_3)^3 + \frac{1}{2}x_{32}(x_{32} - x_3)^2 + x_{22}(x_{32} - x_3) + x_{12} - x_1 = 0 \tag{44}$$

with x_{12}, x_{22}, x_{32} *being points on* Γ^- *found from* (42), (43) *and:*

$$x_{32} = \left(\frac{1}{2}(x_3^2 + x_3^{0^2}) + x_2^0 - x_2\right)^{1/2} \tag{45}$$

The domain $X_{W^+} \subset \mathbb{R}^3$ *on which* W^+ *is defined is:*

$$X_{W^+} = \left\{ x \middle| x_2 < \begin{cases} \frac{1}{2}(x_3^2 - x_3^{0^2}) + x_2^0 \text{ for } x_3 \leq 0 \\ -\frac{1}{2}|x_3^2 - x_3^{0^2}| + x_2^0 \text{ for } x_3 > 0 \end{cases} \right\} \tag{46}$$

The curve and surface Γ^+ *and* W^- *can be found in a similar manner starting from the point* x^+*. Now define a new function describing the surface dividing the state space*

$M = W^+ \cup W^-$. *This function is given as:*

$$g(x) = \begin{cases} g^+(x) \text{ for } x(t) \in X_{W^+} \\ g^-(x) \text{ for } x(t) \in X_{W^-} \end{cases} \tag{47}$$

Finally, define the space above the surface M *as* M^- *and the space below as* M^+ *being regions of the state space where a negative input or a positive input can take the state to one of the switching surfaces.*
Now a feedback law can be designed to steer the state to the limit cycle as:

$$u(t) = \begin{cases} 1 \text{ for } x(t) \in M^+ \\ -1 \text{ for } x(t) \in M^- \\ 1 \text{ for } x(t) \in W^+ \setminus \Gamma^- \\ -1 \text{ for } x(t) \in W^- \setminus \Gamma^+ \\ 1 \text{ for } x(t) \in \Gamma^+ \\ -1 \text{ for } x(t) \in \Gamma^- \\ u(t) \text{ for } x(t) \in \mathbb{R}^3 \setminus (X_{W^+} \cup X_{W^-}) \end{cases} \tag{48}$$

The switching surfaces for this control law are shown in Figure 3. The optimal limit cycle is also plotted as a blue curve.
The control law (48) *and the one using Method A have been simulated, and the results are shown in Figure 4.*
The top plot shows the value of the cost functional. The blue line corresponds to the cost associated with the optimal limit cycle. The red line is the cost achieved by applying Method A, and the green line is the cost achieved by applying Method B. The performance is evaluated using the performance in (4)*. The bottom plots show the trajectory of the closed loop in the phase plane projected onto the* x_1, x_3 *plane left and onto the* x_2, x_3 *plane right. The red curve is the state evolution using Method A, the green curve is the state evolution using Method B, and the blue curve is the state trajectory corresponding to the optimal limit cycle.*
As can be seen, both methods result in the state converging to the limit cycle.

Example 4.2. *Complex stable pole pair: The system is described by the differential equation:*

$$\begin{bmatrix} \dot{x}_1 \\ \dot{x}_2 \end{bmatrix} = \begin{bmatrix} \alpha & \beta \\ -\beta & \alpha \end{bmatrix} \begin{bmatrix} x_1 \\ x_2 \end{bmatrix} + \begin{bmatrix} 0 \\ 1 \end{bmatrix} u \tag{49}$$

where again $u(t) \in \{-1, 1\}$, $\alpha = -0.2$, $\beta = 0.1$ *and* $y(t) = x_1(t)$ *and* $r(t) = 0$*. The limit cycle is found from* (19) *to get switching points* x^+, x^-, *with* $q = 1$ *and* $\rho = \pi/4$*. In this example we would again like to use the geometric representation of the limit cycle, see* (36)*. However, as the equation representing the curve on the optimal cycle produces a complex number, it has not been found obvious how to define an analogue*

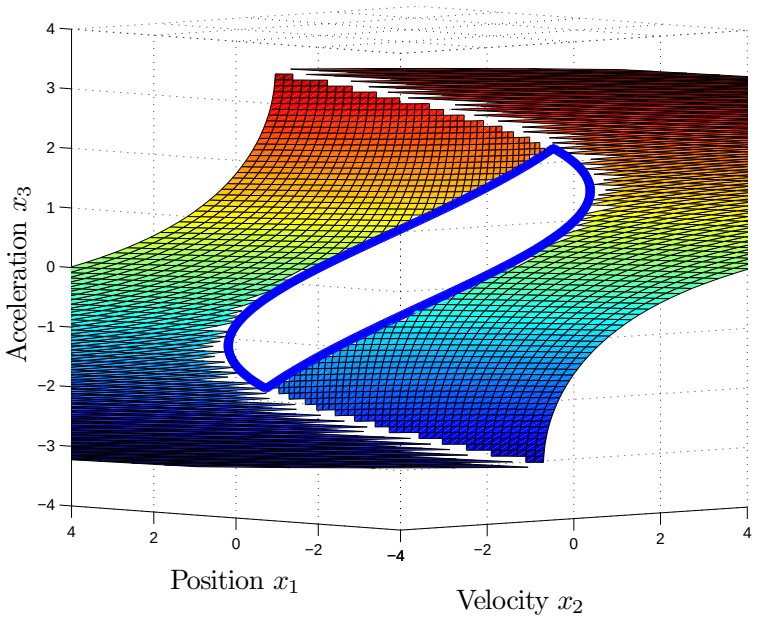

Figure 3: Switching surfaces and optimal limit cycle for the triple integrator example.

law to the one in the previous example. Furthermore, time-optimal control of systems with complex pole pairs is known to generate switching surfaces which cannot be described analytically. Further, in time-optimal control one cannot hold the same input level for more than π/β seconds which will result in a large number of switches when far from the limit cycle. However, this method does not take into account that a cost is assigned to switches. For these reasons, we propose a switching curve for keeping the state trajectory on the limit cycle which is not directly related to time-optimal control. The proposed switching curve is shown in Figure 5 as the black line. It is composed of the three line segments Γ^+, Γ^- and Γ^0. Γ^+, Γ^- are defined as the natural extension of the curves representing the limit cycle along the line described by the vector field evaluated in the points x^+, x^-.

$$\Gamma^-(x) = \{(x_1, x_2) | (Ax^- - B)^T (x - x^-) = 0, x_2 < x_2^-\} \tag{50}$$

$$\Gamma^+(x) = \{(x_1, x_2) | (Ax^+ + B)^T (x - x^+) = 0, x_2 > x_2^+\} \tag{51}$$

Γ^0 is simply the line connecting the point x^+, x^- and therefore the sets Γ^+, Γ^-. Hence the switching curve becomes $\Gamma = \Gamma^+ \cup \Gamma^0 \cup \Gamma^-$. This curve divides the state space into two regions: one M^+ in which the input is positive, and one M^- in which the input is

negative. The control law then becomes:

$$u(t) = \begin{cases} 1 \text{ for } x(t) \in M^+ \setminus \Gamma \\ -1 \text{ for } x(t) \in M^- \end{cases} \tag{52}$$

The control law (52) *together with Method A have been simulated and the results are shown in Figure 5.*
On the left the value of the cost functional is plotted. The blue line corresponds to the cost associated with the optimal limit cycle. The red line is the cost achieved by applying Method A, and the green line is the cost achieved by applying Method B. The performance is evaluated using (4)*. On the right the trajectory of the closed loop is shown. The red curve is the state evolution using Method A, the green curve is the state evolution using Method B, and the blue curve is the state trajectory corresponding to the optimal limit cycle.*
As can be seen, both methods result in the state converging to the limit cycle.
In fact, as the system is stable, many other lines could have been used as switching curves. The curves chosen are those which are tangents to the ones defined from time-optimal control to the two points defining the limit cycle.

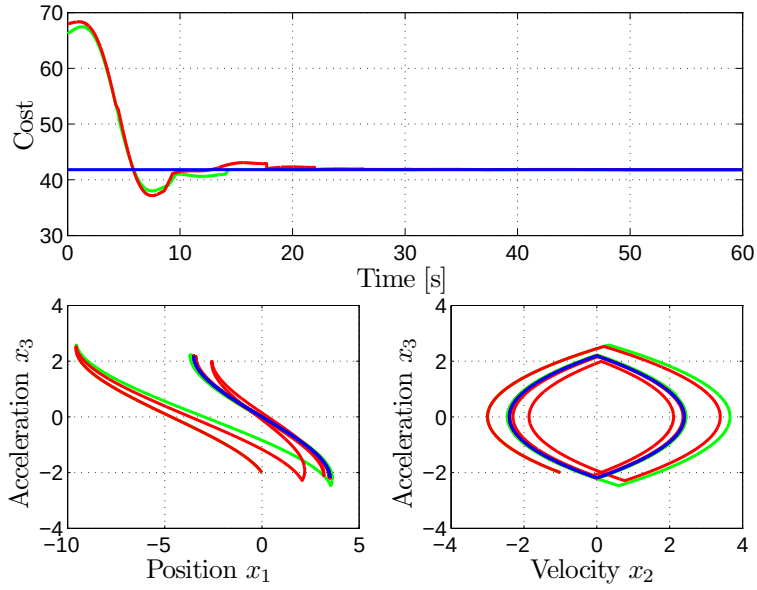

Figure 4: Simulation results for triple integrator example. Top: performance plots. Bottom: state trajectory in the phase plane.

5 Discussion

In the examples above only systems of up to third order were treated. The methods apply to systems of higher order, although it is obvious that the complexity of both Method A and Method B increases when increasing the state dimension. However, the authors also think that these small examples are important in their own right, as many processes in the industry often can be approximated by first, second or third order systems.

Method A suffers from the fact that it requires a certain time synchronisation. This is an extra constraint that results in an unnecessary cost. This is especially a problem when disturbances are acting on the system. However, by defining a more elaborate projection map $Pr(x, \dot{x})$, these shortcomings can be avoided.

The time-optimal strategy, Method B, can be seen as a way of finding hysteresis bounds dependent on the state and not only the controlled output.

Stability and robustness issues for both the proposed methods have not yet been rigorously analysed. Especially Method B will be sensitive to model uncertainties and disturbances leading to a scattering behaviour around the limit cycle. However, as the number of input switches is costly, this cannot be tolerated. In such cases one could define a region around the limit cycle where the input is only changed upon entry and at the switching point defining the limit cycle.

Regarding implementation, Method A is fairly straight forward, whereas Method B will to some degree depend on the chosen sample time in order to detect crossing of switching surfaces in time. To overcome this problem, one could run the algorithm at a low sample rate and then project the current state one sample ahead to see if the state

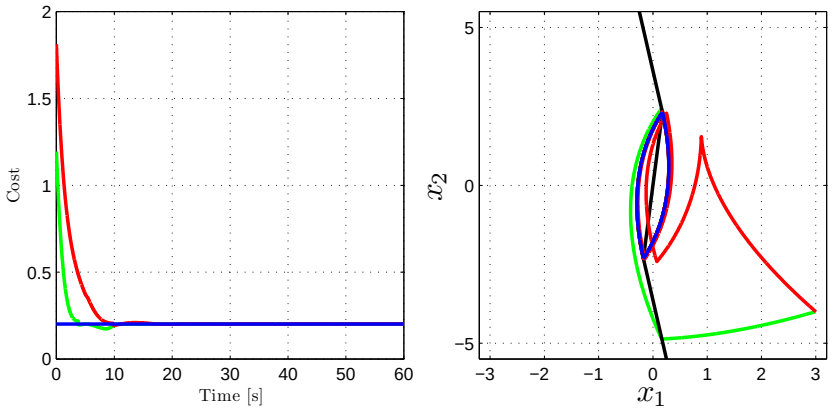

Figure 5: Simulation results for complex pole pair example. Left: performance plots. Right: state trajectory in the phase plane.

trajectory is going to cross the switching surface in between samples. If an estimate of the time at which the crossing takes place can be generated, this could be sent to an underlying faster process handling input/output sampling.

5.1 Complexity

Concerning the reference tracking strategy, Method A, we can conclude as in [Sarabia et al., 2005] that the optimisation problem is unfortunately nonlinear and non-convex which makes it hard to solve. However, integer variables are avoided as the optimisation is over switching times.
The limit cycle can be calculated off line, and a lookup table can be generated as a function of the measurable disturbance or changing reference value.
Like Method A, some calculations might be done off line for Method B. For instance one could find switching surfaces for a number of reference values and disturbances off line and then implement it as a lookup table.
The calculations in Method B, once the switching surfaces are known, are very fast as it amounts to evaluating the sign of certain functions. This makes this method applicable to systems requiring a high sample frequency as opposed to Method A.

5.2 Mixed Continuous/discrete Decision Variables

It is not obvious how to add continuous variables to the problem. [Sarabia et al., 2005] suggested one method described in Section 2.1 from which ideas can be used to include continuous variables in Method A. However, this increases the already high complexity of this algorithm.
Another far simpler approach is to make sequential loop closing. If there is only one discrete variable, this could be ignored when designing controllers for the other loops and then finally use the methods proposed in this paper on the partially closed loop system.

6 Conclusions and Future Works

6.1 Conclusions

It was shown that receding horizon control algorithms, using a finite prediction horizon for systems with mixed discrete and continuous decision variables does not converge to the optimal solution when this state converges to a limit cycle and the cost functional is discontinuous. The problem is that using a finite horizon control law there will be a prediction mismatch. Intuitively, a finite horizon algorithm will not “invest” in a discrete decision with a cost, if the “return-of-investment” takes a significant time, so the predicted decisions will always be postponed relative to their optimal times. Hence there is a need for algorithms for handling the infinite horizon aspects. Such a method

has been presented using sampling of the prediction horizon and a notation of absolute time. However, as a pure infinite horizon approach is not computationally tractable, two methods for handling this problem were presented. One approach was based on tracking the optimal limit cycle in a receding horizon manner, whereas the other method bears resemblance to time-optimal control by using a geometrical approach, which defines switching surfaces for the input in the state space.
Analytic expressions for the limit cycles were found and proved helpful in designing switching surfaces for systems with no complex eigenvalues.
Both the suggested methods were illustrated on the triple integrator and showed convergence of the state to the limit cycle. In case of systems with complex pole pair, convergence was also established. Simple heuristic switching surfaces for this system were also presented.

6.2 Future Work

In general there is a need to consider infinite horizon strategies when designing controllers for systems using discontinuous cost functional. There is a challenge in making both the suggested methods proposed in this paper work for systems with multiple inputs/multiple outputs and mixed discrete/continuous inputs; even though the ideas from [Sarabia et al., 2005] can be considered in case of the reference following method. Also robustness and stability issues for the proposed methods remain an open question.
Further, there might be other more suitable and less involved strategies for using the geometric representation of the limit cycles directly in the controller design.
Finally, unstable systems with positive real part of the eigenvalues need attention.

References

M. Athans and P. L. Falb. *Optimal control : an introduction to the theory and its applications*. New York McGraw-Hill, 1966.

A. Bemporad and M. Morari. Control of systems integrating logic, dynamics, and constraints. *Automatica*, 35:407–427, 1999.

A. Bemporad, F. Borelli, and M. Morari. Piecewise linear optimal controlles for hybrid systems. In *American Control Conference*, pages 1190–1194, June 2000.

A. Bemporad, A. Giua, and C. Seatzu. A master-slave algorithm for the optimal control of continuous-time switched affine systems. In *Proceedings of the IEEE Conference on Decision and Control*, volume 2, pages 1976–1981, 2002.

S. D. Cairano, M. Lazar, A. Bemporad, and W. P. M. H. Heemels. *Hybrid Systems: Computation and Control*, volume 4981, chapter A Control Lyapunov Approach to

Predictive Control of Hybrid Systems, pages 130–143. Springer-Verlag, Saint Louis, USA, 2008. Lecture Notes in Computer Science.

M. Egerstedt, Y. Wardi, and H. Axelsson. Transition-time optimization for switched-mode dynamical systems. *IEEE Transactions on Automatic Control*, 51(1):110–115, 2006.

A. Giua, C. Seatzu, and C. Van der Mee. Optimal control of switched autonomous linear systems. In *Proceedings of the IEEE Conference on Decision and Control*, volume 3, pages 2472–2477, 2001a.

A. Giua, C. Seatzu, and C. Van der Mee. Optimal control of autonomous linear systems switched with a pre-assigned finite sequence. In *IEEE International Symposium on Intelligent Control - Proceedings*, pages 144–149, 2001b.

S. Hedlund and A. Rantzer. Optimal control of hybrid systems. In *Proceedings of the 38th IEEE Conference on Decision and Control*, volume 4, pages 3972–3977, 1999.

R. A. Horn and C. R. Johnson. *Matrix Analysis*. Cambridge University Press, 1999.

L. F. S. Larsen, T. Geyer, and M. Morari. Hybrid MPC in supermarket refrigeration systems. In *16th IFAC World Congress*, Prague, Czech Republic, 2005.

M. Lazar, W. P. M. H. Heemels, S. Weiland, and A. Bemporad. Stabilizing model predictive control of hybrid systems. *IEEE Transactions on Automatic Control*, 51 (11):1813–1818, 2006.

E. B. Lee and L. Markus. *Foundations of optimal control theory*. New York John Wiley & Sons, 1967.

H. C. Lim. Classical approach to bang-bang control of linear processes. *Industrial and Engineering Chemistry, Process Design and Development*, 8(3):9, 1969.

J. M. Maciejowski. *Predictive Control With Constraints*. Harlow: Pearson Education Limited, 2001.

D. Q. Mayne, J. B. Rawlings, C. V. Rao, and P. O. M. Scokaert. Constrained model predictive control: Stability and optimality. *Automatica*, 36(6):789–814, June 2000.

P. Riedinger, C. Zanne, and F. Kratz. Time optimal control of hybrid systems. In *Proceedings of the American Control Conference*, volume 4, pages 2466–2470, 1999.

J. A. Rossiter. *Model-based Predictive Control: A Practical Approach*. CRC Press LLC, 2003.

D. Sarabia, C. de Prada, S. Cristea, and R. Mazaeda. Hybrid model predictive control of a sugar end section. In *European Symposium on Computer Aided Process Engineering, ESCAPE 16*, 2005.

C. Seatzu, D. Corona, A. Giua, and A. Bemporad. Optimal control of continuous-time switched affine systems. *IEEE Transactions on Automatic Control*, 51(5):726–741, May 2006.

E. D. Sontag. *Mathematical control theory : deterministic finite dimensional systems*. New York Springer, 1998.

K. Tsuda, D. Mignone, G. Ferrari-Trecate, and M. Morari. Reconfiguration strategies for hybrid systems. Technical Report AUT00-24, Automatic Control Laboratory, ETH Zurich, 2000.

E. Verriest, M. Egerstedt, Y. Wardi, and M. Boccadoro. Optimal control of switching surfaces in hybrid dynamical systems. *Discrete Event Dynamic Systems*, 14(4):433–448, 2005.

X. Xuping and P. Antsaklis. Quadratic optimal control problems for hybrid linear autonomous systems with state jumps. In *Proceedings of the American Control Conference*, volume 4, pages 3393–3398, 2003.